Lawrence Berkeley Laboratory
UNIVERSITY OF CALIFORNIA

Materials & Chemical Sciences Division

Theoretical Methods for the Study of Chemical Dynamics

N. Makri
(Ph.D. Thesis)

April 1989

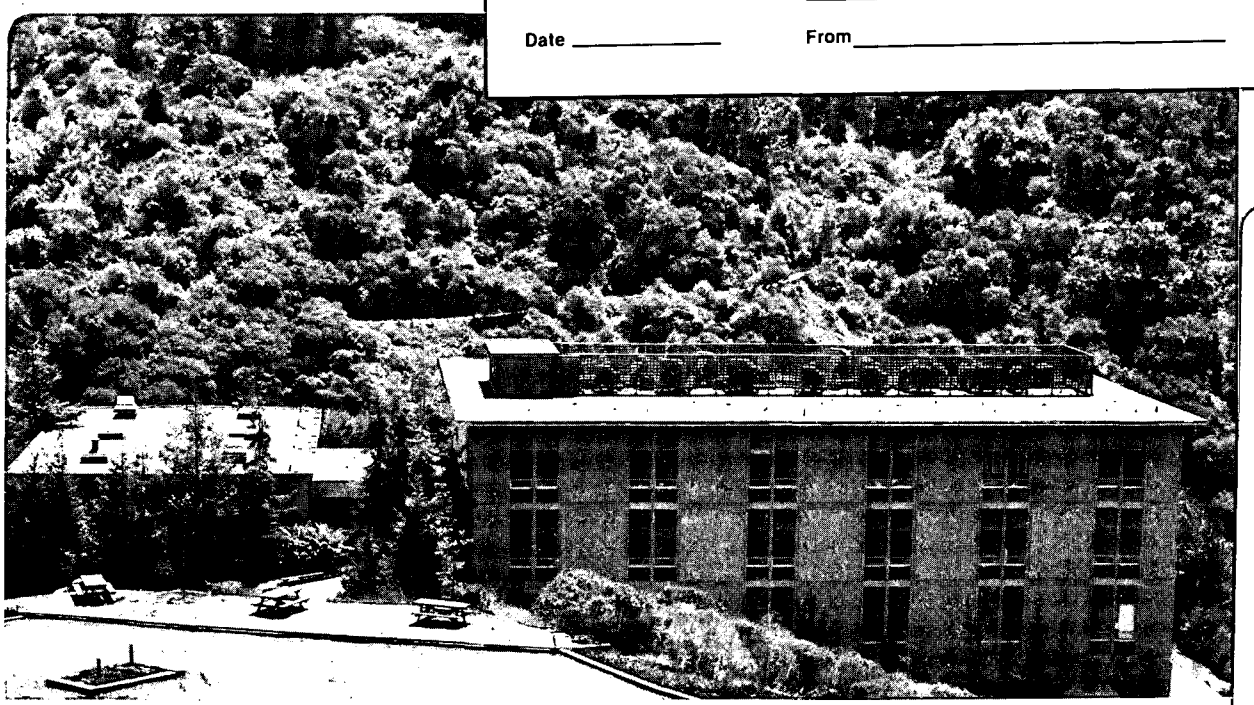

Prepared for the U.S. Department of Energy under Contract Number DE-AC03-76SF00098.

DISCLAIMER

LBL-27938

Theoretical Methods for the Study of Chemical Dynamics

Nancy Makri
(Ph.D. Thesis)

Department of Chemistry
University of California

and

Materials and Chemical Sciences Division
Lawrence Berkeley Laboratory
1 Cyclotron Road
Berkeley, California 94720

April 1989

Theoretical Methods for the Study of Chemical Dynamics

Nancy Makri

Abstract

Theoretical methods are developed for studying the dynamics of chemical reactions. Many chemical processes can be adequately described as a "system" of one or two reaction coordinates coupled to a "bath" of harmonic oscillators. Such a formulation of the problem has obvious advantages, as it is often possible to integrate out the harmonic bath, thus reducing the many degree of freedom problem to a one or two dimensional calculation. A basis set which explicitly incorporates the coupling provides an approximate but fairly accurate way of eliminating the harmonic bath. The time dependent self consistent field approximation is also considered as another approximate way of accomplishing the same goal and is generalized to a multiconfigurational procedure. A simple semiclassical model for incorporating tunneling effects in classical trajectory simulations is constructed and shown to give excellent results over a variety of conditions.

Feynman path integration provides an exact way of calculating quantum dynamical properties and is in principle applicable to problems of involving many degrees of freedom. However, the standard Monte Carlo methodology which must be used to evaluate the multidimensional integrals that occur, is not directly applicable to the path integral expression for the real time propagator, because the integrand of the latter is highly oscillatory. A technique which helps circumvent this problem by sampling about the stationary phase points of the integrand is developed and illustrated with several numerical applications. A new effective real time propagator is also constructed, which is localized and devoid of rapid oscillations. Finally, accurate

approximations to the short time propagator are derived, which drastically improve the convergence characteristics of path integrals. These techniques are expected to extend the applicability of path integral calculations to more complex chemical problems.

Acknowledgments

It is perhaps not possible to express in words my gratitude to my research director, Professor William H. Miller, for his guidance and encouragement during the past four years. My interaction with Bill has had an enormous influence on my scientific development. I have learned a great deal from his way of approaching science and from his profound scientific insight. Bill has given me invaluable scientific knowledge and has encouraged me to develop independent thinking and to pursue my own ideas. Above all, Bill has been a real friend, and it would be difficult to describe how much I have enjoyed working with him.

I wish to express my appreciation to Professor Robert A. Harris for his friendship and support throughout my graduate career at Berkeley, and for many interesting discussions. I thank Professor David Chandler for all of his help and for several useful conversations regarding path integration. I am grateful to Professor Robert Littlejohn of the Physics Department for his patience during many lengthy discussions on semiclassical theory. I also thank Professor Anthony Haymet for his encouragement, in particular during my first year in graduate school. These people have made a significant contribution to my career, and I have enjoyed interacting with them very much.

Many other people have made my four years at Berkeley pleasant. Nikos Daphnis and his family have always been good friends. I wish to thank the former and present members of the Miller group, Ned Sibert, Beverly Ruf, John Tromp, Bernadette Jensen op de Haar, Johnny Chang, Kim White, Sherry Chang, Theo Gray, John Zhang, Lee Gaucher, Penny Teal, Miquel Moreno, Weitao Yang, Andrew Peet, and Scott Auerbach for their friendship. Thanks are also due to Cheryn Gliebe and Beth Kuchinsky, who have always been friendly and very helpful. John Gehlen, Theo Kitsopoulos, Alex Weaver, Rosy Georgiadis, Chris Grayce, and several other people in the Chemistry Department have been my friends over these years. I would like to thank Professors Paul Alivisatos and Kenneth Dawson for useful advice, and Dr. Greg Voth for his

friendship and for always being willing to discuss science and other problems with me. I also appreciate the hospitality of the LBL Nuclear Physics group during the past year.

I wish to thank all the people in Athens who have helped me in several ways and encouraged me to come to Berkeley, especially our family friend Costas Symeonidis. I appreciate the help and advice that many of my High School and College teachers have given me, in particular Professors T. Hadjiioannou, A. Mavridis and C. Efstathiou. I am most indebted to Professor Cleanthis A. Nicolaides of the National Hellenic Research Foundation for introducing me to the real world of Theoretical Chemistry, and for all of his support. I am also grateful to Dr. Yannis Komninos for helping me learn the basics of quantum mechanics and for his valuable guidance during my first research project.

Finally, I owe all of my accomplishments to my parents. I will always be grateful to my father for his love, his extraordinary patience and his confidence in me. Among other things, my father managed to teach me some math and physics during my early childhood (as incredible as it may sound!) and to convey his excitement about science to me. I thank my mother for her continuing love and care for me. I appreciate everything she has done for me, in particular her support and encouragement during recent years; I also thank her for proofreading my Thesis. My grandmother has always been very close to me, and I am grateful for her love and understanding. And I thank Martin for the support he has given me and for the good time we have had together.

This research was supported in part by the Director, Office of Energy Research, Office of Basic Energy Sciences, Chemical Sciences Division of the U.S. Department of Energy under contract No. DE-AC03-76SF00098.

Table of Contents

I. Introduction

One of the most fundamental problems in chemistry is understanding how chemical reactions occur, i.e., how reactant species are transformed into products. Such a description is the goal of chemical reaction dynamics,[1.1–1.2] which in recent years has evolved into a very active field in physical chemistry. Due to major advances in experimental excitation and detection techniques, it is now possible to measure quantum state-specific properties of fairly complicated molecules and to probe the dynamics of chemical reactions at the molecular level and at very short times. Most of these advances have come from the development in the past 2-3 decades of molecular beam [1.3–1.9] and laser [1.10–1.15] techniques.

With the advent of crossed molecular beam methods [1.3–1.9] in the late 1950's, it became possible to study chemical reactions at the microscopic single collision level. In simple molecular beam experiments, a beam of reactant molecules is directed toward a beam of target molecules and the reactive scattering that takes place is observed, yielding finally the reaction cross-section as a function of the collision energy. In other experiments, a laser is used to excite one of the reactant molecules, thus initiating a unimolecular reaction. The measurement of angular, velocity and quantum state population distributions of the products is the result of such experiments.

Even though the above techniques provide very useful chemical information about a reaction, they are unable to follow the actual dynamics of the process in detail, i.e., the evolution from reactants to products through the transition state. Because the latter is very short lived (typically of the order of femtoseconds), special ultrafast laser techniques must be utilized in order to obtain experimentally a picture of the reaction process in real time. Ultrafast experiments [1.16–1.26] have become possible in recent years, as laser pulses as short as only a few femtoseconds are now available in the laboratory. Typical femtosecond experiments use a laser pulse to

excite one of the reactant molecules, thus initiating a reaction; subsequent laser pulses of femtosecond duration are used to probe the time evolution of the initially prepared state. Apart from practical problems, the actual limitation of such experiments is of course imposed by the time-energy uncertainty principle.

On the other hand, the quantitative theoretical description of the dynamics during chemical reactions is as yet less developed. The basic reason for this is that even though all of the desirable information about a quantum system is encompassed in the Schrödinger equation, the latter is in practice impossible to solve if several coupled degrees of freedom are involved. One must thus resort to approximate methods for calculating quantum mechanical properties of non-separable multidimensional systems. While considerable progress has been made during the past few decades in developing approximate schemes for this purpose, there is presently no general method that succeeds in providing the answer to this problem.

The fundamental assumption that is common in all molecular dynamics calculations is the Born-Oppenheimer approximation, which is justified on the basis of the separation of time scales between electronic and nuclear degrees of freedom. This hypothesis allows separation of the electronic motion from that of the nuclei and leads to a potential energy surface on which the chemical event takes place. Non-adiabatic couplings constitute corrections to the Born- Oppenheimer approximation; inclusion of more than one Born-Oppenheimer potential surfaces in the calculation is necessary when such non-adiabatic effects are large.

The main difficulty in fully quantum mechanical calculations is their nonlocal nature, which is inherent in the Schrödinger equation. Basis set methods provide a straightforward and virtually exact way of solving quantum problems. However, the size of the basis set that is required grows exponentially with the number of degrees of freedom. It is thus relatively trivial to deal with one or two degrees of freedom by simple matrix diagonalization in a basis set, but prohibitively difficult for three or

more degrees of freedom. Thus, although the first quantum reactive scattering calculations [1.27–1.30] for the collinear $H+H_2$ reaction were performed using the coupled channel method [1.31] more than a decade ago, application of the same techniques to fully three-dimensional collision problems remains a sufficiently difficult task.

Even though significant progress has been made in developing approximate methods for solving quantum mechanical problems and a lot of effort continues to be devoted to this goal, it is often not necessary to solve the full quantum mechanical state to state problem in order to calculate certain properties. This is so because atoms and molecules are relatively heavy particles, and because suitable averages often tend to wash out quantum effects. In such cases, the most widely used method is the classical trajectory approach.[1.32–1.36] In this treatment, the motion of the nuclei on the Born-Oppenheimer potential surface is calculated by solving Newton's equations of motion. The method is easily implemented and has been applied to a large number of classical problems. Moreover, classical trajectory calculations can be combined with the generalized Langevin equation to allow the description of systems in contact with a thermal bath. Despite the general success of the method, severe problems often arise; these are connected with the inability of classical mechanics to describe quantum effects such as tunneling and zero point energy, which are ubiquitous in chemical reactions.

Semiclassical theory [1.37–1.61] provides the link between classical and quantum mechanics and serves both as a computational tool and as a conceptual framework for interpreting quantum effects in chemical phenomena. The theory employs an expansion in Planck's constant $\hbar$ and relies heavily on the topological properties of the potential involved. A very popular semiclassical dynamical method is the Gaussian wavepacket approximation,[1.62–1.74] which has been applied to many systems with success. Nevertheless, semiclassical methods are not straightforward to implement in most cases. Although semiclassical mechanics is a well understood theory

for one dimensional potentials, this is not so for general systems of higher dimensionality and complicated topology. Chaotic behavior and other nonlinear effects,[1.75–1.78] which play an important role in intramolecular vibrational energy redistribution (IVR),[1.79–1.83] complicate the semiclassical picture. The problem of semiclassical quantization is intimately connected with the existence of global constants of the motion and thus with the problem of integrability in many dimensions, and remains an active area of research.

Time dependent quantum mechanical methods [1.84–1.96] often possess advantages for studying dynamical processes. The goal of the time dependent approach is to solve the time dependent Schrödinger equation directly, subject to the given initial conditions. If the reaction of interest is completed in relatively short time, as is often the case, time dependent calculations can be much more economical than solving the complete time independent quantum problem (i.e., computing the full scattering matrix, or extracting the eigenstates and eigenvalues by numerical diagonalization of the Hamiltonian in a basis set). Perhaps the most successful technique is the split operator method,[1.92–1.93] which utilizes the Fast Fourier Transform (FFT) algorithm [1.92–1.96] and is thus very efficient. Unfortunately, the method suffers from the same shortcomings as most other fully quantum mechanical methods, i.e., its applicability is limited to problems of low dimensionality.

Feynman's idea of path integration [1.97–1.98] provides the most powerful and attractive tool for dealing with systems of many degrees of freedom. Unlike the above methods, which are limited to problems of only a few degrees of freedom, path integration is in principle applicable to systems of high dimensionality. As such, it has found extensive use in statistical mechanics for the calculation of equilibrium properties of large systems.[1.99–1.108] Another useful feature of the path integral methodology is that it can be used to integrate out harmonic degrees of freedom *exactly*. This is done by introducing a nonlocal influence functional which

describes the effect of the harmonic bath on the quantum system. Despite these advantages, though, the use of path integral techniques in the study of dynamical processes has so far been limited.[1.109–1.121] The reason for this is that standard Monte Carlo techniques (which are routinely used as a computational tool for performing multidimensional integration) are not directly applicable to the case of the real time propagator, $\exp(-iHt/\hbar)$, for which the integrand is oscillatory. However, new techniques have recently been developed,[1.122–1.125] whereby Monte Carlo path integration can be efficiently performed for the real time propagator. These techniques have generated optimism for studying the dynamics of relatively fast but fairly complex chemical reactions.

A class of reactions of particular interest to the Miller group are hydrogen atom transfer reactions in polyatomic molecules, e.g., the symmetric isomerization of malonaldehyde,

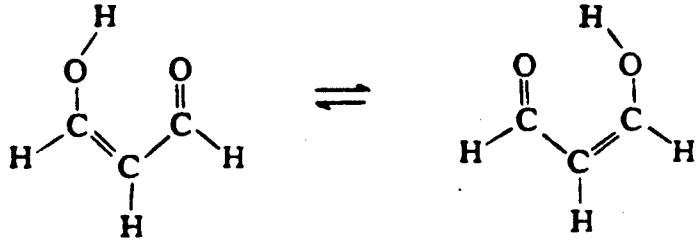

or the unimolecular isomerization of hydrogen isocyanide,

$$HNC \rightarrow HCN.$$

At low temperatures these reactions proceed primarily via tunneling, but at higher temperatures there is a significant probability of the system having an energy above the potential barrier. It is thus of interest to study the effects of tunneling on the thermally averaged reaction rate. Such processes involve large amplitude motion in only one or two coordinates ("reaction coordinates"), while all the other vibrational modes behave like locally harmonic degrees of freedom which affect the reaction of interest through coupling to the reaction coordinate. This picture leads to the *reaction path* (or reaction surface) Hamiltonian formalism,[1.126–1.131] in which the

reaction coordinates constitute the "system" and the remaining degrees of freedom are the "harmonic bath". Having expressed the Hamiltonian according to this model, one tries to integrate out the bath after taking into consideration its effect on the system, thus reducing the problem to a one (or two) dimensional one.

This Thesis is divided into two parts. Part A describes the development of approximate techniques that seem promising for studying the dynamics of systems with several degrees of freedom. Chapters II and III present methods specifically developed for dealing with system-bath problems. In Chapter II a basis set method is described, which provides an approximate way to eliminate the bath degrees of freedom, thus leading to an effective Hamiltonian matrix of small dimensionality. Chapter III explores the possibility of using time dependent mean field approximations in the study of similar problems. A semiclassical model for calculating tunneling rates by integrating the classical equations of motion - a relatively easy task even for multidimensional systems - is described in Chapter IV.

Part B of this Thesis deals almost exclusively with path integral methods. Chapter V develops a technique for performing integration of oscillatory integrands of the type that occur in the path integral formulation of the quantum propagator using the standard Monte Carlo methodology. This is achieved by introducing a weighting function which is constructed to sample primarily about the stationary phase points of the integrand. In Chapter VI it is shown that the highly oscillatory behavior of the real time propagator can be eliminated if the properties of the wavefunction are properly exploited; an effective propagator is constructed, which is well suited for Monte Carlo path integration. Finally, Chapter VII presents a systematic scheme for improving on the short time approximation for the propagator. By using a short time propagator which is valid for longer time increment, the necessary number of integration variables in a path integral can be drastically reduced, resulting in significant savings.

References

1.1 R. D. Levine and R. B. Bernstein, *Molecular Reaction Dynamics and Chemical Reactivity*, Oxford University Press, New York, 1987.

1.2 H. Eyring, S. H. Lin, and S. M. Lin, *Basic Chemical Kinetics*, John Wiley & Sons, New York, 1980.

1.3 S. Datz and E. H. Taylor, in *Recent Research in Molecular Beams*, I. Estermann, Ed. (Academic Press, New York, 1959), p. 157.

1.4 J. Ross, Ed., *Adv. Chem. Phys.* 10 (1966) (special issue on molecular beams).

1.5 D. R. Herschbach, *Molecular Dynamics of Elementary Chemical Reactions*, Les Prix Nobel in 1986, Elsevier Publishing Co., Amsterdam, 1987.

1.6 Y. T. Lee, *Science* 236, 793 (1987).

1.7 J. L. Kinsey, *Int. Rev. Sci. Phys. Chem.* 9, 173 (1972).

1.8 D. R. Herschbach, *Adv. Chem. Phys.* 10, 319 (1966).

1.9 R. B. Bernstein, *Adv. At. Mol. Phys.* 15, 167 (1979).

1.10 K. B. Eisenthal, *Acc. Chem. Res.* 8, 118 (1975).

1.11 A. Laubereau and W. Kaiser, *Rev. Mod. Phys.* 50, 607 (1978).

1.12 V. S. Letokhov, *Nonlinear Laser Chemistry*, Springer Series in Chemical Physics 22, Springer-Verlag, New York, 1983.

1.13 A. E. Siegman, *Lasers*, University Science Books, Mill Valley, California, 1986.

1.14 M. C. Lin, M. E. Umstead, and N. Djeu, *Ann. Rev. Phys. Chem.* 34, 557 (1983).

1.15 R. B. Bernstein, *Chemical Dynamics via Molecular Beam and Laser Techniques*, Oxford, New York, 1982.

1.16 G. R. Fleming and A. E. Siegman, Editors, *Ultrafast Phenomena V*, Springer-Verlag, New York, 1986.

1.17 J. L. Knee and A. H. Zewail, *Spectroscopy*, 3, 44 (1988).

1.18 C. V. Shank, *Science* 233, 1276 (1986).

1.19 A. H. Zewail and R. B. Bernstein, *Chem. & Eng. News* 66, 24 (1988).

1.20 M. Dantus, M. J. Rosker, and A. H. Zewail, *J. Chem. Phys.* 87, 2395 (1987).

1.21 M. Dantus, M. J. Rosker, and A. H. Zewail, *J. Chem. Phys.* 89, 6113 (1988).

1.22 M. Dantus, M. J. Rosker, and A. H. Zewail, *J. Chem. Phys.* 89, 6128 (1988).

1.23 M. J. Rosker, M. Dantus, and A. H. Zewail, *Science* 241, 200 (1988).

1.24 T. S. Rose, M. J. Rosker, and A. H. Zewail, *J. Chem. Phys.* 88, 6672 (1988).

1.25 M. J. Rosker, T. S. Rose, and A. H. Zewail, *Chem. Phys. Lett.* 146, 175 (1988).

1.26 S. Mukamel, in *Ultrafast Phenomena VI* , Springer-Verlag, New York, 1988.

1.27 G. A. Parker, T. G. Shmaltz, and J. C. Light, in *Algorithms and Computer Codes for Atomic and Molecular Quantum Scattering Theory*, L. Thomas, Ed., National Resource for Computation in Chemistry Proceedings 1, 172 (1979).

1.28 J. C. Light, *Discuss. Faraday Soc.* 44, 14 (1969).

1.29 G. C. Schatz and A. Kuppermann, *J. Chem. Phys.* 65, 4668 (1976).

1.30 M. J. Redmon and R. E. Wyatt, *Chem. Phys. Lett.* 63, 209 (1979).

1.31 R. D. Levine, *Quantum Mechanics of Molecular Rate Processes*, Clarendon, Oxford, 1969.

1.32 M. Karplus, R. Porter, and R. D. Sharma, *J. Chem. Phys.* 49, 3259 (1965).

1.33 D. G. Truhlar and T. Muckermanin, in *Physics of Atoms and Molecules*, R. B. Bernstein, Ed., Plenum, New York, 1979.

1.34 R. M. Porter and L. M. Raff, in *Molecular Collisions*, W. H. Miller, Ed., Plenum, New York, 1976.

1.35 S. A. Adelman and J. D. Doll, *J. Chem. Phys.* 61, 4242 (1974).

1.36 J. C. Tully, *Acc. Chem. Res.* 14, 188 (1981).

1.37 J. Bang and J. deBoer, Eds., *Semiclassical Descriptions of Atoms and Nuclear Collisions*, Elsevier, New York, 1985.

1.38 D. W. Noid, M. L. Koszykowski, and R. A. Marcus, *Ann. Rev. Phys. Chem.* 32, 267 (1981).

1.39 M. S. Child, in *Theory of Chemical Reaction Dynamics*, M. Baer, Ed., CRC Press, Boca Raton, FL, 1985, p. 247.

1.40 W. H. Miller, in *Semiclassical Descriptions of Atoms and Nuclear Collisions*, Elsevier, New York, 1985, p. 9-26.

1.41 E. J. Heller, *Acc. Chem. Res.* 14, 368 (1981).

1.42 W. H. Miller, *Adv. Chem. Phys.* 25, 69 (1974).

1.43 W. H. Miller, *Adv. Chem. Phys.* **30**, 77 (1974).

1.44 W. H. Miller, *J. Chem. Phys.* **54**, 5386 (1971).

1.45 W. H. Miller, *J. Chem. Phys.* **81**, 3573 (1984).

1.46 W. H. Miller, *J. Chem. Phys.* **55**, 3146 (1971).

1.47 W. H. Miller, *J. Chem. Phys.* **58**, 1664 (1973).

1.48 S. Chapman, B. C. Garrett, and W. H. Miller, *J. Chem. Phys.* **64**, 502 (1976).

1.49 M. V. Berry and K. E. Mount, *Rep. Prog. Phys.* **35**, 315 (1972).

1.50 J. B. Delos, *Adv. Chem. Phys.* **65**, 161 (1986).

1.51 M. C. Gutzwiller, *J. Math. Phys.* **11**, 1791 (1970).

1.52 I. C. Percival, *Adv. Chem. Phys.* **36**, 1 (1977).

1.53 T. S. Rose, M. J. Rosker, and A. H. Zewail, *J. Chem. Phys.* **88**, 6672 (1988).

1.54 R. A. Marcus, *Annu. Rev. N. Y. Acad. Sci.* **357**, 169 (1980).

1.55 R. A. Marcus, *J. Chem. Phys.* **54**, 3965 (1971).

1.56 J. B. Delos, *Adv. Chem. Phys.* **65**, 161 (1986).

1.57 D. W. Noid and R. A. Marcus, *J. Chem. Phys.* **67**, 559 (1977).

1.58 G. A. Voth and R. A. Marcus, *J. Chem. Phys.* **82**, 4064 (1985).

1.59 G. A. Voth and R. A. Marcus, *J. Phys. Chem.* **89**, 2208 (1985).

1.60 M. C. Gutzwiller, *J. Math. Phys.* **12**, 343 (1971).

1.61 C. C. Martens and G. S. Ezra, *J. Chem. Phys.* **83**, 2990 (1985).

1.62 E. J. Heller, *J. Chem. Phys.* **62**, 1544 (1975).

1.63 E. J. Heller, *Chem. Phys. Lett.* **34**, 321 (1975).

1.64 E. J. Heller, *J. Chem. Phys.* **65**, 1289 (1976).

1.65 E. J. Heller, *J. Chem. Phys.* **65**, 4979 (1976).

1.66 E. J. Heller, *J. Chem. Phys.* **67**, 3339 (1977).

1.67 E. J. Heller, *J. Chem. Phys.* **68**, 2066 (1978).

1.68 E. J. Heller, *J. Chem. Phys.* **68**, 3891 (1978).

1.69 E. J. Heller, *J. Chem. Phys.* **75**, 2923 (1981).

1.70 M. J. Davis and E. J. Heller, *J. Chem. Phys.* **71**, 3383 (1979).

1.71 D. Tannor and E. J. Heller, *J. Chem. Phys.* 77, 202 (1982).

1.72 N. DeLeon, M. J. Davis, and E. J. Heller, *J. Chem. Phys.* 80, 794 (1984).

1.73 N. DeLeon and E. J. Heller, *Phys. Rev.* A **30**, 5 (1984).

1.74 N. DeLeon and E. J. Heller, *J. Chem. Phys.* **81**, 5957 (1984).

1.75 M. V. Berry, in *Chaotic Behaviour in Deterministic Systems* (North Holland Publishing, Amsterdam, 1983), p. 172.

1.76 M. V. Berry, in *Topics in Nonlinear Dynamics* (American Institute of Physics, New York, 1978), v. **46**, p. 16.

1.77 A. J. Lichtenberg and M. A. Lieberman, *Regular and Stochastic Motion*, Springer-Verlag, New York.

1.78 V. I. Arnold, *Mathematical Methods of Classical Mechanics*, Springer, New York, 1978.

1.79 R. A. Marcus, *Ann. N. Y. Acad. Sci.* **357**, 169 (1980).

1.80 E. J. Heller, E. B. Stechel, and M. J. Davis, *J. Chem. Phys.* 73, 4720 (1980).

1.81 C. Jaffe and W. P. Reinhardt, *J. Chem. Phys.* **77**, 3595 (1982).

1.82 E. L. Sibert III, J. T. Hynes, and W. P. Reinhardt, *J. Chem. Phys.* 77, 3595 (1982).

1.83 G. A. Voth, R. A. Marcus, and A. H. Zewail, *J. Chem. Phys.* **81**, 5494 (1984).

1.84 R. G. Gerber, A. T. Yinnon, and R. Kosloff, *Chem. Phys. Lett.* 105,523 (1984).

1.85 R. Kosloff and C. Cerjan, *J. Chem. Phys.* **81**, 3722 (1984).

1.86 G. Wahnstrom and H. Metiu, *Chem. Phys. Lett.* **134**, 531 (1987).

1.87 B. Jackson and H. Metiu, *J. Chem. Phys.* **86**, 1026 (1987).

1.88 D. Huber and E. J. Heller, *J. Chem. Phys.* 87, 5302 (1987).

1.89 D. Huber, E. J. Heller, and R. G. Littlejohn, *J. Chem. Phys.* 89, 2003 (1988).

1.90 Z. Kottler, A. Nitzan, and R. Kosloff, in *Proceedings of the 19th Jerusalem Symposium*, B. Pullman and J. Jortner, Eds., Reidel, Dordrecht, Holland, 1986.

1.91 R. C. Mowrey and K. J. Kouri, *J. Chem. Phys.* **86**, 6140 (1987).

1.92 M. D. Feit, J. A. Fleck, Jr., and A. Steiger, *J. Comp. Phys.* 47, 412 (1982).

1.93 M. D. Feit and J. A. Fleck, Jr., *J. Chem. Phys.* **78**, 301 (1983).

1.94 D. Kosloff and R. Kosloff, *J. Comp. Phys.* **52**, 35 (1983).

1.95 R. Kosloff and D. Kosloff, *J. Chem. Phys.* 79, 1823 (1983).

1.96 R. Kosloff, *J. Phys. Chem.* 92, 2087 (1988).

1.97 R. P. Feynman, *Rev. Mod. Phys.* 20, 367 (1948).

1.98 R. P. Feynman and A. R. Hibbs, *Quantum Mechanics and Path Integrals*, McGraw-Hill, New York, 1965.

1.99 M. Parrinello and A. Rahman, *J. Chem. Phys.* 80, 860 (1984).

1.100 C. D. Jonah, C. Romero, and A. Rahman, *Chem. Phys. Lett.* 123, 209 (1986).

1.101 R. A. Kuharski and P. J. Rossky, *Chem. Phys. Lett.* 103, 357 (1984).

1.102 R. A. Kuharski and P. J. Rossky, *J. Chem. Phys.* 82, 5164 (1985).

1.103 A. Nichols III, D. Chandler, Y. Singh, and D. Richardson, *J. Chem. Phys.* 81, 5109 (1984).

1.104 M. Sprik, M. L. Klein, and D. Chandler, *J. Chem. Phys.* 83, 3042 (1985).

1.105 J. Bartholomew, R. Hall, and B. J. Berne, *Phys. Rev. B* 32, 548 (1985).

1.106 A. Wallquist and B. J. Berne, *Chem. Phys. Lett.* 117, 214 (1985).

1.107 A. Wallquist, D. Thirumalai and B. J. Berne, *J. Chem. Phys.* 85, 1583 (1986).

1.108 See also the entire issue *J. Stat. Phys.* 43, Nos. 5/6 (1986).

1.109 W. H. Miller, S. D. Schwartz, and J. W. Tromp, *J. Chem. Phys.* 79, 4889 (1983).

1.110 R. Jaquet and W. H. Miller, *J. Phys. Chem.* 89, 3139 (1984).

1.111 K. Yamashita and W. H. Miller, *J. Chem. Phys.* 82, 5475 (1985).

1.112 D. Thirumalai and B. J. Berne, *J. Chem. Phys.* 79, 5029 (1983).

1.113 D. Thirumalai and B. J. Berne, *J. Chem. Phys.* 81, 2512 (1984).

1.114 D. Thirumalai, E. J. Bruskin, and B. J. Berne, *J. Chem. Phys.* 79, 5063 (1983).

1.115 D. Thirumalai and B. J. Berne, *Ann. Rev. Phys. Chem.* 37, 401 (1986).

1.116 E. C. Behrman, G. A. Jongeward, and P. G. Wolynes, *J. Chem. Phys.* 79, 6277 (1983).

1.117 E. C. Behrman and P. G. Wolynes, *J. Chem. Phys.* 83, 5863 (1985).

1.118 J. D. Doll, *J. Chem. Phys.* 81, 3536 (1984).

1.119 J. D. Doll and D. L. Freeman, *Science* 234, 1356 (1986).

1.120 J. Chang and W. H. Miller, *J. Chem. Phys.* 87, 1648 (1987).

1.121 J. D. Doll, R. D. Coalson, and D. L. Freeman, *J. Chem. Phys.* 87, 1641 (1987).

1.122 J. D. Doll, R. D. Coalson, and D. L. Freeman, *Phys. Rev. Lett.* 55, 1 (1985).

1.123 R. D. Coalson, D. L. Freeman, and J. D. Doll, *J. Chem. Phys.* 85, 4567 (1986).

1.124 N. Makri and W. H. Miller, *Chem. Phys. Lett.* 139, 10 (1987).

1.125 N. Makri and W. H. Miller, *J. Chem. Phys.* 89, 2170 (1988).

1.126 W. H. Miller, N. C. Handy and J. E. Adams, *J. Chem. Phys.* 72, 99 (1980).

1.127 W. H. Miller, *J. Chem. Phys.* 87, 3811 (1983).

1.128 W. H. Miller, in *The Theory of Chemical Reaction Dynamics*, edited by D. C. Clary (Reidel, Boston, 1986), pp. 27-45.

1.129 W. H. Miller, in *Potential Energy Surfaces and Dynamics Calculations*, D. G. Truhlar, Ed., Plenum Publishing Corporation, 1981.

1.130 W. H. Miller, B. A. Ruf, and Y. T. Chang, *J. Chem. Phys.* 89, 6298 (1988).

1.131 W. H. Miller, *J. Phys. Chem.* 87, 3811 (1983).

PART A

II. The Shifted Oscillator Basis Set

1. Introduction

The model of a system, consisting of a few interesting degrees of freedom, is ubiquitous in chemistry and physics. It is obviously a common situation in statistical mechanics, where the bath may consist of 10^{23} degrees of freedom, but it is also a very relevant and useful point of view in the field of reaction dynamics where the bath may consist of relatively few (e.g., 3-20) degrees of freedom, though still too many to be able to treat the complete system plus bath without approximation.

The specific system-bath model that has concerned this group in recent years arises from the reaction path (or reaction surface) Hamiltonian [2.1] description of a reactive process in a polyatomic molecular system. The reaction coordinate (or coordinates) constitute the system, and the remaining degrees of freedom, which are locally harmonic vibrations perpendicular to the reaction path (or reaction surface), are the bath. In this chapter, though, we consider the simpler generic system-bath model that has been considered by many workers, which is characterized by the Hamiltonian

$$H(p_s,s,\mathbf{P},\mathbf{Q}) = \frac{p_s^2}{2m} + V_0(s) + \sum_k \left[\frac{P_k^2}{2m} + \frac{1}{2}m\omega_k^2 Q_k^2\right] - \sum_k Q_k f_k(s). \qquad (2.1)$$

The system here is the reaction coordinate s. The potential $V_0(s)$ has the topology of the chemical process being described; an intramolecular H-atom transfer process, for example, would be characterized by a double well potential function. The bath consists of harmonic oscillators, which are linearly coupled to the system.

The universal strategy for dealing with a system-bath situation is to find some way, exact or approximate, to eliminate the bath and then to deal accurately with the system. Feynman path integral methodology [2.2] is one very attractive way for doing this that our group,[2.3] and many others,[2.4–2.8] have used. The most powerful

feature of this approach is that the path integral over the bath degrees of freedom can be performed analytically, so that one is left with a path integral for only one degree of freedom which must be performed numerically. For the case of real time dynamics (i.e., the propagator $e^{-iHt/\hbar}$), however, numerical (i.e., Monte Carlo) path integration is a non-trivial task,[2.5–2.7] in particular if the desired information is contained in the long time dynamics.

If one were dealing only with the quantum mechanics of a one (or two) degree of freedom system, then much simpler than evaluating a path integral would be to diagonalize a matrix representation of the Hamiltonian in a basis set. This has been seen,[2.9] for example, in evaluating quantum mechanical reactive flux correlation functions. This is because, as a rule of thumb, basis sets for molecular problems typically require 10-20 basis functions per degree of freedom ; it is thus relatively trivial to deal with one or two degrees of freedom by straightforward matrix diagonalization, but not so for more than three degrees of freedom.

The best of all possible strategies, therefore, would be to use the path integral methodology to eliminate bath degrees of freedom, and then to solve the quantum mechanics of the low-dimensional system by basis set methods. Unfortunately, this seems not to be possible; once the bath modes have been dealt with by path integration, the quantum mechanics for the system does not correspond to a local Schrödinger equation, so that one is forced to deal with it also by path integral methods.

The purpose of this Chapter [2.17] is to describe progress we have made using basis set methods to deal with system-bath problems. As with the path integral approach, we first take account of the bath degrees of freedom and eliminate them from the problem, and then deal accurately with the system. Unlike the path integral approach, though, these basis set methods are unable to incorporate the effects of the bath *exactly* . How well they are able to do so must thus be tested, and we consider

some analytic and numerical examples in the paper. The results are very encouraging that relatively simple basis sets can account for the effect of the bath on the system quite accurately. Once the bath degrees of freedom have been eliminated, the quantum mechanics for the system is dealt with simply by diagonalizing a Hamiltonian matrix whose dimension is only that of the basis set for the system degrees of freedom (i.e., a small matrix).

2. The linearly shifted oscillator basis

The Hamiltonian under consideration is that in Eq. (2.1). To motivate the choice of basis set below, consider first a self-consistent field (SCF) approximation to the wavefunction

$$\psi(s,\mathbf{Q}) = \chi(s)\prod_k u_k(Q_k). \tag{2.2}$$

Taking the diagonal matrix element of the Hamiltonian with respect to $\chi(s)$ gives the following effective Hamiltonian for the Q degrees of freedom:

$$H_{\mathbf{Q}} \equiv \int ds\, \chi(s) H \chi(s) = \text{const} + \sum_k \left[\frac{P_k^2}{2m} + \frac{1}{2} m \omega_k^2 Q_k^2 - \langle \chi | f_k | \chi \rangle Q_k \right]. \tag{2.3}$$

Equation (2.3) is recognized to be the Hamiltonian for a set of *uncoupled*, linearly displaced harmonic oscillators, the eigenfunctions of which are

$$\prod_k \phi_{n_k}(Q_k - \lambda_k)$$

with

$$\lambda_k = \langle \chi | f_k | \chi \rangle / m\omega_k^2, \tag{2.4}$$

where ϕ_{n_k} is the standard harmonic oscillator eigenfunction with frequency ω_k and vibrational quantum number n_k.

We are not interested at the moment in making an SCF approximation, but the above discussion suggests the following basis set for the complete system-bath

Hamiltonian:

$$\psi_{i\mathbf{n}}(s\,\mathbf{Q}) \equiv \langle s,\mathbf{Q}|i\,\mathbf{n}\rangle = \chi_i(s)\prod_k \phi_{n_k}(Q_k-\lambda_k^i), \tag{2.5a}$$

where

$$\lambda_k^i = \langle\chi_i|f_k|\chi_i\rangle/m\,\omega_k^2. \tag{2.5b}$$

Using the shifted oscillator basis functions in Eq. (2.5) takes some account of the coupling directly in the basis set. The amount of the shift for the kth oscillator, λ_k^i, is proportional to the expectation value of the force $f_k(s)$ with respect to basis function $\chi_i(s)$ and is thus different for different values of i. The basis $\chi_i(s)$ for the system is unspecified at present.

It is straightforward to construct the matrix representation of the Hamiltonian (2.1) in the basis (2.4), and one obtains

$$H_{i'\mathbf{n}',i\mathbf{n}} = F_{i'\mathbf{n}',i\mathbf{n}}\,\{\langle\chi_{i'}|H_s|\chi_i\rangle + \sum_k\langle\chi_{i'}|\chi_i\rangle[(n_k+\frac{1}{2})\hbar\omega_k + \frac{m\,\omega_k^2}{2}\lambda_k^{i'}\lambda_k^i]$$

$$-\sum_k\langle\chi_{i'}|f_k|\chi_i\rangle\frac{\lambda_k^{i'}+\lambda_k^i}{2} + \sum_k\frac{\sqrt{\hbar}}{\sqrt{2m\,\omega_k}}[\langle\chi_{i'}|\chi_i\rangle m\,\omega_k^2\lambda_k^i - \langle\chi_{i'}|f_k|\chi_i\rangle]$$

$$\times[\sqrt{n'_k}\frac{\langle\phi_{n'_k-1}(Q_k-\lambda_k^{i'})|\phi_{n_k}(Q_k-\lambda_k^i)\rangle}{\langle\phi_{n'_k}(Q_k-\lambda_k^{i'})|\phi_{n_k}(Q_k-\lambda_k^i)\rangle} + \sqrt{n_k}\frac{\langle\phi_{n'_k}(Q_k-\lambda_k^{i'})|\phi_{n_k-1}(Q_k-\lambda_k^i)\rangle}{\langle\phi_{n'_k}(Q_k-\lambda_k^{i'})|\phi_{n_k}(Q_k-\lambda_k^i)\rangle}]\}, \tag{2.6}$$

where

$$H_s = \frac{p_s^2}{2m} + V_0(s),$$

and F is the Franck-Condon factor between oscillator basis functions,

$$F_{i'\mathbf{n}',i\mathbf{n}} = \prod_k\int dQ_k\ \phi_{n'_k}(Q_k-\lambda_k^{i'})\ \phi_{n_k}(Q_k-\lambda_k^i). \tag{2.7}$$

Were is necessary to diagonalize this entire matrix, then nothing has been accomplished. As a zeroth order approximation, therefore, we choose the part of the

Hamiltonian matrix that is diagonal in the bath quantum numbers **n**; i.e.,

$$H_{i'\mathbf{n}',i\mathbf{n}}^{(0)} = \delta_{\mathbf{n}',\mathbf{n}} H_{i',i}^{\mathbf{n}}, \tag{2.8a}$$

where $H_{i',i}^{\mathbf{n}} \equiv H_{i'\mathbf{n},i\mathbf{n}}$. From Eq. (2.6) one sees that this zeroth order *effective system Hamiltonian* (ESH) is

$$H_{i',i}^{\mathbf{n}} = F_{i',i}^{\mathbf{n}} \{ \langle \chi_{i'} | H_s | \chi_i \rangle + \sum_k [\langle \chi_{i'} | \chi_i \rangle \hbar\omega_k (n_k + 1/2)$$

$$+ \langle \chi_{i'} | \chi_i \rangle \frac{m\omega_k^2}{2} \lambda_k^{i'} \lambda_k^i - \frac{1}{2} (\lambda_k^{i'} + \lambda_k^i) \langle \chi_{i'} | f_k | \chi_i \rangle] \}, \tag{2.8b}$$

where

$$F_{i',i}^{\mathbf{n}} \equiv F_{i'\mathbf{n}',i\mathbf{n}}.$$

We will discuss later how the off-diagonal matrix elements in the bath can be included perturbatively to obtain an ESH to higher order, but the present discussion will deal with the zeroth approximation, Eq. (2.8).

By neglecting off-diagonal matrix elements in the bath quantum numbers, the only remaining step is to diagonalize the ESH, Eq. (2.8), whose dimension is the number of χ_i basis functions. It should be emphasized, though, that the effect of the coupling between system and bath has *not* been neglected by this approximation because the coupling functions $f_k(s)$ enter via the quantities $\lambda_k^i \sim \langle \chi_i | f_k | \chi_i \rangle$; these parameters enter the ESH most importantly via the Franck-Condon factors in Eq. (2.8). For the ground state of the bath, **n**=**0**, for example, the Franck-Condon factor is

$$F_{i',i}^{0} = \exp\left[-\sum_k \frac{m\omega_k}{4\hbar} (\lambda_k^i - \lambda_k^{i'})^2 \right] \tag{2.9}$$

which shows that the coupling functions $f_k(s)$ enter the ESH *nonlinearly*.

Another obvious, but important feature of the ESH of Eq. (2.8) is that a linear transformation of the basis χ_i,

$$\chi_i \rightarrow \sum_j \chi_j U_{j,i}, \tag{2.10a}$$

does *not* lead to a unitary transformation of the Hamiltonian matrix; i.e., with Eq. (2.10a) one does *not* have

$$H^{\mathbf{n}}_{i',i} \rightarrow \sum_{j,j'} U^{\dagger}_{i',j'} H^{\mathbf{n}}_{j',j} U_{j,i}. \tag{2.10b}$$

This is because the ESH involves the basis functions χ_i via the parameters λ^i_k [Eq. (2.5b)] in a nonlinear fashion. The eigenvalues of the ESH are thus not invariant to a linear transformation of the $\{\chi_i\}$ basis, and this raises the question of which kind of basis $\{\chi_i\}$ gives the best approximation to the true eigenvalues of the complete system-bath Hamiltonian.

It is our intuitive feeling that the shifted oscillator basis of Eq. (2.5) will do the best job of describing the effect of the bath on the zeroth order effective system Hamiltonian Eq. (2.9), if the $\{\chi_i\}$ basis is chosen to be one that is *localized* in coordinate space. The floating Gaussian basis,

$$\chi_i(s) = (\alpha/\pi)^{1/4} \exp[-\alpha(s-s_i)^2/2] \tag{2.11}$$

over some grid of s_i values (see Fig. 2-1), as used recently by Hamilton and Light,[2.10] is an example of what we mean by a localized basis. In contrast, the eigenfunctions of the potential $V_0(s)$, which one might have guessed to be the best $\chi_i(s)$ basis, will typically be delocalized, and in our view the shifted oscillator basis then does not do as good as a job of describing the effect of the bath in the zeroth order ESH.

To illustrate the validity of this point of view we consider the two-state approximation for a symmetric double well potential $V_0(s)$; cf. Fig. 2-2. With the specific choice

$$f_k(s) = c_k s, \tag{2.12}$$

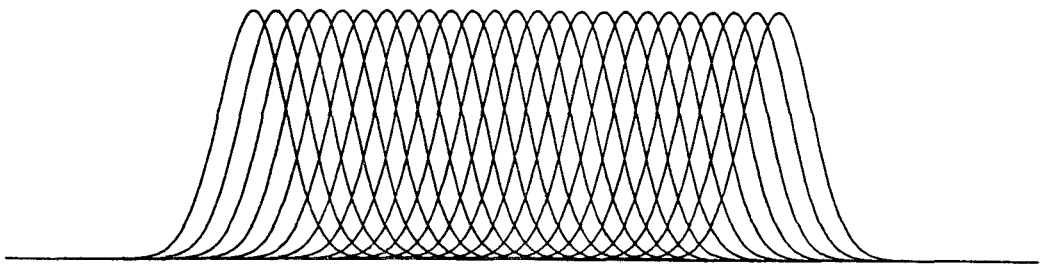

Fig. 2-1
The floating Gaussian basis set [cf. Eq. (2.11)].

this becomes the model considered by Harris and Silbey,[2.11] and a number of others.[2.4] The phenomenon to be described is the effect of the coupling, Eq. (2.12), on the tunneling splitting of the two lowest vibration levels. In the two-state approximation, and with the zeroth order ESH of Eq. (2.9) (with **n=0**), this splitting is given by the usual expression

$$\Delta E = [(H^0_{22}-H^0_{11})^2 + 4(H^0_{12})^2]^{1/2}. \tag{2.13}$$

With the localized basis, Eq. (2.11) with $\chi_1(s)$ located at $s_1=-a$ and $\chi_2(s)$ at $s_2=+a$, it is quite straightforward to show that Eq. (2.13) gives

$$\Delta E = \Delta E_0 \, F^0_{1,2}, \tag{2.14}$$

where $\Delta E_0=2\langle\chi_1|H_s|\chi_2\rangle$ is the splitting that would result if there were no coupling to the bath ($c_k=0$), the Franck-Condon factor is

$$F^0_{1,2} = \exp\left[-a^2\sum_k \frac{c_k^2}{\hbar m \omega_k^3}\right], \tag{2.15}$$

and nonorthogonality has been neglected. This is essentially the correct result, as obtained by other workers;[2.4,2.11] the Franck-Condon factor "renormalizes" the tunneling integral.

If, on the other hand, one chooses the two-state basis to be the delocalized functions $\chi_g(s)$ and $\chi_u(s)$ [which are better approximations to the eigenfunctions of the potential $V_0(s)$],

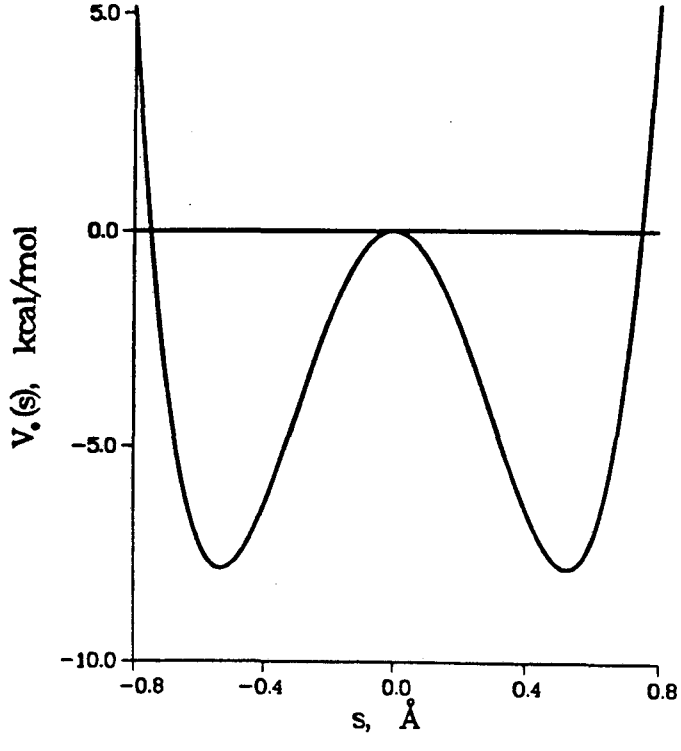

Fig. 2-2
The double well potential $V_0(s)$.

$$\chi_g(s) = \frac{1}{\sqrt{2}}[\chi_1(s)+\chi_2(s)], \tag{2.16a}$$

$$\chi_u(s) = \frac{1}{\sqrt{2}}[\chi_1(s)-\chi_2(s)], \tag{2.16b}$$

then one can easily show that Eq. (2.15) gives

$$\Delta E = \Delta E_0; \tag{2.17}$$

i.e., in this case the zeroth order ESH shows no effect of the coupling on the tunneling splitting, which is incorrect.

This example illustrates very dramatically that the eigenvalues of the zeroth order effective system Hamiltonian, Eq. (2.9), are not invariant to a linear transformation of the $\{\chi_i\}$ basis, and furthermore that the effect of coupling to the bath is best described by the zeroth order ESH if the $\{\chi_i\}$ basis is chosen to be localized. Thus, one should not choose the basis $\{\chi_i\}$ to try to diagonalize the potential $V_0(s)$, for the zeroth order ESH then does not do a good job of incorporating the effect of coupling to the bath. By choosing a localized basis the effective system Hamiltonian matrix $H^{\mathbf{n}}_{i'i}$ is very nondiagonal, but the effect of coupling to the bath is described well. One then diagonalizes $H^{\mathbf{n}}_{i'i}$.

The situation is somewhat reminiscent of the path integral methodology.[2.2–2.4] According to the latter, one makes progress by doing the path integral over the harmonic bath first, and afterwards solving the quantum mechanics (i.e., doing the path integral) for the system degree of freedom. The analogy with the present basis set methodology is that one does not choose the basis $\{\chi_i\}$ to try to diagonalize the s degree of freedom first, but rather chooses it so that when $\mathbf{n}\neq\mathbf{n}'$ matrix elements are neglected the effect of coupling to the bath is described well by the zeroth order ESH. With this choice of the $\{\chi_i\}$ basis, the effective system Hamiltonian matrix $H^{\mathbf{n}}_{i'i}$ is then diagonalized.

3. Application of the shifted oscillator basis: a numerical example

To test the above ideas more fully, we have carried out numerical calculations for the model discussed in Section 2, i.e., tunneling splitting in a symmetric double well potential [see also Ref. 2.17]. The specific form of the potential is

$$V_0(s) = -\frac{1}{2}a_0 s^2 + \frac{1}{4}c_0 s^4, \tag{2.18}$$

with the constants chosen so that the barrier height is 7.8 kcal/mol and the minima are located at $s = \pm 0.53$Å; the mass is chosen to be that of a hydrogen atom. These values correspond roughly to the double-well potential for H-atom transfer in malonaldehyde:

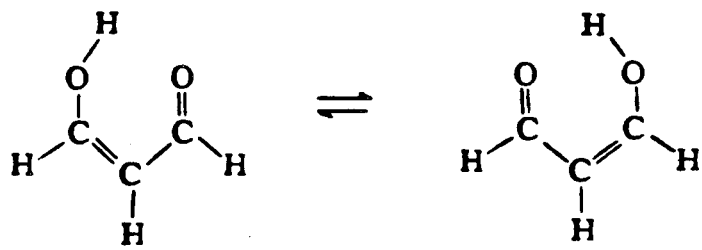

(2.19)

that we have treated earlier by other means.[2.12]

We considered two types of coupling: (i) Linear coupling, i.e., $f_k(s) = c_k s$, which breaks the even symmetry of the double-well potential (one may think of such a coupling as applying in the case of malonaldehyde to a C-O stretch), and (ii) quadratic coupling, i.e., $f_k(s) = c_k s^2$, which preserves the symmetry. (The O-O wag in malonaldehyde is an example of this type of mode).

As the coupling is turned on, the two wells move away from one another and their depth increases, i.e., the height of the barrier increases. As a consequence, the tunneling splitting drops off very rapidly as a function of the coupling strength. Furthermore, the potential shows a singularity (i.e., an infinitely deep well) above some value of the coupling constant in the case of the quadratic coupling, and therefore becomes unphysical. For these reasons, we have incorporated the term

$$\sum_k \frac{[f_k(s)]^2}{2m\omega_k^2} \tag{2.20}$$

in the potential.[2.13] The addition of this term guarantees that the height of the barrier remains constant with increasing coupling constant. The only effect of the coupling is then to change the shape of the double well, i.e., to shift the location of the minima. Contour plots of the double well potential surface coupled to one oscillator are shown in Figs. 2-3(a), 2-3(b) and 2-3(c) for the cases of no coupling, linear coupling, and quadratic coupling, respectively.

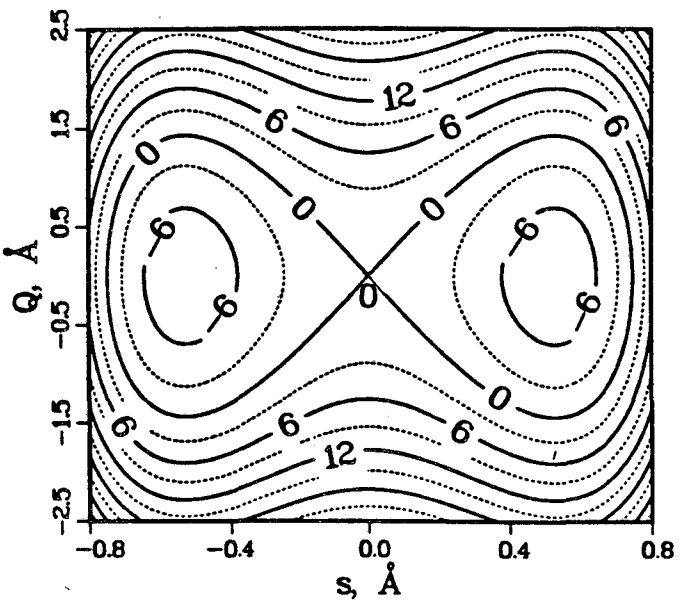

Fig. 2-3(a)

Contour plot of the uncoupled potential surface

$$V_0(s) + \frac{1}{2}m\omega^2 Q^2$$

for ω=298 cm^{-1}. The numbers labeling the curves indicate the height of the potential surface in kcal/mol.

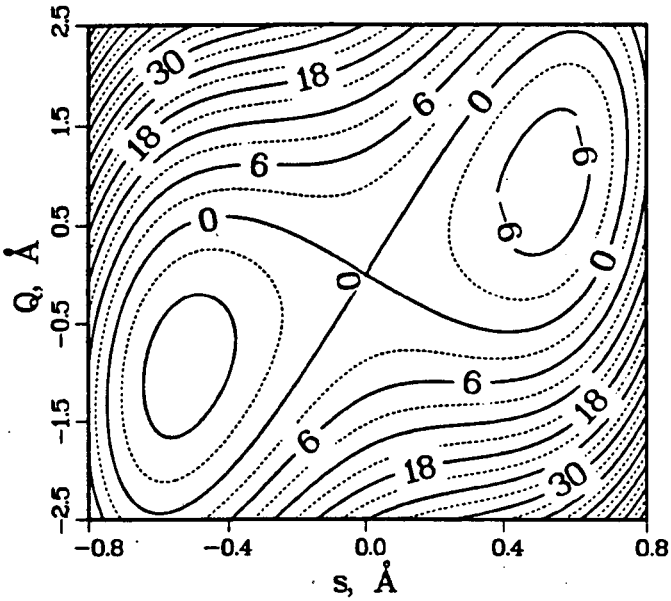

(b)

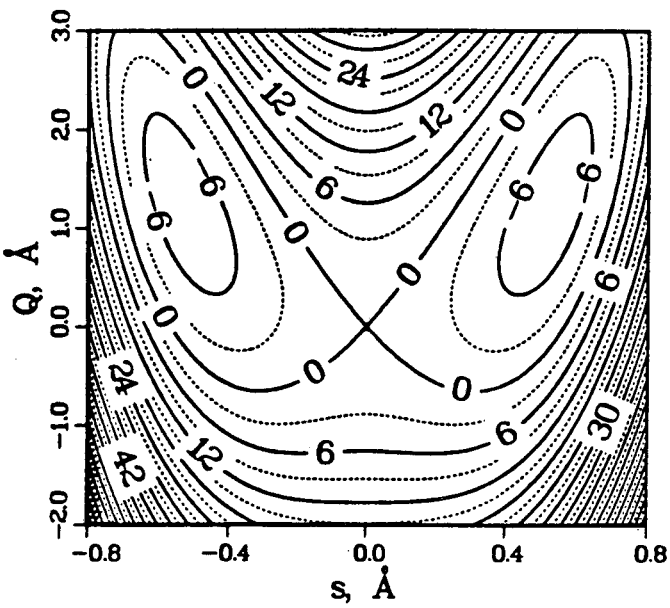

(c)

Fig. 2-3(b),(c)

Contour plot of the potential surface

$$V_0(s) + \frac{1}{2}m\omega^2[Q - f(s)/m\omega^2]^2$$

with ω=298 cm^{-1}. (b) Linear coupling, $f(s)=cs$, with c=0.093 mdyn/Å. (c) Quadratic coupling, $f(s)=cs^2$, with c=0.24 mdyn/Å^2. The numbers labeling the curves indicate the height of the potential surface in kcal/mol.

Only one oscillator is used for these calculations, so in addition to diagonalizing the zeroth order effective system Hamiltonian, Eq. (2.9), it is possible to diagonalize the complete system-bath Hamiltonian, Eq. (2.6), to obtain the exact result. To illustrate the applicability of the method, we considered two extreme cases: a fast ($\omega \approx 3000$ cm^{-1}) and a slow ($\omega \approx 300$ cm^{-1}) bath.

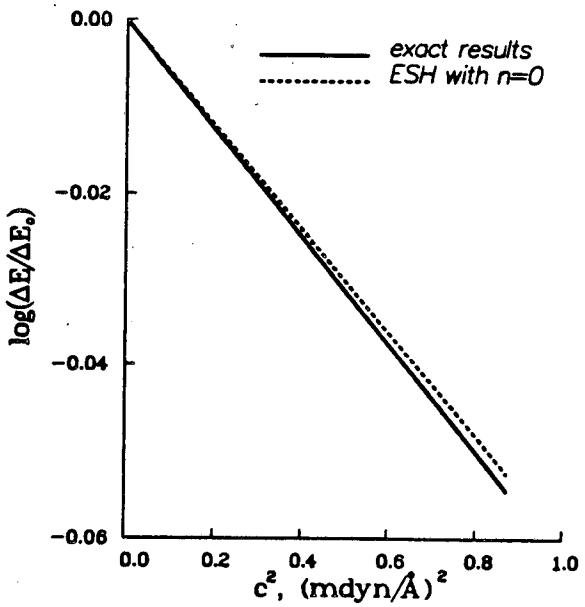

Fig. 2-4

Tunneling splitting for the lowest doublet in the case of fast Q motion (ω=2980 cm^{-1}) vs. the square of the coupling constant c for linear coupling. The results with the ESH, n=0, have been optimized variationally. ΔE_0 is the tunneling splitting at c=0.

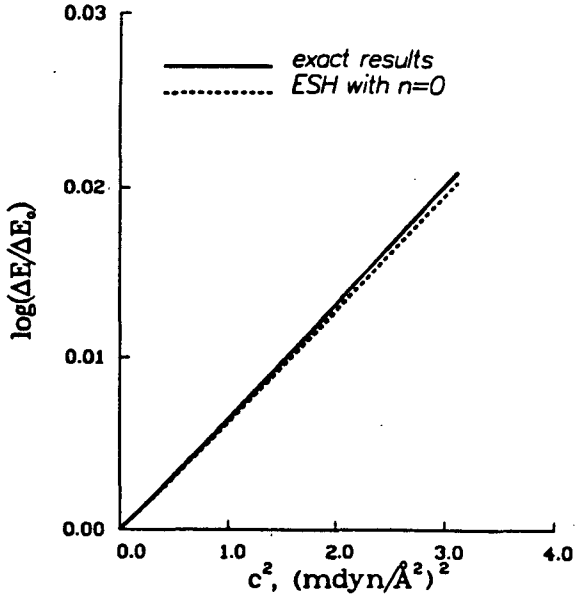

Fig. 2-5

Tunneling splitting for the lowest doublet in the case of fast Q motion (ω=2980 cm^{-1}) vs. the square of the coupling constant c for quadratic coupling. The results with the ESH, n=0, have been optimized variationally. ΔE_0 is the tunneling splitting at c=0.

The case of the fast harmonic bath is very easy to deal with, as one would expect: The potential along the Q coordinate rises very steeply and the spacing between the one dimensional eigenvalues is large. The ESH with n=0 would then be very efficient in describing the lowest doublet of the double well, and indeed this is the case. The exact result is already obtained by including the n=1 excited state of the Q oscillator. Figures 2-4 and 2-5 show the tunneling splitting, referenced to the

value with no coupling, as a function of the coupling constant c. The linearity of the curves in Fig. 2-4 (linear coupling) is an illustration of the approximate result given by Eq. (2.15), and the decrease of the splitting is a consequence of the increase (with respect to the uncoupled case) in the distance between the two minima. The slight increase of the tunneling splitting in Fig. 2-5 is a result of the higher curvature of the wells, which shifts the eigenvalues higher up with respect to the barrier.

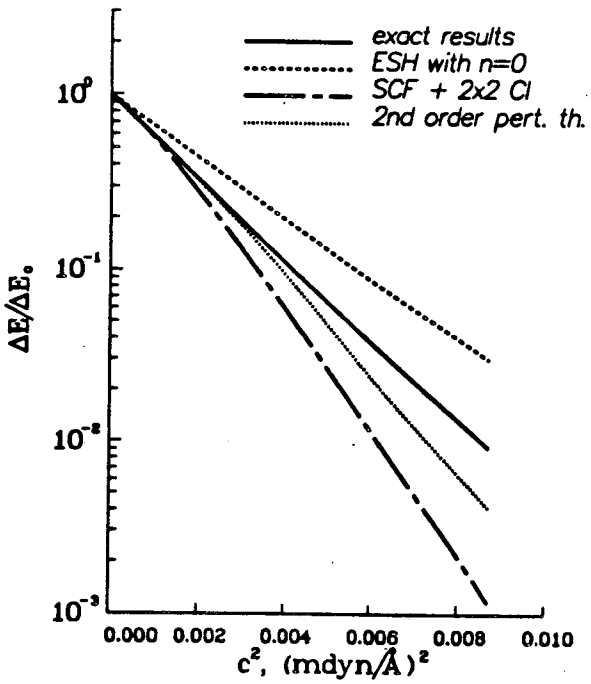

Fig. 2-6

Tunneling splitting for the lowest doublet in the case of slow Q motion (ω=298 cm^{-1}) vs. the square of the coupling constant c for linear coupling. The results with the ESH, n=0, have been optimized variationally. ΔE_0 is the tunneling splitting at c=0. Note the much faster damping of the tunneling splittings compared to the high frequency case of Fig. 2-3.

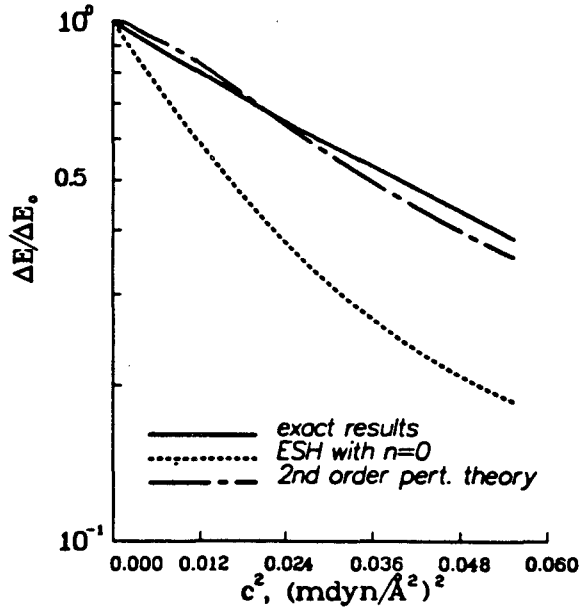

Fig. 2-7

Tunneling splitting for the lowest doublet in the case of slow Q motion (ω=298 cm^{-1}) vs. the square of the coupling constant c for quadratic coupling. The results with the ESH, n=0, have been optimized variationally. ΔE_0 is the tunneling splitting at c=0.

The case of the low frequency bath, on the other hand, is considerably more challenging because the Q eigenstates are now closely packed and mix strongly. As many as five excited states were required for the tunneling splittings to converge to two significant figures at large couplings. The damping of the splitting is much greater here, since a much larger Q amplitude is involved with significant probability within the broader harmonic potential. The results from the ESH with n=0 are not as

good as in the case of fast Q motion. They can be optimized by varying the width of the Gaussians, a nonlinear parameter. The optimum width is larger here than in the high frequency case, as expected intuitively.

The optimized zeroth order version of this calculation is correct to within a factor of 4, even when the coupling is so strong as to have altered the splitting by two orders of magnitude (cf. Fig 2-6). This is quite encouraging, particularly so when one notes that if the zeroth order Hamiltonian, Eq. (2.8), were used without the oscillator basis being shifted, the splitting would be independent of the coupling. Thus, the shifted oscillator basis, even at the zeroth order level, does a reasonably good job of describing the effect of coupling to the bath on the system.

Furthermore, it is relatively simple to go beyond the zeroth level of the theory and include off-diagonal coupling in the ESH, without much more computational effort. The methodology for this is known variably as Van Vleck perturbation theory,[2.14] Löwdin partitioning theory,[2.15] or the Feshbach optical potential [2.16] (in scattering theory). For the present situation, this gives the effective system Hamiltonian matrix, through second order in the off-diagonal bath coupling, as

$$H^{\mathrm{eff}}_{i'',i} = H^{\mathbf{n}}_{i'',i} + \sum_{\mathbf{n}'\neq\mathbf{n}} \sum_{i''',i'''} H_{i''\mathbf{n},i'''\mathbf{n}'} \left(E<\chi_{i''}|\chi_{i'''}> - H^{\mathbf{n}'}_{i''',i'''}\right)^{-1} H_{i'''\mathbf{n}',i\mathbf{n}}. \qquad (2.21)$$

The first term of Eq. (2.20) is the zeroth order ESH matrix considered so far, and the second term the approximate (second order perturbation theory) contribution from nondiagonal coupling ($\mathbf{n}'\neq\mathbf{n}$) in the bath. [The notation $(M_{i'',i'''})^{-1}$ is shorthand for the (i'',i''') element of the inverse of the matrix $(M_{i'',i'''})$.]

The results of the application of this method are very satisfactory. In the high frequency case, the splittings obtained this way are essentially indistinguishable from the exact ones. The second order low frequency results, although still different from the exact ones, nevertheless represent an appreciable improvement over the zeroth order ESH results, as is obvious from Figures 2-6 and 2-7. It is worth emphasizing that this approximation is particularly good, especially for low couplings, and is easy

to implement, because it does not increase the size of the matrix to be diagonalized. Of course, since no variational principle holds here, there is no criterion for the quality of the results and optimization is not possible.

4. Vibrationally adiabatic basis and SCF calculation

As mentioned above, the idea underlying the construction of the shifted oscillator basis is that the matrix element of the coupling function $f_k(s)$ with respect to the s-basis function χ_i represents the average force felt as $s=s_i$. If the Gaussians are peaked around s_i, as is the case in the high frequency limit, then

$$<\chi_i|f_k|\chi_i> \approx f_k(s_i),$$

which represents the instantaneous force at s_i. Since the basis functions $\chi_i(s)$ are localized to the regions $s\approx s_i$, the replacement of $f_k(s_i)$ by $f_k(s)$ would not make a significant difference. This suggests the vibrationally adiabatic basis for the coupled oscillators,

$$\psi_{in}(s,\mathbf{Q}) = \chi_i(s)\prod_k \phi_{n_k}(Q_k - \frac{f_k(s)}{m\omega_k^2}). \tag{2.22}$$

The matrix elements of the Hamiltonian with respect to this basis do not involve any Franck-Condon factors and the eigenvalues are thus invariant to any linear transformation of the basis functions. The vibrationally adiabatic basis has been tested and found to be very similar to the basis discussed above in the limit of high frequencies.

On the other hand, the more demanding case is that with the low frequency bath, as shown above. One may suggest adopting an SCF scheme, as motivated in Section 2, i.e., average over the fast s motion and solve iteratively. We tested this idea vs. the ones mentioned above, and the results are shown in Fig. 2-6.

In order to apply the analytic SCF scheme, we expand the s eigenfunctions in terms of Gaussian basis functions:

$$X_i(s) = \sum_j C_{ij}\chi_j(s), \tag{2.23}$$

where the coefficients c_{ij} are to be determined. The matrix elements of the effective SCF Hamiltonian are

$$H_{i',i}^{\mathrm{eff,SCF}} = \langle\chi_{i'}|\mathrm{H_s}|\chi_i\rangle - \sum_k \left[\frac{\langle\chi_{i'}|f_k|\chi_i\rangle}{m\omega_k^2} \sum_{j,j'} C_{i'j'}C_{ij}\langle\chi_{j'}|f_k|\chi_j\rangle + \frac{\langle\chi_{i'}|f_k^2|\chi_i\rangle}{2m\omega_k^2} \right]. \tag{2.24}$$

For the SCF scheme to succeed in the case of linear coupling, the initial coefficients must not represent a symmetric function, otherwise the odd symmetry of the coupling force would give $\langle X_i|f_k|X_i\rangle=0$. One iteration is enough to break the even symmetry of the uncoupled problem, so that the eigenfunctions after each iteration are asymmetric. Starting from a left (or right) localized function, we obtain a left (or right) localized solution. The method converges within 10-20 iterations, and the SCF limit is reached with approximately 25 Gaussians. The left and the right solution constitute a pair of degenerate eigenfunctions at the SCF level, and one must perform a 2×2 configuration interaction (CI) calculation to obtain tunneling splittings. Since the calculation of the splittings for the lowest doublet involves only the ground state SCF solution, which is the one that was optimized, the results are expected to be good. Figure 2-6 shows that the SCF splittings are somewhat worse than the zeroth order ESH splittings at high values of the coupling, but they are substantially better at low couplings. However, the results obtained by second order perturbation theory are by far the best ones obtained within this level of computational effort, so that the SCF scheme does not constitute any improvement.

On the other hand, the SCF results are less promising in the case of quadratic coupling, where their disagreement from the exact calculations is large. This is to be expected, since both of the g and u solutions are involved in the calculation of the tunneling splitting, while only the lowest (g) wavefunction has been optimized.

5. Concluding remarks

It is seen that the shifted oscillator basis presented in Section 2, even in its zeroth order version, does a very good job of describing the effect on a reaction coordinate of coupling to a harmonic bath, even when the effect of the coupling is quite large. (For this to be true, however, it is necessary that a localized basis set be used for the reaction coordinate). The numerical examples treated in this paper utilized only one mode for the harmonic bath - so as to be able to compare with exact values - but it should be clear that the methods of Sections 2 and 3 are readily applicable with little additional effort to the case of many harmonic bath modes. Application to a three-atom model incorporating the basic features of *H* atom transfer in malonaldehyde further demonstrated the efficiency and success of the method. We believe that the shifted oscillator basis should find extensive use in studying the dynamics of isomerization reactions in polyatomic molecules.

References

2.1 For reviews see

(a) W. H. Miller, *J. Phys. Chem.* **87**, 3811 (1983);

(b) W. H. Miller, in *The Theory of Chemical Reaction Dynamics*, edited by D. C. Clary (Reidel, Boston, 1986), pp. 27-45.

2.2 (a) R. P. Feynman, *Rev. Mod. Phys.* **20**, 367 (1948);

(b) R. P. Feynman and A. R. Hibbs, *Quantum Mechanics and Path Integrals*, McGraw-Hill, New York, 1965.

2.3 (a) W. H. Miller, S. D. Schwartz, and J. W. Tromp, *J. Chem. Phys.* **79**, 4889 (1983);

(b) R. Jaquet and W. H. Miller, *J. Phys. Chem.* **89**, 3139 (1984);

(c) K. Yamashita and W. H. Miller, *J. Chem. Phys.* **82**, 5475 (1985).

2.4 (a) A. O. Caldeira and A. J. Leggett, *Ann. Phys.* (N.Y.) 149, 374 (1983);

(b) S. Chakravarty and A. J. Leggett, *Phys. Rev. Lett.* **52**, 5 (1984);

(c) H. Grabert and U. Weiss, *Phys. Rev. Lett.* **54**, 1605 (1985);

(d) A. T. Dorsey, M. P. A. Fisher, and M. S. Wartak, *Phys. Rev.* A **33**, 1117 (1986).

2.5 (a) D. Thirumalai and B. J. Berne, *J. Chem. Phys.* **79**, 5029 (1983); **81**, 2512 (1984);

(b) D. Thirumalai, E. J. Bruskin, and B. J. Berne, *J. Chem. Phys.* **79**, 5063 (1983);

(c) D. Thirumalai and B. J. Berne, *Ann. Rev. Phys. Chem.* **37**, 401 (1986).

2.6 (a) J. D. Doll, *J. Chem. Phys.* **81**, 3536 (1984);

(b) D. L. Freeman, R. D. Coalson, and J. D. Doll, *J. Stat. Phys.* **43**, 931 (1986).

2.7 (a) E. C. Behrman, G. A. Jongeward, and P. G. Wolynes, *J. Chem. Phys.* **79**, 6277 (1983);

(b) E. C. Behrman and P. G. Wolynes, *J. Chem. Phys.* **83**, 5863 (1985).

(c) R. W. Hall and P. G. Wolynes, *J. Stat. Phys.* **43**, 935 (1986).

2.8 (a) D. Chandler and P. G. Wolynes, *J. Chem. Phys.* 74, 4078 (1981);

(b) M. Sprik, M. L. Klein, and D. Chandler, *J. Chem. Phys.* **83**, 3042 (1985);

(c) M. Sprik, R. W. Impey, and M. L. Klein, *J. Chem. Phys.* **83**, 5802 (1985);

(d) C. D. Jonah, C. Romeo, and A. Rahman, *Chem. Phys. Lett.* **123**, 209 (1986);

(e) R. J. Rossky, J. Schnitker, and R. A. Kuharski, *J. Stat. Phys.* **43**, 949 (1986);

(f) A. Wallquist, D. Thirumalai and B. J. Berne, *J. Chem. Phys.* **85**, 1583 (1986).

2.9 J. W. Tromp and W. H. Miller, *J. Phys. Chem.* **90**, 3482 (1986).

2.10 I. P. Hamilton and J. C. Light, *J. Chem. Phys.* 84, 306 (1986).

2.11 R. Silbey and R. A. Harris, *J. Chem. Phys.* 80, 2615 (1984).

2.12 (a) J. Bicerano, J. F. Schaefer, and W. H. Miller, *J. Am. Chem. Soc.* 105, 2550 (1983);
(b) T. Carrington, Jr., and W. H. Miller, *J. Chem. Phys.* 84, 4364 (1986).

2.13 This is also done by most of the authors in Ref. 2.4.

2.14 See, for example, E. C. Kemble, *The Fundamental Principles of Quantum Mechanics* (Dover, New York, 1958), pp. 394-396.

2.15 P. O. Lowdin, *J. Math. Phys.* 3, 969 (1962).

2.16 (a) H. Feshbach, *Ann. Phys.* (N.Y.) 5, 357 (1958);
(b) H. Feshbach, *Ann. Phys.* (N.Y.) 19, 287 (1962).

2.17 The methods and numerical examples of this Chapter appeared previously in the following article:
N. Makri and W. H. Miller, *J. Chem. Phys.* 86, 1451 (1987).

III. The TDSCF Approximation

1. Introduction

As discussed in Chapter II, dynamical processes in polyatomic molecules can often be described as a "system" of one or two "interesting" degrees of freedom that characterize the process of interest, plus a "bath" of the many remaining degrees of freedom which, though coupled to the "system", do not play a principal role. Very often the bath is taken to be a set of harmonic modes (with perhaps variable frequencies, functions of the system coordinates). An example of such a model is the reaction path (or surface) Hamiltonian, [3.1] where the "system" is the reaction coordinate (i.e. the distance along the minimum energy reaction path through the transition state), and the "bath" are local harmonic vibrations orthogonal to the reaction path. Since it is not possible in general to deal accurately with more than three or so degrees of freedom by brute force quantum mechanical methods, all strategies for treating the dynamics of "system-bath" models involve eliminating the "bath" degrees of freedom, after taking account of their effect on the "system" as best as possible, and then dealing with the few degrees of freedom of the system by straightforward means.

In Chapter II we presented a simple basis set method capable of providing a good description of the effect of bath coupling on tunneling in a symmetric double well potential (the system). The key to the accuracy of this model is that one uses a *localized* basis set for the system, and a basis set for the harmonic bath that has its equilibrium position shifted to incorporate the average effect of the coupling.[3.2] One needs only to diagonalize a Hamiltonian matrix whose dimension is that of the number of basis functions of the system. The principal limitation of this model – at least in its zeroth order version which is computationally the simplest – is that it is not able to describe energy transfer between system and bath, a feature that would

clearly be important in very asymmetric double well problems, e.g. exothermic isomerizations.

The purpose of this Chapter [3.12] is to explore another class of approximate models for treating system-bath dynamics, namely the time-dependent self consistent field (TDSCF) approximation.[3.3–3.6] Its potential advantage over the zeroth order basis set method noted above is that it can describe energy transfer between system and bath. Though a fully quantum mechanical method, the TDSCF approach has a very semiclassical character to it, especially with regard to the harmonic bath. Since several different groups [3.7–3.9] are currently advocating these "quantum system" plus "classical bath" approaches, it is of interest to see how useful they are for describing the effect of bath coupling on isomerizations.

We first consider the standard (single configuration) TDSCF scheme, noting that for this problem [3.10] it is identical to the semiclassical Ehrenfest model, [3.11] i.e. "quantum system plus classical bath". Unfortunately, this model is totally inadequate for our test problem, a double well potential coupled to a harmonic bath. The essential difficulty, which is inherent to this approximation, is that the bath responds only to the *average* force exerted on it by the system, rather than a force that is different for different values of the system coordinate.

We have therefore generalized the TDSCF procedure to a *multi-configuration* treatment.[3.12] Specifically, the wavefunction for the double well system is divided into two components, with a different bath wavefunction for each component. The time-dependence of all the wavefunctions is determined from the time-dependent variational principle.[3.13] This multi-configuration TDSCF (MC-TDSCF) model is seen to provide a much better description of the effect of coupling on tunneling in the double well system.

Section 2 gives the formal development of the single and multi- (two-) configuration treatment of the system-bath problem, and results of application to a

symmetric double well system coupled to a harmonic bath are presented is Section 3. Discussion of these results and some concluding remarks appear in Section 4.

2. The TDSCF equations for the system-bath model

The model under consideration is described by the Hamiltonian

$$H\ (p_s,\ s\ ,\ \mathbf{P},\ \mathbf{Q}) = \frac{p_s^2}{2m} + V_0(s) + \sum_k [\frac{P_k^2}{2m} + \frac{1}{2} m\,\omega_k^2 Q_k^2] - \sum_k Q_k\ f_k(s)$$

$$= H_s + \sum_k H_{Q_k} - \sum_k Q_k\ f_k(s) \tag{3.1}$$

Here s is the reaction coordinate and $Q_1, Q_2, ..., Q_N$ are the harmonic degrees of freedom that constitute the bath, which is linearly coupled to the system. For the specific examples treated in this Chapter $V_0(s)$ is a double well potential function corresponding roughly to motion of a hydrogen atom with a barrier of 6 kcal/mol.

a) Single configuration TDSCF

Consider first the standard TDSCF scheme, with the wavefunction represented by a single Hartree product:

$$\Psi(s\ ,\ \mathbf{Q};\ t) = \chi(s;\ t) \prod_k \phi_{n_k}(Q_k;\ t) \tag{3.2}$$

Substitution of Eq. (3.2) into the time-dependent Schrödinger equation

$$H\Psi = i\hbar \frac{\partial}{\partial t}\Psi \tag{3.3}$$

and projection onto $\prod_k <\phi_{n_k}|$ gives [3.14] the TDSCF equation for $\chi(s;\ t)$:

$$i\hbar\ \frac{\partial}{\partial t}\chi(s;\ t) = [\ H_s - \sum_k \frac{<\phi_{n_k}|Q_k|\phi_{n_k}>}{<\phi_{n_k}|\phi_{n_k}>}\ f_k(s)$$

$$+ \sum_k (\frac{<\phi_{n_k}|H_{Q_k}|\phi_{n_k}>}{<\phi_{n_k}|\phi_{n_k}>} - i\hbar \frac{<\phi_{n_k}|\dot{\phi}_{n_k}>}{<\phi_{n_k}|\phi_{n_k}>})]\ \chi(s;\ t) \tag{3.4a}$$

while projection onto $\langle\chi| \prod_{k' \neq k} \langle\phi_{n_{k'}}|$ gives the TDSCF equation for ϕ_{n_k}:

$$i\hbar \frac{\partial}{\partial t}\phi_{n_k}(Q_k; t) = [\, H_{Q_k} - favQ_k + Hs - i\hbar \frac{\langle\chi|\dot{\chi}\rangle}{\langle\chi|\chi\rangle}$$

$$- \sum_{k' \neq k} \frac{\langle\chi|f_{k'}|\chi\rangle}{\langle\chi|\chi\rangle} \frac{\langle\phi_{n_{k'}}|Q_{k'}|\phi_{n_{k'}}\rangle}{\langle\phi_{n_{k'}}|\phi_{n_{k'}}\rangle} + \sum_{k' \neq k} \frac{\langle\phi_{n_{k'}}|H_{Q_{k'}}|\phi_{n_{k'}}\rangle}{\langle\phi_{n_{k'}}|\phi_{n_{k'}}\rangle}$$

$$- i\hbar \sum_{k' \neq k} \frac{\langle\phi_{n_{k'}}|\dot{\phi}_{n_{k'}}\rangle}{\langle\phi_{n_{k'}}|\phi_{n_{k'}}\rangle} \,]\, \phi_{n_k}(Q_k; t) \qquad (3.4b)$$

Equations (3.4a) and (3.4b) can be simplified by defining the functions X and Φ_{n_k} that include appropriate phase factors:

$$X(s; t) = \chi(s; t)\, e^{\frac{i}{\hbar}\int_0^t dt' \,[\sum_k hQ - i\hbar \sum_k \frac{\langle\phi_{n_k}|\dot{\phi}_{n_k}\rangle}{\langle\phi_{n_k}|\phi_{n_k}\rangle}]} \qquad (3.5a)$$

$$\Phi_{n_k}(Q_k; t) = \phi_{n_k}(Q_k; t)\, \exp\{\frac{i}{\hbar}\int_0^t dt' [\, Hs + \sum_{k' \neq k} \frac{\langle\phi_{n_{k'}}|H_{Q_{k'}}|\phi_{n_{k'}}\rangle}{\langle\phi_{n_{k'}}|\phi_{n_{k'}}\rangle}$$

$$- \sum_{k' \neq k} \frac{\langle\phi_{n_{k'}}|Q_{k'}|\phi_{n_{k'}}\rangle}{\langle\phi_{n_{k'}}|\phi_{n_{k'}}\rangle} \frac{\langle\chi|f_{k'}|\chi\rangle}{\langle\chi|\chi\rangle}$$

$$- i\hbar \frac{\langle\chi|\dot{\chi}\rangle}{\langle\chi|\chi\rangle} - i\hbar \sum_{k' \neq k} \frac{\langle\phi_{n_{k'}}|\dot{\phi}_{n_{k'}}\rangle}{\langle\phi_{n_{k'}}|\phi_{n_{k'}}\rangle}]\} \qquad (3.5b)$$

Then the equations to be solved become

$$i\hbar \frac{\partial}{\partial t}X(s; t) = [H_s - \sum_k \frac{\langle\Phi_{n_k}(t)|Q_k|\Phi_{n_k}(t)\rangle}{\langle\Phi_{n_k}(t)|\Phi_{n_k}(t)\rangle} f_k(s)]\, X(s; t) \qquad (3.6a)$$

$$i\hbar \frac{\partial}{\partial t}\Phi_{n_k}(Q_k; t) = [H_{Q_k} - \frac{\langle X(t)|f_k|X(t)\rangle}{\langle X(t)|X(t)\rangle} Q_k]\, \Phi_{n_k}(Q_k; t). \qquad (3.6b)$$

The TDSCF scheme proceeds by solving the N+1 differential equations, one for each mode. Thus the time evolution of each mode is governed by a time-dependent potential which is the average of the full interaction potential over all other modes.

Notice that the TDSCF equations are not linear and therefore the rate depends on the initial conditions.

In the present application, where the bath consists of only harmonic degrees of freedom linearly coupled to the system, one can actually solve Equations (3.6b) analytically; this is because they have the form of uncoupled, linearly forced harmonic oscillators. Specifically, the time-dependent bath wavefunctions $\Phi_{n_k}(Q_k; t)$, the solution of Eq. (3.6b), are given by

$$\Phi_{n_k}(Q_k; t) = \int_{-\infty}^{\infty} dQ_k' \, K(Q_k, Q_k'; t) \, \Phi_{n_k}(Q_k'; 0) \tag{3.7}$$

where K is the Feynman kernel (propagator) [3.15]

$$K(Q_k, Q_k'; t) = \left(\frac{m\omega_k}{2\pi i \hbar \sin\omega_k t}\right)^{1/2} e^{\frac{i}{\hbar} S_k^{Cl}}. \tag{3.8a}$$

In the last equation, S_k^{Cl} is the classical action for the kth oscillator:

$$\begin{aligned} S_k^{Cl} = {} & \frac{m\omega_k}{2\sin\omega_k t} \left[(Q_k^2 + Q_k'^2)\cos\omega_k t - 2Q_k Q_k'\right. \\ & + \frac{2Q_k}{m\omega_k} \int_0^t dt' f_k(t') \sin\omega_k t' + \frac{2Q_k'}{m\omega_k} \int_0^t dt' f_k(t') \sin\omega_k (t-t') \\ & \left. - \frac{2}{m^2\omega_k^2} \int_0^t dt' \int_0^{t'} dt'' \, f_k(t') f_k(t'') \sin\omega_k t'' \sin\omega_k (t-t')\right] \end{aligned} \tag{3.8b}$$

It is then straightforward to show that the expectation value of Q_k that appears in Eq. (3.6a) is given by

$$\begin{aligned} \langle \Phi_{n_k}(t) | Q_k | \Phi_{n_k}(t) \rangle = {} & \langle \Phi_{n_k}(0) | P_k | \Phi_{n_k}(0) \rangle \frac{\sin\omega_k t}{m\omega_k} \\ & + \langle \Phi_{n_k}(0) | Q_k | \Phi_{n_k}(0) \rangle \cos\omega_k t \\ & + \frac{1}{m\omega_k} \int_0^t dt' \sin\omega_k (t-t') \, \frac{\langle X(t') | f_k | X(t') \rangle}{\langle X(t') | X(t') \rangle}. \end{aligned} \tag{3.9}$$

Eq. (3.9) is the same as the classical expression for the position of a forced oscillator at time t, in terms of the initial position $<\Phi_{n_k}(0)|Q_k|\Phi_{n_k}(0)>$ and initial momentum $<\Phi_{n_k}(0)|P_k|\Phi_{n_k}(0)>$.

Thus, the problem reduces to the solution of only one differential equation, namely Eq. (3.6a), which is closed by virtue of Eq. (3.9). This result has been obtained previously,[3.10] where it was emphasized that Eq. (3.6a) plus Eq. (3.9) is essentially the Schrödinger equation analog of the classical generalized Langevin equation; i.e., equations (3.6a) and (3.9) have memory effects [$\dot{X}(t)$ depends on $X(t')$ for $t'<t$] and a "random force" that involves initial conditions of the bath. The full quantum mechanical solution can be easily obtained by expanding $X(s;t)$ in a basis set.

It is easy to show that equations (3.4a) and (3.4b) conserve the norm of the wavefunction for each mode, as well as the average total energy, i.e.,

$$<X(t)|X(t)> = <\Phi_{n_k}(t)|\Phi_{n_k}(t)> = 1$$

and

$$\frac{d}{dt}<\Psi(t)|H|\Psi(t)> = 0.$$

b) Multi-configuration TDSCF

As noted in the Introduction (and *vide infra*), the standard single configuration TDSCF is completely inadequate for describing the effect of the bath on the rate of tunneling between the two local minima of the double well potential $V_0(s)$. This is perhaps to be expected of any such mean field approximation when the coupling between the degrees of freedom is of a very specific nature. The root of the problem can be seen in Eq. (3.6), where the oscillator wavefunction is determined by the *average* force,

$$<X(t)|f_k|X(t)> = \int ds\ X^*(s;t)\, f_k(s)\, X(s;t).$$

If the force $f_k(s)$ varies significantly from the region of one local minimum of $V_0(s)$ to the other, then one intuitively feels that the oscillator should experience these varying forces in a more specific fashion than simply the average. This is true even more so when one is wishing to describe the *rate* of passage from one local minimum to the other.

To this end we consider a two-configuration TDSCF trial wavefunction [3.12] for the present case of a double well reaction coordinate. To simplify the notation, we restrict the description below to the case where the bath consists of only one harmonic mode and drop the subscripts k, but it should be clear that the method should apply in the case of many modes in general, with the number of differential equations being linearly related to the number of modes. The specific form of the wavefunction is thus

$$\Psi(s, Q; t) = \chi_a(s; t)\phi_a(Q; t) + \chi_b(s; t)\phi_b(Q; t), \tag{3.10a}$$

where the subscripts "a" and "b" refer to the two wells of the double well potential $V_0(s)$. The transition state divides the reaction coordinate into two distinct regions that correspond to the two wells. Thus, the wavefunctions of the two configurations in the reaction coordinate can be taken to be orthogonal to one another:

$$\langle\chi_a(t)|\chi_b(t)\rangle = 0. \tag{3.10b}$$

Substitution of Eq. (10a) into the Schrödinger equation, as before, gives the coupled differential equations

$$\begin{aligned} i\hbar\frac{\partial}{\partial t}\chi_a = [H_s - \frac{\langle\phi_a|Q|\phi_a\rangle}{\langle\phi_a|\phi_a\rangle}f(s) + \frac{\langle\phi_a|H_Q|\phi_a\rangle}{\langle\phi_a|\phi_a\rangle} - i\hbar\frac{\langle\phi_a|\dot{\phi}_a\rangle}{\langle\phi_a|\phi_a\rangle}]\,\chi_a \\ + [\frac{\langle\phi_a|\phi_b\rangle}{\langle\phi_a|\phi_a\rangle}H_s - \frac{\langle\phi_a|Q|\phi_b\rangle}{\langle\phi_a|\phi_a\rangle}f(s) + \frac{\langle\phi_a|H_Q|\phi_b\rangle}{\langle\phi_a|\phi_a\rangle} \\ - i\hbar\frac{\langle\phi_a|\dot{\phi}_b\rangle}{\langle\phi_a|\phi_a\rangle}]\,\chi_b - i\hbar\frac{\langle\phi_a|\phi_b\rangle}{\langle\phi_a|\phi_a\rangle}\dot{\chi}_b \end{aligned} \tag{3.11a}$$

$$i\hbar\frac{\partial}{\partial t}\phi_a = [H_Q - \frac{<\chi_a|f|\chi_a>}{<\chi_a|\chi_a>}Q + \frac{<\chi_a|H_s|\chi_a>}{<\chi_a|\chi_a>} - i\hbar\frac{<\chi_a|\dot{\chi}_a>}{<\chi_a|\chi_a>}]\,\phi_a$$

$$+ [\frac{<\chi_a|H_s|\chi_b>}{<\chi_a|\chi_a>} - \frac{<\chi_a|f|\chi_b>}{<\chi_a|\chi_a>}Q]\,\phi_b \tag{3.11b}$$

and similarly for $\dot{\chi}_b$, $\dot{\phi}_b$.

Because of the presense of the $<\phi_a|\dot{\phi}_a>$ term in Eq. (3.11a) and the $<\chi_a|\dot{\chi}_a>$ term in Eq. (3.11b), it is difficult to solve these equations simultaneously. (One would have to evaluate $<\phi_a|\dot{\phi}_a>$ of Eq. (3.11a) using Eq. (3.11b), which contains $<\chi_a|\dot{\chi}_a>$, so that $\frac{\partial}{\partial t}\chi_a$ would be expressed in terms of $<\chi_a|\dot{\chi}_a>$.) This problem can be overcome by introducing appropriate phase factors:

$$X_a(s;t) = \chi_a(s;t)\,e^{i\alpha(t)} \tag{3.12a}$$

$$X_b(s;t) = \chi_b(s;t)\,e^{i\beta(t)} \tag{3.12b}$$

$$\Phi_a(Q;t) = \phi_a(Q;t)\,e^{i\gamma(t)} \tag{3.12c}$$

$$\Phi_b(Q;t) = \phi_b(Q;t)\,e^{i\delta(t)}. \tag{3.12d}$$

It is easily verified that with the choice

$$\gamma(t) = -\alpha(t), \quad \delta(t) = -\beta(t) \tag{3.13}$$

any diagonal coordinate-independent term in Eq. (3.11a) (plus the corresponding equation for $\dot{\chi}_b$), or in Eq. (3.11b) (plus the corresponding equation for $\dot{\phi}_b$), but not in both pairs, can be eliminated. Specifically, by defining

$$\gamma(t) = \frac{1}{\hbar}\int_0^t dt'\,[\frac{<\chi_a|H_s|\chi_a>}{<\chi_a|\chi_a>} - i\hbar\frac{<\chi_a|\dot{\chi}_a>}{<\chi_a|\chi_a>}] \tag{3.14a}$$

$$\delta(t) = \frac{1}{\hbar}\int_0^t dt'\,[\frac{<\chi_b|H_s|\chi_b>}{<\chi_b|\chi_b>} - i\hbar\frac{<\chi_b|\dot{\chi}_b>}{<\chi_b|\chi_b>}] \tag{3.14b}$$

equations (3.11a) and (3.11b) reduce to

$$i\hbar\frac{\partial}{\partial t}X_a = [H_s - \frac{\langle\Phi_a|Q|\Phi_a\rangle}{\langle\Phi_a|\Phi_a\rangle}f(s) + \frac{\langle\Phi_a|H_Q|\Phi_a\rangle}{\langle\Phi_a|\Phi_a\rangle} - i\hbar\frac{\langle\Phi_a|\dot{\Phi}_a\rangle}{\langle\Phi_a|\Phi_a\rangle}]\,X_a$$

$$+ [\frac{\langle\Phi_a|\Phi_b\rangle}{\langle\Phi_a|\Phi_a\rangle}H_s - \frac{\langle\Phi_a|Q|\Phi_b\rangle}{\langle\Phi_a|\Phi_a\rangle}f(s)$$

$$+ \frac{\langle\Phi_a|H_Q|\Phi_b\rangle}{\langle\Phi_a|\Phi_a\rangle} - i\hbar\frac{\langle\Phi_a|\dot{\Phi}_b\rangle}{\langle\Phi_a|\Phi_a\rangle}]\,X_b$$

$$- i\hbar\frac{\langle\Phi_a|\Phi_b\rangle}{\langle\Phi_a|\Phi_a\rangle}\dot{X}_b, \tag{3.15a}$$

$$i\hbar\frac{\partial}{\partial t}\Phi_a = [H_Q - \frac{\langle X_a|f|X_a\rangle}{\langle X_a|X_a\rangle}Q]\,\Phi_a$$

$$+ [\frac{\langle X_a|H_s|X_b\rangle}{\langle X_a|X_a\rangle} - \frac{\langle X_a|f|X_b\rangle}{\langle X_a|X_a\rangle}Q]\Phi_b \tag{3.15b}$$

and similarly for $\dot{X}_b$ and $\dot{\Phi}_b$. Equations (3.15a) and (3.15b) conserve the total energy.

So far, the MC-TDSCF equations, Eq. (3.15), involve no approximations other than the MC-TDSCF *ansatz* for the wavefunction, Eq. (3.10). Unlike the single configuration TDSCF equations, however, here it is not possible to solve Eq. (3.15b) analytically for the oscillator wavefunctions $\Phi_a(Q;t)$ and $\Phi_b(Q;t)$; this is because there are now *two* oscillator wave functions (for each bath mode), rather than just one, and the equations for the two are coupled to each other. For a problem with N bath modes, the complete quantum-mechanical solution of the $2(N+1)$ equations that are involved in this method is still a relatively simple calculation for N not too large, especially if this is compared to a full basis set calculation.

Nevertheless, it would clearly be a considerable simplification if one could solve the equations for the bath modes analytically and thus eliminate them from the problem. This can be done approximately by neglecting the terms in Eq. (3.15b) that couple Φ_a and Φ_b. Thus Eq. (3.15b) is approximated by

$$i\hbar \frac{\partial}{\partial t}\Phi_a = [H_Q - \frac{<X_a|f|X_a>}{<X_a|X_a>} Q]\Phi_a \tag{3.16}$$

which, like Eq. (3.6b), can be solved analytically by using the Feynman kernel; a similar approximate equation holds for $\dot{\Phi}_b$. In the case of zero coupling, Eq. (3.16) is exact. For non-zero coupling, the physical meaning of this approximation, Eq. (3.16), is that the time-dependent force that the bath wavefunction Φ_a experiences is determined by averaging the force $f(s)$ only over the region of well "a", i.e. with respect to the wavefunction $X_a(s;t)$,

$$\frac{<X_a(t)|f|X_a(t)>}{<X_a(t)|X_a(t)>},$$

rather than averaging it over both wells as happens in single configuration TDSCF. Note here that $X_a(s;t)$ is itself not normalized to 1, but rather $<X_a(t)|X_a(t)>$ is the probability that the system is in well "a" at time t.

Therefore, with Eq. (3.16) approximating Eq. (3.15b), Φ_a is given by Equations (3.7) and (3.8), and similarly for Φ_b. It is then possible to evaluate analytically the overlap quantities $<\Phi_a|\Phi_b>$ and $<\Phi_a|Q|\Phi_b>$ that appear in Eq. (3.15a) for $\dot{X}_a$; these expressions are

$$<\Phi_a(t)|\Phi_b(t)>$$

$$= <\Phi_a(Q-q;0)\,|\, e^{\frac{i}{\hbar}Q\int_0^t dt' \,[f_b(t')-f_a(t')]\cos\omega t'} \,|\, \Phi_b(Q;0)>$$

$$\times \exp\{\frac{im\omega}{2\hbar\sin\omega t}\,[\frac{2q}{m\omega}\int_0^t dt'\, f_a(t')\sin\omega(t-t') - q^2\cos\omega t$$

$$- \frac{2}{m^2\omega^2}\int_0^t dt' \int_0^{t'} dt''\, [f_b(t')f_b(t'')$$

$$-f_a(t')f_a(t'')]\,\sin\omega t''\sin\omega(t-t')]\}, \tag{3.17a}$$

and

$$<\Phi_a(t)|Q\,|\Phi_b(t)>$$

$$= \{<\Phi_a(Q-q;\,0)\,|\,P\;e^{\frac{i}{\hbar}Q\int_0^t dt'\,[f_b(t')-f_a(t')]\cos\omega t'}\,|\Phi_b(Q;\,0)>\,\frac{\sin\omega t}{m\omega}$$

$$+\,<\Phi_a(Q-q;\,0)|\,Q\;e^{\frac{i}{\hbar}Q\int_0^t dt'\,[f_b(t')-f_a(t')]\cos\omega t'}\,|\Phi_b(Q;\,0)>\cos\omega t$$

$$+\,[\frac{\sin\omega t}{m\omega}\int_0^t dt'\,f_a(t')\cos\omega t' - \frac{\cos\omega t}{m\omega}\int_0^t dt'\,f_b(t')\sin\omega t']$$

$$\times\,<\Phi_a(Q-q;\,0)|\,e^{\frac{i}{\hbar}Q\int_0^t dt'\,[f_b(t')-f_a(t')]\cos\omega t'}\,|\Phi_b(Q;\,0)>\}$$

$$\times\exp\{\frac{im\omega}{2\hbar\sin\omega t}\,[\frac{2q}{m\omega}\int_0^t dt'\,f_a(t')\sin\omega(t-t') - q^2\cos\omega t$$

$$-\,\frac{2}{m^2\omega^2}\int_0^t dt'\int_0^{t'} dt''\,[f_b(t')f_b(t'')-f_a(t')f_a(t'')]\,\sin\omega t''\sin\omega(t-t')]\},\quad (3.17b)$$

where

$$q(t) = \frac{1}{m\omega}\int_0^t dt'\,[f_b(t')-f_a(t')]\sin\omega t'. \qquad (3.17c)$$

With this approximation, Eq. (3.16), for the bath dynamics, the problem has thus been reduced to only the two coupled equations for $X_a(s;\,t)$ and $X_b(s;\,t)$, i.e., Eq. (3.15a) [with Eq. (3.17)] for $\dot{X}_a$ and a similar one for $\dot{X}_b$.

3. Numerical application: tunneling rate in a double well

To test the various TDSCF schemes presented in Section 2, calculations were carried out for a summetric double well potential $V_0(s)$ coupled to a bath consisting of one harmonic oscillator.[3.12] (The limitation to one or two bath modes for these tests is necessary in order to be able to generate exact results for comparison.) The specific form of $V_0(s)$ is

$$V_0(s) = -\frac{1}{2}a_0 s^2 + \frac{1}{4}c_0 s^4,$$

where the two constants are chosen so that (with the mass m equal to that of an H atom) the frequency at the local minima is 1530 cm^{-1} and the height of the barrier is 6.3 kcal/mol, roughly typical of an H atom transfer process. The frequency of the bath mode is 2980 cm^{-1}. The time evolution of a state initially localized in well "a" of the double well potential, as determined by TDSCF, was studied and compared to the exact time evolution, obtained by basis set calculations.

The potential surface of Eq. (3.1) for the case of one bath mode and $f(s) = cs$ (linear coupling) is shown in Fig. 3-1. The wavefunction for the initial state was chosen to be of the form

$$\Psi(s, Q; 0) = \tilde{\chi}_0(s)\, \tilde{\phi}_0(Q-\lambda). \tag{3.18a}$$

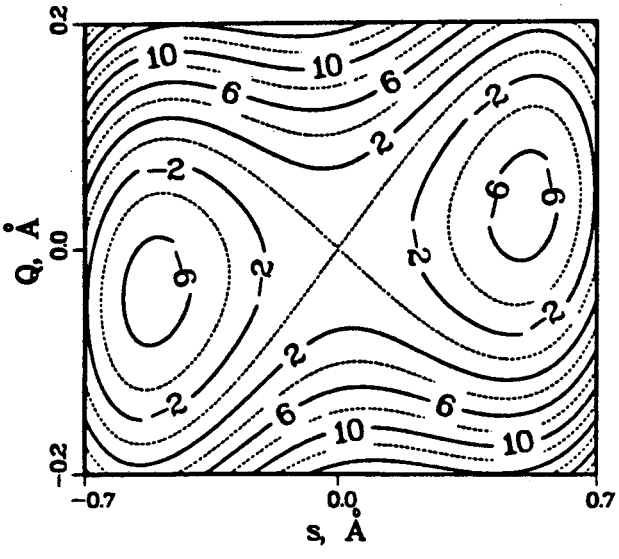

Fig. 3-1

Contour plot of the potential

$$V(s,Q) = V_0(s) + \frac{1}{2}m\omega^2Q^2 - f(s)Q, \qquad f(s)=cs,$$

with c=0.39 mdyn/Å for ω=2980 cm^{-1}. The numbers labeling the curves indicate the height of the potential surface in kcal/mol.

Here $\tilde{\chi}_0$ is a Gaussian that is centered at the minimum of well "a" and corresponds to the lowest eigenstate of the locally harmonic potential,

$$\lambda = \frac{\langle\tilde{\chi}_0|f|\tilde{\chi}_0\rangle}{m\omega^2} \tag{3.18b}$$

is the shift in the Q coordinate from $Q=0$ due to the coupling, and $\tilde{\phi}_0$ is the ground state harmonic oscillator function of frequency ω.

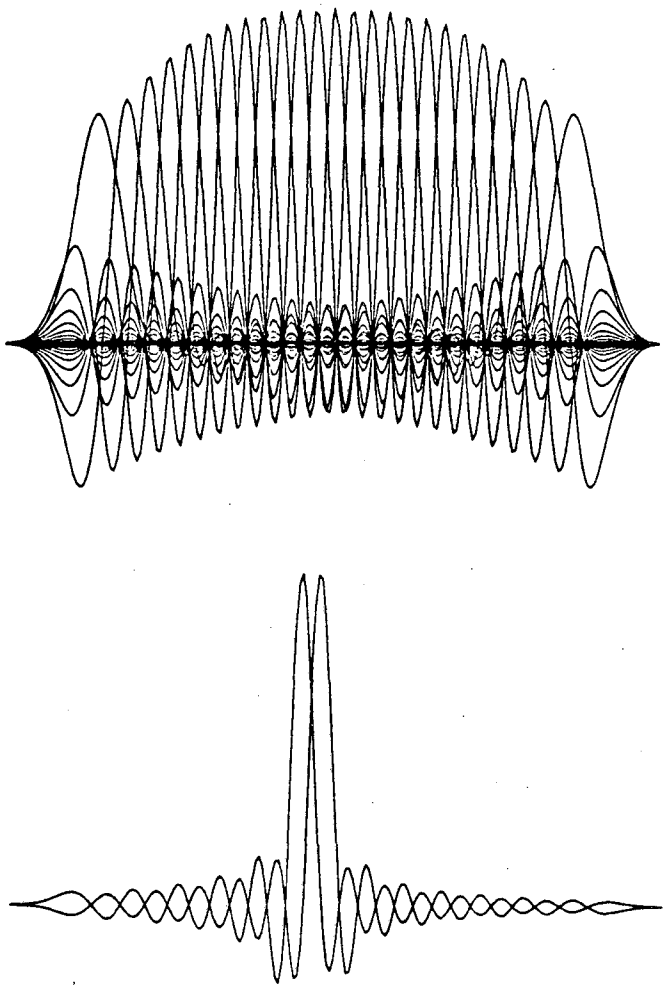

Fig. 3-2

The orthogonal basis functions x_i of Eq. (3.19). These are orthogonalized Gaussians that span the reaction coordinate. (a) The set of all (25) basis functions that were used in the double well calculation of Section 3. (b) Only two such basis functions are shown for clarity.

Consider first the single configuration TDSCF approach. Eq. (3.6a), with Eq. (3.9), is solved by expanding $X(s;t)$ in an orthonormal basis set:

$$X(s;t) = \sum_{i=1}^{M} c_i(t)\, x_i(s); \tag{3.19a}$$

$$\langle x_i | x_j \rangle = \delta_{ij}, \tag{3.19b}$$

thereby converting the equation for $X(s;t)$ into a set of M first order ordinary differential equations for the coefficients $\{c_i(t)\}$. The basis functions $x_i(s)$ are chosen to be localized about grid points s_i; specifically, they are the orthogonalized distributed Gaussians used recently by Hamilton and Light [3.16], and here they are distributed over the region encompassing both potential wells (and the barrier between them). The basis functions $x_i(s)$ are shown in Fig. 3-2. The survival probability

$$P(t) = |\langle X(0) | X(t) \rangle|^2, \tag{3.20}$$

is plotted as a function of the time t, and from this the tunneling period is obtained for a given coupling constant. If τ is the time at which $P(t)$ decays to zero, the tunneling splitting of the ground state is given by

$$\Delta E = \frac{\pi\hbar}{\tau}. \tag{3.21}$$

The time evolution of the initial state of Eq. (3.18) for the case of zero coupling is shown in Fig. 3-3. Plotted is the absolute square of the wavefunction, $|\Psi(s, Q; t)|^2$, as a function of t for total time τ, i.e., half the tunneling period. Fig. 3-4 shows the corresponding survival probability, Eq. (3.20), for $c=0$. The high frequency beats are due to the mixing of other eigenstates of the double well (mainly the third and fourth) besides the lowest two in the wave function at $t=0$.

The single configuration TDSCF calculation is obviously exact in the case of zero coupling. Fig. 3-5, however, which shows how ΔE varies as the coupling constant c is increased from zero, shows that this single configuration TDSCF

approximation is extremely poor for essentially any non-zero value of c. It greatly overestimates the degree to which the coupling diminishes the tunneling splitting.

We thus move on to the two-configuration MC-TDSCF model. The functions X_a and X_b of Equations (3.12a) and (3.12b) are expanded as follows:

$$X_a(s;t) = \sum_{i=1}^{M/2} c_{ia}(t)x_i(s) \tag{3.22a}$$

$$X_b(s;t) = \sum_{i=M/2+1}^{M} c_{ib}(t)x_i(s), \tag{3.22b}$$

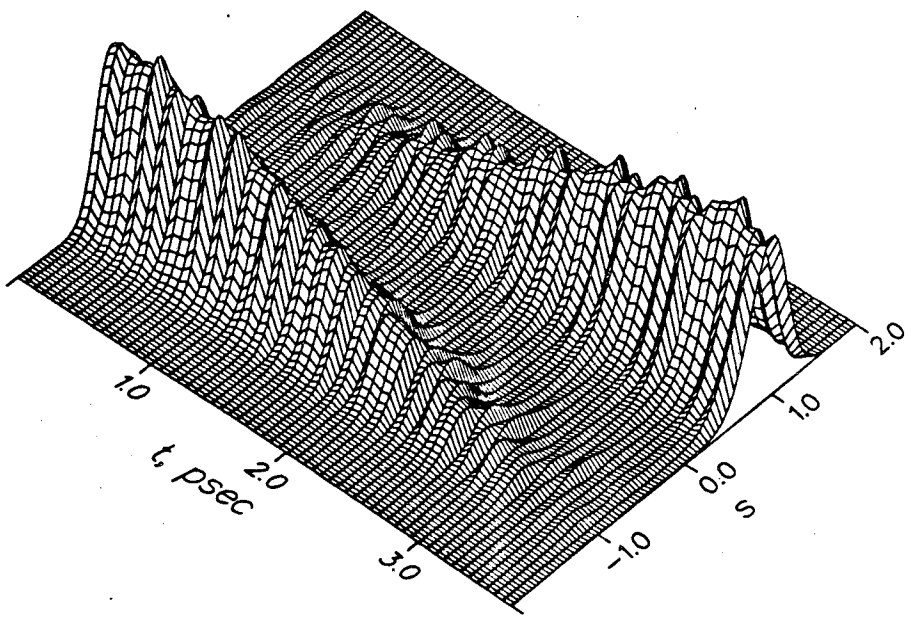

Fig. 3-3

Time evolution of the wavefunction given by Eq. (3.18) for the case of zero coupling. Plotted is the probability density, $|\Psi(s, Q; t)|^2$, as a function of the reaction coordinate s and the time t. The time evolution was computed by basis set expansion.

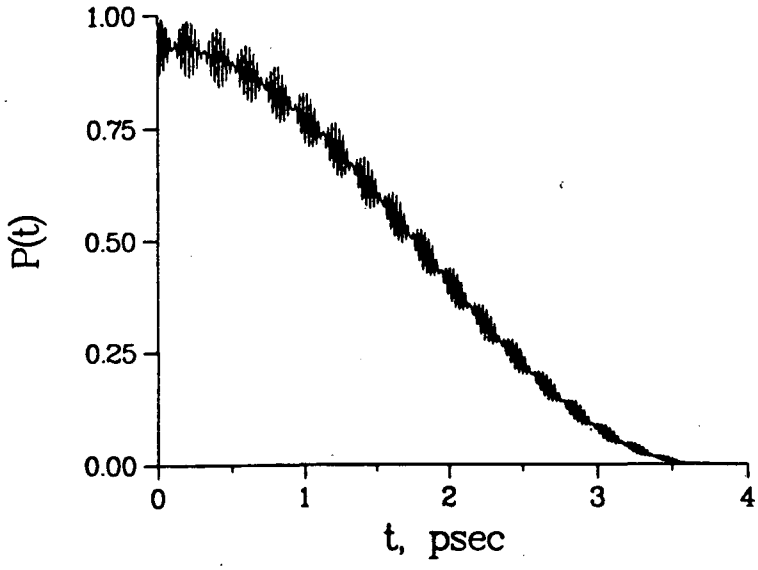

Fig. 3-4
The survival probability, Eq. (3.20), for the uncoupled double well potential $V_0(s)$ as a function of time t.

where $\{x_i(s)\}$ are the localized basis functions noted above; $x_i(s)$ is localized in well "a" for $i \leq M/2$ and in well "b" if $i > M/2$. Note that, by construction, $\langle X_a | X_b \rangle = 0$ at all times.

The exact TDSCF equations [Eqs. (3.15a) and (3.15b)] are solved numerically by expanding $\Phi_a(Q; t)$ and $\Phi_b(Q; t)$ in another basis set:

$$\Phi_a(Q; t) = \sum_{i=1}^{K} d_{ia}(t)\psi_i(Q) \tag{3.23a}$$

$$\Phi_b(Q; t) = \sum_{i=1}^{K} d_{ib}(t)\psi_i(Q) \tag{3.23b}$$

where $\{\psi_i(Q)\}$ is also an orthogonalized distributed Gaussian basis. Note that here $\langle \Phi_a | \Phi_b \rangle \neq 0$ (in the special case of zero coupling, $\langle \Phi_a | \Phi_b \rangle = 1$).

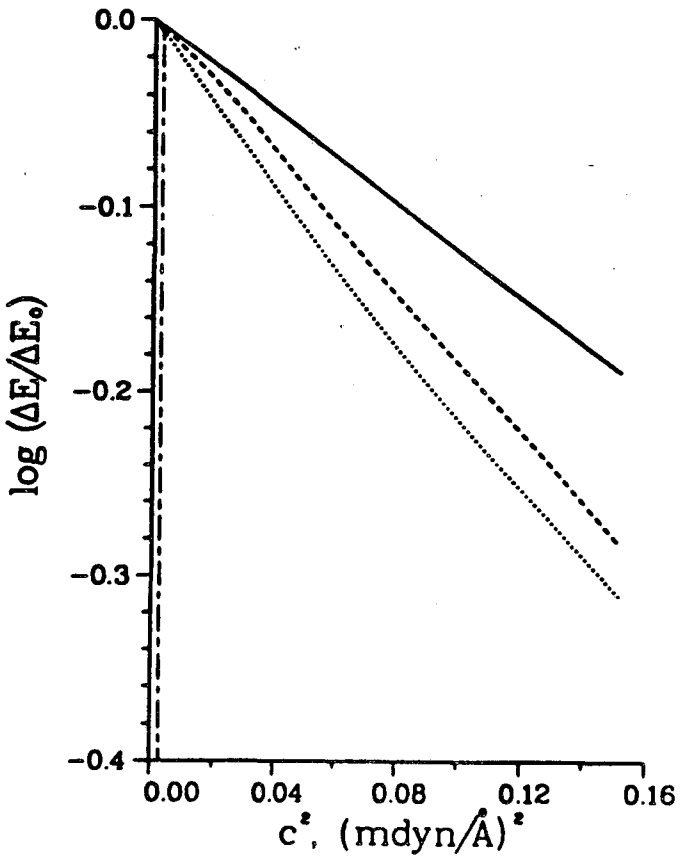

Fig. 3-5

Tunneling splitting between the two lowest levels of the double well potential as a function of the square of the coupling constant c for ω=2980 cm^{-1}. The solid line indicates the exact results. The dashed line shows the results of the exact solution of the two-configuration MC-TDSCF equations, Eq. (3.15a) and (3.15b), while the dotted line shows the results of the approximate, analytically solvable MC-TDSCF model, with Eq. (3.16) replacing Eq. (3.15b). The single configuration TDSCF results are shown by the chain-dashed line. The tunneling splittings that are calculated by using the shifted oscillator basis of Chapter II are in this case practically indistinguishable from the exact results.

The results of this MC-TDSCF calculation, as seen in Fig. 3-5, are orders of magnitude better than the one-configuration results. Also shown in Fig. 3-5 are the results of the approximate MC-TDSCF model [where the exact equation for the bath wavefunction, Eq. (3.15b), is replaced by the approximate, analytically solvable Eq. (3.16)], and they are seen to be only slightly less accurate than the values from the exact MC-TDSCF calculation.

Thus the MC-TDSCF model (two configurations for this example) is seen to be a dramatic improvement over the standard, single configuration TDSCF description for this model of an isomerization process. It is encouraging, too, that the approximate version of the MC-TDSCF approach is almost as accurate as the exact version, for the former allows one to eliminate the bath degrees of freedom completely analytically and thus be left with only the two coupled equations for the two configurations of the reaction coordinate.

Finally, though, even the exact version of the MC-TDSCF model does not give results for this example that are as accurate as the shifted oscillator basis set model presented in Chapter II [see also Ref. 3.2]. For the coupling strengths shown in Fig. 3-5, the results given by the latter approach are indistinguishable (within the resolution of the figure) from the exact values shown there.

4. Concluding remarks

Perhaps the most striking result of this work is how poorly the standard, single configuration TDSCF model works for describing the effect of system-bath coupling on the isomerization rate. This is particularly disturbing because for this system, this treatment is equivalent to the "quantum system" plus "classical bath" model that many workers hope will be sufficient to describe the effect of a bath on a system of interest. Our results thus suggest caution in this regard. (It is worth pointing out that one could improve the single configuration TDSCF results by defining new

coordinates that are linear combinations of the system coordinate and the bath coordinates. This is not desirable for these system-bath problems, though, because it would prevent one from integrating out the bath degrees of freedom.)

The multi-configuration TDSCF description, however, is seen to correct the major shortcoming of the single configuration model. Here each "configuration", or component, of the system wavefunction has its own separate bath wavefunction, and each bath wavefunction responds only to the force averaged over its associated configuration of the system. The equations of Section 2b can clearly be extended to deal with more than two configurations. The MC-TDSCF equations are more complicated than the standard TDSCF, but with the approximate version – which was seen to be almost as accurate as the exact MC-TDSCF – the number of coupled equations to be solved numerically is only the number of configurations of the system.

The MC-TDSCF approach should thus find considerable utility for treating the dynamics of these system-bath problems.

References

3.1 (a) W. H. Miller, N. C. Handy and J. E. Adams, *J. Chem. Phys.* 72, 99 (1980);
(b) W. H. Miller, *J. Chem. Phys.* **87**, 3811 (1983).

3.2 N. Makri and W. H. Miller, *J. Chem. Phys.* 86, 1451 (1987).

3.3 (a) R. B. Gerber, V. Buch and M. A. Ratner, *J. Chem. Phys.* 77, 3022 (1982);
(b) V. Buch, R. B. Gerber and M. A. Ratner, *Chem. Phys. Lett.* **101**, 44 (1983);
(c) R. B. Gerber, V. Buch and M. A. Ratner, *Chem. Phys. Lett.* **91**, 173 (1982);
(d) G. C. Schatz, V. Buch, M. A. Ratner and R. B. Gerber, *J. Chem. Phys.* **79** , 1808 (1983).

3.4 R. B. Gerber, V. Buch, and M. A. Ratner, in *Intramolecular Dynamics*, Proceedings of the 15th Jerusalem Symposium on Quantum Chemistry and Biochemistry, Eds. J. Jortner and B. Pullman (Reidel, Dortrecht, 1982).

3.5 (a) R. A. Harris, *J. Chem. Phys.* **72**, 1776 (1980);
(b) D. L. Yeager and P. Jorgensen, *Chem. Phys. Lett.* 65, 77 (1979);
(c) P. Albertsen, P. Jorgensen and D. L. Yeager, *Mol. Phys.* 41, 409 (1980).

3.6 E. J. Heller, *J. Chem. Phys.* 62, 1544 (1975).

3.7 K. M. Christoffel and J. M. Bowman, *J. Chem. Phys.* 74, 5057 (1981).

3.8 B. Carmeli and H. Metiu, *Chem. Phys. Lett.* 133, 543 (1987).

3.9 E. C. Behrman and P. G. Wolynes, *J. Chem. Phys.* 83, 5863 (1985).

3.10 W. H. Miller, in *Stochasticity* and *Intramolecular Redistribution of Energy*, R. Lefebvre and S. Mukamel, Eds., D. Reidel, Boston, 1987.

3.11 See, for example,
(a) G. D. Billing, *Chem. Phys. Lett.* 30, 391 (1975);
(b) G. D. Billing, *J. Chem. Phys.* 64, 908 (1976).

3.12 The methods and numerical examples presented in this Chapter appeared previously in the following article:
N. Makri and W. H. Miller, *J. Chem. Phys.* 87, 5781 (1987).

3.13 P. A. M. Dirac, *Proc. Cambridge Philos. Soc.* 26, 376 (1930).

3.14 This procedure is what results from using the Dirac time-dependent variational principle, i.e., requiring that the functional $\int dt \; \langle \Psi(t) | i\hbar \frac{\partial}{\partial t} - H | \Psi(t) \rangle$ be stationary with respect to variation of the wavefunction Ψ.

3.15 (a) R. P. Feynman, *Rev. Mod. Phys.* **20**, 367 (1948);

(b) R. P. Feynman and A. R. Hibbs, *Quantum Mechanics* and *Path Integrals*, McGraw-Hill, New York, 1965.

3.16 I. P. Hamilton and J. C. Light, *J. Chem. Phys.* 84, 306 (1986).

IV. A Semiclassical Tunneling Model

1. Introduction

Classical mechanics is known to provide a powerful method for studying the dynamics of large molecular systems.[4.1] Unlike quantum mechanical methods, which become prohibitively difficult to implement as the dimensionality of the system increases, the classical equations of motion are comparatively easy to solve even for systems with many degrees of freedom. The fact that atoms and molecules are relatively heavy particles suggests that chemical reactions should in general be successfully approximated by classical trajectory simulations. Indeed, use of classical mechanics in molecular processes has been found to yield results that agree well with those of quantum calculations, in particular if the comparison is made on averaged rather than state-to-state properties; this is so because suitable averaging tends to smear out quantum effects.[4.2]

Perhaps the most serious limitation of classical mechanics, which hinders its application to many interesting chemical problems, is its inability to describe tunneling effects. However, the quantum mechanical phenomenon of tunneling is often quite prominent in chemical reactions that involve significant motion of light atoms. Typical examples include unimolecular dissociation or isomerization, e.g.,

$$H_2CO \rightarrow H_2 + CO, \tag{4.1}$$

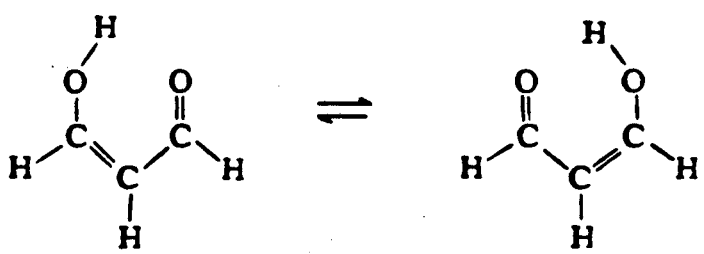

(4.2)

as well as bimolecular reactions that involve H-atom transfer, e.g.,

$$H_2 + H \rightarrow H + H_2, \tag{4.3}$$

$$H_2 + F \rightarrow H + HF. \tag{4.4}$$

There do exist "rigorous" semiclassical theories that describe how classical trajectories tunnel, e.g., classical S-matrix theory [4.3] and the "instanton" (periodic orbit in pure imaginary time) model,[4.4,4.5] but they are difficult to apply routinely to sizable (e.g., more than three atom) molecular systems. There also exist a host of simple tunneling corrections to transition state theory [4.6] expressions for thermal rate constants; these often work well for this purpose, but they are not applicable to more general dynamical phenomena.

What we seek is a semiclassical model, as generally applicable as possible, for including tunneling in a classical trajectory simulation of the full molecular dynamics; the purpose of this Chapter is to present such a model. The model we have developed is similar in spirit to the Tully-Preston [4.7] surface hopping model for electronically non-adiabatic processes. In the Tully-Preston model a classical trajectory moving on one potential energy surface (i.e., Born-Oppenheimer electronic state) has a probability of making "hops", i.e., instantaneous transitions, to another potential energy surface at certain times. In the tunneling model presented herein the classical trajectory evolving in one classically allowed region of space will, at specific times, have a probability for making an instantaneous (in real time) transition to another classically allowed region of space. The model may also be viewed as the *classical* version of the semiclassical branching model of Waite and Miller,[4.8] but generalized to allow for a more general tunneling path. This more general tunneling path is very closely related to that used by Heller and Brown [4.9] in their semiclassical treatment of radiationless transitions.

In Section 2 we first give a qualitative discussion/motivation for the model, and then define it more precisely. Section 3 gives the results of some test calculations on model Hamiltonians that illustrate some of its quantitative features. More

specifically, we present in that Section calculations of the tunneling splitting in symmetric double wells and of the unimolecular decay rate for quasi-bound initial states. In general the model is seen to provide an excellent description of these tunneling phenomena over a wide range of conditions (e.g., coupling constants, different symmetries of coupling). Finally, some concluding remarks appear in Section 4.

2. The semiclassical tunneling model

a) One dimensional case

It is well known that the rate of unimolecular decay from a one-dimensional well, as in Fig. 4-1, is given semiclassically (and accurately!) by [4.10]

$$k = \frac{\omega}{2\pi} e^{-2\theta} \tag{4.5a}$$

where ω is the vibrational frequency in the well and $e^{-2\theta}$ is the probability of tunneling through the barrier; θ is the classical action integral through the barrier,

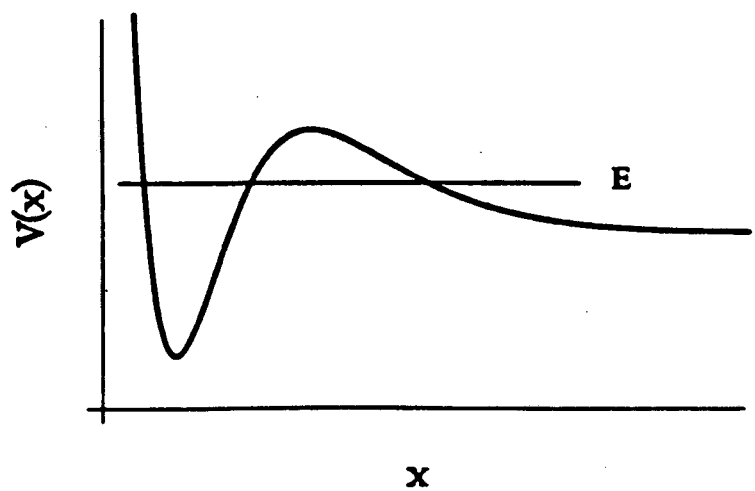

Fig. 4-1
A typical one-dimensional potential for unimolecular decay (cf. Section 2a). An energy level that corresponds to a quasi-bound state is indicated.

$$\theta = \frac{1}{\hbar} \mathrm{Im} \int_{barrier} p(x)dx. \tag{4.5b}$$

Since $\omega/2\pi$ is the frequency that the trajectory experiences a classical turning point at the barrier, one may interpret Eq. (4.5) as a classical trajectory that oscillates in the well, tunneling out with probability $e^{-2\theta}$ every time it "hits" the barrier. If the particle is considered to be in the well at time t=0, the *net probability that the particle has tunneled*, $P_{net}(t)$, is [4.11]

$$P_{net}(t) = \sum_n h(t-t_n)P_n \tag{4.6a}$$

where $h(\xi)$ is the usual step function (=1 if $\xi>0$, =0 if $\xi<0$), t_n are the various "tunneling times", the times that the classical trajectory $x(t)$ is at its outer turning point (i.e., "hits the barrier"), and

$$P_n = e^{-2\theta} \tag{4.6b}$$

is the tunneling probability for time t_n (here the same at each tunneling time). Fig. 4-2 indicates the "staircase" character of $P_{net}(t)$. Averaging over the initial phase of the vibrational motion in the well will smooth out these steps, and it is not hard to see that the tunneling rate of Eq. (4.5a) is equivalently given by the slope of the averaged net tunneling probability $P_{net}(t)$, i.e.,

$$k = \frac{d}{dt}\langle P_{net}(t)\rangle. \tag{4.6c}$$

The above discussion, which involves tunneling *probabilities*, applies to unimolecular dissociation, as pictured in Fig. 4-1, and also to isomerization in an asymmetric double well potential that is irreversible on the time scale of physical interest. (Without the pre-exponential factor, it also gives the reaction probability for tunneling in bimolecular reactions, either symmetric or asymmetric.) The above description is *not* appropriate, however, to resonant tunneling in a *symmetric* double well potential, for the quantity of interest there, the splitting of the two degenerate energy

levels, involves the tunneling *amplitude*.[4.10,4.12] For the present one-dimensional case this tunneling splitting is given semiclassically by

$$\Delta E = \frac{\hbar\omega}{\pi} e^{-\theta}, \tag{4.7a}$$

where ω and θ are the same quantities as above. Following the same analysis as in the preceding paragraph, however, one can express ΔE in terms of the *net tunneling amplitude*

$$S_{net}(t) = \sum_n h(t - t_n) S_n, \tag{4.7b}$$

$$S_n = e^{-\theta}, \tag{4.7c}$$

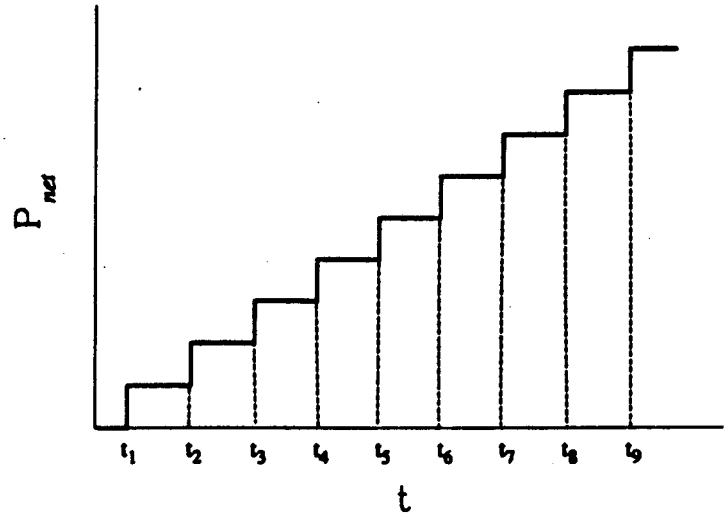

Fig. 4-2

The net tunneling probability, $P_{net}(t)$, as a function of the time t, for a one dimensional potential of the type shown in Fig. 4-1. The "tunneling times" $t_1, t_2, \ldots$, i.e., the times at which the trajectory experiences an outer turning point, are indicated.

as follows:

$$\Delta E = 2\hbar \frac{d}{dt} \langle S_{net}(t) \rangle, \tag{4.7d}$$

where the bracket implies an average over the initial phase of vibrational motion. We note that the same relation, Eq. (4.7d), also results from first order time dependent perturbation theory, whereby one has (to within a constant phase factor)

$$S(t) = H_{ab}\, t/\hbar,$$

$$\Delta E = 2H_{ab},$$

where H_{ab} is the exchange matrix element between states localized in wells "a" and "b".

b) Separable multidimensional case

Now consider a separable N-dimensional potential

$$V(s, Q_1, \ldots, Q_{N-1}) = V_0(s) + \sum_{i=1}^{N-1} V_i(Q_i), \tag{4.8}$$

where the potential for the s coordinate has a barrier, and the potentials V_i are simple oscillators. Fig. 4-3 shows a contour plot of such a potential for N=2, and a classical trajectory for energy E below the top of the barrier is shown in Fig. 4-4. A separable potential is a special case of an integrable system, with the N constants of the motion E_i, i=1,...,N specified by energy conservation in each degree of freedom individually. All trajectories that correspond to the same constants of the motion are confined on an N-dimensional manifold embedded in $2N$-dimensional phase space. If the motion is bounded, this manifold has the topology of a torus [cf. Fig. 4-5] and its projection onto configuration space is an N-dimensional parallelepiped (a "box"), with the sides (caustic surfaces) traced out by the trajectories as they go through turning points in each degree of freedom. A typical trajectory gives rise to a Lissajous-type figure (see Fig. 4-4). For N=2, the trajectory manifold touches the boundary of

the energetically allowed region at four points, the "corners".

Since the potential is separable, tunneling involves only the s degree of freedom and is described as in Section 2(a). Thus, the tunneling times $\{t_n\}$ occur whenever the s degree of freedom experiences an outer turning point, and the tunneling path is a straight line - the s axis - perpendicular to the trajectory at time t_n. The passage through the barrier takes place in pure imaginary time, during which the $N-1$ momenta $P_1, \ldots, P_{N-1}$ remain constant. The decay rate is the same as that of the one-dimensional potential V_0, i.e., given by Eq. (4.6). Note that the action integral is

$$\theta = \frac{1}{\hbar} \operatorname{Im} \int p_s ds = \frac{1}{\hbar} \operatorname{Im} \int_{\text{tunneling path}} \mathbf{p} \cdot d\mathbf{q}, \tag{4.9}$$

where $\mathbf{q} \equiv (s, Q_1, \ldots, Q_{N-1})$ and $\mathbf{p} \equiv (p_s, P_1, \ldots, P_{N-1})$.

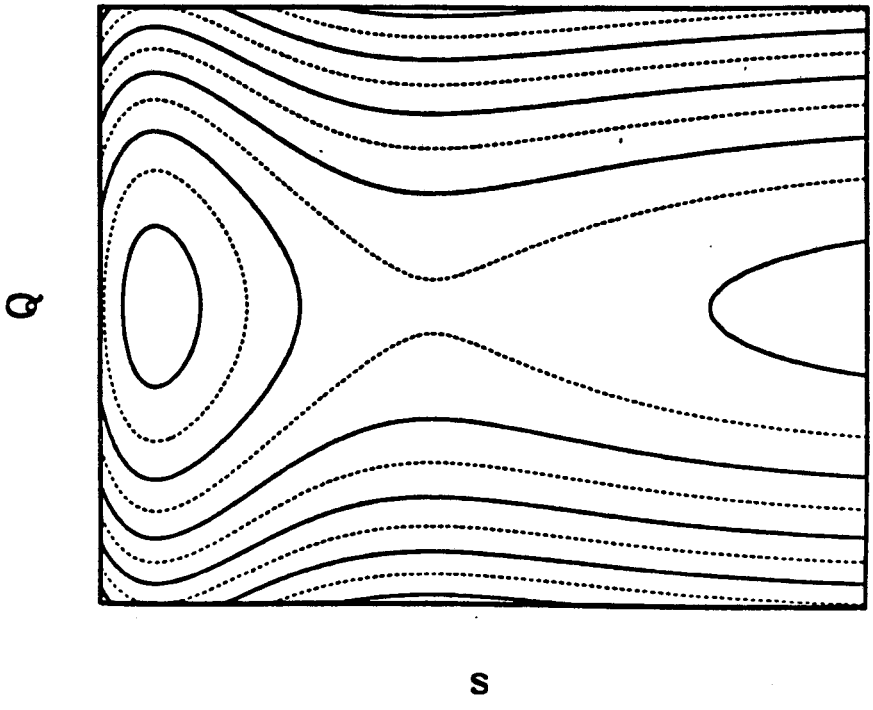

Fig. 4-3

Contour plot of a separable two-dimensional potential. The potential in the s coordinate is that of Fig. 1, while the Q coordinate is a simple harmonic oscillator.

Finally we note that the trajectory reaches the products region with the same momentum **p** with which it began to tunnel and at the *same real time* (i.e., the tunneling involves only a pure imaginary time increment). The semiclassical picture is thus that the tunneling process is instantaneous (in real time) and conserves the momentum **p**.

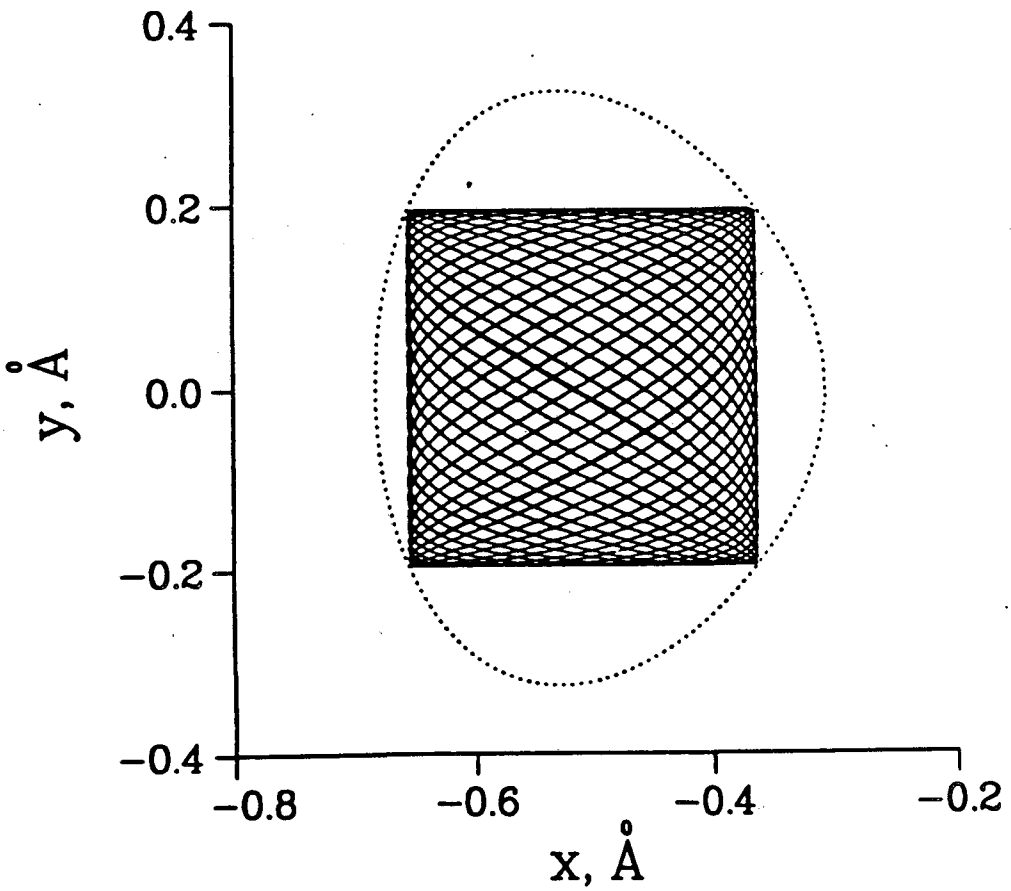

Fig. 4-4

A trajectory corresponding to the semiclassical ground state of a separable two-dimensional potential. The trajectory (or a set of trajectories that correspond to the same semiclassical state) defines a rectangular region bounded by the caustics. The dotted line shows the energy contour.

c) General (non-separable) case

We consider a generic Cartesian Hamiltonian

$$H(\mathbf{q},\mathbf{p}) = \sum_{i=1}^{N} \frac{p_i^2}{2m} + V(\mathbf{q}), \tag{4.10}$$

where the potential function V is in general non-separable. The above tunneling model is generalized by allowing the trajectory to tunnel along a *straight line path* in a specified direction $\hat{\mathbf{n}}_0$ every time the component of the momentum $\mathbf{p}$ along $\hat{\mathbf{n}}_0$, $\mathbf{p}\cdot\hat{\mathbf{n}}_0$, experiences a classical turning point (i.e., goes through zero) in the outward direction; equivalently, this corresponds to the times that the component of the coordinate vector $\mathbf{q}$ along the direction $\hat{\mathbf{n}}_0$, $\mathbf{q}\cdot\hat{\mathbf{n}}_0$, goes through a relative maximum.

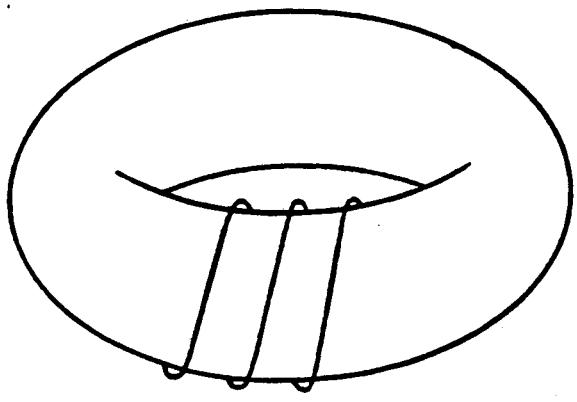

Fig. 4-5
Schematic representation of a two-dimensional torus, corresponding to a separable two degree of freedom system. A trajectory which winds around the torus is also indicated.

(We note parenthetically that a straight line tunneling path is one of the many models used by Truhlar and co-workers [4.6a,b] for making tunneling corrections to transition state theory. The termini of the straight line are sometimes chosen to lie at vibrationally adiabatic turning points and in other cases to lie on reference paths in the reactant and product region.[4.6b] The former version of their model is closest in spirit to the present work, though we note that the present model is defined in terms of the numerically exact classical trajectories of the system and is applicable to more general dynamical processes.)

The choice of the tunneling direction $\hat{\mathbf{n}}_0$ will be discussed more fully in part (d) of this Section. Requiring the tunneling path to be a straight line (in the full dimensional coordinate space) is, of course, an approximation in the general non-separable case, but a reasonable one. Calculations based on the more rigorous classical S-matrix [4.13] and "instanton" [4.14] theories show that the optimum tunneling path is relatively straight in the tunneling region.

To describe the tunneling model more specifically, it is useful to make a change of coordinates (a point transformation) $\{q_i\} \rightarrow \{x, y_1, \ldots, y_{N-1}\}$, where x is the component of $\mathbf{q}$ along the tunneling path,

$$x = \mathbf{q}\cdot\hat{\mathbf{n}}_0, \tag{4.11}$$

and $\{y_1,\ldots,y_{N-1}\}$ define $N-1$ orthogonal directions perpendicular to $\hat{\mathbf{n}}_0$. The Hamiltonian is then expressed in the new coordinate system:

$$\tilde{H}(x,\mathbf{y},p_x,\mathbf{p}_y) = \frac{p_x^2}{2m} + \sum_{i=1}^{N-1}\frac{p_{y_i}^2}{2m} + \tilde{V}(x,\mathbf{y}), \tag{4.12}$$

where $\mathbf{y}\equiv(y_1, \ldots, y_{N-1})$ and $\mathbf{p}_y$ is the vector of conjugate momenta. Since by our choice of tunneling path all components of $\mathbf{y}$ and $\mathbf{p}_y$ remain constant during the straight line tunneling process, the tunneling integral is given by

$$\theta = \frac{1}{\hbar}\,\mathrm{Im}\int_{\textit{tunneling path}} \mathbf{p}\cdot d\,\mathbf{q} = \frac{1}{\hbar}\,\mathrm{Im}\int p_x\,dx. \tag{4.13}$$

Furthermore, due to energy conservation along the tunneling path, we have

$$\frac{p_x(t)^2}{2m} + \frac{\mathbf{p}_y(t)^2}{2m} + \tilde{V}(x(t),\mathbf{y}(t)) = \frac{p_x(t_0)^2}{2m} + \frac{\mathbf{p}_y(t_0)^2}{2m} + \tilde{V}(x_0,\mathbf{y}_0), \qquad (4.14)$$

where $(x_0,\mathbf{y}_0)$ are the coordinates of the trajectory at the tunneling time t_0, and $t-t_0$ is pure imaginary. But $p_x(t_0)=0$, $\mathbf{p}_y(t)=\mathbf{p}_y(t_0)$, and $\mathbf{y}(t) = \mathbf{y}_0$, so we obtain

$$p_x = i\sqrt{2m[\tilde{V}(x,\mathbf{y})-\tilde{V}(x_0,\mathbf{y}_0)]} = i\sqrt{2m[V(\mathbf{q}_0+(x-x_0)\hat{\mathbf{n}}_0)-V(\mathbf{q}_0)]}. \qquad (4.15)$$

The tunneling integral is thus given by

$$\theta_0 = \frac{1}{\hbar}\int_0^{\xi_{max}} \sqrt{2m[V(\mathbf{q}_0+\xi\hat{\mathbf{n}}_0)-V(\mathbf{q}_0)]}\,d\xi \qquad (4.16)$$

and the probability for tunneling at time t_0 is

$$P_0 = e^{-2\theta_0} \qquad (4.17)$$

where ξ_{max} is the value of ξ at which the integrand of Eq. (4.16) equals zero, i.e., the value for which the tunneling trajectory reaches another classically allowed region of space.

It is useful to emphasize that the above algorithm is easily implemented in the original coordinates and momenta $(\mathbf{q}, \mathbf{p})$ of Eq. (4.10) without actually having to make the canonical transformation used above to describe it. Thus one monitors the quantity $x(t)$ of Eq. (4.11) while the trajectory $(\mathbf{q}(t), \mathbf{p}(t))$ is being computed; t_0 is a time at which x(t) experiences a local maximum, and $\mathbf{q}_0\equiv\mathbf{q}(t_0)$, $\mathbf{p}_0\equiv\mathbf{p}(t_0)$. The tunneling integral is then given by Eq. (4.16), where ξ_{max} is the value of the integration variable at which the integrand vanishes, and the tunneling probability is given by Eq. (4.17). [If the integrand of Eq. (4.16) never vanishes for $\xi>0$, then one has $\theta_0\rightarrow+\infty$ and thus $P_0\rightarrow 0$; i.e., the tunneling path never finds another classically allowed region.] If one wishes to follow the trajectory in the new classically allowed region - e.g., in order to determine the product state distribution - then the initial conditions for it are

$$\mathbf{q}_{new}(t_0) = \mathbf{q}_0 + \hat{\mathbf{n}}_0 \xi_{max}, \tag{4.18a}$$

$$\mathbf{p}_{new}(t_0) = \mathbf{p}_0. \tag{4.18b}$$

d) Choice of the tunneling path

To complete the description of the model, we must specify the "tunneling direction" $\hat{\mathbf{n}}_0$ introduced in the preceding Section. We have actually investigated a variety of choices and describe here the one which has proved most satisfactory in general and which seems most justifiable on theoretical grounds.

Consider first the initial conditions for a trajectory in the reactant potential well. For the semiclassical picture to be meaningful, we assume that the motion in the reactant potential well does not explore all energetically accessible regions of phase space, but is constrained to lie on an N-dimensional KAM torus,[4.15] as in the separable case, for the energy that corresponds to the desired initial conditions. This is a reasonable assumption, especially if one is interested in tunneling from low lying initial states (e.g., from the ground state). More specifically, we will be considering trajectories that start out with initial conditions $(\boldsymbol{\phi},\mathbf{J})$ in action-angle variables,[4.15a] where the actions

$$J_i = \frac{1}{2\pi}\int_{\Gamma_i} \mathbf{p}\cdot d\mathbf{q} = (n_i + \frac{1}{4}\mu_i)\hbar \tag{4.19}$$

are defined along the N topologically distinct paths (basis contours) Γ_i on the torus and are quantized, and μ_i is the corresponding Maslov index.[4.16] Averaging over initial conditions then corresponds to averaging over the angles $\{\phi_i\}$, $i=1,...,N$. These are the polyatomic version of the standard quasiclassical initial conditions (EBK quantization).[4.17]

Since the motion is assumed to sweep out a torus, its projection onto configuration space still gives rise to "box"-like shapes (see Fig. 4-6). Unlike the separable case, the edges of such a "box" need no longer be straight lines, though

one can show that they still cross at right angles near a corner;[4.18] i.e., the motion is locally separable about a corner.

We now employ the concept of the semiclassical wavefunctions that correspond to these box-like trajectories and a simple argument from quantum mechanics to motivate our choice of the tunneling path. Quantum mechanically, the amplitude for a transition from the initial state $|\Psi_i>$ to the final state $|\Psi_f>$ is given by

$$<\Psi_f|\hat{T}|\Psi_i>, \tag{4.20}$$

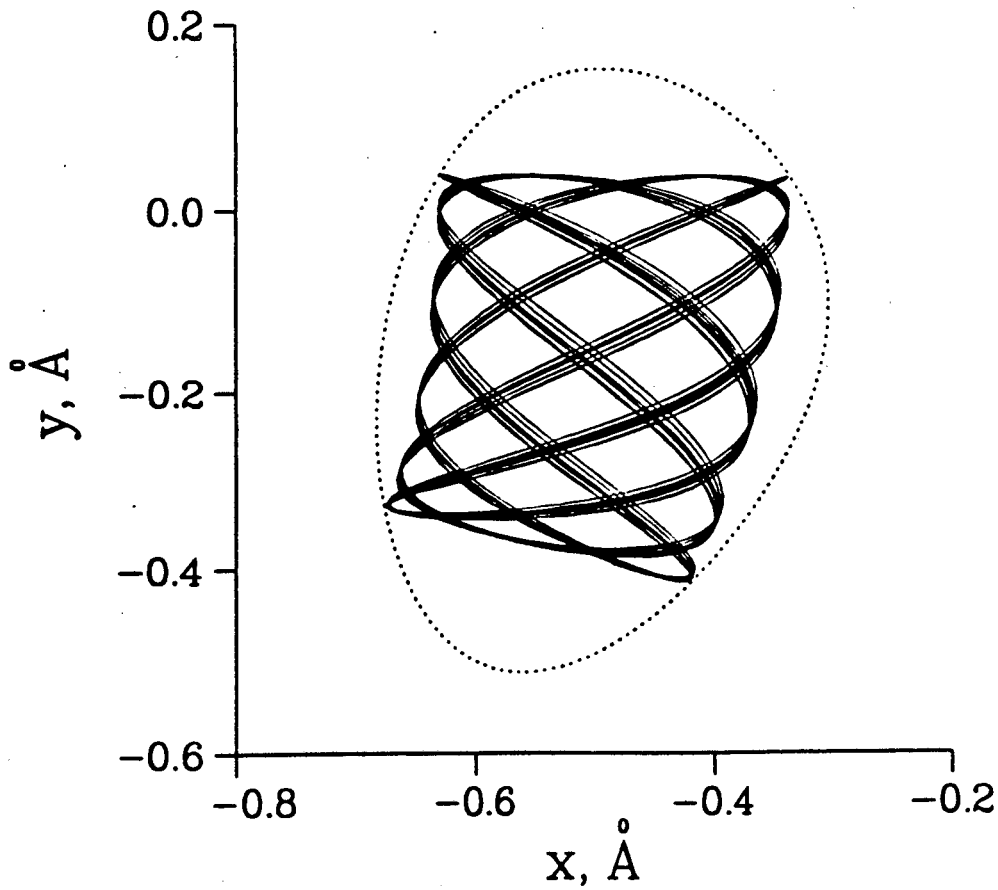

Fig. 4-6

A trajectory corresponding to the semiclassical ground state of a non-separable two-dimensional potential. The classical motion is regular, i.e., the trajectory lies on a KAM torus and will, over time, trace out a two-dimensional region which is a subset of the energy shell. This region (the "trajectory manifold") is the projection of the KAM torus onto configuration space; it touches the energy contour at four points, the "corners", and is bounded by caustics. The dotted line shows the energy contour.

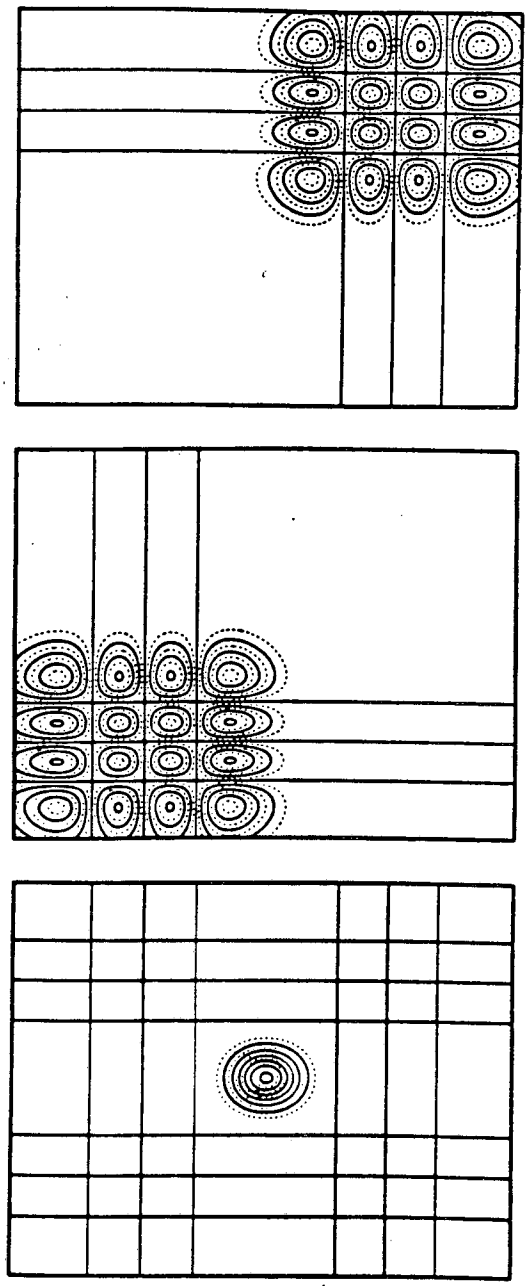

Fig. 4-7

(a)-(b): Schematic representation of the semiclassical wavefunctions that correspond to two tori, whose projections onto configuration space do not overlap. The wavefunctions have been analytically continued into the classically forbidden region. (c) The product of the two wavefunctions; it is seen that the overlap of the two wavefunctions is maximized along the direction that connects the nearest corners of the trajectory manifolds.

where $\hat{T}$ is the appropriate transition operator, in our case the Hamiltonian. The semiclassical wavefunction in the region near the caustic surfaces but *outside* the trajectory manifold can be defined (by generalizing the well known one-dimensional WKB results) as the analytic continuation of the WKB wavefunction on the manifold.[4.19] The wavefunction will be proportional to the exponential of a properly defined action integral, and is largest near the edges of the manifold. The tunneling amplitude accumulates its magnitude from the regions of space where the initial and final state wavefunctions overlap the most. The overlap of these wavefunctions is clearly maximized along the shortest straight line that joins these manifolds (see Fig. 4-7); We thus choose the tunneling direction $\hat{\mathbf{n}}_0$ as *the straight line that connects the manifolds* that correspond to the initial and final state *in the shortest possible way*. Fig. 4-8 shows three typical cases, and the tunneling path for each case.

We note that the above choice for the tunneling direction is the same in spirit as that of Heller and Brown [4.9] in their treatment of semiclassical matrix elements for radiationless transitions. The primary difference is that our model does not restrict tunneling only to the "corner to corner" (or corner to edge) path, but allows for tunneling in the "corner to corner" *direction* every time the component of the motion along this direction experiences a classical turning point. We also note that this "corner to corner" tunneling direction is also very similar to that yielded in some applications of "rigorous" semiclassical theories, i.e., classical S-matrix theory [4.13] and the instanton model.[4.14]

3. Application: tunneling rates in model potentials

We envision the present model to be most useful for describing tunneling processes in complex molecular systems involving unimolecular decomposition and isomerization. In this Section we illustrate its success by presenting test applications on simple two-dimensional Hamiltonians of the form

$$H = \frac{p_s^2}{2m} + \frac{p_Q^2}{2m} + V(s,Q).$$

We performed calculations of the tunneling splitting in symmetric double wells and of unimolecular decay rates from quasi-bound initial states.

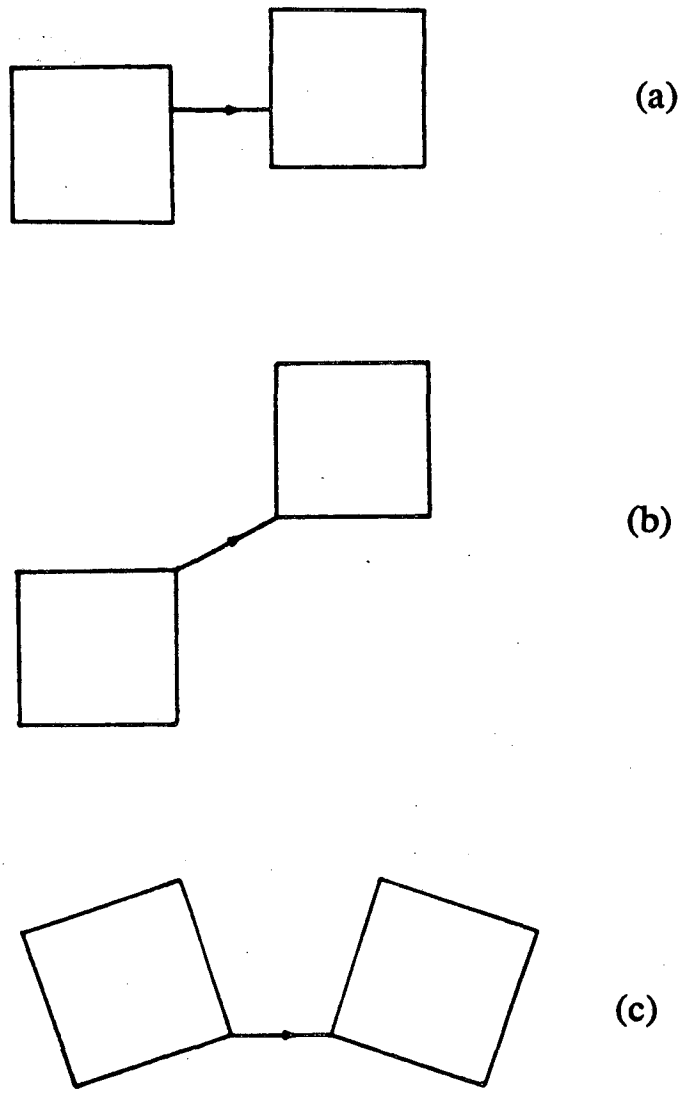

Fig. 4-8

The boundary of the trajectory manifolds and the "tunneling path" according to the definition of Section 2d in three typical cases.

a) Choice of initial conditions

To describe tunneling from a given "regular" quantum state semiclassically, we must choose classical trajectories that lie on a quantizing torus (J_1,J_2) and average over all initial angles (ϕ_1,ϕ_2). (By "regular" we mean a state that corresponds to a KAM torus, i.e., a torus on which classical motion is regular.) We used the adiabatic switching technique [4.20,4.21] to quantize the actions. According to this method, initial conditions are chosen from the appropriate quantizing torus of a zeroth order Hamiltonian H_0, with the initial angles uniformly distributed in the interval $[0,2\pi)$. Then the perturbation $H-H_0$ is slowly switched on; i.e., the trajectories evolve according to the time dependent Hamiltonian

$$H(t) = H_0 + \lambda(t)(H-H_0), \tag{4.21}$$

where $\lambda(t)$ starts out with zero value and reaches unity at some time T. Because of the principle of adiabatic invariance,[4.15a] the actions remain approximately constant during the switching process, while the energy changes as the Hamiltonian is changed. At the end of this process the trajectories uniformly cover a torus that corresponds to the desired semiclassical local eigenstate of the full Hamiltonian H.

There is no unique way of choosing the zeroth order Hamiltonian H_0 or the switching function $\lambda(t)$. The particular form of H_0 that we used contains the kinetic energy terms and the harmonic approximation to $V(s,Q)$ about the potential minimum (s_0,Q_0). Such a Hamiltonian is separable in the normal mode type coordinates,

$$\begin{bmatrix} x_1 \\ x_2 \end{bmatrix} = \mathbf{U}^T \cdot \begin{bmatrix} \Delta s \\ \Delta Q \end{bmatrix} \tag{4.22a}$$

where $\Delta s = s - s_0$ and $\Delta Q = Q - Q_0$. Here $\mathbf{U}$ is the orthogonal matrix that diagonalizes the second derivative matrix $\mathbf{K}$,

$$\mathbf{K}\cdot\mathbf{U} = \mathbf{U}\cdot\mathbf{\Lambda}, \tag{4.22b}$$

Λ being the diagonal matrix of eigenvalues,

$$\Lambda_{ii} \equiv m\omega_i^2, \qquad i=1,2. \tag{4.22c}$$

The transformation to action-angle variables for the harmonic zeroth order potentials is given by

$$x_i = \sqrt{\frac{2J_i}{m\omega_i}}\,\sin\phi_i \tag{4.23a}$$

$$p_i = \sqrt{2m\omega_i J_i}\,\cos\phi_i \tag{4.23b}$$

with i=1,2. The anharmonicities constitute the perturbation term, which is then switched on according to the function [4.21]

$$\lambda(t) = \frac{t}{T} - \frac{1}{2\pi}\sin\frac{2\pi t}{T}, \tag{4.24}$$

where T is the "switching time", and is taken to be large compared to the two vibrational periods.

At the end ($t=T$) of this process the time t is set equal to zero, and the equations of motion are integrated with the full potential. As explained in Section 2, a tunneling time t_n occurs whenever the component of the velocity vector along the tunneling direction $\hat{\mathbf{n}}_0$ goes through zero (in the outward direction), i.e., whenever the trajectory experiences a classical turning point in that direction; stated perhaps more simply, this is when the component of the coordinate vector (s,Q) along $\hat{\mathbf{n}}_0$ experiences a local maximum.

b) Symmetric double well linearly coupled to a harmonic oscillator

We now apply the model of Section 2 to calculate the tunneling splitting of the ground state in a symmetric double well. The specific form of the model potential that we used for this application is the same as that in Chapters II and III (see also Ref. 4.22)

$$V(s,Q) = V_0(s) + \frac{1}{2}m\omega^2[Q - \frac{f(s)}{m\omega^2}]^2. \qquad (4.25a)$$

Here s is the reaction coordinate, $V_0(s)$ is a symmetric double well,

$$V_0(s) = -\frac{1}{2}a_0 s^2 + \frac{1}{4}c_0 s^4, \qquad (4.25b)$$

$f(s)$ is the coupling function, and Q is the orthogonal harmonic degree of freedom, which is linearly coupled to the reaction coordinate. Notice that the term $[f(s)]^2/2m\omega^2$ in Eq. (4.25a) renormalizes the height of the barrier so that it is independent of the strength of the coupling, and the dependence of the tunneling splitting on the coupling is merely due to the distortion of the potential surface away from the separable case. The constants were chosen such that the barrier height is 7.8 kcal/mol and the two potential minima are located at $s_{\pm}=\pm 0.53$Å; The mass was chosen to be that of a hydrogen atom, and the frequency of the harmonic oscillator was 298 cm^{-1}. These parameters are the same as those in Chapter II (and Ref. 22a) and are typical of H-atom transfer processes.

We considered two different forms of the coupling function $f(s)$, which give rise to different symmetries in the full (coupled) potential: (i) linear coupling, $f(s)=cs$, for which V possesses inversion symmetry, and (ii) quadratic coupling, $f(s)=cs^2$, in which case V has reflection symmetry with respect to the Q axis. Contour plots of the potential in these two different cases for typical values of the coupling constant c are shown in Figures 2-2(b) and 2-2(c) (Chapter II).

In the case of linear coupling, the two wells move apart in the Q direction as the coupling increases. For small values of c, our rule for choosing the tunneling path gives $\hat{n}_0=\hat{s}$, i.e., the trajectories tunnel purely in the s direction (cf. Fig. 4-8a). As the coupling constant gets larger, however, the shortest line that connects the "boxes" becomes the line that connects the nearest corners passing through the transition state (cf. Fig. 4-8b). In the case of quadratic coupling, the tunneling path is always the line that connects the nearest corners, which is in this case the s direction

(cf. Fig. 4-8c).

Since the double well is symmetric, we use the amplitude version of the model, as described at the end of Section 2. Fig. 4-9 shows a typical graph of the net tunneling amplitude $S_{net}(t)$ defined by Eq. (4.7a), with $S_n = e^{-\theta_n}$, averaged over 1000 trajectories. The linear character of this function is obvious, and the slope gives the tunneling splitting according to Eq. (4.7c). Figures 4-10 and 4-11 show the tunneling splitting ΔE as given by this semiclassical model, normalized by the exact (quantum) value ΔE_0 of the tunneling splitting at zero coupling, as a function of the square of the coupling constant c, for the cases of linear and quadratic coupling. Also shown are the exact quantum mechanical values of $\Delta E/\Delta E_0$, obtained by numerical diagonalization of the Hamiltonian in a basis set. The agreement between the semiclassical results and the exact ones is remarkable, even when the coupling is very strong.

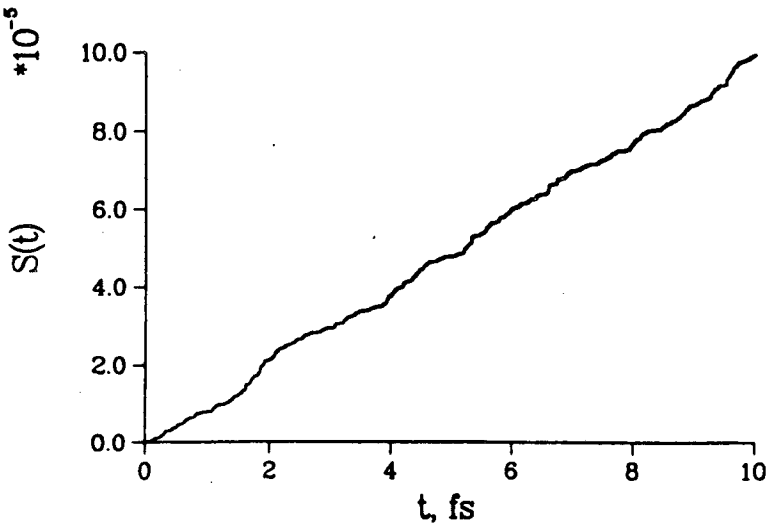

Fig. 4-9

The net tunneling amplitude [cf. Eq. (4.7a)], averaged over 1000 trajectories, for a trajectory in the potential of Fig. 2-2b.

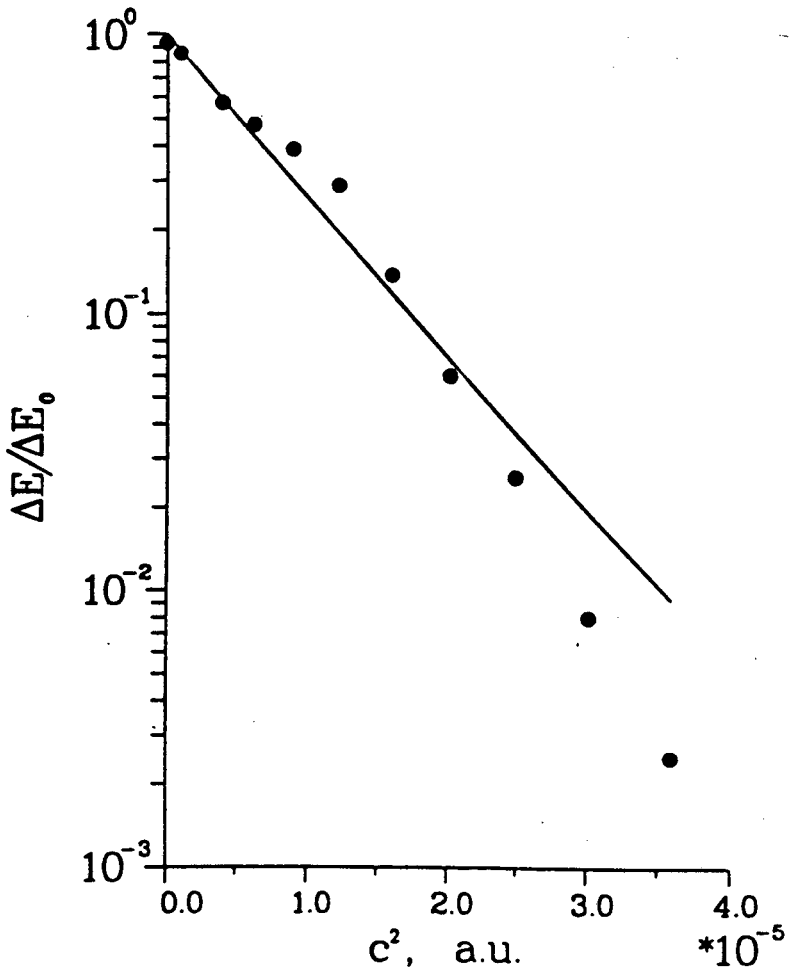

Fig. 4-10

The tunneling splitting ΔE, normalized by the exact quantum value ΔE_0 of the splitting in the one-dimensional double well, as a function of the square of the coupling constant c, for the case of linear coupling, $f(s)=cs$. Solid line: exact quantum results, obtained by a basis set calculation. Circles: results obtained by using the semiclassical model presented in this Chapter.

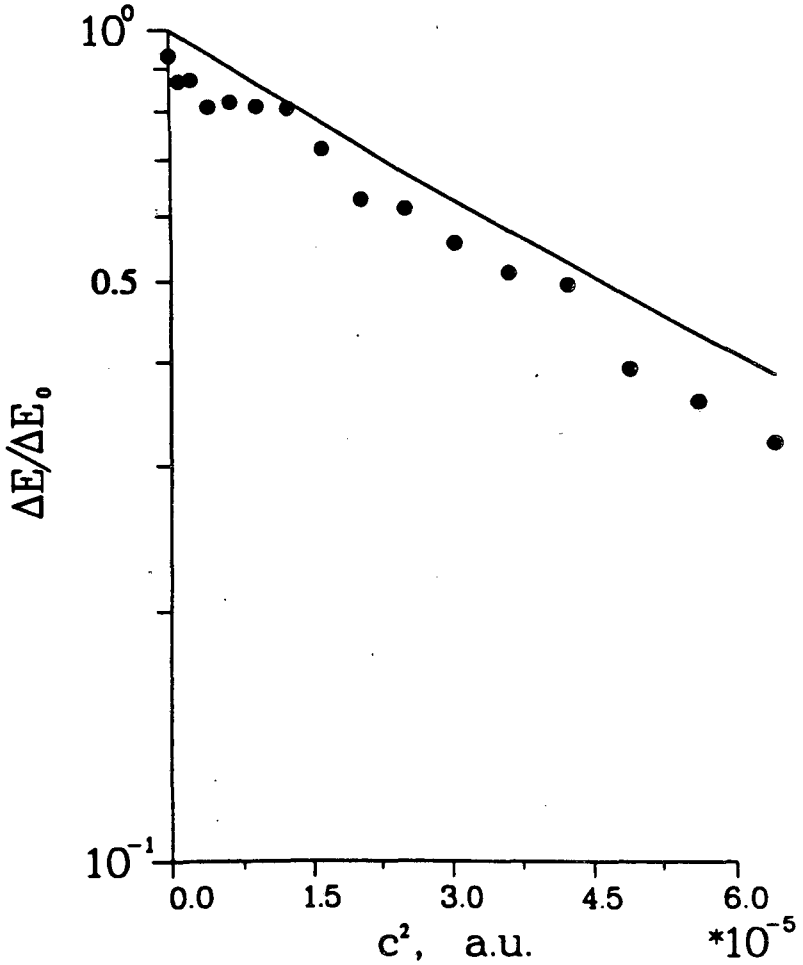

Fig. 4-11

The tunneling splitting ΔE, normalized by the exact quantum value ΔE_0 of the splitting in the one-dimensional double well, as a function of the square of the coupling constant c, for the case of quadratic coupling, $f(s)=cs^2$. Solid line: exact quantum results, obtained by a basis set calculation. Circles: results obtained by using the semiclassical model presented in this Chapter.

c) *Two-dimensional potentials for H atom transfer in malonaldehyde and in the formic acid dimer*

We now present calculations for the tunneling splittings in two H-atom reactions, approximated by two-dimensional potentials, using the semiclassical tunneling model of Section 2.

The first reaction is the symmetric isomerization of malonaldehyde, reaction (4.2). The reaction coordinate s corresponds to the displacement of the hydrogen atom, and the orthogonal degree of freedom Q in our two-dimensional model is the symmetric O-O stretch, which is strongly coupled to the H motion. The Hamiltonian is written in the reaction path form:[4.23]

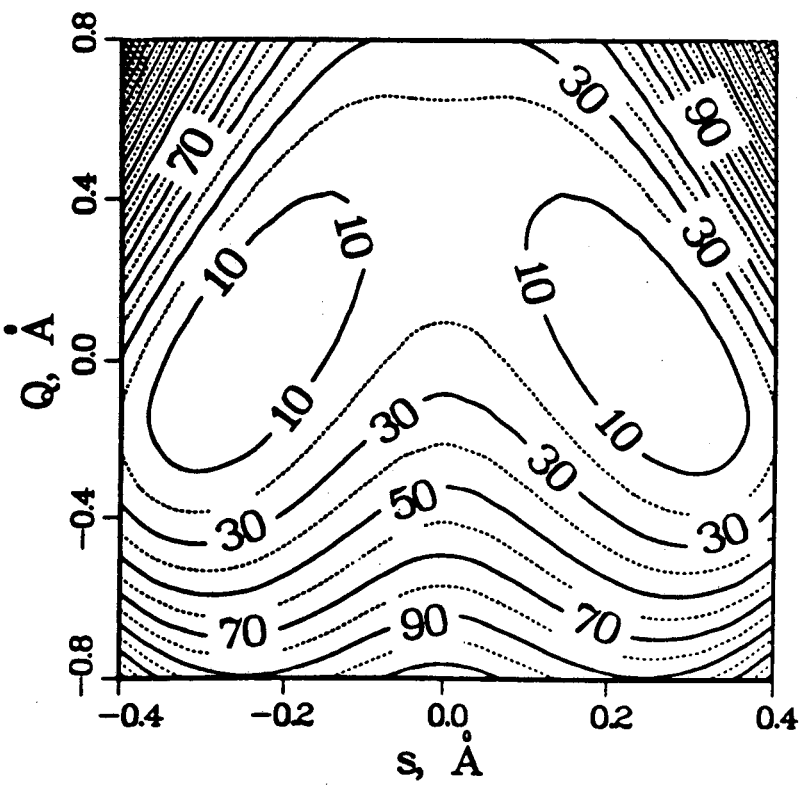

Fig. 4-12

Contour plot of the two-dimensional potential that incorporates the most important features of the H-atom transfer in malonaldehyde [cf. Eq. (4.2)].

$$H = \frac{p_s^2}{2m} + \frac{p_Q^2}{2m} + V_0(s) + f(s)Q + \frac{1}{2}K(s)Q^2, \tag{4.26}$$

with m=5367.8 in atomic units. A contour plot of the potential of Eq. (4.26) is shown in Fig. 4-12.

Because of the symmetry of the potential, the tunneling direction is the s axis. The value of the tunneling splitting predicted for this potential by the semiclassical model is equal to 2.8 cm^{-1}. To compare with exact results, we diagonalized the Hamiltonian in a two-dimensional basis set composed out of particle in a box basis functions. The numerically exact splitting obtained this way is 11.9 cm^{-1} and compares well with the result of the semiclassical calculation, given the fact that the tunneling splitting that corresponds to the one-dimensional potential V_0 is 0.042 cm^{-1}, i.e., the coupling is so strong that it increases the value of the splitting by a factor of 280.

The second tunneling reaction involves the simultaneous transfer of two H atoms in the formic acid dimer:

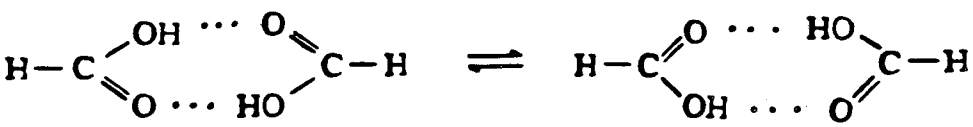

(4.27)

The two-dimensional Hamiltonian that we used to model this reaction has the form

$$H = \frac{p_s^2}{2} + \frac{p_Q^2}{2} + V(s,Q). \tag{4.28}$$

Here s and Q are mass-weighted cartesian coordinates and $V(s,Q)$ is a polynomial 4th order in s and 15th order in Q.[4.24] Fig. 4-13 shows a contour plot of this potential. The tunneling direction is the line connecting nearest corners and because of the inversion symmetry of the potential, the tunneling path passes through the transition state.

The tunneling splitting predicted by our semiclassical model is 0.9 cm^{-1} while numerical diagonalization [4.24] of the Hamiltonian yields a value of 1.8 cm^{-1}. Thus the result of the semiclassical tunneling model agrees with the exact splitting to within a factor of 2.

d) Unimolecular decay rates

Finally, we apply the tunneling model (the probability version of it) to calculate the decay rate from the ground quasi-bound state (i.e., lowest energy resonance) of a two-dimensional potential which has the form

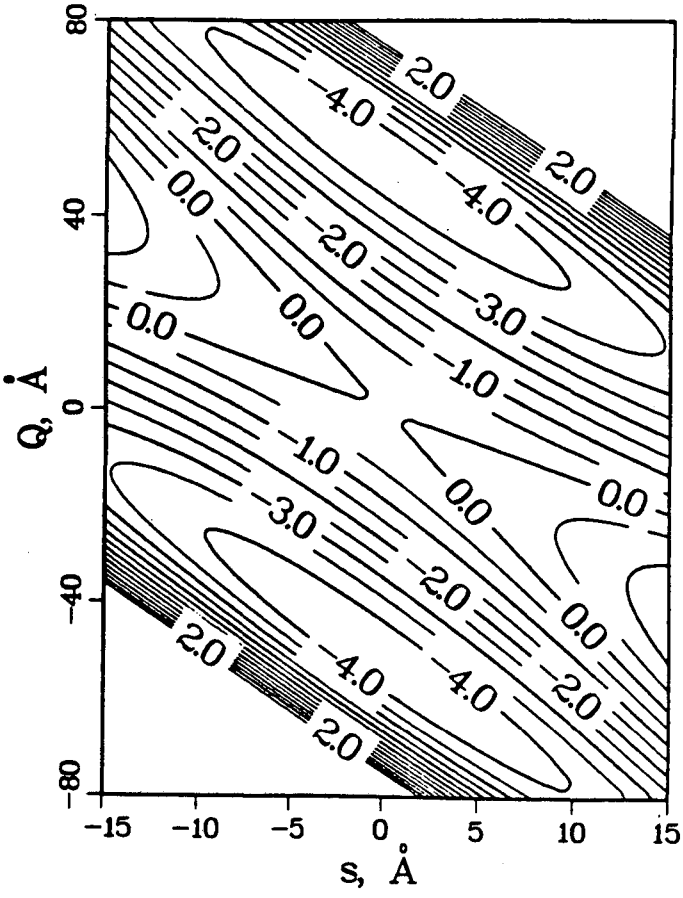

Fig. 4-13

Contour plot of the two-dimensional potential that incorporates the most important features of the H-atom transfer in the formic acid dimer [cf. Eq. (4.27)].

$$V(s,Q) = V_0(s) + \frac{1}{2}m\omega^2 Q^2 - csQ \tag{4.29a}$$

where

$$V_0(s) = \frac{1}{2}a_0 s^2 - \frac{1}{3}b_0 s^3. \tag{4.29b}$$

The one-dimensional potential V_0 is shown in Fig. 4-14; the local maximum occurs at s=0.71 Å and the barrier height is 7.4 kcal/mol. The mass was chosen to be that of a hydrogen atom, and the frequency of the harmonic oscillator was 298 cm^{-1}. Fig. 4-15 shows a contour plot of the two-dimensional potential for a typical value of the coupling parameter c. The semiclassical decay rate was calculated according to Eq. (4.6).

In order to generate accurate quantum mechanical results for comparison, we computed the width of the resonance using the method of complex scaling.[4.25] The s coordinate was rotated as $s \rightarrow se^{i\alpha}$, while the Q coordinate remained real. The complex scaled Hamiltonian was then diagonalized in a basis set of (real) particle in a box basis functions and the complex eigenvalues

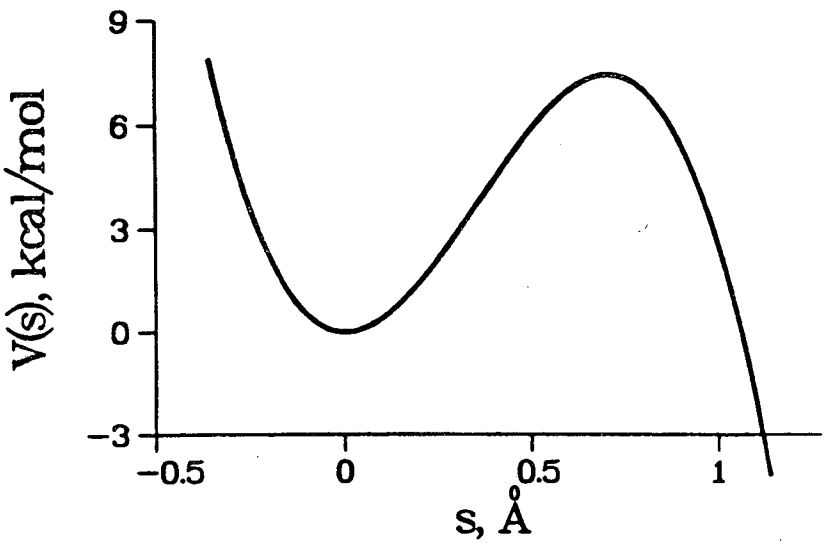

Fig. 4-14

The potential V_0 which was used in the calculation of the unimolecular decay rate of Section 3d [cf. Eq. (4.29b)].

$$E = E_R + iE_I \tag{4.30a}$$

which were stable under change of the scaling angle α were identified as resonances, whose width is

$$\Gamma = -2E_I. \tag{4.30b}$$

The decay rate k is obtained in terms of the resonance width according to

$$k = \frac{\Gamma}{\hbar}. \tag{4.30c}$$

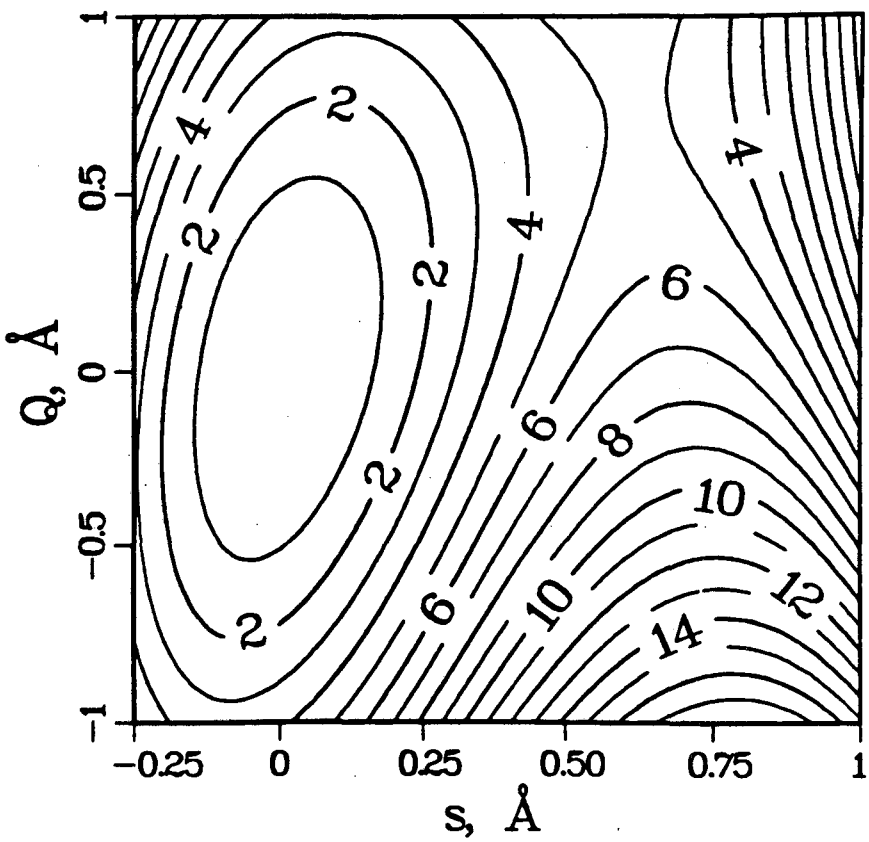

Fig. 4-15

Contour plot of the two-dimensional potential used in the calculations of Section 3d [cf. Eq. (4.29)], for c=0.004 hartree/bohr^2. The potential in the s coordinate is shown in Fig. 4-14, while the Q coordinate is a harmonic oscillator of frequency 298 cm^{-1}.

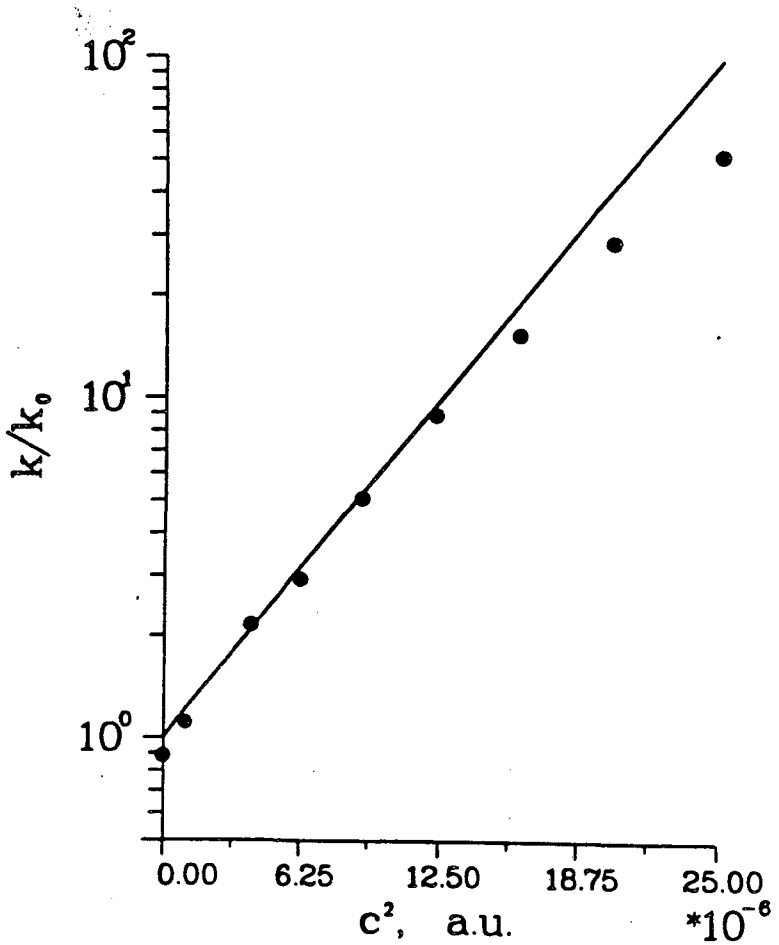

Fig. 4-16

The decay rate k, normalized by the exact quantum value k_0 of the rate in the one-dimensional potential V_0, as a function of the square of the coupling constant c. Solid line: exact quantum results, obtained by the method of complex scaling. Circles: results obtained by using the semiclassical model described in this Chapter.

Fig. 4-16 compares the results of the semiclassical model for the decay rate with the quantum mechanical ones, i.e., those of the complex scaling calculation. Plotted is the decay rate k (normalized by the exact quantum value of the rate for the uncoupled potential) as a function of the square of the coupling constant c. The agreement is of the same quality as in the previous applications - within a factor of 2 in the worst case, while the coupling is so strong that it has increased the value of k by two orders of magnitude.

4. Discussion and concluding remarks

The examples treated in the previous Section show that the semiclassical model presented in Section 2 provides an excellent description of tunneling in multidimensional systems typical of polyatomic molecules. Although these applications were for two-dimensional systems - so that the exact quantum results could be easily generated for comparison - the important feature of the semiclassical model is that it can be readily applied to truly *multi*dimensional systems. Applicability was, in fact, the essential criterion we have kept in mind in constructing the model; there do exist more rigorous semiclassical descriptions of multidimensional tunneling,[4.3–4.5] but they are not easily implemented within a standard classical trajectory simulation.

The necessary condition for the validity of the semiclassical model is that the classical phase space that corresponds to the given quantum state be regular. Stochastic regions generally occupy a small fraction of phase space at low energies, much smaller than Planck's quantum, and thus semiclassical eigenstates are well defined there. Semiclassical theory is unable to deal with highly excited states, for which phase space is dominated by chaotic regions [see Figures 4-17 and 4-18].

Finally, in order to keep the description simple, we assumed that the projection of the trajectory manifold onto configuration space has a simple box-like structure, as is typical of motion away from low order resonances. Classically, resonances occur

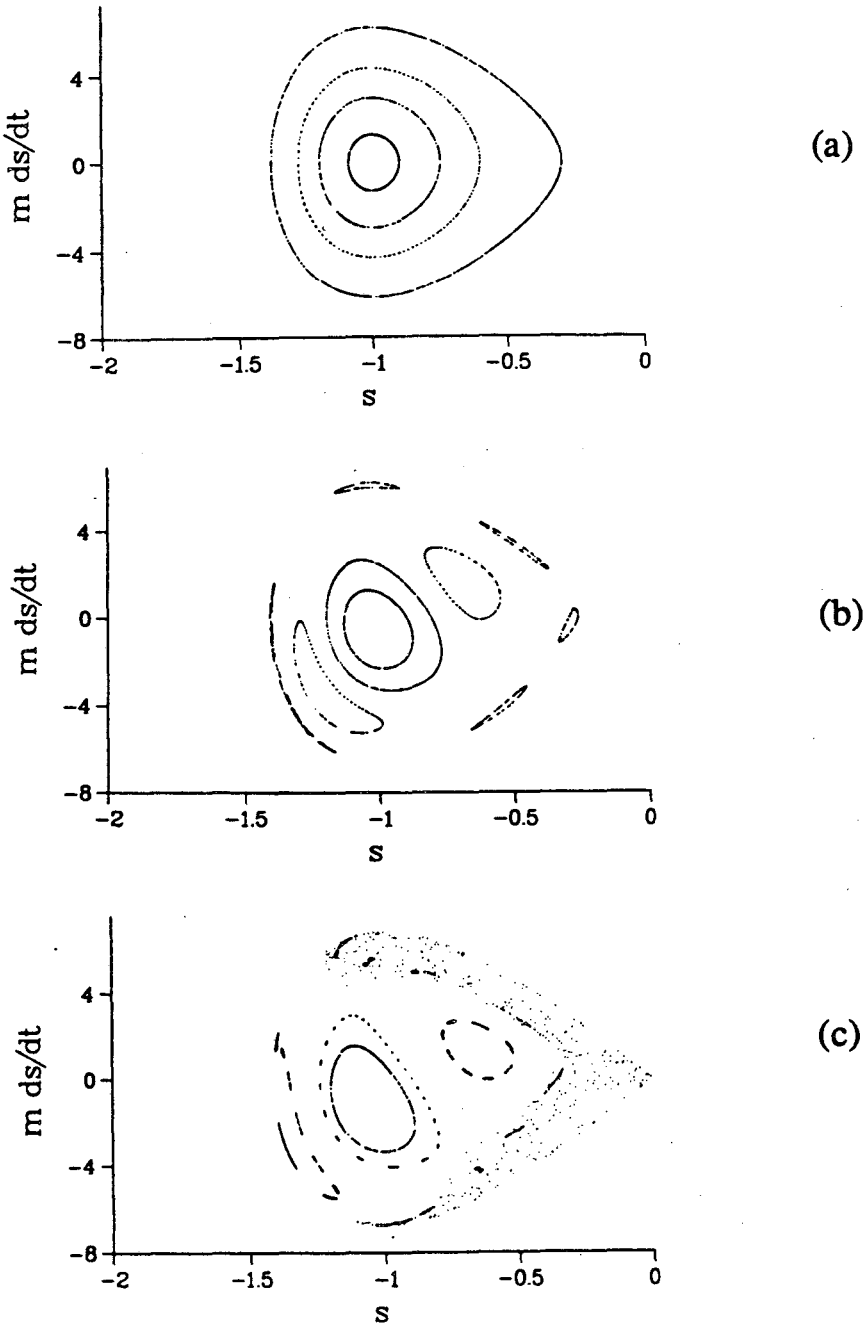

Fig. 4-17

Poincare surfaces of section [4.15a] for the double well system of Section 3 with linear coupling, at energy corresponding to the top of the potential barrier, for three different values of the coupling constant. Plotted is the momentum p_s as a function of the coordinate s every time the trajectory intersects the $Q=0$ plane with $p_Q>0$. (a) Uncoupled case, $c=0$. (b) $c=0.02$. (c) $c=0.04$. It is seen that the area occupied by stochastic motion increases as the coupling increases.

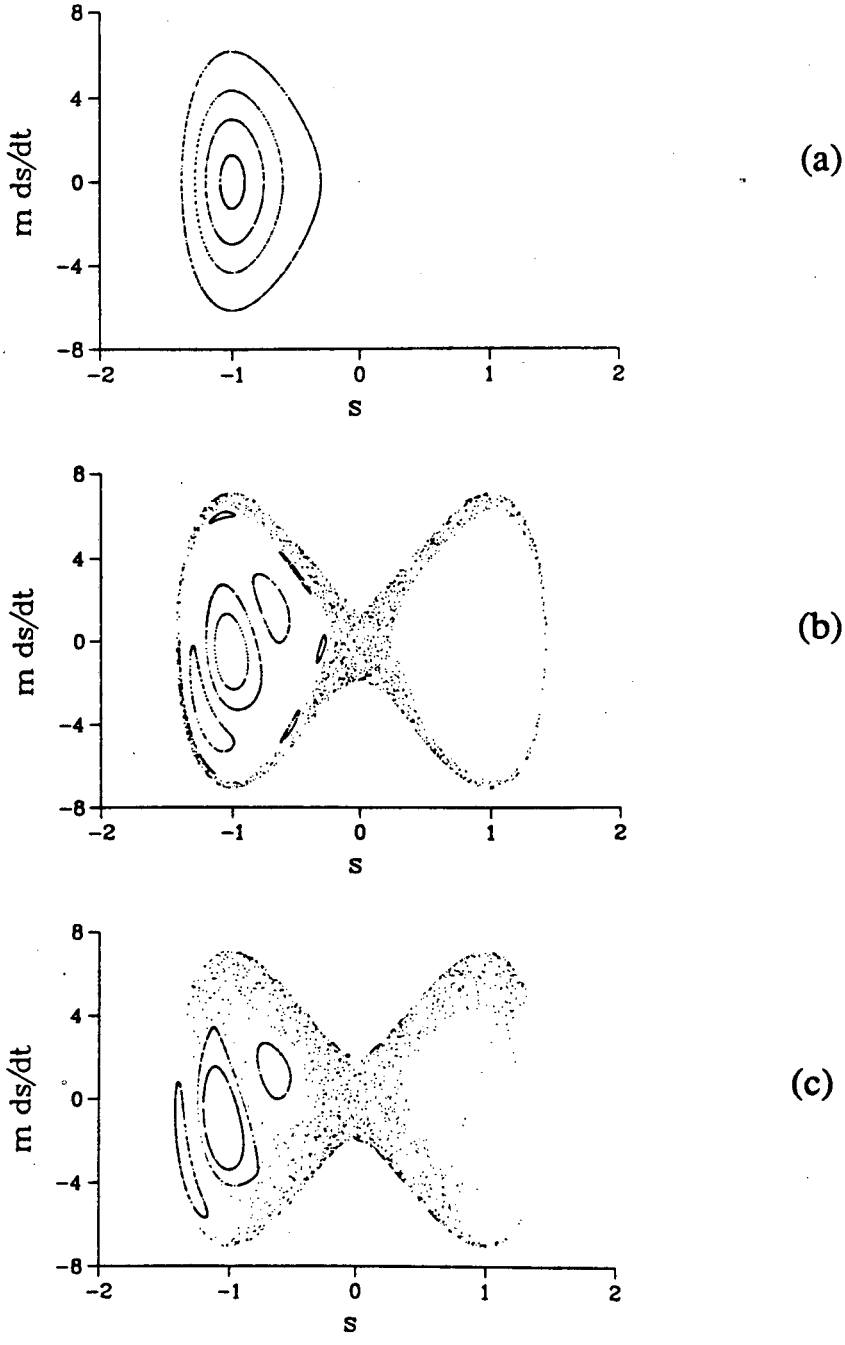

Fig. 4-18

Poincare surfaces of section [4.15a] for the double well system of Section 3 with linear coupling, at energy above the top of the potential barrier, for three different values of the coupling constant. Plotted is the momentum p_s as a function of the coordinate s every time the trajectory intersects the $Q=0$ plane with $p_Q>0$. (a) Uncoupled case, $c=0$. (b) $c=0.02$. (c) $c=0.04$. It is seen that the area occupied by stochastic motion is in each case larger than that shown in Fig. 4-17, and increases as the coupling increases.

when the frequencies of the N degrees of freedom are rationally dependent, i.e., when there exist N integer coefficients which make a linear combination of the frequencies equal to zero. Thus, for two degrees of freedom, resonances appear when the ratio of the two frequencies (the *winding number*) is a rational number. The presence of resonances, especially of low order (i.e., such that the winding number is a fraction whose numerator and denominator are small integers) complicate the structure of phase space. A resonant trajectory for the double well system of Section 3b and the Poincare surfaces of section [4.15a] which correspond to the same energy are shown in Figures 4-19 and 4-20. Tunneling from resonant tori can probably be treated in a similar way, although we have not dealt with such complications in the present work. (For example, the picture would simplify drastically if one could perform a canonical transformation that would "unfold" the resonant trajectory.

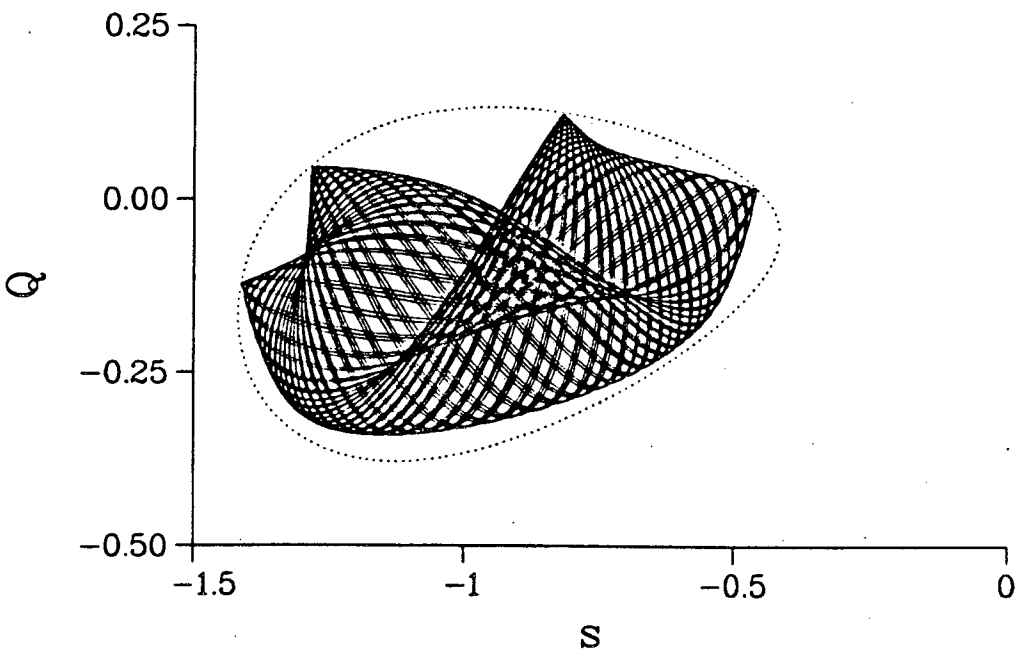

Fig. 4-19

A resonant trajectory for the double well system of Section 3 with linear coupling for higher frequency and at higher energy than the examples treated in Section 3. The dotted line shows the boundary of the energetically accessible region.

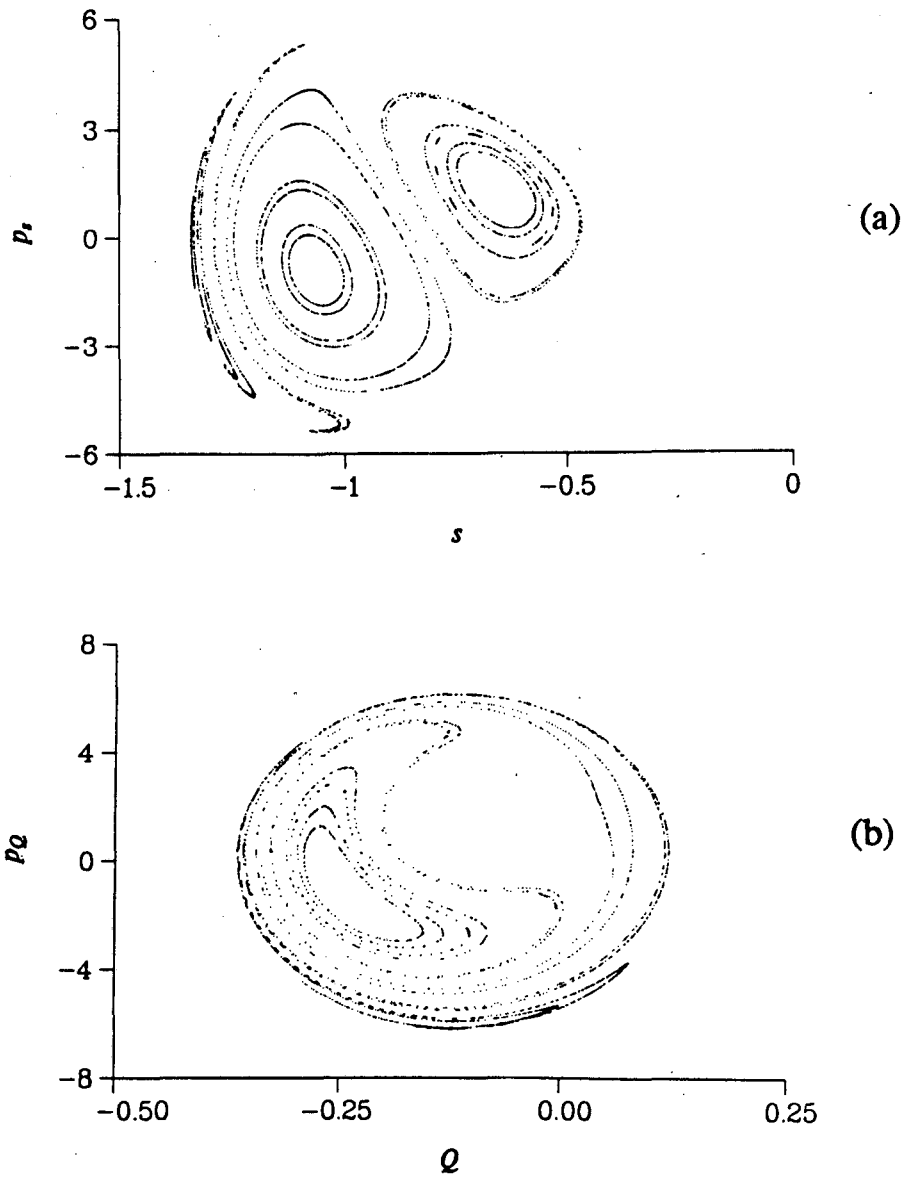

Fig. 4-20

The Poincare surfaces of section [4.15a] at the energy of the trajectory shown in Fig. 4.19. (a) Plotted is the momentum p_s as a function of the coordinate s every time the trajectory intersects the Q=0 plane with p_Q>0. (b) Plotted is the momentum p_Q as a function of the coordinate Q every time the trajectory intersects the s=0 plane with p_s>0.

In conclusion, the results of the applications in Section 3 are quite impressive. If the two degrees of freedom are uncoupled, then the semiclassical model is for all practical purposes exact (i.e., correct to about 10% typically), but the accuracy of the results (tunneling splittings or decay rates) decreases to only a factor of 2 or so error even when the coupling between the degrees of freedom is so strong as to change the result by 2 orders of magnitude from its uncoupled value. This is as good as (or even better than) some of the best approximate quantum methods, e.g., the multi-configuration time dependent Hartree-Fock approximation,[4.22b] that are much more difficult to apply.

References

4.1 For a recent survey of classical trajectory methodology and application, see L. M. Raff and D. L. Thompson, in *Theory of Chemical Reaction Dynamics* vol. III, edited by M. Baer, CRC Press, Boca Raton, FL 1985, pp. 1-122.

4.2 W. H. Miller, *J. Chem. Phys.* **54**, 5386 (1971).

4.3 (a) W. H. Miller, *Adv. Chem. Phys.* **25**, 69 (1974);
(b) W. H. Miller, *Adv. Chem. Phys.* **30**, 74 (1975);
(c) W. H. Miller, *Science*, **233**, 171 (1986).

4.4 W. H. Miller, *J. Chem. Phys.* **62**, 1899 (1975).

4.5 (a) S. Coleman, Uses of instantons, in *The Whys of Subnuclear Physics*, edited by A. Zichichi, Plenum, N.Y., 1979, pp. 805-916;
(b) A. O. Caldiera and A. J. Leggett, *Ann. Phys.* (N.Y.) **149**, 374 (1983).

4.6 Some examples are:
(a) D. G. Truhlar and B. C. Garrett, *Ann. Rev. Phys. Chem.* **35**, 159 (1984);
(b) G. C. Lynch, D. G. Truhlar, and B. C. Garrett, fIJ. Chem. Phys. **90**, 3102 (1989);
(c) R. A. Marcus and M. E. Coltrin, *J. Chem. Phys.* **67**, 2609 (1977);
(d) C. J. Cerjan, S. Shi, and W. H. Miller, *J. Phys. Chem.* **86**, 2244 (1982).

4.7 J. C. Tully and R. K. Preston, *J. Chem. Phys.* **55**, 562 (1971).

4.8 B. A. Waite and W. H. Miller, *J. Chem. Phys.* **76**, 2412 (1982).

4.9 E. J. Heller and R. C. Brown, *J. Chem. Phys.* **79**, 3336 (1983).

4.10 See, for example, K. W. Ford, D. L. Hill, M. Wakano, and J. A. Wheeler, *Ann. Phys.* (N.Y.) **7**, 239 (1959).

4.11 Eq. (2.2a) is correct for small tunneling probabilities, $P_n \ll 1$. More generally, one must include a "survival probability" factor, so that Eq. (2.2a) becomes

$$P_{net}(t) = \sum_{n=1} h(t-t_n)p_n ,$$

where $p_1 = P_1$ and $p_n = P_n(1 - \sum_{n'=1}^{n-1} p_{n'})$ for n>1, with P_n still given by Eq. (2.2b).

4.12 Also see the discussion by W. H. Miller, *J. Chem. Phys.* **83**, 960 (1979).

4.13 (a) T. F. George and W. H. Miller, *J. Chem. Phys.* **56**, 5722 (1972);
(b) T. F. George and W. H. Miller, *J. Chem. Phys.* **57**, 2458 (1972).

4.14 S. Chapman, B. C. Garrett, and W. H. Miller, *J. Chem. Phys.* 63, 2710 (1975).

4.15 (a) A. J. Lichtenberg and M. A. Lieberman, *Regular and Stochastic Motion* (Springer, New York, 1983);
(b) M. V. Berry, Regular and irregular motion, in *Topics in Nonlinear Dynamics*, S. Joma, ed. A.I.P. Conference Proceedings 46, 1976;
V. I. Arnold, *Mathematical Methods of Classical Mechanics* (Springer, New York, 1978).

4.16 V. P. Maslov and M. V. Fedoriuk, *Semiclassical Approximation in Quantum Mechanics*, Reidel, Boston, 1981.

4.17 (a) A. Einstein, *Verh. Dtsch. Phys. Ges.* 19, 82 (1917);
(b) M. L. Brillouin, *J. Phys.* 7, 353 (1926);
(c) J. B. Keller, *Ann. Phys.* 4, 180 (1958).

4.18 P. Pechukas, *J. Chem. Phys.* **57**, 5577 (1972).

4.19 M. Wilkinson, *Physica* **21***D*, 341 (1986).

4.20 (a) E. A. Solv'ev, *Soviet Physics JETP* 48, 635 (1978);
(b) R. T. Skodje, F. Borondo, and W. P. Reinhardt, *J. Chem. Phys.* **82**, 4611 (1985).

4.21 B. R. Johnson, *J. Chem. Phys.* **83**, 1204 (1984).

4.22 (a) N. Makri and W. H. Miller, *J. Chem. Phys.* **86**, 1451 (1987);
(b) N. Makri and W. H. Miller, *J. Chem. Phys.* **87**, 5781 (1987).

4.23 B. A. Ruf, private communication.

4.24 Y. T. Chang, private communication.

4.25 (a) B. R. Junker, *Adv. Atom. Mol. Phys.* **18**, 207 (1982);
(b) W. P. Reinhardt, *Ann. Rev. Phys. Chem.* **33**, 223 (1982);
(c) B. A. Waite and W. H. Miller, *J. Chem. Phys.* 74, 3910 (1981).

PART B

V. Monte Carlo Path Integration in Real Time

1. Introduction

Feynman path integration [5.1] provides an alternate formulation of quantum mechanics. Over the past several years, the path integral representation of the propagator, $\exp(-iHt/\hbar)$, has found extensive use as a starting point for deriving semiclassical approximations to quantum dynamical phenomena and has proved to be a powerful technique for evaluating equilibrium statistical mechanical properties. Its power lies in the fact that, unlike basis set methods, it can be used effectively to deal with systems of many degrees of freedom. Another attractive feature is that harmonic "bath" type degrees of freedom (which occur in many areas of chemical physics) can be integrated out *exactly* using the influence functional theory [5.2] of the path integral formalism, thus reducing the problem to one of low dimensionality.

In order to evaluate the coordinate matrix element of the propagator $\langle \mathbf{x}_f | \exp(-iHt/\hbar) | \mathbf{x}_0 \rangle$ according to the path integral idea, one utilizes the fact that accurate approximations for the former are available for *short* (real or imaginary) time. The total time t is thus split into N "short" time increments $\Delta t = t/N$, and the propagator is written as the product of N short time propagators. Insertion of $N-1$ complete sets of position eigenstates allows then the propagator to be expressed in the form

$$\langle \mathbf{x}_f | \exp(-iHt/\hbar) | \mathbf{x}_0 \rangle = \int d\mathbf{x}_{N-1} \cdots \int d\mathbf{x}_1 \prod_{k=1}^{N} \langle \mathbf{x}_k | \exp(-iH\Delta t/\hbar) | \mathbf{x}_{k-1} \rangle, \qquad (5.1)$$

where $\mathbf{x}_N \equiv \mathbf{x}_f$. Each set of coordinate points $\{\mathbf{x}_k\}$ in Eq. (5.1) defines a discrete path that connects $\mathbf{x}_0$ and $\mathbf{x}_f$ (see Fig. 5-1). Integrating over all points $\{\mathbf{x}_k\}$ is (in the limit $N \rightarrow \infty$) equivalent to *summing over all paths* that connect the given initial and final points in time t.

All such paths contribute with the same weight, but different phases in the sum.

The phase factor for a given path α is proportional to the classical action $S[\mathbf{x}_\alpha(t)]$ along the path,[5.1] and the propagator is given by

$$\langle \mathbf{x}_f | \exp(-iHt/\hbar) | \mathbf{x}_0 \rangle \propto \sum_\alpha e^{\frac{i}{\hbar} S[\mathbf{x}_\alpha(t)]}, \tag{5.2}$$

where

$$S[\mathbf{x}_\alpha(t)] = \int_0^t L(\mathbf{x}_\alpha(t'); \dot{\mathbf{x}}_\alpha(t'); t')dt' = \int_0^t [\frac{1}{2} m \dot{\mathbf{x}}_\alpha(t')^2 - V(\mathbf{x}_\alpha(t'))]dt'. \tag{5.3}$$

The oscillatory character of the integrand in Eq. (5.2) results in enormous cancellation; the main contribution to the result comes from paths for which the action is slowly varying. In the limit $\hbar \to 0$, only paths for which the action is *stationary* contribute. But such paths are those determined from the classical equations of motion, and thus classical mechanics is obtained from the quantum mechanical path integral formalism in the small $\hbar$ limit.

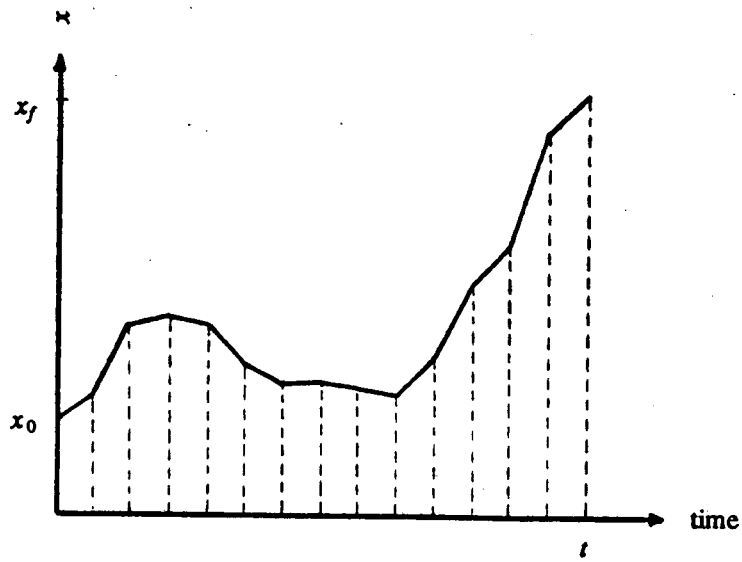

Fig. 5-1

A discretized path that connects points x_0 and x_f in time t.

Numerical evaluation of the propagator according to the path integral prescription, Eq. (5.1), requires multidimensional integration, even for a one degree of freedom problem. Importance sampling techniques [5.3] are ideally suited for this task when the integrand is positive definite. While the computational effort that is required for the numerical evaluation of a path integral is much greater than the effort required to obtain the complete quantum mechanical solution of a one dimensional problem by other techniques (e.g., by basis set calculations), the situation changes entirely as the dimensionality of the problem increases. This is so because the difficulty in carrying out a path integral grows *slowly* (unlike other methods) with the number of degrees of freedom.

Until recently, Feynman path integration has found most utility in chemical/molecular dynamics as an elegant tool for deriving semiclassical approximations to quantum dynamical processes.[5.4,5.5] Only in the last few years has there begun to be interest in using it as a numerical method for carrying out completely quantum mechanical simulations for the dynamics of complex (i.e., non-analytically solvable) systems.[5.6–5.11] The reason for this slow development is that the path integral expression for the propagator is a multidimensional integral whose integrand is a *complex* exponential function, and thus oscillatory. This appears to obviate the use of the Monte Carlo integration method, which is the only general approach one has for dealing with highly multidimensional integrals. (In contrast, the integrand of the corresponding path integral representation of the Boltzmann operator, $e^{-\beta H}$, is a *real* exponential and thus directly amenable to Monte Carlo integration methods. A number of impressive calculations for the quantum statistical mechanics of quite complex systems have been carried out this way.[5.12–5.16])

In this Chapter we present a new approach to Monte Carlo evaluation of integrals with oscillatory integrands,[5.17] of the type occuring in the path integral representation of the time evolution operator. The method is quite general and has

the highly desirable feature that it incorporates the stationary phase approximation - i.e., the semiclassical limit of the path integral - as its worst limit. Section 2 develops the new idea and Section 3 illustrates the method with a simple but non-trivial example. Specifics of applying the method to real time path integrals are detailed in Section 4, and the results of test calculations are presented and discussed in Section 5.

2. The method

a) The basic idea

In this Section we consider the generic multidimensional integral

$$K = \int_{-\infty}^{\infty} d\mathbf{x}\, e^{iS(\mathbf{x})}. \tag{5.4}$$

We begin, following Filinov,[5.18] by inserting unity in the form

$$1 = \int_{-\infty}^{\infty} d\mathbf{x}_0 \sqrt{\det(\mathbf{B}/2\pi)}\; e^{-\frac{1}{2}(\mathbf{x}-\mathbf{x}_0)\cdot\mathbf{B}\cdot(\mathbf{x}-\mathbf{x}_0)} \tag{5.5}$$

(where **B** is a positive matrix) into the integrand of Eq. (5.4). By interchanging the order of integration, the integral becomes

$$K = \int_{-\infty}^{\infty} d\mathbf{x}_0 \sqrt{\det(\mathbf{B}/2\pi)} \int_{-\infty}^{\infty} d\mathbf{x}\; e^{iS(\mathbf{x}) - \frac{1}{2}(\mathbf{x}-\mathbf{x}_0)\cdot\mathbf{B}\cdot(\mathbf{x}-\mathbf{x}_0)}. \tag{5.6}$$

Since the Gaussian factor insures that values of $\mathbf{x}$ near $\mathbf{x}_0$ dominate the integral over $\mathbf{x}$, we expand $S(\mathbf{x})$ in a Taylor series about $\mathbf{x}_0$ through quadratic terms:

$$S(\mathbf{x}) \approx S(\mathbf{x}_0) + \mathbf{S}_1(\mathbf{x}_0)\cdot(\mathbf{x}-\mathbf{x}_0) + \frac{1}{2}(\mathbf{x}-\mathbf{x}_0)\cdot\mathbf{S}_2(\mathbf{x}_0)\cdot(\mathbf{x}-\mathbf{x}_0), \tag{5.7}$$

where $\mathbf{S}_1(\mathbf{x}) = \partial S/\partial\mathbf{x}$ and $\mathbf{S}_2(\mathbf{x}) = \partial^2 S/\partial\mathbf{x}\partial\mathbf{x}$. This allows the $\mathbf{x}$-integration to be performed analytically, yielding

$$K \approx K(\mathbf{B})$$

$$\equiv \int_{-\infty}^{\infty} d\mathbf{x}_0 \, e^{iS(\mathbf{x}_0)} [\det(1 - i\,\mathbf{S}_2(\mathbf{x}_0)\cdot\mathbf{B}^{-1})]^{-1/2} \, e^{-\frac{1}{2}\mathbf{S}_1(\mathbf{x}_0)\cdot[\mathbf{B}-i\,\mathbf{S}_2(\mathbf{x}_0)]^{-1}\cdot\mathbf{S}_1(\mathbf{x}_0)} . \tag{5.8}$$

At this point we depart from Filinov's procedure and note that Eq. (5.5) is true if **B** is complex, and is approximately true even if **B** is a function of x_0; we make the specific choice

$$\mathbf{B} = \mathbf{B}(\mathbf{x}_0) = i\,\mathbf{S}_2(\mathbf{x}_0) + \mathbf{c}^{-1}, \tag{5.9}$$

so that Eq. (5.8) becomes

$$K \approx K(\mathbf{c}) \equiv \int_{-\infty}^{\infty} d\mathbf{x}_0 \, e^{iS(\mathbf{x}_0)} \sqrt{\det[1 + i\,\mathbf{c}\cdot\mathbf{S}_2(\mathbf{x}_0)]} \, e^{-\frac{1}{2}\mathbf{S}_1(\mathbf{x}_0)\cdot\mathbf{c}\cdot\mathbf{S}_1(\mathbf{x}_0)} . \tag{5.10}$$

The matrix **c** is a constant positive matrix; for example, one may take $\mathbf{c} = c\,\mathbf{1}$, where $c > 0$.

Eq. (5.10) is the basic result of this Section and appeared first in Ref. 5.17. This multidimensional integral is evaluated by Monte Carlo with the function

$$p(\mathbf{x}_0) = e^{-\frac{1}{2}\mathbf{S}_1(\mathbf{x}_0)\cdot\mathbf{c}\cdot\mathbf{S}_1(\mathbf{x}_0)} \tag{5.11a}$$

as the (un-normalized) probability distribution from which points are sampled, i.e., the Monte Carlo approximation to the integral is

$$K(\mathbf{c}) = \int_{-\infty}^{\infty} d\mathbf{x}\, p(\mathbf{x}) \, \frac{1}{M} \sum_{j=1}^{M} e^{iS(\mathbf{x}_j)} \sqrt{\det[1 + i\,\mathbf{c}\cdot\mathbf{S}_2(\mathbf{x}_j)]}, \tag{5.11b}$$

where the M values $\mathbf{x}_j$ are chosen at random from the distribution $p(\mathbf{x})$. The Metropolis algorithm [5.3], the stochastic dynamics algorithm [5.19], etc., are standard ways for doing this. The error in Eq. (5.11b) decreases with increasing M as $M^{-1/2}$.

The method is similar to the original idea of "stationary phase Monte Carlo" first suggested by Doll.[5.20] This is so because the distribution p most strongly weights the regions about the stationary phase points [values of $\mathbf{x}_0$ for which $\mathbf{S}_1(\mathbf{x}_0)=0$].

Choosing a large value for the constant c causes very narrow sampling about the stationary phase points, and the Monte Carlo statistics are thus excellent. There is the question, though, of how well $K(\mathbf{c})$ approximates the original integral K when c is large; in the limit $c \to \infty$, in fact, one can show that $K(\mathbf{c})$ becomes the *stationary phase approximation* to K[5.21]:

$$\lim_{c \to \infty} K(\mathbf{c}) = \sum_{\mathbf{x}_{SP}} e^{iS(\mathbf{x}_{SP})} \sqrt{\det(2\pi i / S_2)}. \tag{5.12a}$$

In the opposite limit, that c is small, it is easy to see that the exact integral is recovered:

$$\lim_{c \to 0} K(\mathbf{c}) \to K, \tag{5.12b}$$

but the Monte Carlo statistics become poor because the distribution p becomes very broad. In practice, therefore, one evaluates $K(\mathbf{c})$ for several values of c, taking it as small as acceptable Monte Carlo error allows, knowing that in the "worst" limit, $c \to \infty$, $K(\mathbf{c})$ becomes the stationary phase approximation to K. This feature renders our method superior to Doll's original stationary phase Monte Carlo idea. In Section 2b we show how one can actually calculate the error introduced by finite c, i.e., a Monte Carlo estimate of the difference between $K(\mathbf{c})$ and K. Finally, Eq. (5.10) has the useful property that $K(\mathbf{c})=K$ identically for all values of c if $S(\mathbf{x})$ is a quadratic function of the integration variables.

Since the stationary phase approximation to a path integral gives semiclassical dynamics,[5.4,5.5] one interesting way to view the application of the modified Filinov procedure to path integrals is as a systematic way to correct semiclassical approximations (e.g., the classical S-matrix [5.5] in scattering, etc.). This is a major step forward for, although semiclassical approximations are often quite accurate,[5.4,5.5] there has heretofore been no systematic way to improve on semiclassical results when they were not sufficiently accurate. The modified Filinov algorithm for $c<\infty$ may thus be viewed as a way of "turning on" full quantum mechanics, progressively so as c is

decreased, and letting the Monte Carlo calculation correct the semiclassical ($c=\infty$) result.

Finally, it is also useful to note the analogy of the present Monte Carlo calculation to those in classical equilibrium statistical mechanics, for which the (unnormalized) probability distribution function is $p(\mathbf{x}) = e^{-\beta U(\mathbf{x})}$. Comparing to Eq. (2.8), the analogy is $\beta \equiv c$, and the effective "potential" that determines the sampling is $U(\mathbf{x}) \equiv \frac{1}{2}|\mathbf{S}_1(\mathbf{x})|^2$. Stationary phase points thus correspond to local minima of the "potential", with the value $U_{min}=0$. There may be other local minima in this "potential" that are not zero, i.e., where the phase is not stationary but only more slowly varying than in neighboring regions; these are often related to the existence of nearby *complex* stationary phase regions that characterize tunneling-like contributions to the integral.[5.22]

b) The error estimate

It is not difficult to obtain an estimate of the absolute error that is introduced by using a non-zero matrix $\mathbf{c}$ in Eq. (5.10) to approximate the integral of interest, K. The validity of the first approximation that was used in deriving $K(\mathbf{c})$ depends on how well Eq. (5.7) describes $S(\mathbf{x})$ in the region of space that is selected by the exponential

$$e^{-\frac{1}{2}(\mathbf{x}-\mathbf{x}_0)\cdot\mathbf{B}\cdot(\mathbf{x}-\mathbf{x}_0)}$$

in Eq. (5.6). If $\mathbf{B}$ is large, for example, then the integration with respect to $\mathbf{x}$ is restricted to points very close to $\mathbf{x}_0$, in which case the expansion of S through quadratic terms about $\mathbf{x}_0$ will be accurate, even though $S(\mathbf{x})$ itself may be a non-quadratic function when viewed in the entire domain of $\mathbf{x}$ between $-\infty$ and ∞. This can be checked by comparing the integrand of Eq. (5.8),

$$e^{iS(\mathbf{x}_0)}[\det(1-i\,\mathbf{S}_2(\mathbf{x}_0)\cdot\mathbf{B}^{-1})]^{-1/2}\, e^{-\frac{1}{2}\mathbf{S}_1(\mathbf{x}_0)\cdot[\mathbf{B}-i\,\mathbf{S}_2(\mathbf{x}_0)]^{-1}\cdot\mathbf{S}_1(\mathbf{x}_0)} \tag{5.13}$$

which incorporates the approximation of Eq. (5.7), to the true integrand before any approximation was made, that of Eq. (5.6):

$$\sqrt{\det(\mathbf{B}/2\pi)}\int_{-\infty}^{\infty} d\mathbf{x}\, e^{iS(\mathbf{x})-\frac{1}{2}(\mathbf{x}-\mathbf{x}_0)\cdot\mathbf{B}\cdot(\mathbf{x}-\mathbf{x}_0)}. \tag{5.14}$$

The second approximation was introduced by Eq. (5.9). The accuracy of this approximation, however, is closely related to that of the approximation described in the previous paragraph; the integrand of Eq. (5.5) is only large for values of $\mathbf{x}_0$ near $\mathbf{x}$, within a range determined by the magnitude of $\mathbf{B}$. If S is well described by a quadratic function in this region, i.e., $\mathbf{S}_2(\mathbf{x}_0)$ is nearly constant there, then $\mathbf{B}(\mathbf{x}_0)$ will also be nearly constant, and Eq. (5.5) will be accurate. Therefore, if one compares

$$e^{iS(\mathbf{x}_0)}\sqrt{\det[1+i\,\mathbf{c}\cdot\mathbf{S}_2(\mathbf{x}_0)]}\, e^{-\frac{1}{2}\mathbf{S}_1(\mathbf{x}_0)\cdot\mathbf{c}\cdot\mathbf{S}_1(\mathbf{x}_0)} \tag{5.15}$$

to

$$\sqrt{\det[(i\,\mathbf{S}_2(\mathbf{x}_0)+\mathbf{c}^{-1})/2\pi)]}\int_{-\infty}^{\infty} d\mathbf{x}\, e^{iS(\mathbf{x})-\frac{1}{2}(\mathbf{x}-\mathbf{x}_0)\cdot[i\,\mathbf{S}_2(\mathbf{x}_0)+\mathbf{c}^{-1}]\cdot(\mathbf{x}-\mathbf{x}_0)}, \tag{5.16}$$

which are obtained by substituting Eq. (5.9) in Equations (5.13) and (5.14) respectively, one will be testing both approximations. The integral in Eq. (5.16) can be performed using

$$e^{-\frac{1}{2}(\mathbf{x}-\mathbf{x}_0)\cdot\mathbf{c}^{-1}\cdot(\mathbf{x}-\mathbf{x}_0)} \tag{5.17}$$

as the weighting function. If this comparison is carried out at several different values of $\mathbf{x}_0$ and the above quantities [Equations (5.15) and (5.16)] are in good agreement with one another, then Eq. (5.10) will be a good approximation to the exact integral, Eq. (5.4). This test is easy to perform. The rule will be to take c to be as small as the Monte Carlo statistics permit; in general, this means $c<1$. Then c^{-1} will be

large, and Eq. (5.17) will be a sharp weighting function, so that the integral of Eq. (5.16) can be evaluated using a small number of Monte Carlo points. Another attractive feature of this method is that the sampling function that is used is a normalized distribution, and thus no normalization integral (see Section 4) need be computed numerically.

This method was originally reported by Makri and Miller at the American Conference on Theoretical Chemistry (July 1987), and essentially the same idea has recently been suggested by Doll, Freeman and Gillan.[5.23] Tests of this approach have been made on the Airy integral of Section 3 (originally used in Ref. 5.17), as well as in all the applications considered in Section 5, verifying that this procedure does indeed provide an accurate estimate of the difference between $K(c)$ and K. As stated above, it is easier to implement if c is assigned small values, in which case the Monte Carlo integral of Eq. (5.16) has very good statistics. Estimating the error is thus an excellent way to determine (without too much additional effort) whether the results of Eq. (5.10) for a specific value of c should be trusted. Unlike Doll *et al*'s results,[5.23] however, our work indicates that the actual calculation of the correction to Eq. (5.10) by means of integrating the difference between equations (5.15) and (5.16) requires (in multidimensional problems, in particular) a large amount of additional computational effort. Since our method gives very accurate results with small values of c, the correction would be needed only if one wanted to evaluate Eq. (5.10) with relatively large c, a choice that would render the Monte Carlo error bars small. Unfortunately, this is not easily feasible, because the statistics of the correction integral are then poor. Furthermore, as will be explained in detail in Section 5, the computational evaluation of Eq. (5.10) with large c presents certain challenges, which necessitate the use of special Monte Carlo techniques. [Problems of this nature do not, however, occur in the evaluation of the integral involved in estimating the error according to Eq. (5.16).] We therefore conclude that one is more likely to

gain in computational effort and simplicity by using a small value for c, in which case calculating the correction to Eq. (5.10) in the way described in this paragraph will not be necessary.

3. Simple example: the Airy function

Since the method of Section 2 is exact for quadratic functions $S(x)$, a non-trivial test requires a more complicated phase function. The integral representation of the Airy function [5.24]

$$Ai(-z) = \frac{1}{2\pi} \int_{-\infty}^{\infty} dx \; e^{i(xz - \frac{1}{3}x^3)} \tag{5.18}$$

is of the form of Eq. (5.4) with

$$S(x) = xz - \frac{x^3}{3}$$

and this integral has the generic behavior of coalescing stationary phase points in the limit $z \to 0$.

For $z \gg 1$ the stationary phase (i.e., semiclassical, WKB) approximation to $Ai(-z)$

$$Ai(-z) \sim \frac{\sin(\frac{\pi}{4} + \frac{2}{3}z^{3/2})}{\pi^{1/2} z^{1/4}} \tag{5.19}$$

is extremely accurate [5.24], so that here the method of Section 2 will be accurate and efficient for a wide range of values of the constant c. To provide a challenge to the method, therefore, we consider small values of z .

Figures 5-2 through 5-5 show the percentage error,

$$100 \times \frac{(\text{approximate}) - (\text{exact})}{(\text{exact})}, \tag{5.20}$$

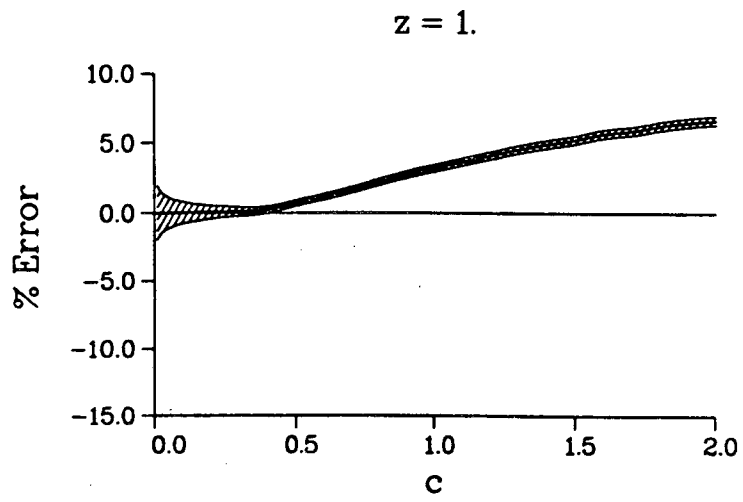

Fig. 5-2

The percentage error [cf. Eq. (5.20)] given by Eqs. (5.10)-(5.11) for the Airy integral, Eq. (5.18), for z=1, as a function of the constant c. The width of the shaded curve shows the Monte Carlo statistical error for N=5000. The stationary phase limit, $c \to \infty$, is off by 4.6% for this case.

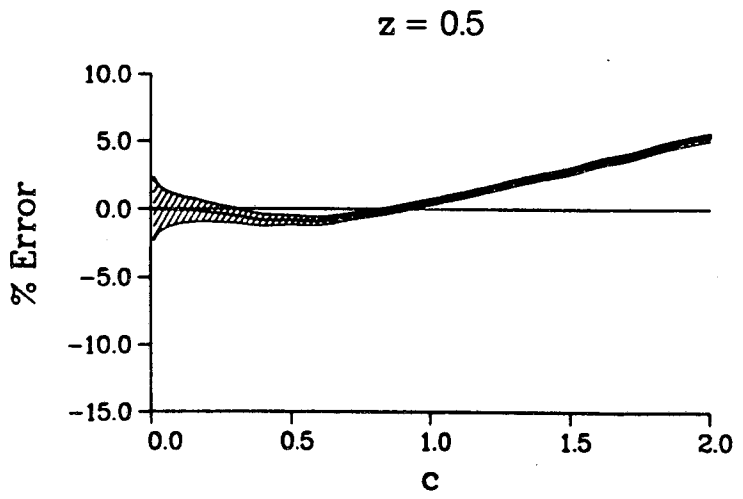

Fig. 5-3

Same as Fig. 5-2 except for z=0.5. The stationary phase limit, $c \to \infty$, is off by 20%.

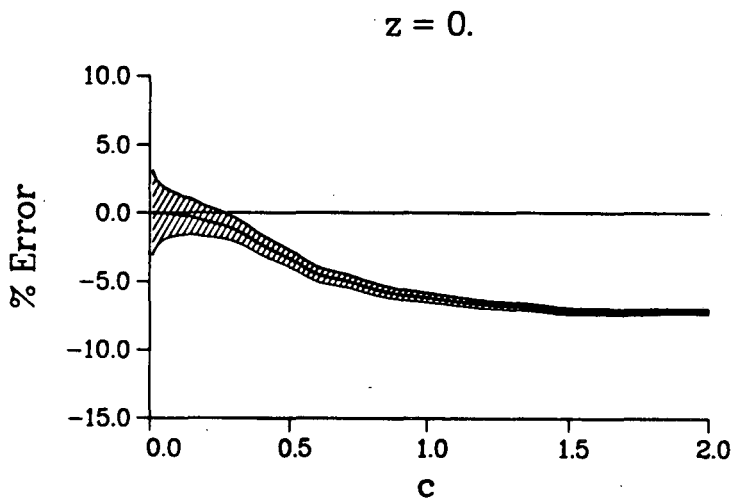

Fig. 5-4

Same as Fig. 5-2 except for z=0. Here the stationary phase limit is divergent.

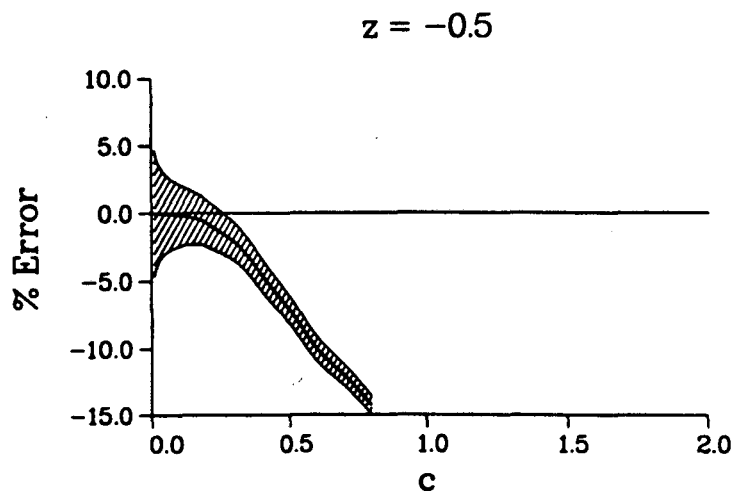

Fig. 5-5

Same as Fig. 5-2 except for z=−0.5. There are no (real) stationary phase points in this case.

given by Eq. (5.11b) for the Airy integral, Eq. (5.18), for z = 1, 0.5, 0, and –0.5, respectively, as a function of the parameter c. In each case the shaded region of the curve denotes the Monte Carlo statistical error for M=5000; the reader can obtain results for different values of M simply by scaling the width of the curves by $(5000/M)^{1/2}$; e.g., the results corresponding to M=1000 are obtained by expanding the width of the shaded curves by $\sqrt{5} \approx 2.2$.

For z=1 (Fig. 5-2) the stationary phase approximation is still quite good (error smaller than 5%), so there is a wide range of c for which the Monte Carlo result, Eq. (5.11b), is accurate and efficient (i.e. gives small statistical error). Smaller z is more of a challenge, but even for z=0 – where the stationary phase result, Eq. (5.19), diverges – there is a significant range of c for which Eq. (5.11b) is both accurate and efficient.

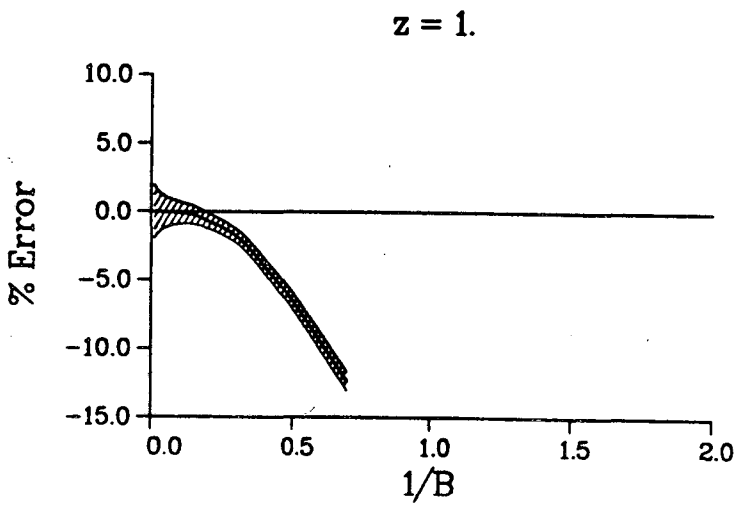

Fig. 5-6 Same as Fig. 5-2 (also z=1), except for the original Filinov method, Eq. (5-8), using the real part of the exponent to define the sampling function $P(x)$ rather than Eq. (5.11a).

Table 5-1
Error Estimate

z	x_0	c	R^*	z	x_0	c	R^*
1	1	0.01	1.00000	1	0.5	0.01	0.99985
		0.1	1.00079			0.1	0.99361
		0.2	1.00647			0.2	0.97720
		0.3	1.01916				
		0.4	1.04289				
		0.5	1.07150			0.5	0.91611
		0.8	1.18121			0.8	0.87324
		1.0	1.26132			1.0	0.84016
0.5	0.5	0.01	0.99997	0.5	0.2	0.01	0.99996
		0.1	0.99838			0.1	0.99607
		0.2	0.99628			0.2	0.98845
		0.3	0.99838				
		0.4	1.00629				
		0.5	1.02022			0.5	0.97801
		0.8	1.08845			0.8	1.00253
		1.0	1.13309			1.0	1.01473
0.	0.5	0.01	1.00002	0.	0.2	0.01	1.00000
		0.1	1.00337			0.1	1.00120
		0.2	1.01595			0.2	1.00865
		0.3	1.03996				
		0.4	1.07499				
		0.5	1.11166			0.5	1.08006
		0.8	1.26258			0.8	1.19181
		1.0	1.35997			1.0	1.27804
-0.5	0.2	0.01	1.00005	-0.5	0.	0.01	1.00006
		0.1	1.00581			0.1	1.00627
		0.2	1.02591			0.2	1.02539
		0.3	1.06218				
		0.4	1.10203				
		0.5	1.15480			0.5	1.15146
		0.8	1.31544			0.8	1.30718
		1.0	1.39692			1.0	1.39659

* $R = \frac{\text{Eq. (5.15)}}{\text{Eq. (5.16)}}$

For $z<0$ there are no (real) points of stationary phase, yet Eq. (5.11b) still provides usefully accurate results (less than 10% error) when c is large enough to have acceptable statistical error. If one distorted the integration path from the real x axis – a trick that has already been shown to be very useful in Monte Carlo path integration [5.10,5.25] – then much more accurate results could be obtained for $z<0$.

Finally, Fig. 5-6 shows similar results for $z=1$ using Filinov's original expression, Eq. (5.8), as a function of the constant B^{-1}. (Here one divides the complex exponent $-\frac{1}{2}S'(x_0)^2/[B-iS''(x_0)]$ into real and imaginary parts and uses the real part to define the Monte Carlo sampling function.) The results are essentially the same as Fig. 5-6 for all values of z tested and behave not nearly so well as those discussed above. One can show analytically that the stationary phase approximation is *not* obtained in the limit $B^{-1}\to\infty$ (or any other limit); in fact, $K(B)\to 0$ as $B^{-1}\to\infty$, i.e., -100% error. The *modified* Filinov expression, Eq. (5.10), is thus clearly superior.

Before concluding this Section, we present a test of the error estimate method of Section 2b to the calculation of the Airy function. Table 5-1 shows the ratio of Eq. (5.15) to Eq. (5.16), evaluated at selected points x_0, as a function of the parameter c for the values of z shown in figures 5-1 through 5-4. The integration of Eq. (5.16) was performed by Monte Carlo with 10000 points. It is clearly seen that the magnitude of the deviation of this ratio from unity does indeed reflect the error in the result that corresponds to the specific value of c.

4. Application: time evolution via path integration

In this Section, we describe the path integral evaluation of the time evolution operator in the coordinate representation and of the survival probability in three one-dimensional potentials: a harmonic potential, a symmetric double well potential, and a Morse potential.

a) The path integral expressions

The path integral expression for the coordinate representation of the propagator for a one-dimensional potential $V(x)$ is

$$\langle x_N | e^{-iHt/\hbar} | x_0 \rangle = \left[\frac{mN}{2\pi i \hbar t}\right]^{N/2} \int_{-\infty}^{\infty} dx_1 \cdots \int_{-\infty}^{\infty} dx_{N-1} \times e^{-\frac{mN}{2i\hbar t}\sum_{k=1}^{N}(x_k - x_{k-1})^2 - \frac{it}{N\hbar}\sum_{k=0}^{N} w_k V(x_k)} \tag{5.21}$$

where $w_k = 1$ for $k=1,...,N-1$, $w_0 = w_N = \frac{1}{2}$, and $N-1$ is the number of time discretizations. This expression becomes exact in the limit where $N \to \infty$. To evaluate Eq. (5.21) using the Monte Carlo algorithm, it is useful first to make a transformation of the integration variables to diagonalize the kinetic energy part; this leads to Coalson's quasi-Fourier representation,[5.26]

$$\langle x_N | e^{-iHt/\hbar} | x_0 \rangle = \sqrt{\frac{m}{2\pi i \hbar t}}\, e^{-i(N-1)\pi/4} e^{-\frac{m}{2i\hbar t}(x_N - x_0)^2} \times \int_{-\infty}^{\infty} da_1 \cdots \int_{-\infty}^{\infty} da_{N-1}\, e^{i\pi\sum_{k=1}^{N-1} a_k^2 - \frac{it}{N\hbar}\sum_{k=0}^{N} w_k V(x_k)} \tag{5.22}$$

where

$$x_k = x_0 + (x_N - x_0)\frac{k}{N} + \sqrt{\frac{\pi\hbar t}{m}}\frac{1}{N}\sum_{k'=1}^{N-1} a_{k'} \frac{\sin(\pi k k'/N)}{\sin(\pi k'/2N)}. \tag{5.23}$$

Eq. (5.22) is an integral of the type discussed in Section 2, with S of Eq. (5.21) given by

$$S = S(\mathbf{a}) = \frac{m}{2\hbar t}(x_N - x_0)^2 + \pi\sum_{k=1}^{N-1} a_k^2 - \frac{t}{N\hbar}\sum_{k=0}^{N} w_k V(x_k). \tag{5.24}$$

The survival probability, $P(t)$, for the time evolution of a state initially described by the wave function $\Phi(x)$, is given by

$$P(t) = |\langle\Phi|e^{-iHt/\hbar}|\Phi\rangle|^2$$

$$= |\int_{-\infty}^{\infty} dx_0 \int_{-\infty}^{\infty} dx_N \langle\Phi|x_N\rangle\langle x_N|e^{-iHt/\hbar}|x_0\rangle\langle x_0|\Phi\rangle|^2$$

$$= \frac{m}{2\pi\hbar t} |\int_{-\infty}^{\infty} dx_0 \int_{-\infty}^{\infty} dx_N \int_{-\infty}^{\infty} da_1 \cdots \int_{-\infty}^{\infty} da_{N-1} \Phi^*(x_N)\, \Phi(x_0)$$

$$\times e^{-\frac{m}{2i\hbar t}(x_N - x_0)^2} e^{i\pi \sum_{k=1}^{N-1} a_k^2 - \frac{it}{N\hbar} \sum_{k=0}^{N} w_k V(x_k)} |^2. \qquad (5.25)$$

In applications below the initial state is taken to be a Gaussian centered at x_{in}:

$$\Phi(x) = \frac{\alpha^{1/4}}{\pi^{1/4}} e^{-\frac{\alpha}{2}(x - x_{in})^2}. \qquad (5.26)$$

b) The normalization integral

After making the transformation described in Section 2a, one must evaluate a multidimensional integral of the type of Eq. (5.4). The most common way of doing this is via the Metropolis algorithm,[5.3] which gives a normalized average over the chosen relative distribution function. Eq. (5.4) must thus be multiplied and divided by the normalization integral,

$$I \equiv \int_{-\infty}^{\infty} d\mathbf{x}\, e^{-\frac{1}{2}\mathbf{S}_1(\mathbf{x})\cdot\mathbf{c}\cdot\mathbf{S}_1(\mathbf{x})} = \int_{-\infty}^{\infty} d\mathbf{x}\, p(\mathbf{x}), \qquad (5.27)$$

so that the Metropolis expression for $K(\mathbf{c})$ of Eq. (5.4) is

$$K(\mathbf{c}) = \frac{I}{M} \sum_{j=1}^{M} e^{iS(\mathbf{x}_j)} \sqrt{\det[1 + i\,\mathbf{c}\cdot\mathbf{S}_2(\mathbf{x}_j)]}, \qquad (5.28)$$

where $\{\mathbf{x}_j\}$ are the M points selected from the distribution $p(\mathbf{x})$ by the Metropolis procedure.

The normalization integral, Eq. (5.27), is similar to integrals that occur in statistical mechanics, where one wants to compute partition functions. We have used the "charging" algorithm [5.27] to evaluate it. The exponent of the weighting function is

thus split into two parts,

$$p(\mathbf{x}) = e^{-[g_0(\mathbf{x}) + g_1(\mathbf{x})]}, \tag{5.29}$$

such that $e^{-g_0(\mathbf{x})}$ is analytically integrable. [In the case of the Monte Carlo evaluation of path integrals, there is always a quadratic (and thus analytically integrable) part in the exponent of the weighting function, and therefore this algorithm is directly applicable.] Defining

$$I_\lambda \equiv \int_{-\infty}^{\infty} d\mathbf{x}\, e^{-[g_0(\mathbf{x}) + \lambda g_1(\mathbf{x})]}, \tag{5.30}$$

one has

$$-\frac{d}{d\lambda}\ln I_\lambda = -\frac{1}{I_\lambda}\frac{d}{d\lambda}I_\lambda = \frac{\int_{-\infty}^{\infty} d\mathbf{x}\, g_1(\mathbf{x})\, e^{-[g_0(\mathbf{x}) + \lambda g_1(\mathbf{x})]}}{\int_{-\infty}^{\infty} d\mathbf{x}\, e^{-[g_0(\mathbf{x}) + \lambda g_1(\mathbf{x})]}} = \langle g_1 \rangle_\lambda \tag{5.31}$$

and therefore

$$I = I_{\lambda=1} = I_{\lambda=0}\, e^{-\int_0^1 d\lambda \langle g_1 \rangle_\lambda}. \tag{5.32}$$

One must thus compute the normalized average of g_1 with respect to the distribution

$$p_\lambda(\mathbf{x}) = e^{-[g_0(\mathbf{x}) + \lambda g_1(\mathbf{x})]} \tag{5.33}$$

at selected values of λ between 0 and 1 and numerically integrate over λ to obtain the normalization integral I. The Metropolis procedure is used to compute $\langle g_1 \rangle_\lambda$.

In most of the cases presented in this Chapter, the integrand of Eq. (5.32), $\langle g_1 \rangle_\lambda$, is a very non-smooth function of λ; however, by properly selecting the values of λ (typically, 10-20 points are sufficient) at which $\langle g_1 \rangle_\lambda$ is evaluated, this function can be accurately and efficiently integrated.

c) *Computation of the survival probability*

The exponent of the integrand in Eq. (5.25) for the survival probability, with $\Phi(x)$ given by Eq. (5.26), has a real as well as an imaginary part. Our first inclination was to deal with this by applying the modified Filinov transformation, Eq. (5.10), only to the $\{a_k\}$ variables since there is already a real exponential factor that can serve as the weighting function for integrating over the variables x_0 and x_N. This turns out not to be a good idea, however, because the resulting Metropolis sampling function does not sample the regions of x_0 and x_N about the stationary phase points of these variables. This causes the phase factor e^{iS} to oscillate wildly with x_0 and x_N, and thus gives poor Monte Carlo statistics.

We have found that it is much better simply to generalize Eqs. (5.4)-(5.10) to the case that the phase $S(\mathbf{x})$ is complex.[5.28] With the replacement

$$S(\mathbf{x}) \rightarrow S(\mathbf{x}) + iW(\mathbf{x}), \tag{5.34}$$

all of the manipulations leading to Eq. (5.10) are the same (at least if W is a quadratic function of $\mathbf{x}$), so that one obtains

$$K(\mathbf{c}) = \int_{-\infty}^{\infty} d\mathbf{x}\, e^{iS(\mathbf{x})} e^{-W(\mathbf{x})} \sqrt{\det[1+i\,\mathbf{c}\cdot\mathbf{S}_2(\mathbf{x})-\mathbf{c}\cdot\mathbf{W}_2(\mathbf{x})]}$$

$$\times\, e^{-\frac{1}{2}(\mathbf{S}_1+i\mathbf{W}_1)\cdot\mathbf{c}\cdot(\mathbf{S}_1+i\mathbf{W}_1)}, \tag{5.35}$$

where

$$\mathbf{W}_1(\mathbf{x}) = \partial W(\mathbf{x})/\partial\mathbf{x}, \qquad \mathbf{W}_2 = \partial^2 W(\mathbf{x})/\partial\mathbf{x}\partial\mathbf{x}.$$

Choosing the Metropolis sampling function as

$$p(\mathbf{x}) = e^{-\left[\frac{1}{2}\mathbf{S}_1(\mathbf{x})\cdot\mathbf{c}\cdot\mathbf{S}_1(\mathbf{x}) + \mathbf{W}(\mathbf{x}) - \frac{1}{2}\mathbf{W}_1(\mathbf{x})\cdot\mathbf{c}\cdot\mathbf{W}_1(\mathbf{x})\right]}, \tag{5.36}$$

Eq. (5.35) becomes

$$K(\mathbf{c}) = \int_{-\infty}^{\infty} d\mathbf{x}\, p(\mathbf{x})\, e^{i[S(\mathbf{x})-\mathbf{W}_1(\mathbf{x})\cdot\mathbf{c}\cdot\mathbf{S}_1(\mathbf{x})]} \sqrt{\det[1+i\,\mathbf{c}\cdot\mathbf{S}_2(\mathbf{x})-\mathbf{c}\cdot\mathbf{W}_2(\mathbf{x})]}. \tag{5.37}$$

Equations (5.36) and (5.37) are thus the generalization of Eqs. (5.10) and (5.11). For the present application, the integration variables are x_0, x_N and $\{a_k\}$, S is the real part of the phase given by Eq. (5.24), and W the imaginary part, given by

$$W = \frac{\alpha}{2}[(x_0-x_{in})^2+(x_N-x_{in})^2]. \tag{5.38}$$

Our choice for the matrix $\mathbf{c}$ is an $N+1$-dimensional diagonal matrix whose $N-1$ elements (the ones corresponding to the a_k variables) are equal to a constant c and the two elements that correspond to the integration of the endpoints x_0 and x_N are equal to another constant c'. Eq. (5.36) thus gives the Metropolis sampling function as

$$p(x_0,x_N,\mathbf{a}) = e^{-\frac{c}{2}\sum_{k=1}^{N-1}\left[\frac{\partial S}{\partial a_k}\right]^2} e^{-\frac{\alpha}{2}(1-\alpha c')[(x_0-x_{in})^2+(x_N-x_{in})^2]} \times e^{-\frac{c'}{2}\left[\left[\frac{\partial S}{\partial x_0}\right]^2+\left[\frac{\partial S}{\partial x_N}\right]^2\right]}, \tag{5.39}$$

and the expression for the survival amplitude is

$$\langle\Phi|e^{-iHt/\hbar}|\Phi\rangle = \sqrt{\frac{m}{2\pi i\hbar t}}e^{-i(N-1)\pi/4}\sqrt{\frac{\alpha}{\pi}}\int_{-\infty}^{\infty}dx_0\int_{-\infty}^{\infty}dx_N\int_{-\infty}^{\infty}da_1\cdots\int_{-\infty}^{\infty}da_{N-1}$$
$$\times e^{iS(x_0,x_N,a_1,\ldots,a_{N-1})}e^{-ic'\alpha\left[(x_0-x_{in})\frac{\partial S}{\partial x_0}+(x_N-x_{in})\frac{\partial S}{\partial x_N}\right]}$$
$$\times\sqrt{\det[\mathbf{1}+i\,\mathbf{c}\cdot\mathbf{S}_2(\mathbf{x_0})-\mathbf{c}\cdot\mathbf{W}_2(\mathbf{x_0})]}\;p(x_0,x_N,\mathbf{a}). \tag{5.40}$$

Since the term $(x_N-x_0)^2$ [which arises from Eq. (3.4)] in Eq. (5.37) becomes dominant at short times, one must be careful to "move" both x_0 and x_N at each step in the Monte Carlo random walk, so that $|x_0-x_N|$ remains small. (Failure to do so will result in the rejection of most of the steps or — if the step size is small enough so that only half of the steps are rejected — the integration space will be sampled

very poorly.) To guarantee this, we carried out the Metropolis sampling using the variables

$$z_+ = \frac{1}{\sqrt{2}}(x_0+x_N) \quad \text{and} \quad z_- = \frac{1}{\sqrt{2}}(x_0-x_N) \tag{5.41}$$

with the step sizes adjusted to give 50% rejection rate.

5. Results and discussion

The methodology described in Sections 2 and 4 was first tested for a harmonic potential, $V(x) = \frac{1}{2}m\omega^2x^2$. In this case the integrand of the path integral, Eq. (5.21) or (5.22), is the exponential of a quadratic function of the integration variables, and as discussed in Section 2, the modified Filinov transformation gives the integral exactly, for all values of the parameter c. This was verified directly by using the Monte Carlo procedure described in Section 4, and the results are presented below.

We first give the expression for the diagonal element of the propagator, $\langle 0|\exp(-iHt/\hbar)|0\rangle$, that is obtained using Eq. (5.22) with N time slices. Noting that

$$\sum_{k=1}^{N-1} x_k^2 = \frac{\pi\hbar t}{2mN}\sum_{k'=1}^{N-1}\frac{a_{k'}^2}{\sin^2\frac{\pi k'}{2N}}, \tag{5.42}$$

the integrations in Eq. (5.22) can be easily performed, yielding the result [5.29]

$$\langle 0|e^{-iHt/\hbar}|0\rangle \approx \sqrt{\frac{m}{2\pi i\hbar t}}\prod_{k=1}^{N-1}\left[1-\frac{(\omega t)^2}{(2N\sin\frac{\pi k}{2N})^2}\right]^{-1/2}. \tag{5.43}$$

As $N\to\infty$, Eq. (5.43) approaches the exact result for the harmonic potential [5.1]

$$\langle 0|e^{-iHt/\hbar}|0\rangle = \sqrt{\frac{m\omega}{2\pi i\hbar\sin\omega t}}. \tag{5.44}$$

For the case of the harmonic potential there is only one stationary phase point for each integration variable in Eq. (5.24). One can easily get the exact results with

small Monte Carlo error by using large values for the parameter c. To illustrate this, we performed the Metropolis calculation of $\langle 0|\exp(-iHt/\hbar)|0\rangle$ according to Eq. (5.10) for the potential

$$V(x) = \frac{1}{2} m \omega^2 x^2 \tag{5.45}$$

with the mass equal to that of a hydrogen atom and the force constant $m\omega^2$=0.04 atomic units, which corresponds to $\omega \approx 1020\ \mathrm{cm}^{-1}$.

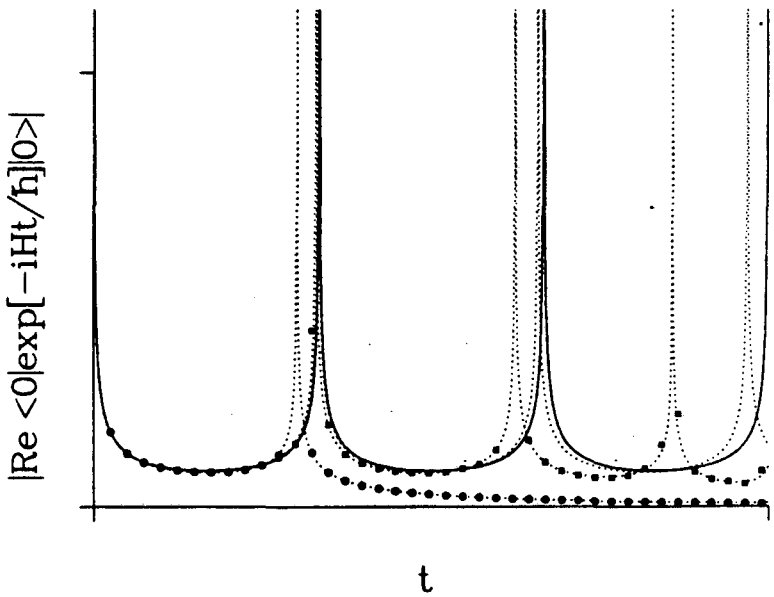

Fig. 5-7

The absolute value of the real part of the 0-0 matrix element of the propagator, $\langle 0|e^{-iHt/\hbar}|0\rangle$, as a function of time, for a harmonic potential, Eq. (5.45). Solid line: exact result, Eq. (5.44). Dotted lines: analytic result for the path integral evaluation with N time slices [cf. Eq. (5.43)] where N=2,5 and 11, respectively. Circles and squares: Monte Carlo path integral evaluation according to Eq. (5.10) with N=2 and 5, respectively. The statistical error bars are smaller than the size of the points.

Fig. 5-7 shows the agreement of various finite-N results, Eq. (5.43), with the exact results, Eq. (5.44), as a function of the time t. Also shown are the results of the Monte Carlo path integral calculation of $\langle 0|\exp(-iHt/\hbar)|0\rangle$ using our method, for N=4, with $\mathbf{c} = c\,\mathbf{1}$, c=50, and 5000 Monte Carlo points per dimension. The Monte Carlo error bars are very small, and the agreement with the analytically obtained results for the same value of N is (as expected) excellent.

A non-trivial application, however, and one that is related to some of the chemical applications that we have in mind for future work, is a symmetric double well potential,[5.28]

$$V(x) = -\frac{1}{2}a_0x^2 + \frac{1}{4}c_0x^4 \tag{5.46}$$

with $a_0 = 0.02$ and $c_0 = 0.04$ atomic units. For a particle with the mass of a hydrogen atom, the harmonic frequency in each well is 1020 cm^{-1}. The barrier that separates the two wells is small and the local potential about each minimum very anharmonic. For this potential, Eq. (5.10) is not exact, except for c=0. Furthermore, this is a case for which semiclassical approximations are not expected to work very well.

Consider first the diagonal element of the propagator, $\langle 0|\exp(-iHt/\hbar)|0\rangle$. This quantity is closely related to the reactive flux correlation function [5.6] (see also Chapter VII) for the transition state (x=0) on this one-dimensional potential energy surface. It is useful first to examine the case with only one time discretization because it provides some useful insight into important aspects of the calculation. Eq. (5.24) then reads

$$S(a_1) = \pi a_1^2 - \frac{t}{2\hbar}V(x_1) \tag{5.47a}$$

with

$$x_1 = \sqrt{\frac{\pi\hbar t}{2m}}a_1 \tag{5.47b}$$

and one can readily show that the integral over a_1 in Eq. (3.2) has *three* points of stationary phase,

$$a_1^{SP} = 0, \quad \pm \left[\frac{2\pi + \frac{\pi t^2}{4m} a_0}{\frac{\pi^2 \hbar t^3}{8m^2} c_0} \right]^{1/2} . \tag{5.48}$$

For short times, i.e., $t \to 0$, these are all well separated, and the stationary phase approximation to the integral,

$$\langle 0 | e^{-iHt/\hbar} | 0 \rangle^{SPA} \approx e^{-i\pi/4} \frac{\sqrt{\frac{m}{2\pi i \hbar t}}}{\sqrt{2 + \frac{t^2}{4m} a_0}} \left[\sqrt{2} e^{i\pi/4} + 2\, e^{-i\pi/4}\, e^{i \frac{2 + (t^2 a_0/4m)^2}{\hbar t^3 c_0 / 2m^2}} \right], \tag{5.49}$$

is accurate. As t increases, however, the three stationary phase points approach each other (coalescing as $t \to \infty$), and Eq. (5.49) becomes incorrect. (Of course one would not attempt to do the calculation for long times with only one time discretization; our purpose here is merely to examine the behavior of the specific integral.)

Now consider Monte Carlo evaluation of the integral over a_1 with the modified Filinov transformation, Eq. (5.10). It is useful to refer to the analogy with classical statistical mechanics noted at the end of Section 2a. Thus the Monte Carlo distribution function

$$p(a_1) = e^{-\frac{c}{2} S'(a_1)^2}, \tag{5.50a}$$

here with S of Eq. (5.43), is identified with

$$p(a_1) \equiv e^{-\beta U(a_1)}, \tag{5.50b}$$

so that

$$\beta \equiv c \tag{5.50c}$$

$$U(a_1) \equiv \frac{1}{2} S'(a_1)^2. \tag{5.50d}$$

The three stationary phase points of Eq. (5.48) are thus local minima of the "potential" $U(a_1)$, $U(a_1^{SP})=0$, and when applying the Metropolis algorithm in such cases one must be careful to sample the various local minima appropriately. When c ($\equiv\beta$) is small enough (high "temperature"), this is easily accomplished, because the optimum step size for the random walk is large enough to provide multiple jumps from one minimum to the other.[5.28] For larger c ($=\beta$, i.e., low "temperature"), however, the Metropolis calculation often gets trapped in one minimum, without "seeing" the others within realistic time scales. This problem is often encountered in statistical mechanics, and sophisticated Monte Carlo procedures have been developed for successfully populating the various local minima. The most commonly used procedure, the simulated annealing algorithm,[5.30] starts the random walk with very small c (high temperature), so that all the local minima can be populated, and successively increases c (i.e., lowers the temperature) to the desired value.

The annealing procedure works well for the above case that the three local minima in $U(a_1)$ all have the same value, $U_{min}=0$. It is less efficient, though, for computing the normalization integral, Eq. (5.30), because for $0<\lambda<1$ the relative minima in $U_\lambda(a_1)$ [p_λ of Eq. (5.33) $\equiv\exp(-U_\lambda)$] do not all have the same value [See Figures 5-8 and 5-9]. In this case, we used a technique similar to the staging algorithm;[5.31] we first carried out a preliminary Metropolis random walk with a large step size in order to provide the correct relative population of all important regions of space, and then used these configurations to initiate Metropolis sampling with the optimum step size.

We demonstrate the success of this latter method by presenting the Metropolis computation of the real part of $\langle 0|\exp(-iHt/\hbar)|0\rangle$ for the double well potential with $N=2$. The reason for restricting the calculation to just one time discretization is to be able to compare with exact results, which can then be computed by simple numerical integration. Basis set calculations (which would normally provide the exact answer)

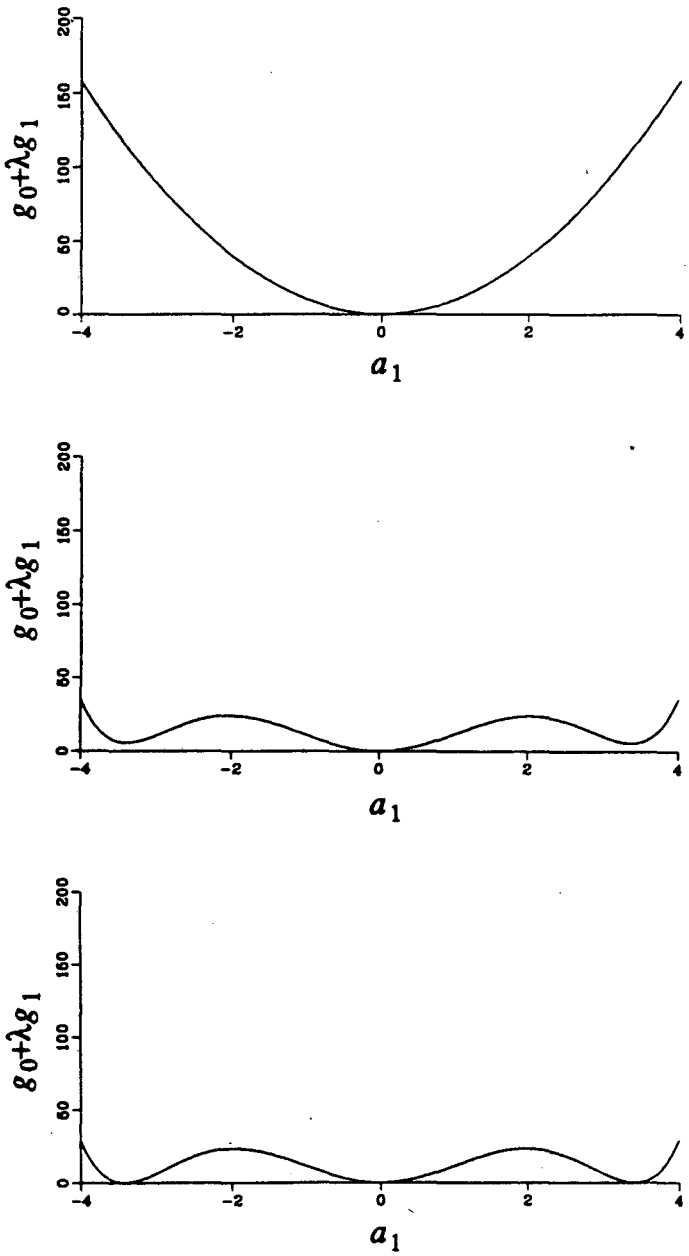

Fig. 5-8

The exponent $g_0+\lambda g_1$ of the integrand [Eq. (5.33)] required to evaluate the normalization integral, Eq. (5.30), as a function of the integration variable a_1 [cf. Eq. (5.47)] for the double well example discussed in Section 5, at three different values of λ. (a) $\lambda=0$, (b) $\lambda=0.95$, (c) $\lambda=1$.

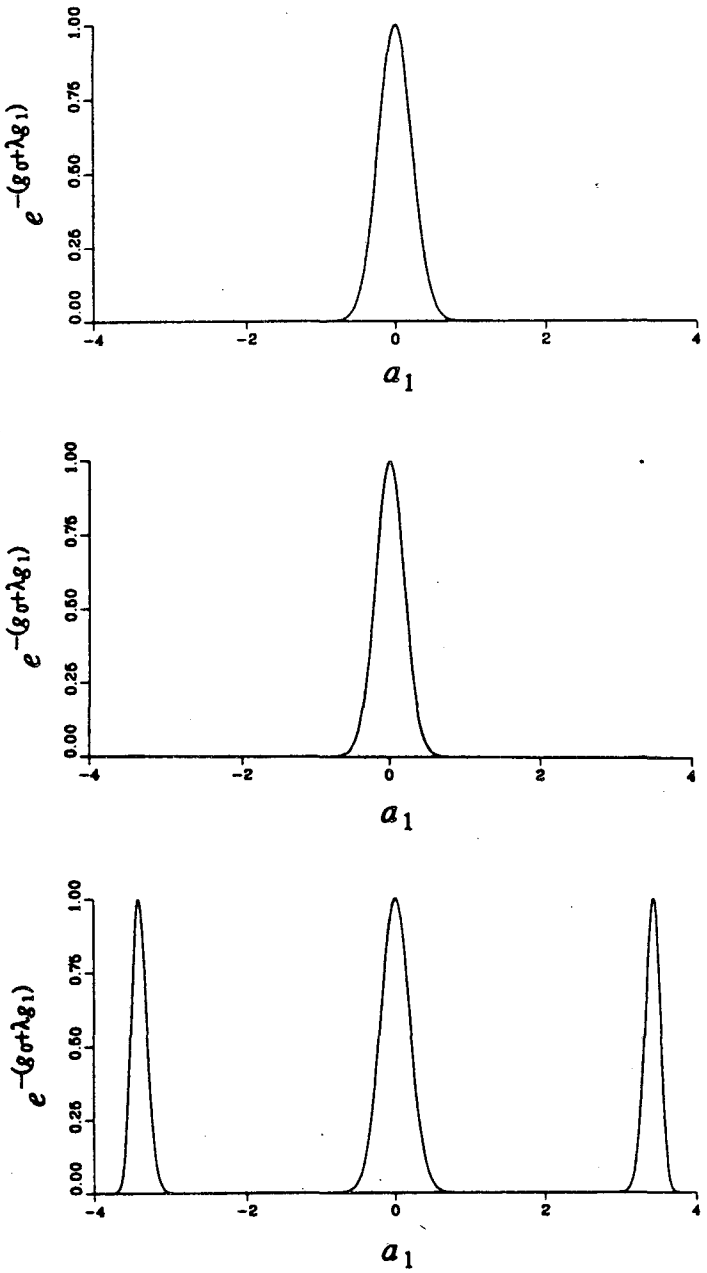

Fig. 5-9

The integrand $e^{-(g_0+\lambda g_1)}$ required to evaluate the normalization integral, Eq. (5.30), as a function of the integration variable a_1 [cf. Eq. (5.47)] for the double well example discussed in Section 5, at three different values of λ. (a) λ=0, (b) λ=0.95, (c) λ=1.

converge extremely slowly in the case of the purely real time propagator. Fig. 5-10 shows the results of this calculation for three different values of c, and compares to the exact results. The results for c=0.05 were obtained using straightforward Metropolis sampling with 500000 points. The c=0.5 and c=1 results were obtained by carrying out the Metropolis calculation with large step size to create 5000 configurations in the important regions of space, and then sampling about each of these configurations using 100 Monte Carlo points with the optimum step size. All three calculations were performed with the same total number of Monte Carlo points (5000×100=500000); although the quality of the results is the same, the small c calculation is obviously preferable as being the simplest computationally.

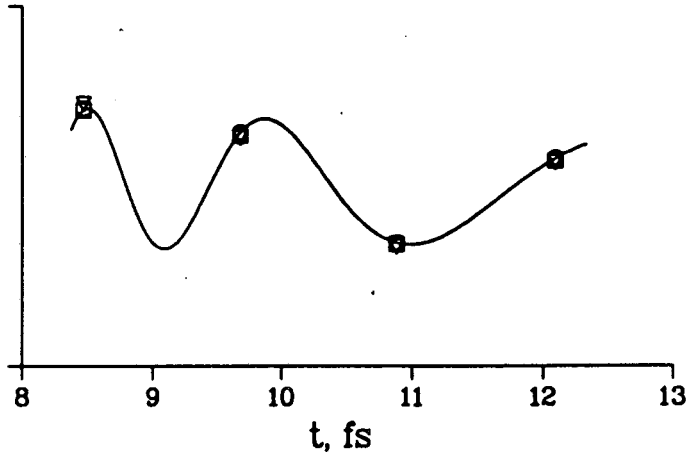

Fig. 5-10

Calculation of Eq. (5.21) with x_N=x_0=0 and N=2 for the double well potential. The solid line shows exact results, generated by means of numerical integration. The points show the Monte Carlo evaluation of the same quantity using three different values for the parameter c: circles, c=0.05; squares, c=0.5; and triangles, c=1. The c=0.05 results were obtained by straightforward Metropolis sampling, while the c=0.5 and c=1 results were obtained by sampling about 5000 configurations that were created using a larger step size for the random walk (see the discussion in Section 5).

Next, we present the calculation of the survival probability, $P(t)$, for the double well potential. The initial state was taken to be a Gaussian centered at one minimum. We used two different values for α, one with which the initial state is an eigenstate of the harmonic approximation to the potential about this minimum (α=8.57), and a smaller value (α=2), which corresponds to a broader initial state. In the first case (see Figures 5-11 and 5-12) the decay of $P(t)$ is primarily from tunneling of the initial state through the barrier to the other potential well, while in the latter case (see Figures 5-13 and 5-14) it is via relaxation of the initial state in its own potential well.

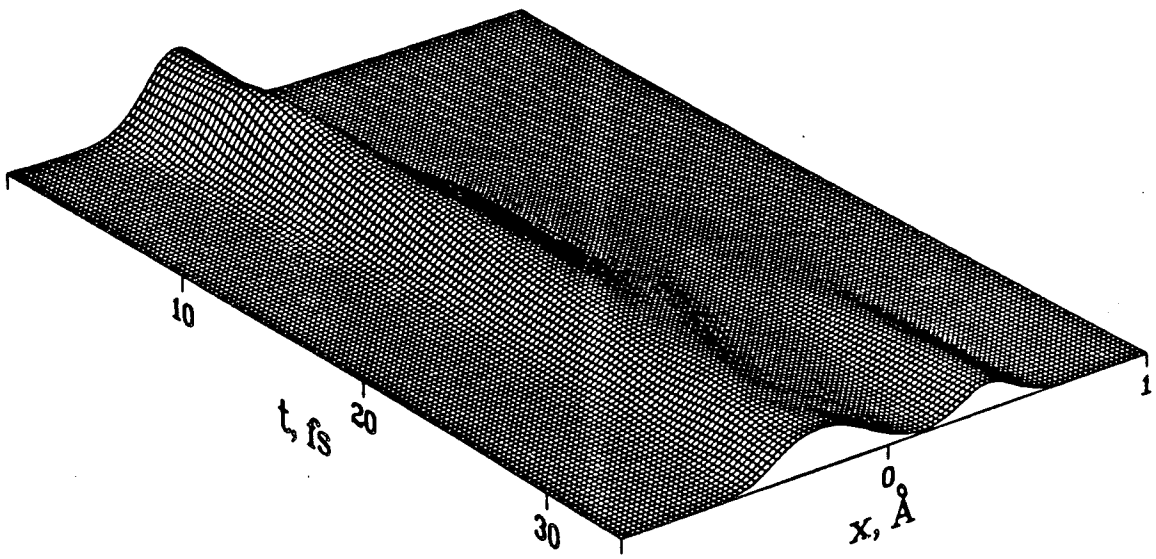

Fig. 5-11

Time evolution of a Gaussian which starts out as an eigenstate of the local harmonic approximation to the double well potential, Eq. (5.46), about one minimum. Plotted is the probability density, $|\Phi(x;t)|^2$, as a function of the coordinate x and the time t. The time evolution was computed by basis set expansion.

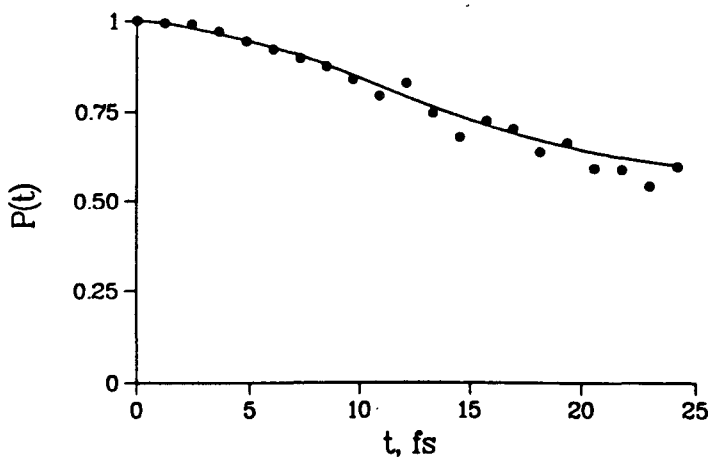

Fig. 5-12

The survival probability, $P(t)$, for a Gaussian which starts out as an eigenstate of the local harmonic approximation to the double well potential, Eq. (5.46), about one minimum. The points show the results of evaluating Eq. (5.10) by Monte Carlo, with the parameter c ranging between 0.02 and 0.1; 100000 - 1000000 Monte Carlo points were used per dimension of the integral. The solid line shows exact results, generated by basis set methods.

The error estimate of Section 2b has also been applied. In each calculation, the average absolute difference between Equations (5.15) and (5.16) was of the same order of magnitude or smaller than the Monte Carlo error bars for the values of c that were used.

It is worth pointing out that the computation could also be performed with larger values of the parameter c, as was pointed out when discussing the case of the diagonal element of the propagator. However, small values of c have yet another advantage: in order to calculate the square root of the determinant that appears in Eq.

(5.10), one must in general diagonalize the matrix $1+i\,\mathbf{c}\cdot\mathbf{S}_2$ $(-\mathbf{c}\cdot\mathbf{W}_2)$, in order to be able to determine the correct phase factors of the product by taking the complex square root of each of the eigenvalues separately. If c is small though, the determinant has a positive real part; therefore the correct phase of the square root can be found without diagonalizing the matrix, and thus the calculation can be considerably accelerated.

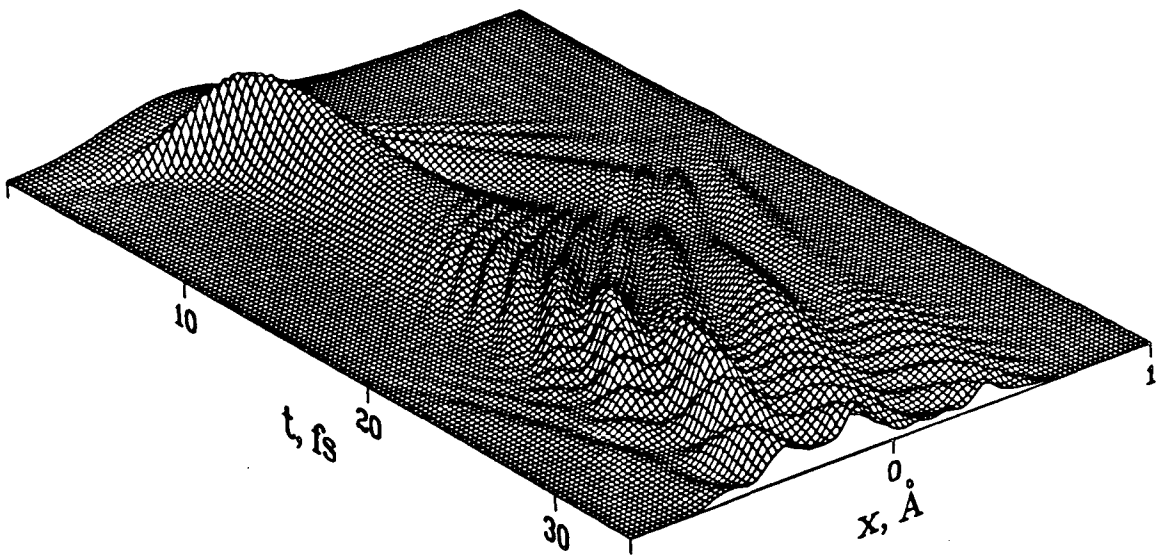

Fig. 5-13

Time evolution of a Gaussian with α=2 [cf. Eq. 5.26] in the double well potential, Eq. (5.46). Plotted is the probability density, $|\Phi(x;t)|^2$, as a function of the coordinate x and the time t. The time evolution was computed by basis set expansion.

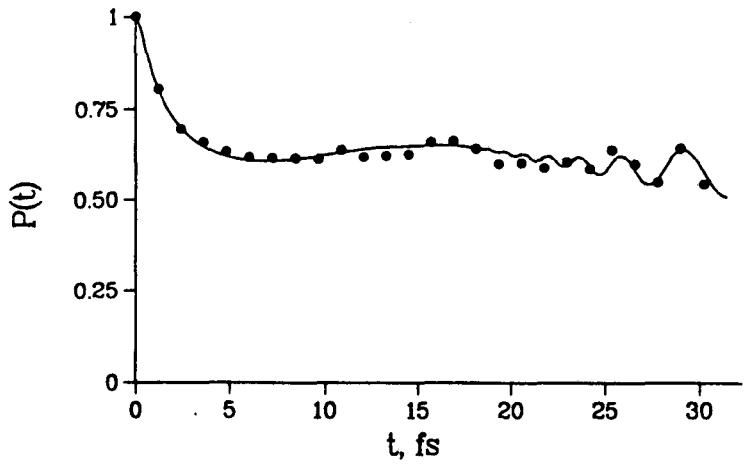

Fig. 5-14

Same as Fig. 5-12, except that the initial state was broader (α=2). The Metropolis computation was performed with c ranging between 0.1 and 0.2, with 100000 - 200000 Monte Carlo points per dimension.

Finally, we present a similar calculation for a Morse potential,

$$V(x) = D_e(e^{-2\beta x} - 2e^{-\beta x}). \tag{5.47}$$

We chose the parameters to correspond roughly to those for the vibrational motion of H_2, i.e., the well depth D_e = 4.476 eV and the harmonic frequency at the bottom of the well ω_e = 4395 cm^{-1}. The initial state was a Gaussian with the width of the ground state wave function and centered at x_{in} = –0.21 Å(see Fig. 5-15); the energy of this state corresponds approximately to that of the fourth eigenstate, where the potential is very anharmonic. Fig. 5-16 shows the evolution of the square of the wave function, $|\Phi(x;t)|^2$, with time. The shape of the wavepacket is distorted as it moves to the right, especially as it approaches the outer turning point of the Morse potential; although the wave function is very broad there, it is too far away from its

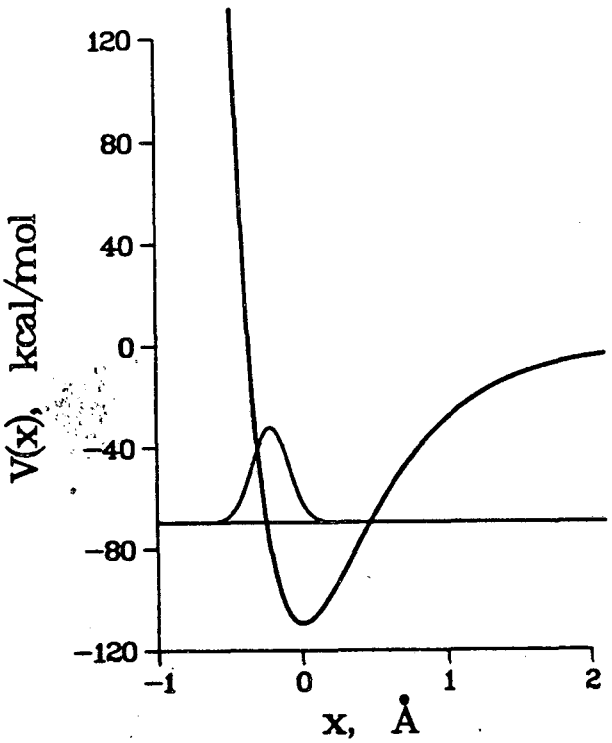

Fig. 5-15

The Morse potential with parameters that correspond roughly to the vibrational motion of H_2 (D_e = 4.476 eV, ω_e = 4395 cm^{-1}). Also shown is the initial Gaussian wavepacket, which has the width of the ground vibrational state and is displaced by -0.21 Å from the equilibrium position; the energy of this state corresponds approximately to the fourth eigenstate of the potential.

original location to have any significant overlap with the initial state, and the survival probability (see Fig. 5-18) approaches zero. The wave function partially regains its initial localization as it starts moving back toward the left, while the survival probability rises from zero and develops a maximum. However, the localization of the wavepacket is totally destroyed as it bounces off the hard wall of the Morse

potential. The wave function breaks apart as it starts moving to the right after the reflection, while the survival probability decays to zero again. Other local maxima appear in the survival probability at subsequent times, when the original Gaussian overlaps with smaller peaks of the reflected wave.[5.28]

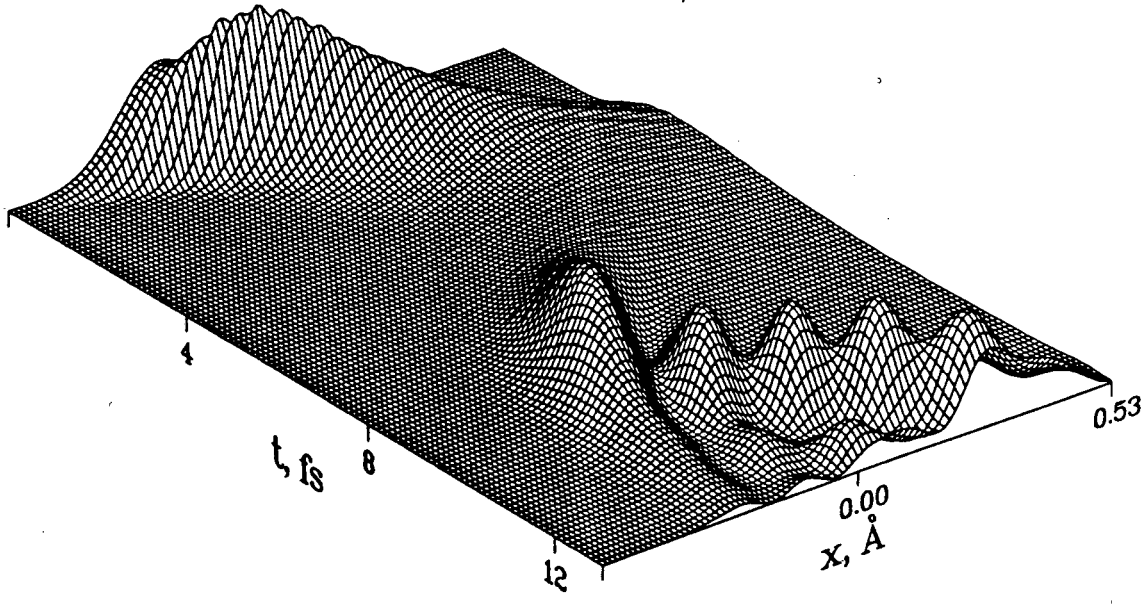

Fig. 5-16

Time evolution of the wave function shown in Fig. 5-15 in the Morse potential shown in Eq. (5.47). Plotted is the probability density, $|\Phi(x;t)|^2$, as a function of the coordinate x and the time t. The time evolution was computed by basis set expansion.

To illustrate the magnitude and the importance of the anharmonicity of the Morse potential at this energy, we show in Fig. 5-17 the time evolution of the same initial wavepacket in a *harmonic* potential which was chosen to fit the Morse potential at the minimum. In this case the wavepacket remains localized at all times, while its center bounces back and forth between the classical turning points following the classical equations of motion.

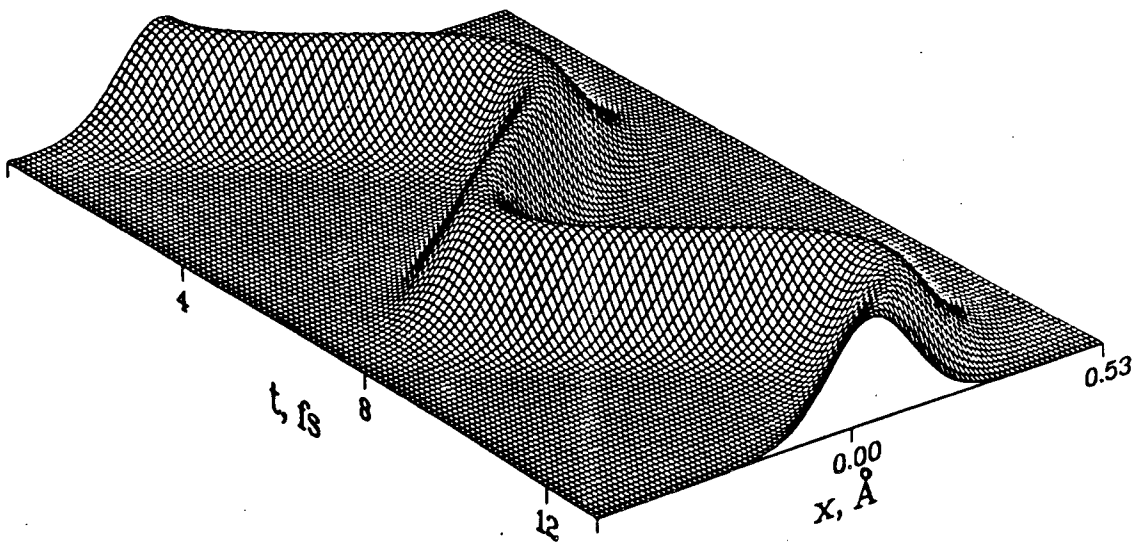

Fig. 5-17

Time evolution of the wave function shown in Fig. 5-15 in a harmonic potential with frequency equal to the equilibrium frequency of the Morse potential. Plotted is the probability density, $|\Phi(x;t)|^2$, as a function of the coordinate x and the time t.

Fig. 5-18 shows the survival probability for time evolution in the Morse potential, as calculated by Monte Carlo path integration, and compares with exact results, generated by basis set methods. The agreement is very good at all times; the path integral results have been obtained using as many as 20 time discretizations for the points of the second peak. More accurate approximations to the short time propagator (see Chapter VII) would allow the time evolution to be followed for longer times with the same number of time discretizations. We therefore conclude that the modified Filinov method is accurate and efficient for describing the dynamics, even when the processes that are taking place are sufficiently complicated.

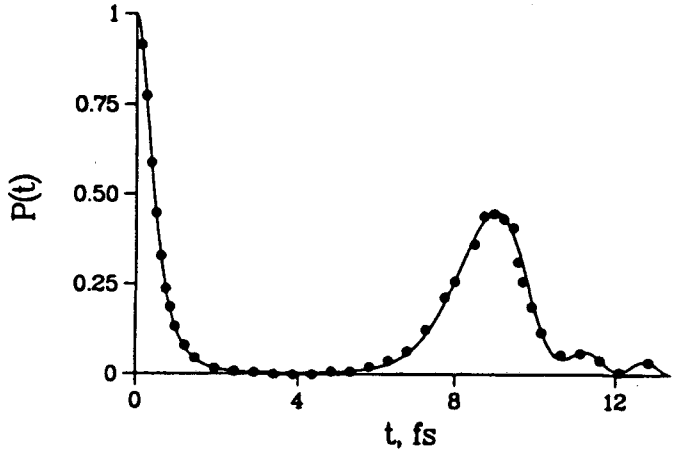

Fig. 5-18

The survival probability, $P(t)$ (see Eq. 5.25), for the wavepacket in the Morse potential of Fig. 5-15. The calculation was performed with 100000 points, with c=0.2 and c'=0.03; the Monte Carlo error bars are smaller than the size of the points, even when the dimensionality of the integral is ≥20. The solid line shows exact results.

6. Concluding remarks

The purpose of this Chapter has been to show that real time propagator path integrals can indeed be evaluated by Monte Carlo methods via the modified Filinov algorithm. The fact that Monte Carlo methods are used means that the integrand of the path integral can be augmented by a non-local influence functional that arises, for example, by integrating out other degrees of freedom to which the remaining one is coupled. Such possibilities show the potential power of this approach.

The applications discussed in Section 5 also show some of the challenges presented to this approach. Namely, when there is more than one stationary phase region in the integrand, the Metropolis procedure must be "smart" enough to insure that it samples them all and in the correct relative amounts. (This is identical to the problem in classical statistical mechanics of evaluating a partition function for a potential with several local minima.) Semiclassical theory, which is the stationary phase approximation to the path integral, explicitly searches out these stationary phase points (i.e., the classical paths) and then adds their contributions appropriately. Presently, though, we do not wish to make the stationary phase approximation but rather let the Monte Carlo procedure sample these regions (in principle, exactly). There exist a variety of sophisticated Monte Carlo techniques for dealing with these multiple minima situations, and they will undoubtedly be useful for application to these modified Filinov-type calculations. For the applications in this Chapter, however, we have taken the simpler alternative of choosing the constant matrix $\mathbf{c}$ small enough that the Monte Carlo weighting function [Eq. (5.10)] samples broadly enough to encompass all the various stationary phase regions. More experience with further applications will be necessary to see which combinations of these various Monte Carlo techniques will be most generally useful for these path integral calculations.

References

5.1 (a) R. P. Feynman, *Rev. Mod. Phys.* **20**, 367 (1948);

(b) R. P. Feynman and A. R. Hibbs, *Quantum Mechanics and Path Integrals*, McGraw-Hill, New York, 1965.

5.2 Ref. 1b, pp. 68-71, 343-354.

5.3 (a) N. Metropolis, A. W. Rosenbluth, M. N. Rosenbluth, H. Teller, and E. Teller, *J. Chem. Phys.* **21**, 1087 (1953);

(b) J. P. Valleau and S. G. Whittington in *Modern Theoretical Chemistry*, B.J. Berne, Ed., Phenum, New York, 1977, vol. 5, pp. 137-168.

5.4 P. Pechukas, *Phys. Rev.* **181**, 166, 174 (1969).

5.5 (a) W. H. Miller, *J. Chem. Phys.* 53, 1949 (1970);

(b) W. H. Miller, *Adv.Chem. Phys.* **25**, 69 (1974).

5.6 (a) W. H. Miller, S. D. Schwartz, and J. W. Tromp, *J. Chem. Phys.* **79**, 4889 (1983);

(b) R. Jaquet and W. H. Miller, *J. Phys. Chem.* **89**, 3139 (1984);

(c) K. Yamashita and W. H. Miller, *J. Chem. Phys.* **82**, 5475 (1985).

5.7 (a) D. Thirumalai and B. J. Berne, *J. Chem. Phys.* **79**, 5029 (1983); **81**, 2512 (1984);

(b) D. Thirumalai, E. J. Bruskin, and B. J. Berne, *J. Chem. Phys.* **79**, 5063 (1983);

(c) D. Thirumalai and B. J. Berne, *Ann. Rev. Phys. Chem.* **37**, 401 (1986).

5.8 (a) E. C. Behrman, G. A. Jongeward, and P. G. Wolynes, *J. Chem. Phys.* **79**, 6277 (1983);

(b) E. C. Behrman and P. G. Wolynes, *J. Chem. Phys.* **83**, 5863 (1985).

5.9 (a) J. D. Doll, *J. Chem. Phys.* **81**, 3536 (1984);

(b) J. D. Doll and D. L. Freeman, *Science* **234**, 1356 (1986).

5.10 J. Chang and W. H. Miller, *J. Chem. Phys.* **87**, 1648 (1987).

5.11 J. D. Doll, R. D. Coalson, and D. L. Freeman, *J. Chem. Phys.* **87**, 1641 (1987).

5.12 (a) M. Parrinello and A. Rahman, *J. Chem. Phys.* **80**, 860 (1984);

(b) C. D. Jonah, C. Romero, and A. Rahman, *Chem. Phys. Lett.* **123**, 209 (1986).

5.13 (a) R. A. Kuharski and P. J. Rossky, *Chem. Phys. Lett.* **103**, 357 (1984);

(b) R. A. Kuharski and P. J. Rossky, *J. Chem. Phys.* **82**, 5164 (1985).

5.14 (a) A. Nichols III, D. Chandler, Y. Singh, and D. Richardson, *J. Chem. Phys.* **81**, 5109 (1984);
(b) M. Sprik, M. L. Klein, and D. Chandler, *J. Chem. Phys.* 83, 3042 (1985).

5.15 (a) J. Bartholomew, R. Hall, and B. J. Berne, *Phys. Rev. B* 32, 548 (1985);
(b) A. Wallquist and B. J. Berne, *Chem. Phys. Lett.* 117, 214 (1985);
(c) A. Wallquist, D. Thirumalai and B. J. Berne, *J. Chem. Phys.* 85, 1583 (1986).

5.16 See also the entire issue *J. Stat. Phys.* 43, Nos. 5/6 (1986).

5.17 This method appeared previously in the following article:
N. Makri and W. H. Miller, *Chem. Phys. Lett.* 139, 10 (1987).

5.18 V. S. Filinov, *Nucl. Phys. B* 271, 717 (1986).

5.19 (a) B. I. Halperin and P. C. Hohenberg, *Rev. Mod. Phys.* 49, 435 (1977);
(b) D. J. E. Callaway, F. Cooper, J. R. Klauder, H. A. Rose, *Nucl. Phys. B* 262, 19 (1985).

5.20 J. D. Doll, private communication to W. H. Miller.

5.21 See, for example, G.F. Carrier, M. Krook, and C.E. Pearson, *Functions of a Complex Variable*, Mc Graw-Hill, 1966.

5.22 See the discussion in Ref. 5.17.

5.23 J. D. Doll, D. L. Freeman, and M. J. Gillan, *Chem. Phys. Lett.* 143, 277 (1988).

5.24 M. Abramowitz and I. A. Stegun, *Handbook of Mathematical Functions*, U.S. Government Printing Office, 1964, p. 446 *et seq.*.

5.25 (a) J. D. Doll, R. D. Coalson, and D. L. Freeman, *Phys. Rev. Lett.* 55, 1 (1985);
(b) R. D. Coalson, and D. L. Freeman, and J. D. Doll, *J. Chem. Phys.* 85, 4567 (1986);

5.26 R. D. Coalson, *J. Chem. Phys.* 85, 926 (1986).

5.27 C. H. Bennett, *J. Comp. Phys.* 22, 245 (1976).

5.28 Most of the path integral calculations presented in Section 4 appeared in the following article:
N. Makri and W. H. Miller, *J. Chem. Phys.* 89, 2170 (1988).

5.29 N. Makri and W. H. Miller, *Chem. Phys. Lett.* 151, 1 (1988).

5.30 (a) S. Kirkpatrick, C. D. Gelatt, Jr., and M. P. Vecchi, *Science* 220, 671 (1983);
(b) M. Sprik and M. L. Klein, *J. Chem. Phys.* 87, 5987 (1987).

5.31 M. Sprik, M. L. Klein, and D. Chandler, *Phys. Rev. B* 31, 4234 (1985).

VI. Effective Non-oscillatory Real Time Propagator

1. Introduction

In recent years, Feynman path integration [6.1] has found extensive use in the study of equilibrium statistical mechanical properties. Discretization of the integration variables on a grid converts the path integral into matrix multiplication,[6.2] an iterative scheme which is very efficient for systems of only a few degrees of freedom. Many body problems cannot be dealt with the above technique, though, as the size of the coordinate grid grows exponentially with the number of degrees of freedom. Monte Carlo methods, [6.3] which are specifically designed to handle multidimensional integrals, provide an efficient tool in that case and have been successfully used in statistical mechanical calculations.

However, the above methodology is much less straightforward to apply for studying dynamical properties, as was made clear in the previous Chapter. Although the path integral formalism for the real time propagator, $\exp(-iHt/\hbar)$, is identical to that for the Boltzmann operator, $\exp(-\beta H)$, the standard coordinate representation of the former is highly oscillatory. Matrix multiplication is then inappropriate as a propagation scheme. There exist numerical techniques that propagate a wavefunction on a grid using the fast Fourier transform (FFT) method,[6.4,6.5] and which are very efficient for problems of only a few degrees of freedom. For multidimensional systems, though, Monte Carlo path integration provides the only known alternative. Unfortunately, ordinary importance sampling methods cannot be used to evaluate the rapidly oscillatory integrals encountered in dynamical calculations. Approximate techniques for performing integration of oscillatory integrands by using the existing Monte Carlo methodology have recently been developed and were described in Chapter V (see also references 6.6 and 6.7). These methods introduce a weighting function which is constructed to sample primarily about the stationary phase points of

the integrand, and show promise for studying the real time dynamics of chemical systems.

The purpose of this Chapter is to describe a new approach to real time path integration. It is shown that the highly oscillatory behavior of the short time propagator in its standard (coordinate) representation can be eliminated if the properties of the wavefunction are properly exploited. An effective system-specific real time propagator is obtained, which is localized and devoid of rapid oscillations. This effective propagator is thus well suited for time propagation by matrix multiplication and – more importantly – for straightforward Monte Carlo path integration. The method is strictly quantum mechanical and yet very easy to implement. Another attractive feature of this approach is that its convergence characteristics are determined from the Fourier spectrum of the wavefunction in a simple and straightforward way.

Section 2 describes the idea and constructs the new effective propagator. Some numerical examples which illustrate the properties of this propagator are presented in Section 3, and conclusions regarding the possible applications of the method appear in Section 4.

2. The effective propagator

Suppose we wish to propagate an initial state $|\Psi(0)>$ for a short time t by performing a single step path integral. The procedure is expressed formally by inserting a complete set of position eigenstates between the time evolution operator and the initial state ket:

$$<x|\Psi(t)> = \int_{-\infty}^{\infty} dx' <x|e^{-iHt/\hbar}|x'><x'|\Psi(0)>. \qquad (6.1)$$

This is the traditional idea which when used repeatedly leads to the notion of an "integral over all paths". Unfortunately, the coordinate matrix element of the propagator in the previous equation is a rapidly oscillatory function of x' – behaving as $\exp[\frac{i}{\hbar}\frac{m}{2t}(x-x')^2]$ through leading order – and thus numerical integration of Eq. (6.1)

is a demanding task, particularly so if t is small. Since all known approximations to the coordinate representation of the propagator are only valid for short time, the problems associated with the numerical evaluation of a path integral become apparent.

Another formally exact way of arriving at an expression similar to Eq. (6.1), i.e., of expressing the time evolved wavefunction as an integral of a time dependent kernel times the initial state wavefunction, is to use the completeness property of momentum eigenstates; this leads to the relation

$$<x|\Psi(t)> = \int_{-\infty}^{\infty} dp <x|e^{-iHt/\hbar}|p><p|\Psi(0)>. \tag{6.2}$$

The $x-p$ matrix element of the propagator which appears in Eq. (6.2), i.e., the *mixed representation kernel*, can be interpreted as the coordinate representation of a propagated plane wave, which at $t=0$ had the form

$$<x|p> = \frac{1}{\sqrt{2\pi\hbar}} e^{ipx/\hbar}. \tag{6.3}$$

It is important to emphasize that the $t \to 0$ limit of the $x-p$ propagator is a well defined function, in contrast to the $x-x'$ kernel of Eq. (2.1), which behaves as $\delta(x-x')$ and is thus very singular in that limit.

One can obtain a quite good approximation for the short time evolution of a wavefunction by expressing it as the exponential of a power series in time, and requiring that the wavefunction satisfy the time dependent Schrödinger equation through various orders in t. This procedure (which is similar to the exponential power series expansion for the propagator described in Chapter VII and in Ref. 6.14) determines the expansion coefficients in a simple recursive scheme and is outlined in the Appendix. Assuming a one-dimensional cartesian Hamiltonian of the form

$$H = \frac{p^2}{2m} + V(x),$$

the result for the propagation of a plane wave through order t is

$$<x|e^{-iHt/\hbar}|p> = \frac{1}{\sqrt{2\pi\hbar}}\, e^{\frac{i}{\hbar}\{px - [\frac{p^2}{2m}+V(x)]t\}} \qquad (6.4)$$

Higher order terms are easy to obtain, and the multidimensional generalization is straightforward.

Eq. (6.2), with the propagator given by Eq. (6.4), should be easy to integrate numerically for small values of t, since the $x-p$ propagator is well behaved. However, one can readily see that the stationary phase point for the p-integration occurs at $p=mx/t$, i.e., at higher values of momentum as t becomes smaller. Thus the rapidly oscillatory behavior of the integrand shows up in Eq. (6.2) as well, and it appears that we have gained nothing by introducing the mixed representation.

However, such high values of p are of no significance to the actual time evolution of a given initial state, even though they are important for the propagator itself. This is so because the integrand of Eq. (6.2) includes the momentum representation of the wavefunction, which will typically decay exponentially with p. That is, the presence of the momentum space wavefunction in the integrand of Eq. (6.2) effectively prevents the latter from being rapidly oscillatory, and thus allows numerical evaluation of the integral.

The physically relevant range of momentum values for a particular problem can be identified by examining the Fourier transform of the initial wavefunction. This gives a cut-off value p_{max}, which can be chosen according to the desired accuracy. Wavefunctions usually spread in position space under propagation, which makes their Fourier transform a narrower function as the time progresses. Convergence is easily tested by increasing the cut-off value p_{max}.

Once the momentum range that is relevant to the time evolution of the state of interest has been estimated, one can bring the problem in the traditional form, namely the position representation of Eq. (6.1). Noting that the completeness relation in the momentum representation becomes for the present purpose

$$1 = \int_{-p_{max}}^{p_{max}} |p><p|, \tag{6.5}$$

an *effective coordinate propagator* can be defined as

$$<x|e^{-iHt/\hbar}|x'>_{eff} = \int_{-p_{max}}^{p_{max}} dp <x|e^{-iHt/2\hbar}|p><p|e^{-iHt/2\hbar}|x'>. \tag{6.6}$$

The second factor in Eq. (6.6) is easily obtained from Eq. (6.4) by invoking time reversal symmetry arguments, i.e., by replacing t by $-t$ and complex conjugating. In light of the arguments presented above, this effective propagator is expected to exhibit smooth behavior for finite values of p_{max}.

It is useful to obtain an explicit formula for the effective propagator, and for this purpose we integrate Eq. (6.6) analytically. The integration is possible because the exponent of the propagator [cf. Eq. (6.4)] is *quadratic* in p. (This is actually true up to order t^3.) The result is

$$<x|e^{-iHt/\hbar}|x'>_{eff} = \sqrt{\frac{m}{2\pi i\hbar t}}\, e^{\frac{i}{\hbar}\{\frac{m}{2t}(x-x')^2 - \frac{t}{2}[V(x)+V(x')]\}}$$

$$\times f_{smooth}(x-x';p_{max};t) \tag{6.7a}$$

with f_{smooth} given by

$$f_{smooth}(x-x';p_{max};t) = \frac{1}{2}[\mathrm{erf}\,(\sqrt{\frac{it}{2m\hbar}}p_{max} + \sqrt{\frac{im}{2\hbar t}}(x-x'))$$

$$+\mathrm{erf}\,(\sqrt{\frac{it}{2m\hbar}}p_{max} - \sqrt{\frac{im}{2\hbar t}}(x-x'))], \tag{6.7b}$$

where $\mathrm{erf}\,(z)$ is the error function of complex argument,[6.8]

$$\mathrm{erf}\,(z) = \frac{2}{\sqrt{\pi}}\int_0^z e^{-x^2}dx.$$

The first factor in Eq. (6.7) is recognized as the standard expression for the coordinate representation of the propagator, which is obtained by using the Trotter

product rule. The part involving the error functions (the *smoothing factor*), though, is the new result of this Section. It is this part of the effective propagator that smooths out the oscillations present in the kinetic energy part of the Trotter propagator. It is easy to check that Eq. (6.7) reduces to the standard Trotter form of the short time propagator if $p_{\max}\to\infty$:

$$\lim_{p_{\max}\to\infty} \langle x|e^{-iHt/\hbar}|x'\rangle_{\text{eff}} = \sqrt{\frac{m}{2\pi i\hbar t}}\, e^{\frac{i}{\hbar}\{\frac{m}{2t}(x-x')^2-\frac{t}{2}[V(x)+V(x')]\}} . \tag{6.8}$$

To establish the properties of this effective propagator, it is useful to distinguish between two cases:

(a) For points x' sufficiently far from x, such that

$$\frac{m}{t}|x-x'|\gg p_{\max} \qquad \text{and} \qquad \sqrt{\frac{m}{\hbar t}}|x-x'|\to\infty, \tag{6.9a}$$

(the *classically inaccessible region*), one can use the asymptotic properties of the error function [6.8] to show that the smoothing factor of Eq. (6.7) is proportional to

$$f_{\text{smooth}}(x-x';p_{\max};t) \sim \frac{1}{x-x'}\, e^{-\frac{i}{\hbar}\frac{m}{2t}(x-x')^2} \sin[p_{\max}(x-x')/\hbar]. \tag{6.9b}$$

The second term in the exponential of the above equation *cancels the fast oscillations* that arise from the kinetic energy part of Eq. (6.7). The only oscillations that remain are of constant wavelength, and the effective propagator is *damped* as $(x-x')^{-1}$ with increasing separation of the coordinate points. These features are very useful for the purpose of numerical integration, and are illustrated in Fig. 6-1.

(b) For x' near x, i.e., if

$$\frac{m}{t}|x-x'|<p_{\max}, \tag{6.10a}$$

(the *classically accessible region*), one can only use the asymptotic behavior of the error function if

$$\sqrt{\frac{t}{\hbar m}}p_{\max}\gg 1. \tag{6.10b}$$

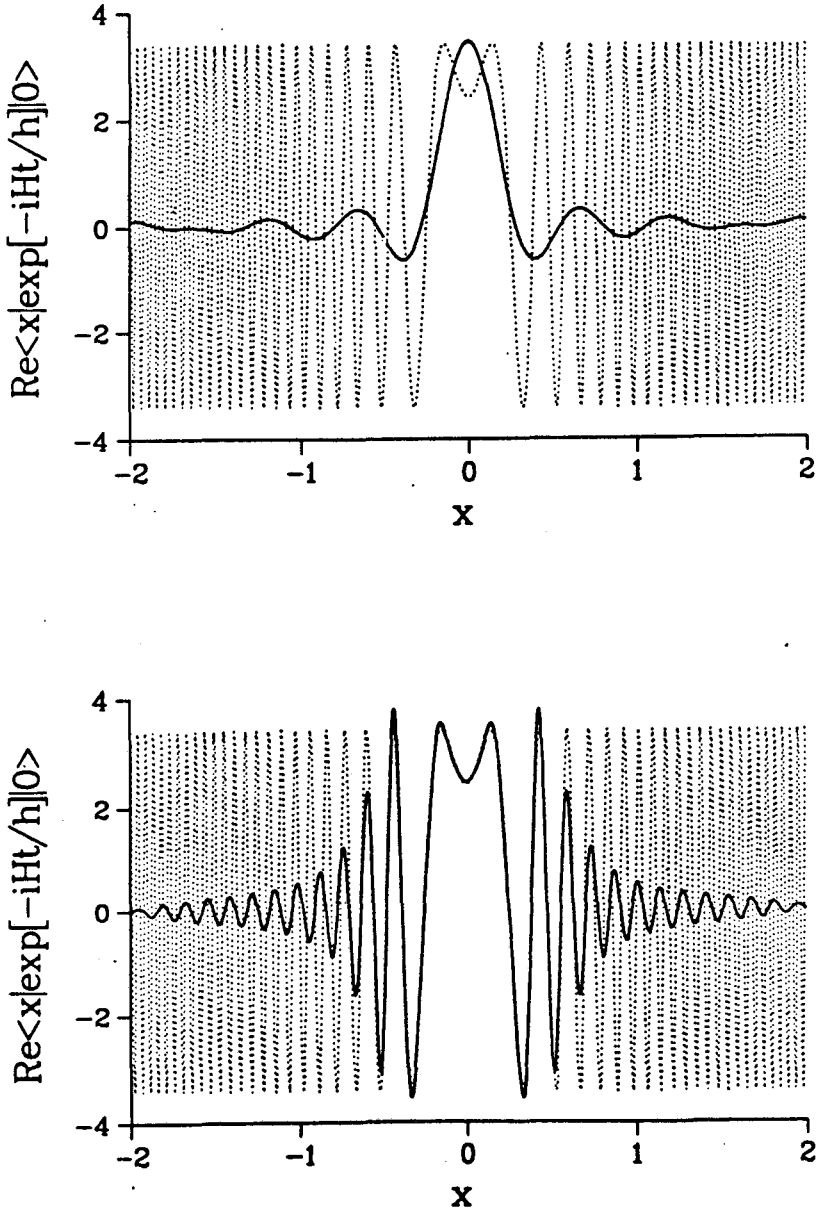

Fig. 6-1

Comparison of the effective propagator, Eq. (6.7), to the standard propagator, Eq. (6.8), for two different values of cut-off momentum p_{max}. Plotted is the real part of the propagator with $x'=0$ as a function of x, for the double well potential of Eq. (6.12). The time step is equal to 1/40 of the period that corresponds to the harmonic potential at the minimum. Solid line: effective propagator, Eq. (6.7), with cut-off momentum value p_{max}. Dotted line: standard propagator, Eq. (6.8). (a) p_{max}=12 atomic units; this is the value which was used in the first application of Section 3. (b) p_{max}=48 atomic units.

This is the case with large time increment t, large momentum cut-off p_{max}, or small $\hbar$. Then the smoothing factor approaches unity and the effective propagator behaves like the standard short time propagator. If one were to integrate Eq. (6.7) over x' in order to propagate a wavefunction, stationary phase points would occur whenever

$$\frac{m}{t}(x-x') = -\frac{t}{2}V'(x'), \tag{6.10c}$$

i.e., on the classical path. [Points x' that satisfy Eq. (6.10c) but do *not* lie within the range dictated by Eq. (6.10a) are to be ignored. Phrased in different words, this fact states that classical paths of momentum higher that p_{max} are not allowed in the present situation.]

Fig. 6-1 shows the real part of the effective propagator, Eq. (6.7), with $x'=0$, for the case of a double well potential (see Section 3) for two different cut-off values p_{max}. For Fig. 6-1a, p_{max} was chosen based on the momentum distribution of the initial state used in the first numerical example of Section 3. In Fig. 6-1b, a much larger value of p_{max} was used. The behavior described above is clearly seen. The standard Trotter propagator, Eq. (6.8), is also shown in the same figures for comparison. It is interesting to point out that the asymptotic property, Eq. (6.9a), is satisfied faster for shorter t. This means that the above behavior is approached for relatively small separations $x-x'$ if the time increment is small.

Consider now using the effective propagator, Eq. (6.7), to evaluate a path integral by Monte Carlo methods. Since the damping of the integrand at large separation is built in the propagator, one can multiply and divide the integrand by a function

$$F(x,x') = \sqrt{\frac{\lambda}{\pi}}\, e^{-\lambda(x-x')^2} \tag{6.11}$$

which is to be used as the sampling function. The parameter λ is chosen such that Eq. (6.11) resembles the true $(x-x')^{-1}$ behavior of the integrand as closely as

possible over a fixed interval which is determined to be important in the integration. Since the weighting function, Eq. (6.11), is normalized one need not calculate normalization integrals numerically.[6.6b]

Comparison of the method proposed here with stationary phase based Monte Carlo schemes [6.6,6.7] is due at this point. When the standard highly oscillatory expression, Eq. (6.8), is used as the short time propagator in a path integral, *all* conceivable paths that connect the given initial and final points contribute with the *same absolute weight* (probability) but different phases. The numerical value of the integral is then the result of enormous cancellation, with the dominant contributions coming from the stationary phase regions of the integrand, which correspond to classical paths. If, on the other hand, the effective short time propagator of Eq. (6.7) is used instead, then phase cancellation is a relatively unimportant issue in determining the numerical value of the result. The reason for this is that different paths are *weighted differently* and give rise to slowly varying phases in the present case. Thus, short paths tend to dominate, as they enter the path integral with relatively large probability, while paths involving steps in the "classically inaccessible region" contribute with much smaller absolute weight. Classical paths of the latter type (i.e., of high kinetic energy) have essentially zero contribution, and short classical paths are not treated more favorably than other short paths. Stated more explicitly, in the present method one sums over *all* paths that are allowed by the momentum range of the wavefunction. This is now doable and efficient, provided that the effective propagator is not rapidly oscillatory in the region where it has significant amplitude. The fact that it is not necessary to exclude non-classical-like paths from the summation means that quantum effects are fully accounted for when the effective propagator of Eq. (6.7) is used.

It is also of interest to point out a remote connection of the present approach with the partial averaging technique of Ref. 6.9. According to the partial averaging

method, one tries to include paths of high frequency Fourier components in order to obtain a more accurate short time propagator. In the approach taken here, though, one eliminates all large momentum components from the effective propagator, knowing that their contribution is exponentially small when the propagator is multiplied by a wavefunction with a bound Fourier spectrum.

The efficiency of the scheme suggested above depends heavily on how smoothly the effective propagator behaves in the "classically accessible region". It is not hard to show that the generic behavior of the effective propagator is that indicated in Fig. 6-1a, i.e., the "asymptotic region" where the propagator is damped has been reached by the time *only one* or so phase oscillation has been completed, as long as the problem belongs to the quantum regime (small quantum numbers). To illustrate this we examine the $\hbar \to 0$ limit of the effective propagator when the quantum number of the state is held fixed, noting that in that limit the cut-off momentum $p_{\max}$ also vanishes. [This is so because the phase space volume $\Delta x \Delta p$ occupied by a quantum state is (for one degree of freedom) proportional to Planck's constant. (Here Δx and Δp can be defined as the distance between classical turning points in position and in momentum space, respectively.) Typically (e.g., for a harmonic potential) $\Delta x \sim \sqrt{\hbar}$ and $\Delta p \sim \sqrt{\hbar}$, which implies that $p_{\max} \sim \sqrt{\hbar}$.] It then follows that for time increment smaller than the period corresponding to the shortest time scale of the problem, the change in the action through the entire "classically accessible region" of Eq. (6.10a) (beyond which the effective propagator is damped) is only of order $\hbar$.

We thus anticipate the effective propagator of Eq. (6.7) to be most useful in situations where quantum effects are large. Such cases are intimately connected with the existence of coalescing or complex stationary phase points of the integrand and tend to render stationary phase based approximations inaccurate. In the opposite limit, where classical mechanics plays the principal role in determining the dynamics (e.g., with highly excited states of with very harmonic-like potentials), semiclassical

approximations are already quite accurate; in such cases calculation of quantum corrections using stationary phase Monte Carlo methods should be an easier task than attempting to obtain the full quantum solution directly according to the method described in this Section, which is not biased toward sampling near classical paths.

Finally, we point out that the analytic integration of Eq. (6.6) can be performed as easily with the propagator of Eq. (6.4) including terms up to order t^3. This results in more accurate expressions, and also brings derivatives of the potential in the arguments of Eq. (6.8). The smooth part of the resulting propagator can then be used for evaluation of a path integral using Metropolis sampling techniques.

3. Numerical applications

In this Section we present several numerical calculations that illustrate the features of the effective propagator discussed in Section 2 and its usefulness for evaluating path integrals by Monte Carlo methods.

The most important property of the effective propagator is that it is localized and relatively smooth. To demonstrate this we first use it to propagate a wavefunction according to the matrix multiplication scheme.[6.2] Specifically, a vector containing the values of the wavefunction at selected grid points is generated at each time step; this vector is then multiplied by the propagator matrix, to yield the wavefunction vector at the next time increment. This is equivalent to doing a path integral but has the advantage of being free of statistical error, thus permitting unambiguous assessment of the accuracy of the method.

For the first application, a Gaussian wavepacket is propagated in a one dimensional symmetric double well potential of the form

$$V(x) = -\frac{1}{2}a_0x^2 + \frac{1}{4}c_0x^4, \tag{6.12}$$

with the parameters chosen such that the mass is that of a hydrogen atom and the barrier height is approximately 4 kcal/mol. The initial Gaussian wavepacket is

centered at one minimum of the double well and has a width equal to that of the ground state of the local harmonic approximation to the potential. The duration of the tunneling process corresponds to many vibrational periods. The wavefunction was propagated for a full tunneling period using the effective propagator of Section 2 with the time step equal to about 1/40 of the harmonic vibrational period and the results were compared to those of numerically exact calculations performed by standard basis set methods. (Such short time step was necessary in order to obtain results of the accuracy mentioned below for time as long as a full tunneling period.) A grid of only 25 points was used to span the x coordinate. Had we used the standard coordinate propagator instead of the effective propagator of Section 2, hundreds of points would have been necessary to construct an adequate propagation matrix. The coordinate matrix element of the propagator that was used in the calculation with $x'=0$ is shown in Fig. 6-1a. Figure 6-2 shows the survival probability (the time autocorrelation function squared) as a function of time. The agreement of the results obtained by using the effective propagator scheme with the exact ones is seen to be excellent at all times. In fact, the results converged to 3 decimal figures, and arbitrary precision can be achieved by adjusting the cut-off value of the momentum range used in the calculation.

The second example involves a two dimensional model that describes the dynamics of energy transfer between the CH stretch and the CCH in-plane wag in benzene. For quantum numbers v=4-8, where broad spectra are observed experimentally, the process takes place via a Fermi resonance type interaction [6.10] and the local mode picture is appropriate. Our model potential has the form

$$V(s,Q) = D(1-e^{-as})^2 + \frac{1}{2}m_Q\omega_0^2 e^{-cs}Q^2. \qquad (6.13)$$

Here s represents the CH stretch coordinate and Q the CCH in-plane wag, with the parameters chosen to fit those of Ref. 6.10. A contour plot of the potential is shown in Fig. 6-3.

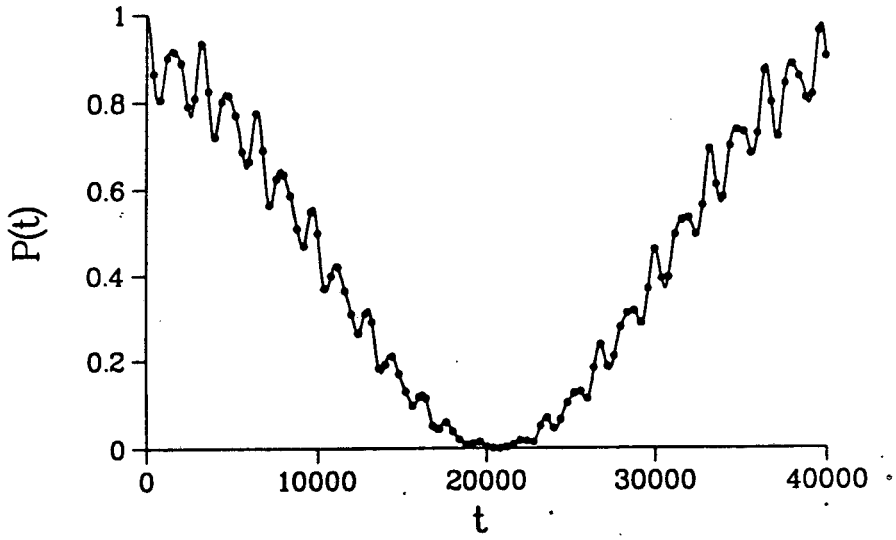

Fig. 6-2

The survival probability, $P(t)=|\langle\Psi(0)|e^{-iHt/\hbar}|\Psi(0)\rangle|^2$, for a Gaussian which starts out as an eigenstate of the local harmonic approximation to the double well potential [Eq. (6.12)] about one minimum. The points show results obtained by propagating the wavefunction according to the matrix multiplication scheme, with time step equal to that used in Fig. 6-1. Exact results, obtained by a basis set calculation, are indicated by the solid line for comparison.

In order to test the ability of the present method to accurately describe the dynamics of energy flow, we propagate an initial state which is an eigenstate of the uncoupled ($c=0$) Hamiltonian with 4 quanta in the CH oscillator. Fig. 6-4 shows the survival probability as a function of time and compares with exact results obtained by a basis set calculation.

Finally, we present a path integral calculation of the survival probability for a Gaussian wavepacket in a one dimensional Morse potential,

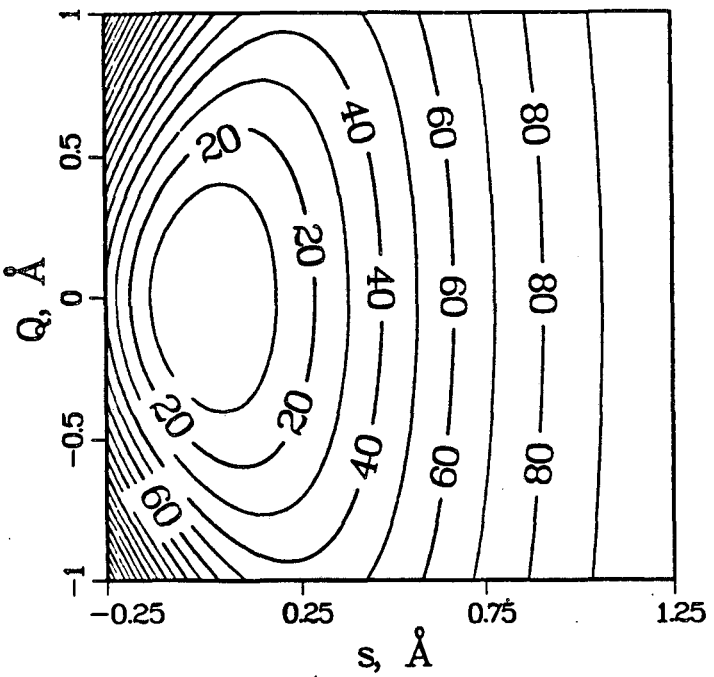

Fig. 6-3

Contour plot of the two dimensional potential that describes the dynamics of energy flow between the CH stretch and the CCH in-plane wag in benzene [cf. Eq. (6.13)]. The numbers labeling the curves indicate the height of the potential surface in kcal/mol.

$$V(x) = D\ (e^{-2\alpha x} - 2e^{-\alpha x}), \tag{6.14}$$

with D=0.164 and α=0.9374 in atomic units (see also Ref. 6.5c), using the Monte Carlo integration scheme. The parameters are chosen to correspond roughly to the vibrational motion of H_2, i.e., the well depth is 4.46 eV and the harmonic frequency at the minimum is 3910 cm^{-1}. The initial wavepacket is displaced by –0.1 Å from the equilibrium position and has width which corresponds to the frequency at the bottom of the potential well. The calculation was performed with a time step equal to about 1/20 of the vibrational period, with 100000 Monte Carlo points per integration

variable. The computational details are as described in Ref. 6.6b, except that in the present case a sampling function of the type given by Eq. (6.11) was used and thus the normalization integral [6.6b] was obtained analytically. Fig. 6-5 shows the survival probability as given by the Monte Carlo calculation with the effective propagator of Section 2 and compares with the exact results. It is seen that accurate results with reasonably small statistical error can be obtained, while an extremely simple Monte Carlo algorithm was used.

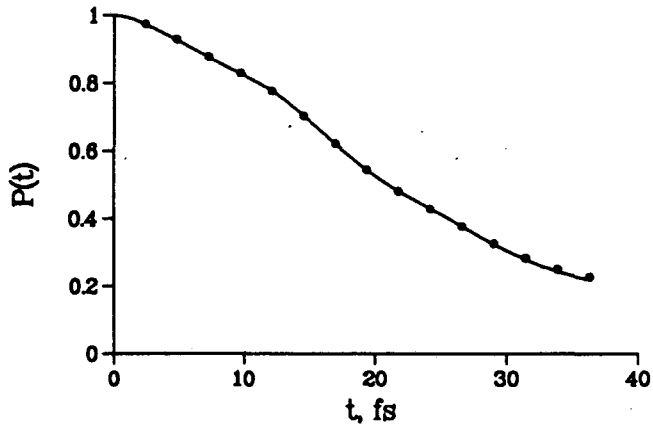

Fig. 6-4

The survival probability for a wavefunction in the potential of Fig. 6-3 [Eq. (6.13)]. The initial state is an eigenstate of the uncoupled (c=0) Hamiltonian, with 4 energy quanta in the CH coordinate. The points show results obtained by propagating the wavefunction according to the matrix multiplication scheme. Exact results, obtained by a basis set calculation, are indicated by the solid line for comparison.

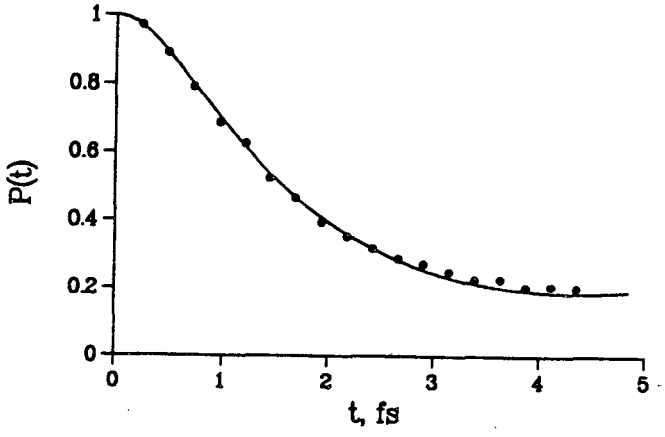

Fig. 6-5

The survival probability for a wavefunction in a Morse potential. The initial state is a Gaussian wavepacket which is displaced by –0.1Å from the equilibrium position and has width equal to that of the eigenstate of the harmonic approximation at the potential minimum. The points show results obtained by a Monte Carlo calculation using a time step equal to about 1/20 of the vibrational period with 100000 Monte Carlo points per integration variable. The solid line shows exact result, obtained by a basis set calculation.

4. Discussion and concluding remarks

The analysis of Section 2, along with the numerical calculations of Section 3, shows that the effective propagator defined in Section 2 possesses the important properties of localization and smooth behavior which are essential to numerical evaluation of a path integral. The most important feature is that the calculation can be made as accurate as desired by adjusting the cut-off value of momentum explored by the wavefunction of interest. Furthermore, the fact that the sampling function for the Monte Carlo calculation has an extremely simple form results in considerable savings, as it is analytically normalizable (a fact important in real time dynamics), and

also eliminates the need for search of stationary phase points of the integrand, which is usually a demanding task. We therefore believe that the effective propagator will prove useful for studying the dynamics of multidimensional systems by path integral methods.

Furthermore, we suggest that the effective propagator should also find utility in the calculation of correlation functions,

$$C(t) = \mathrm{tr}\,[e^{iHt_c^*/\hbar}\hat{A}e^{-iHt_c/\hbar}\hat{B}\,], \tag{6.15}$$

where $\hat{A}$ and $\hat{B}$ are quantum mechanical operators, and $t_c \equiv t - i\hbar\beta/2$, with $\beta = 1/kT$. [By setting both $\hat{A}$ and $\hat{B}$ equal to the flux operator,

$$F = \frac{1}{2m}[\delta(\hat{s}-s_0)\hat{p}_s + \hat{p}_s\delta(\hat{s}-s_0)], \tag{6.16}$$

one obtains the flux correlation function,[6.11] whose time integral yields the rate of a reactive process. In Eq. (6.16) s is the reaction coordinate and s_0 its value at the dividing surface, i.e., the surface through which the flux is measured.]

To evaluate Eq. (6.15) in a path integral fashion, one must be able to compute the complex time propagator. Expressing the latter as

$$\langle x|e^{-iHt_c/\hbar}|x'\rangle = \int dx'' \langle x|e^{-iHt/\hbar}|x''\rangle\langle x''|e^{-\beta H}|x'\rangle \tag{6.17}$$

allows one to think of the problem in a way similar to Eq. (6.1). Specifically, the coordinate matrix element of the Boltzmann operator that appears in Eq. (6.17) effectively plays the role of a wavefunction [6.12] and thus defines a momentum cut-off value. Small temperature (large β) should be easier to deal with, as only low energy states are occupied in that case. The calculation should be rather similar to the time propagation of wavefunctions treated in this Chapter, but numerical tests are necessary in order to assess the actual feasibility and usefulness of the method for studying non-equilibrium properties of complex systems.

Finally we wish to emphasize that the method suggested in this Chapter should

be more difficult to implement for studying long time dynamics, as is true of all path integral methods. [By "long time" we mean time much longer than the shortest time scale that appears in the problem, i.e., time for which many (e.g., hundreds of) time slices will be required to yield convergent results.] Apart from reasons pertaining to the dimensionality of the integral itself, which increases with the time, additional problems often arise. These are usually associated with the existence of multiple classical paths that connect the given endpoints. Stationary phase based methods must explicitly search for these classical paths, and this is a non-trivial task. Use of the effective non-oscillatory propagator scheme excludes paths of large momentum steps but samples all paths of momentum smaller than the cut-off value. While the method does so in a very efficient way, i.e., by circumventing the problem of highly oscillatory behavior that would arise if the standard propagator were used, it is still expected that the statistical error will grow with time, since larger fluctuations from the straight line path will then be included. The staging algorithm [6.13] is ideally suited for dealing with such problems, and we believe that it will help to extend the range of applicability of the effective propagator technique described in this Chapter to problems requiring much longer time propagation.

Appendix

Here we describe a simple recursive procedure for obtaining analytically the short time evolution of a wavefunction in a Hamiltonian of the form

$$H = \frac{\mathbf{p}^2}{2m} + V(\mathbf{x}).$$

The procedure is similar to the exponential power series expansion of the propagator presented in Ref. 6.14. We *assume* that the propagated wavefunction can be written as a single exponential, i.e.,

$$\Psi(\mathbf{x},t) \equiv e^{iW(\mathbf{x},t)/\hbar} \tag{6.18a}$$

and expand the exponent in a power series in time:

$$W(\mathbf{x},t) = \sum_{n=0} W_n(\mathbf{x}) t^n. \tag{6.18b}$$

[The above assumption is *not* always valid, e.g., Eq. (6.18) cannot describe the evolution of a wavepacket near a turning point, where the resulting wavefunction is composed of an indident plus a reflected wave.] Substituting Eq. (6.18) into the time dependent Schrödinger equation and equating like powers of t yields the following recursion relations which determine the expansion coefficients $W_n(\mathbf{x})$:

$$W_1 = -V + \frac{i\hbar}{2m}\nabla^2 W_0 - \frac{1}{2m}(\nabla W_0)^2, \tag{6.19a}$$

$$W_{n+1} = \frac{1}{n+1}\left[\frac{i\hbar}{2m}\nabla^2 W_n - \frac{1}{2m}\sum_{k=0}^{n} \nabla W_k \cdot \nabla W_{n-k}\right], \qquad n \geq 1 \tag{6.19b}$$

where W_0 is given by the logarithm of the initial wavefunction:

$$W_0 = -i\hbar \ln \Psi(0). \tag{6.19c}$$

Application to the time evolution of a plane wave (see Section 2) is straightforward.

References

6.1 (a) R. P. Feynman, *Rev. Mod. Phys.* **20**, 367 (1948);

(b) R. P. Feynman and A. R. Hibbs, *Quantum Mechanics and Path Integrals*, McGraw-Hill, New York, 1965.

6.2 D. Thirumalai, E. J. Bruskin, and B. J. Berne, *J. Chem. Phys.* 79, 5063 (1983);

6.3 (a) N. Metropolis, A. W. Rosenbluth, M. N. Rosenbluth, H. Teller, and E. Teller, *J. Chem. Phys.* 21, 1087 (1953);

(b) J. P. Valleau and S. G. Whittington in *Modern Theoretical Chemistry*, B. J. Berne, Ed., Phenum, N.Y., 1977, vol. 5, pp. 137-168.

6.4 (a) M. D. Feit, J. A. Fleck, Jr., and A. Steiger, *J. Comp. Phys.* 47, 412 (1982);

(b) M. D. Feit and J. A. Fleck, Jr., *J. Chem. Phys.* 78, 301 (1983).

6.5 (a) R. Kosloff and D. Kosloff, *J. Chem. Phys.* 79, 1823 (1983);

(b) R. Kosloff and C. Cerjan, *J. Chem. Phys.* 81, 3722 (1984);

(c) R. Kosloff, *J. Phys. Chem.* 92, 2087 (1988).

6.6 (a) N. Makri and W. H. Miller, *Chem. Phys. Lett.* 139, 10 (1987);

(b) N. Makri and W. H. Miller, *J. Chem. Phys.* 89, 2170 (1988).

6.7 (a) J. D. Doll and D. L. Freeman, *Adv. Chem. Phys.* 73, 120 (1988);

(b) J. D. Doll, D. L. Freeman, and M. J. Gillan, *Chem. Phys. Lett.* 143, 277 (1988);

(c) J. D. Doll, T. L. Beck, and D. L. Freeman, *J. Chem. Phys.* 89, 5753 (1988).

6.8 M. Abramowitz and I. A. Stegun, *Handbook of Mathematical Functions*, Dover, New York.

6.9 (a) J. D. Doll, R. D. Coalson, and D. L. Freeman, *Phys. Rev. Lett.* 55, 1 (1985);

(b) R. D. Coalson, D. L. Freeman, and J. D. Doll, *J. Chem. Phys.* 85, 4567 (1986).

6.10 E. L. Sibert, W. P. Reinhardt, and J. T. Hynes, *J. Chem. Phys.* 81, 1115 (1984).

6.11 W. H. Miller, S. D. Schwartz, and J. W. Tromp, *J. Chem. Phys.* 79, 4889 (1983).

6.12 (a) B. Hellsing, A. Nitzan, and H. Metiu, *Chem. Phys. Lett.* 123, 523 (1986);

(b) G. Wahnstrom and H. Metiu, *Chem. Phys. Lett.* 134, 531 (1987).

6.13 M. Sprik, M. L. Klein, and D. Chandler, *Phys. Rev.* B 31, 4234 (1985).

6.14 N. Makri and W. H. Miller, *J. Chem. Phys.* 90, 904 (1989).

VII. Improved Short Time Propagators

1. Introduction

A very important application of the path integral formulation of quantum mechanics [7.1] is that it enables the actual computation of equilibrium or dynamical properties of many body quantum systems. In the path integral formalism the problem of calculating quantum mechanical observables is transformed into an exercise in multidimensional integration. For this reason, an enormous amount of effort has recently been devoted to the development and application of Monte Carlo path integration techniques. However, the utility of Monte Carlo path integration approaches relies on the convergence characteristics of the approximations involved.

Numerical evaluation of a path integral requires that a discretized representation be used. One "slices" the total time t into N segments, each with time increment $\Delta t = t/N$:

$$\langle x_N | e^{-iHt/\hbar} | x_0 \rangle = \int dx_{N-1} \cdots \int dx_1 \prod_{k=1}^{N} \langle x_k | e^{-iH\Delta t/\hbar} | x_{k-1} \rangle, \tag{7.1}$$

and uses some short time approximation for each factor in the integrand of the above equation. The most popular approximation to the short time propagator for a Cartesian Hamiltonian of the form

$$\hat{H} = \frac{\hat{p}^2}{2m} + V(\hat{x}) \equiv \hat{T} + \hat{V}, \tag{7.2}$$

which results from use of the Trotter product formula,[7.2–7.4] is

$$\langle x_k | e^{-iH\Delta t/\hbar} | x_{k-1} \rangle$$

$$= \sqrt{\frac{m}{2\pi i \hbar \Delta t}} \exp\left[\frac{im}{2\hbar\Delta t}(x_k - x_{k-1})^2 - \frac{i\Delta t}{\hbar}\frac{1}{2}[V(x_k) + V(x_{k-1})] \right]. \tag{7.3}$$

Eq. (7.3), substituted in Eq. (7.1), has been extensively used for numerical evaluation

of path integrals. Another choice that has been used [7.1] corresponds to replacing the average potential by the potential at the average position,

$$\frac{1}{2}[V(x_k)+V(x_{k-1})] \rightarrow V(\frac{x_k+x_{k-1}}{2}) \tag{7.4}$$

in Eq. (7.3). There are a number of other, more sophisticated (and thus more difficult to apply) short time approximations that have also been suggested.[7.5–7.9]

In this Chapter we point out that even though Eq. (7.3), (7.4) and other previously suggested short time propagators all give the correct $N \rightarrow \infty$ limit in Eq. (7.1), *none* of them are actually correct through first order in Δt for finite N. We consider the exponent in the short time propagator as a power series in Δt, and derive the correct coefficients of these various orders. Neither Eq. (7.3), (7.4), nor any of the other more sophisticated approximations (that we are aware of) have even the first order term correct. The pre-exponential factor is also modified in our result. [The reason that Eq. (7.3), (7.4) and others give the correct $N \rightarrow \infty$ limit is because the first term in the exponent, the kinetic energy term, effectively restricts $(x_k - x_{k-1})$ in the integration in Eq. (7.1) to be of order $\Delta t^{1/2}$. In our treatment, though, we consider x_k and x_{k-1} to be independent variables.]

Apart from this formal improvement, though, the practically significant feature is that our short time approximation converges to the correct result more rapidly with increasing N in Eq. (7.1), while it is still simple and thus directly amenable to Monte Carlo integration methodology. Section 2 uses the semiclassical expression to derive a short time propagator up to order Δt^4. The result of this method is actually the correct quantum mechanical result through order Δt^2. In Section 3 we generate a power series expansion for the exponent of the propagator and obtain fully quantum expressions for the various terms. Corrections to the semiclassical result which are of quantum mechanical nature appear in the cubic and in higher order terms. Successive terms in the series can be calculated recursively to any order. This way, short to

intermediate (real or imaginary) time dynamics can be obtained *analytically* for any number of degrees of freedom. Analytic and numerical applications are given in Section 4, and Hamiltonians with vector potentials are treated in Section 5. The derivations in this Chapter will be presented for the real time propagator, $e^{-iHt/\hbar}$. All results are readily generalizable to complex time (for example, the corresponding expression for the Boltzmann operator is obtained by setting $it/\hbar=\beta$).

2. Semiclassical first and third order short time propagators

We will consider first a system of one degree of freedom, with a Cartesian Hamiltonian of the form shown in Eq. (7.2). The coordinate matrix element of the propagator (time dependent Green's function), $\langle x|e^{-iHt/\hbar}|x_0\rangle$, can be viewed as a wavefunction $G(x;t)$ which satisfies the time dependent Schrödinger equation and the initial condition $G(x;0)\propto\delta(x-x_0)$. The semiclassical expression for the propagator is then obtained by time evolving the initial wavefunction $\delta(x-x_0)$ according to time dependent WKB theory. Thus the initial state is considered as an *ensemble* of classical particles which are all located at x_0 at $t=0$ but whose momenta have - according to the uncertainty principle - all values from $-\infty$ to ∞. These particles are propagated for time t according to the laws of classical dynamics. If $S(x,x_0;t)$ is the action along the classical trajectory $x(t')$ of such a particle from x_0 to x in time t , i.e.,

$$S(x,x_0;t)=\int_0^t L(x(t'),\dot{x}(t');t')\,dt'=\int_0^t [\frac{1}{2}m\dot{x}(t')^2-V(x(t'))]\,dt', \qquad (7.5)$$

then the semiclassical expression for the propagator is [7.2]

$$\langle x|e^{-iHt/\hbar}|x_0\rangle=(2\pi i\hbar)^{-1/2}\left[-\frac{\partial^2 S}{\partial x_0\partial x}\right]^{1/2} e^{\frac{i}{\hbar}S(x,x_0;t)}. \qquad (7.6)$$

The quantity $\partial^2 S/\partial x_0\partial x$, which appears in the pre-exponential factor, is called the Van Vleck determinant.[7.11] The final momentum distribution of the particles is given by the x-derivative of the action:[7.10]

$$p(x,x_0;t) = \frac{\partial}{\partial x} S(x,x_0;t). \tag{7.7a}$$

The Van Vleck determinant can then be interpreted as the derivative of the final momentum with respect to the initial coordinate point:

$$\frac{\partial^2 S}{\partial x_0 \partial x} = \frac{\partial}{\partial x_0} p(x,x_0;t). \tag{7.7b}$$

The action $S(x,x_0;t)$ and the corresponding momentum distribution $p(x,x_0;t)$ may actually be *multi*valued functions of x. In that case the semiclassical expression for the propagator is modified by summing over all branches b of the momentum field $p(x,x_0;t)$: [7.23]

$$\langle x | e^{-iHt/\hbar} | x_0 \rangle = \sum_b (2\pi i \hbar)^{-1/2} \left| \frac{\partial^2 S_b}{\partial x_0 \partial x} \right|^{1/2} e^{\frac{i}{\hbar} S_b(x,x_0;t)} e^{-i\mu_b \pi/2}. \tag{7.8}$$

In the above formula μ_b is the Maslov index;[7.12] this is an integer which increments by 1 at caustics, i.e., at points where the Van Vleck determinant $\partial^2 S/\partial x_0 \partial x = \infty$. The momentum distribution $p(x,x_0;t)$ is shown in Fig. 7-1 for two different cases: a harmonic potential, $V(x) = \frac{1}{2} m\omega^2 x^2$, and a quartic potential, $V(x) \propto x^4$. In the former case, $p(x,x_0;t)$ can be shown to remain a linear function of x at all times, and therefore has only one branch for all times $t \neq \pi/\omega$, while at times $t_n = n\pi/\omega$ (caustics), the momentum distribution becomes a vertical line. This is a consequence of the fact that the frequency of the classical motion is in the case of a harmonic potential independent of the energy. In the case of the quartic potential this is no longer true. Fig. 7-2 shows some classical trajectories for these two potentials. The period of the classical motion decreases with the energy in the case of a quartic potential. As a result, a classical particle can get from x_0 to x in time t in an infinite number of ways - by performing 0,1,2,...,∞ reflections at the potential walls - for *any* (however small) t[7.2]. The corresponding action has an infinity of branches, as can be seen in Fig. 7-1. This behavior is typical of potentials steeper than x^2.

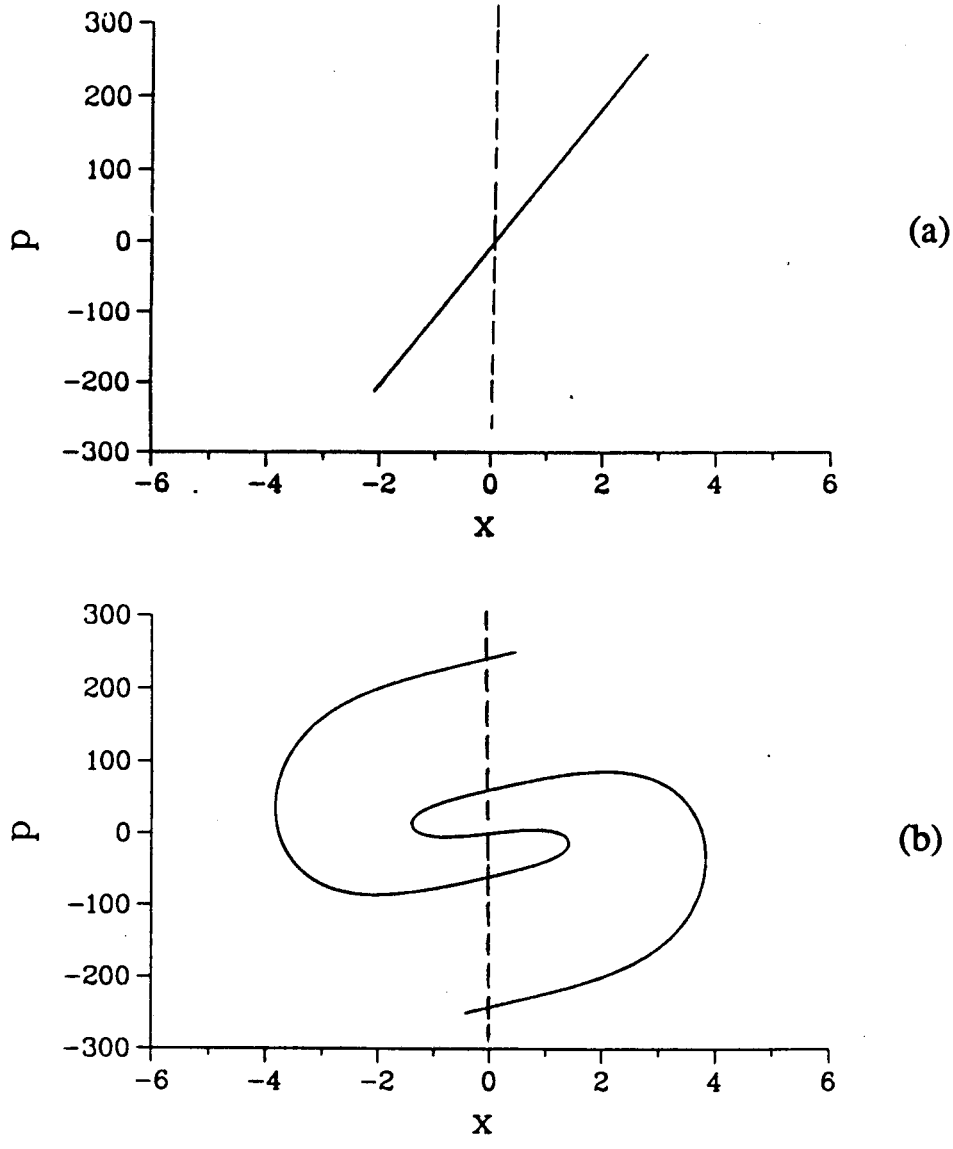

Fig. 7-1

Time evolution of the momentum distribution $p(x,x_0;t)$, plotted as a function of x, in two one dimensional potentials. Initially (t=0) all particles are localized at $x=x_0$ with any possible value of momentum. Dashed line: momentum distribution at t=0. Solid line: momentum distribution after a short time t. (a) Harmonic potential, $V=\frac{1}{2}m\omega^2x^2$. The momentum distribution remains linear at all times. (b) Quartic potential, $V\propto x^4$. The momentum distribution develops an infinity of branches for any $t>0$; only part of this complicated evolution is shown, while in reality the curve continues to wrap around itself for ever.

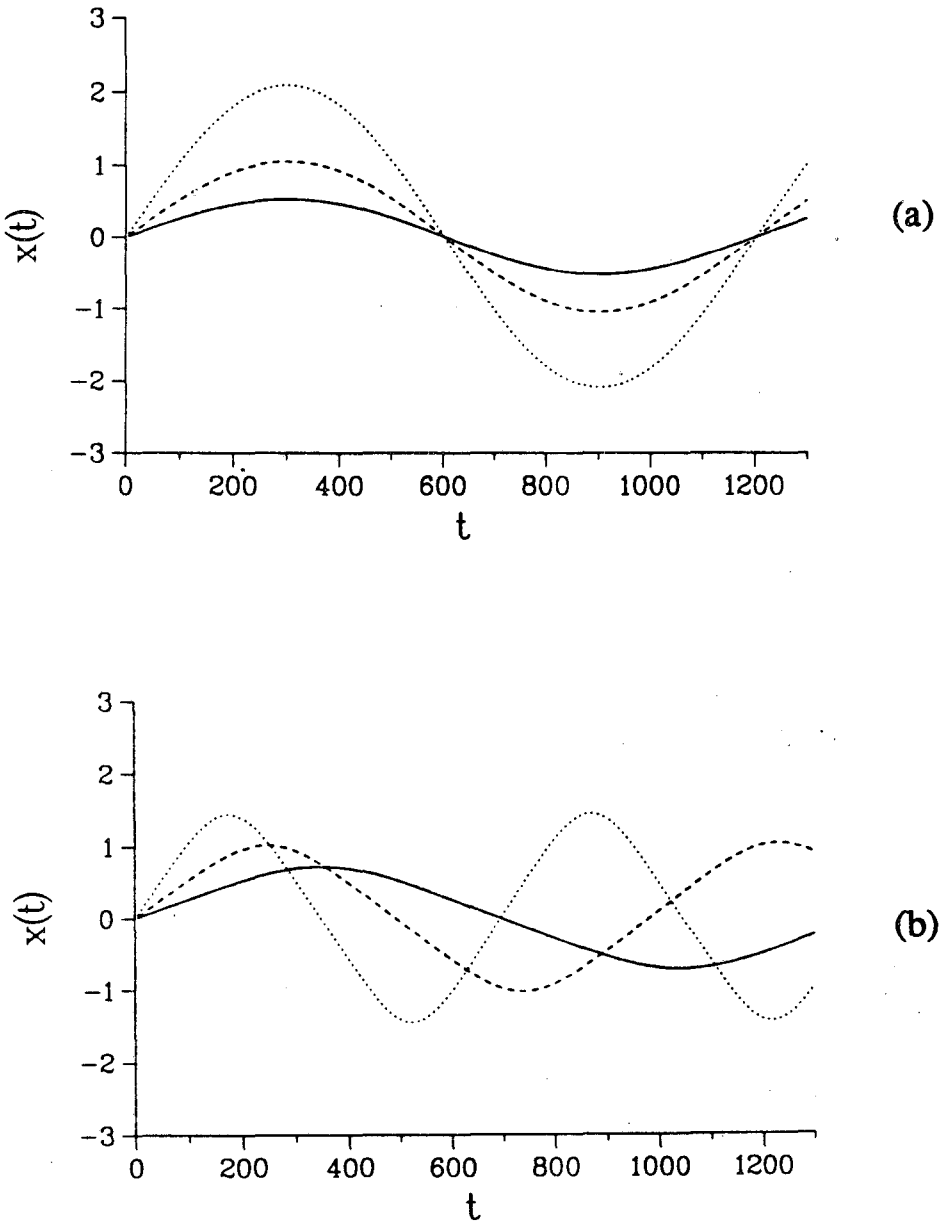

Fig. 7-2

Classical trajectories at different energies for the two potentials shown in Fig. 7-1. (a) Harmonic potential, $V=\frac{1}{2}m\omega^2x^2$. All trajectories focus at times $t_n=n\pi/\omega$, while there is only one trajectory that reaches a specified coordinate point at any time $t\neq n\pi/\omega$. (b) Quartic potential, $V\propto x^4$. In this case there are an infinite number of trajectories that reach a specified coordinate point at any time.

Fortunately, we only need to consider one term in Eq. (7.8) - that of smallest action - to obtain the short time propagator. This is so because the action behaves as t^{-1} for the lowest energy trajectory (the "direct" trajectory, i.e., the one with the smallest number of bounces) and as t^{-n}, $n>1$, for all other trajectories; terms of the form $\exp(it^{-n}/\hbar)$ oscillate very fast (or are exponentially small if the time is imaginary) for $n>1$ (compared to the $n=1$ term) and do not contribute in the limit $t\rightarrow 0$.

Our plan is to express the classical action $S(x,x_0;\,t)$ as a power series in t and then use Eq. (7.6) to obtain the short time propagator. Because of time reversal symmetry, i.e.,

$$\langle x|e^{-iHt/\hbar}|x_0\rangle^* = \langle x|e^{iHt/\hbar}|x_0\rangle,$$

the action (which is a real quantity) contains no even powers in t. (This is also true for the matrix elements of the Boltzmann operator, as follows by analytic continuation of the real time expressions.)

To find the action through first order in t, we begin by expanding $x(t')$ and $V(x(t'))$ in a Taylor series in t':

$$x(t') = \sum_{n=0}^{\infty} x_0^{[n]} \frac{t'^n}{n!}, \tag{7.9}$$

$$V(x(t')) = \sum_{n=0}^{\infty} \left[\frac{d^n V(x(t'))}{dt'^n}\right]_{t'=0} \frac{t'^n}{n!} \tag{7.10}$$

where

$$x_0^{[n]} \equiv \left[\frac{d^n x(t')}{dt'^n}\right]_{t'=0} \tag{7.11}$$

and $x(t)=x$. For the lowest energy trajectory, the leading term in $\dot{x}_0 \equiv x_0^{[1]}$ is $\dfrac{x-x_0}{t}$.

Using this and the equation of motion $\ddot{x}_0 = -\dfrac{V_0'}{m}$, we see that

$$x_0^{[n]}\, t^n = -\frac{V_0^{[n-1]}}{m}(x-x_0)^{n-2}\, t^2 + O(t^4) \tag{7.12}$$

where

$$V_0^{[n]} = \left[\frac{d^n V(x')}{dx'^n}\right]_{x'=x_0}. \tag{7.13}$$

Solving Eq. (7.9) with $t'=t$ for $\dot{x}_0$ gives

$$\dot{x}_0 = \frac{x-x_0}{t} + \frac{t}{m}\sum_{n=0}^{\infty} V_0^{[n+1]}\frac{(x-x_0)^n}{(n+2)!}. \tag{7.14}$$

The integral of Eq. (7.5) is straightforward to evaluate through order t. It is important to emphasize that *all* terms of the form

$$V_0^{[n]}\,\dot{x}^n\frac{t'^n}{n!}$$

in $d^n V(x(t'))/dt'^n$ contribute to $\int_0^t V(x(t'))dt'$ through first order. It is then easy to show that

$$\int_0^t V(x(t'))dt' = t\sum_{n=0}^{\infty} V_0^{[n]}\frac{(x-x_0)^n}{(n+1)!} + O(t^3). \tag{7.15}$$

Recognizing the sum in Eq. (7.24b) as $\frac{1}{x-x_0}\int_{x_0}^{x} V(x')dx'$, we get the result

$$\int_0^t V(x(t'))dt' = \frac{t}{x-x_0}\int_{x_0}^{x} V(x')dx' + O(t^3). \tag{7.16}$$

This can also be written in the form

$$\int_0^t V(x(t'))dt' = \int_0^t V(x_0+\frac{t'}{t}x)dt', \tag{7.17}$$

i.e., as the integral of the potential along a constant velocity (straight line) trajectory.

To find the integral of the kinetic energy through order t, we first point out that

$$\int_0^t \dot{x}(t')^2dt' = \int_0^t [\dot{x}_0^2 + 2\dot{x}_0(x_0^{[n+1]}\frac{t'^n}{n!})]dt' + O(t^3). \tag{7.18}$$

Using Eq. (7.14), we obtain

$$\int_0^t \dot{x}(t')^2 dt' = \frac{m}{2t}(x-x_0)^2 + O(t^3). \tag{7.19}$$

Thus, our final result for the action is

$$S(x,x_0;\,t) = \frac{m}{2t}(x-x_0)^2 - \frac{t}{x-x_0}\int_{x_0}^{x} V(x')dx' + O(t^3). \tag{7.20}$$

It is instructive and useful to carry out the derivation in a different way. The derivation that follows has the extra advantage that it is easy to generalize to higher order terms in t. We thus proceed to calculate the action through third order in time.

The action can be expressed (for the one-dimensional case) as [7.10]

$$S(x,x_0;\,t) = \Phi(E) - Et, \tag{7.21a}$$

$$\Phi(E) = \int_{x_0}^{x} \sqrt{2m\,[E-V(x')]}\,dx' \tag{7.21b}$$

where the energy E is determined implicitly by the equation

$$\Phi'(E) = t. \tag{7.22}$$

Expanding Φ in a Taylor series in $V(x')$ gives the following equations which correspond to Eqs. (7.21) and (7.22):

$$\Phi(E) = \sqrt{2m}\sum_{n=0}^{\infty}\binom{1/2}{n}(-1)^n E^{\frac{1}{2}-n}\int_{x_0}^{x} V(x')^n dx', \tag{7.23}$$

$$S(x,x_0;\,t) = \sqrt{2m}\sum_{n=0}^{\infty}\binom{1/2}{n}\left(\frac{1}{2}+n\right)(-1)^n E^{\frac{1}{2}-n}\int_{x_0}^{x} V(x')^n dx', \tag{7.24a}$$

$$\sqrt{E} = \frac{\sqrt{2m}}{t}\sum_{n=0}^{\infty}\binom{1/2}{n}\left(\frac{1}{2}-n\right)(-1)^n E^{-n}\int_{x_0}^{x} V(x')^n dx'. \tag{7.24b}$$

Combining Equations (7.24a) and (7.24b) gives

$$S(x,x_0;\,t) = \frac{2m}{t}\sum_{n=0}^{\infty}\sum_{n'=0}^{\infty}\binom{1/2}{n}\binom{1/2}{n'}\left(\frac{1}{2}-n\right)\left(\frac{1}{2}+n'\right)(-1)^{n+n'}E^{-n-n'}$$

$$\times\int_{x_0}^{x} V(x')^n dx' \int_{x_0}^{x} V(x')^{n'} dx'. \tag{7.25}$$

Solving Eq. (7.24b) through $O(t^2)$ by successive iteration and substituting into Eq. (7.25) gives the following result for the action through third order in t[7.13]

$$S(x,x_0;\,t) = \frac{m}{2t}\Delta x^2 - t\langle V\rangle - \frac{t^3}{2m\Delta x^2}[\langle V^2\rangle - \langle V\rangle^2] + O(t^5), \qquad (7.26a)$$

where

$$\Delta x = x - x_0 \qquad (7.26b)$$

and

$$\langle V^n\rangle = \frac{1}{\Delta x}\int_{x_0}^{x} V(x')^n\,dx', \quad n=1,2. \qquad (7.26c)$$

We note that the averages of the potential (and its square) in Eq. (7.26c) can also be written as

$$\langle V^n\rangle = \frac{1}{t}\int_0^t V(x_0+(x-x_0)\frac{t'}{t})^n\,dt', \qquad (7.27a)$$

which emphasizes that they are time averages over the straight line, constant velocity trajectory from x_0 to x; in dimensionless form this becomes

$$\langle V^n\rangle = \int_0^1 V((1-\xi)x_0+\xi x)^n\,d\xi. \qquad (7.27b)$$

Consider now the *first order propagator*, i.e., Eq. (7.6) with S given by Eq. (7.20) or by the first two terms of Eq. (7.26a),

$$S(x,x_0;\,t) = \frac{m}{2t}\Delta x^2 - t\langle V\rangle. \qquad (7.28)$$

It is not hard to show that the Van Vleck determinant is given by

$$-\frac{\partial^2 S}{\partial x_0 \partial x} = \frac{m}{t} + t\int_0^1 \xi(1-\xi)V''((1-\xi)x_0+\xi x)\,d\xi; \qquad (7.29a)$$

integration by parts (twice) allows the second term also to be written as

$$\int_0^1 \xi(1-\xi)V''((1-\xi)x_0+\xi x)\,d\xi = \frac{2}{\Delta x^2}\left[\frac{1}{2}[V(x_0)+V(x)] - \langle V\rangle\right]. \qquad (7.29b)$$

It is also easy to see how this first order propagator is related to other simple approximations for the short time propagator. Eq. (7.3), for example, corresponds to the two-point approximation (the trapezoid rule) for the potential energy integral,

$$<V> \rightarrow \frac{1}{2}[V(x_0)+V(x)], \tag{7.30a}$$

and Eq. (7.4) to the one-point approximation to the integral,

$$<V> \rightarrow V(\frac{x+x_0}{2}). \tag{7.30b}$$

Not surprisingly, therefore, Eq. (7.30a) has been seen in practice [7.14,7.9] to work much better than Eq. (7.30b). As will be seen, though, Eq. (7.28) itself is even better. This comparison also makes it clear that both of these approximations approach the correct first order propagator as $\Delta x \rightarrow 0$.

Finally, we note that the multidimensional version of Eq. (7.28)-(7.29) is of the same form. I.e., the action is the time integral over a straight line trajectory,

$$S(\mathbf{x},\mathbf{x}_0; t) = \frac{m}{2t}|\Delta\mathbf{x}|^2 - t\int_0^1 V((1-\xi)\mathbf{x}_0+\xi\mathbf{x})d\xi, \tag{7.31a}$$

where

$$\Delta\mathbf{x} = \mathbf{x}-\mathbf{x}_0,$$

and the Van Vleck determinant is

$$\det\left[-\frac{\partial^2 S}{\partial x_0^i \partial x^j}\right] = \det\left[\frac{m}{t}\delta_{ij} + t\int_0^1 \xi(1-\xi)\frac{\partial^2 V}{\partial x_i \partial x_j}((1-\xi)\mathbf{x}_0+\xi\mathbf{x})d\xi\right]. \tag{7.31b}$$

The first order propagator for an F-dimensional Cartesian Hamiltonian is then

$$<\mathbf{x}|e^{-iHt/\hbar}|\mathbf{x}_0> = \left[\det\left[-(2\pi i\hbar)^{-F}\ \frac{\partial^2 S}{\partial\mathbf{x}\partial\mathbf{x}_0}\right]\right]^{1/2} e^{iS/\hbar}, \tag{7.31c}$$

with S given by Eq. (7.31a).

3. Exponential power series for the quantum propagator

In this Section we expand the exponent of the short time propagator in a power series in time and obtain recursion relations for successive terms. The treatment we follow is strictly quantum mechanical, i.e., we make no assumption about the magnitude of $\hbar$ relative to the other parameters of the problem.

Throughout this Section we consider simple (but multidimensional) Cartesian Hamiltonian operators of the form

$$\hat{H} = \frac{\hat{\mathbf{p}}^2}{2m} + V(\hat{\mathbf{x}}), \tag{7.32}$$

where $\hat{\mathbf{x}}$, $\hat{\mathbf{p}} = \{\hat{x}_i \equiv x_i, \hat{p}_i \equiv \frac{\hbar}{i}\frac{\partial}{\partial x_i}\}$ for $i=1,...,F$. The generalization of this procedure to Hamiltonians with vector potentials (e.g., electromagnetic fields) is given in Section 5.

We wish to determine an analytic approximation for the coordinate matrix element of the single step propagator

$$<\mathbf{x}|e^{-iHt/\hbar}|\mathbf{x}_0>. \tag{7.33}$$

The approximation must be correct in the limit $t \rightarrow 0$, but for the sake of efficiency in a path integral one would like it to be accurate for as long a time as possible.

In the limit $t \rightarrow 0$ one knows the limiting form of the propagator to be

$$\lim_{t\rightarrow 0} <\mathbf{x}|e^{-iHt/\hbar}|\mathbf{x}_0> = \left[\frac{m}{2\pi i \hbar t}\right]^{F/2} \exp[\frac{im}{2\hbar t}|\mathbf{x}-\mathbf{x}_0|^2], \tag{7.34}$$

so the *ansatz* we choose is

$$<\mathbf{x}|e^{-iHt/\hbar}|\mathbf{x}_0> = t^{-F/2} e^{\frac{i}{\hbar}W(\mathbf{x},t)}, \tag{7.35a}$$

where $W(\mathbf{x},t)$ is expanded as a power series in t as [7.15]

$$W(\mathbf{x},t) = \frac{1}{t}\sum_{n=0} t^n W_n(\mathbf{x}) = \sum_{n=0} t^{n-1} W_n(\mathbf{x}). \tag{7.35b}$$

(W also depends on the initial condition $\mathbf{x}_0$, but to keep the notation simple we do not indicate this explicitly.) In light of Eq. (7.34), we anticipate the form for the first two terms in the expansion (7.35b) to be

$$W_0(\mathbf{x}) = \frac{m}{2}|\mathbf{x}-\mathbf{x}_0|^2 \tag{7.36a}$$

$$e^{\frac{i}{\hbar}W_1(\mathbf{x})} = \left[\frac{m}{2\pi i\hbar}\right]^{F/2}, \tag{7.36b}$$

so that Eqs. (7.35) and (7.36) may also be combined to read

$$\langle \mathbf{x}|e^{-iHt/\hbar}|\mathbf{x}_0\rangle = \langle \mathbf{x}|e^{-iH_0t/\hbar}|\mathbf{x}_0\rangle \exp[\frac{i}{\hbar}\sum_{n=2} t^{n-1}W_n(\mathbf{x})], \tag{7.37}$$

where the first factor on the right hand side is the free particle propagator, Eq. (7.34) (i.e., $H_0 = \hat{\mathbf{p}}^2/2m$).

To determine the various terms $\{W_n(\mathbf{x})\}$ in the expansion (7.35b) we use the fact that the propagator satisfies the time-dependent Schrödinger equation

$$[-\frac{\hbar^2}{2m}\nabla^2 + V(\mathbf{x}) - i\hbar\frac{\partial}{\partial t}]\ \langle \mathbf{x}|e^{-iHt/\hbar}|\mathbf{x}_0\rangle = 0, \tag{7.38}$$

where $\nabla^2 = \sum_{i=1}^{F}\frac{\partial^2}{\partial x_i^2}$. Substituting Eq. (7.35) into (7.38) and equating like powers of t leads in a straightforward way to the following equations for the functions $\{W_n(\mathbf{x})\}$:

$$0 = i\hbar\frac{F}{2}\delta_{n,1} + V(\mathbf{x})\delta_{n,2} + (n-1)W_n(\mathbf{x})$$

$$+ \frac{1}{2m}\sum_{n'=0}^{n}\nabla W_{n'}(\mathbf{x})\cdot\nabla W_{n-n'}(\mathbf{x}) - \frac{i\hbar}{2m}\nabla^2 W_{n-1}(\mathbf{x}), \tag{7.39}$$

for n=0,1,2,... ($W_{-1}\equiv 0$). For n=0 and 1 these equations are, respectively,

$$W_0(\mathbf{x}) = \frac{1}{2m}|\nabla W_0(\mathbf{x})|^2 \tag{7.40a}$$

$$0 = i\hbar\frac{F}{2} + \frac{1}{m}\nabla W_0(\mathbf{x})\cdot\nabla W_1(\mathbf{x}) - \frac{i\hbar}{2m}\nabla^2 W_0(\mathbf{x}), \tag{7.40b}$$

and one can easily verify that the previously anticipated solutions for $W_0(\mathbf{x})$ and $W_1(\mathbf{x})$, namely Eq. (7.36), do indeed satisfy Eq. (7.40) (noting the fact that $\nabla^2|\mathbf{x}-\mathbf{x}_0|^2 = 2F$). Using these solutions [Eq. (7.36)] for $W_0(\mathbf{x})$ and $W_1(\mathbf{x})$, Eq. (7.39) then gives the following equations for $W_2(\mathbf{x})$ and for all higher order terms:

$$(\mathbf{x}-\mathbf{x}_0)\cdot\nabla W_2(\mathbf{x}) + W_2(\mathbf{x}) = -V(\mathbf{x}) \tag{7.41a}$$

$$(\mathbf{x}-\mathbf{x}_0)\cdot\nabla W_n(\mathbf{x}) + (n-1)W_n(\mathbf{x}) = -\frac{1}{2m}\sum_{n'=2}^{n-2}\nabla W_{n'}(\mathbf{x})\cdot\nabla W_{n-n'}(\mathbf{x}) + \frac{i\hbar}{2m}\nabla^2 W_{n-1}(\mathbf{x}) \tag{7.41b}$$

for n=3,4,....

Note that Equations (7.41) are all linear inhomogeneous first order differential equations of the form

$$(\mathbf{x}-\mathbf{x}_0)\cdot\nabla y(\mathbf{x}) + (n-1)y(\mathbf{x}) = a(\mathbf{x}), \tag{7.42}$$

where the right hand side $a(\mathbf{x})$ is a known inhomogeneity. One can verify by direct substitution that the solution to Eq. (7.42) is

$$y(\mathbf{x}) = \int_0^1 d\xi\, \xi^{n-2} a(\mathbf{x}_0+(\mathbf{x}-\mathbf{x}_0)\xi). \tag{7.43}$$

To show this, note first that

$$\nabla y(\mathbf{x}) \equiv \frac{\partial}{\partial \mathbf{x}} y(\mathbf{x}) = \int_0^1 d\xi\, \xi^{n-2}\frac{\partial}{\partial \mathbf{x}} a(\mathbf{x}_0+(\mathbf{x}-\mathbf{x}_0)\xi)$$

$$= \int_0^1 d\xi\, \xi^{n-1}\frac{\partial}{\partial \mathbf{x}'} a(\mathbf{x}')|_{\mathbf{x}'=\mathbf{x}_0+(\mathbf{x}-\mathbf{x}_0)\xi}, \tag{7.44}$$

so that

$$(\mathbf{x}-\mathbf{x}_0)\cdot\nabla y(\mathbf{x}) = \int_0^1 d\xi\, \xi^{n-1}(\mathbf{x}-\mathbf{x}_0)\cdot\frac{\partial}{\partial \mathbf{x}'} a(\mathbf{x}')|_{\mathbf{x}'=\mathbf{x}_0+(\mathbf{x}-\mathbf{x}_0)\xi}. \tag{7.45}$$

But

$$(\mathbf{x}-\mathbf{x}_0)\cdot\frac{\partial}{\partial \mathbf{x}'}a(\mathbf{x}')|_{\mathbf{x}'=\mathbf{x}_0+(\mathbf{x}-\mathbf{x}_0)\xi} = \frac{d}{d\xi}a(\mathbf{x}_0+(\mathbf{x}-\mathbf{x}_0)\xi), \tag{7.46}$$

so that Eq. (7.45) becomes

$$(\mathbf{x}-\mathbf{x}_0)\cdot\nabla y(\mathbf{x}) = \int_0^1 d\xi\ \xi^{n-1}\frac{d}{d\xi}a(\mathbf{x}_0+(\mathbf{x}-\mathbf{x}_0)\xi). \tag{7.47}$$

Integration by parts on the right hand side of (7.47) gives

$$\begin{aligned}
&\xi^{n-1}a(\mathbf{x}_0+(\mathbf{x}-\mathbf{x}_0)\xi)|_0^1 - \int_0^1 d\xi\ (n-1)\xi^{n-2}a(\mathbf{x}_0+(\mathbf{x}-\mathbf{x}_0)\xi) \\
&\quad = a(\mathbf{x}) - (n-1)\int_0^1 d\xi\ \xi^{n-2}a(\mathbf{x}_0+(\mathbf{x}-\mathbf{x}_0)\xi) \\
&\quad = a(\mathbf{x}) - (n-1)y(\mathbf{x}),
\end{aligned}$$

whereby Eq. (7.47) becomes Eq. (7.42), thus verifying that Eq. (7.43) is indeed the solution.

Applying the results of the previous paragraph to Eq. (7.41a) gives the solution for $W_2(\mathbf{x})$ as

$$W_2(\mathbf{x}) = -\int_0^1 d\xi\ V(\mathbf{x}_0+(\mathbf{x}-\mathbf{x}_0)\xi), \tag{7.48}$$

and application to Eq. (7.41b) gives an expression for $W_n(\mathbf{x})$ in terms of lower order terms,

$$\begin{aligned}
W_n(\mathbf{x}) = \int_0^1 d\xi\ \xi^{n-2}[&\frac{i\hbar}{2m}\nabla^2 W_{n-1}(\mathbf{x}') \\
&- \frac{1}{2m}\sum_{n'=2}^{n-2}\nabla W_{n'}(\mathbf{x}')\cdot\nabla W_{n-n'}(\mathbf{x}')]|_{\mathbf{x}'=\mathbf{x}_0+(\mathbf{x}-\mathbf{x}_0)\xi},
\end{aligned} \tag{7.49}$$

for n=3,4,..... All higher order terms W_3, W_4,... can thus be determined recursively from Eq. (7.49).[7.15,7.24]

For example, the explicit solution for $W_3(\mathbf{x})$ is

$$W_3(\mathbf{x}) = \frac{i\hbar}{2m}\int_0^1 d\xi\ \xi\nabla^2 W_2(\mathbf{x}')|_{\mathbf{x}'=\mathbf{x}_0+(\mathbf{x}-\mathbf{x}_0)\xi}, \tag{7.50}$$

with $W_2(\mathbf{x})$ given by (7.48). Since

$$\nabla^2 W_2(\mathbf{x}') \equiv -\int_0^1 d\xi' \, \frac{\partial^2}{\partial \mathbf{x}'^2} V(\mathbf{x}_0+(\mathbf{x}'-\mathbf{x}_0)\xi')$$

$$= -\int_0^1 d\xi' \, \xi'^2 \frac{\partial^2}{\partial \mathbf{x}''^2} V(\mathbf{x}'')|_{\mathbf{x}''=\mathbf{x}_0+(\mathbf{x}'-\mathbf{x}_0)\xi'},$$

Eq. (7.50) becomes

$$W_3(\mathbf{x}) = -\frac{i\hbar}{2m}\int_0^1 d\xi \, \xi \int_0^1 d\xi' \, \xi'^2 \frac{\partial^2}{\partial \mathbf{x}''^2} V(\mathbf{x}'')|_{\mathbf{x}''=\mathbf{x}_0+(\mathbf{x}-\mathbf{x}_0)\xi\xi'}.$$

Changing integration variables appropriately allows one of these integrations to be performed, giving finally

$$W_3(\mathbf{x}) = -\frac{i\hbar}{2m}\int_0^1 d\xi \, \xi(1-\xi)\nabla^2 V(\mathbf{x}')|_{\mathbf{x}'=\mathbf{x}_0+(\mathbf{x}-\mathbf{x}_0)\xi}. \tag{7.51}$$

The next term, $W_4(\mathbf{x})$, is then given from Eq. (7.49) as

$$W_4(\mathbf{x}) = \int_0^1 d\xi \, \xi^2 [\frac{i\hbar}{2m}\nabla^2 W_3(\mathbf{x}') - \frac{1}{2m}|\nabla W_2(\mathbf{x}')|^2]|_{\mathbf{x}'=\mathbf{x}_0+(\mathbf{x}-\mathbf{x}_0)\xi}. \tag{7.52}$$

Using the previously obtained solutions for W_2 and W_3 and proceeding in a manner similar to the above paragraph, one obtains the following result for W_4:

$$W_4(\mathbf{x}) = -\frac{1}{m}\int_0^1 d\xi \int_0^\xi d\xi' \, \xi'(1-\xi)\nabla V(\mathbf{x}')\cdot\nabla V(\mathbf{x}'')$$

$$+ \frac{\hbar^2}{8m^2}\int_0^1 d\xi \, \xi^2(1-\xi)^2(\nabla^2)^2 V(\mathbf{x}') \tag{7.53}$$

with $\mathbf{x}'=\mathbf{x}_0+(\mathbf{x}-\mathbf{x}_0)\xi$ and $\mathbf{x}''=\mathbf{x}_0+(\mathbf{x}-\mathbf{x}_0)\xi'$, and where

$$(\nabla^2)^2 = \left[\sum_{i=1}^F \frac{\partial^2}{\partial x_i^2}\right]^2 = \sum_{i,j=1}^F \frac{\partial^4}{\partial x_i^2 \partial x_j^2}.$$

It is clear that one can continue using Eq. (7.49) to construct higher order terms, though the algebra becomes tedious. If the potential is sufficiently simple (e.g., a polynomial) that the various integrals are doable analytically, then computer algebra

manipulators (e.g., MACSYMA or *Mathematica*) can be used to do this very efficiently. This is what has been done, in fact, for some of the examples discussed in Section 4 to obtain terms up to W_{10}.

It is also possible, of course, to attempt to extend the region of usefulness of the power series expansion for $W(\mathbf{x},t)$ by converting it into a Padé [13] approximant, i.e.,

$$\sum_{n=0}^{L+M} t^n W_n(\mathbf{x}) \rightarrow \sum_{n=0}^{L} t^n p_n(\mathbf{x})/[1+\sum_{n=1}^{M} t^n q_n(\mathbf{x})]. \tag{7.54}$$

There is a well established procedure for determining the L+M+1 coefficients $\{p_n(\mathbf{x})\}$, $\{q_n(\mathbf{x})\}$ from the L+M+1 coefficients $\{W_n(\mathbf{x})\}$, which is also amenable to computer algebraic manipulation. The results discussed in Section 4 do indeed show that the Padé procedure extends the accuracy of the above propagator to longer times.

Before concluding this Section we note that for the case of one dimension (F=1) the above integrals can be simplified by integration by parts. Thus Eqs. (7.48), (7.51) and (7.53) can be written in this case as

$$W_2(x) = -\frac{1}{\Delta x}\int_{x_0}^{x} dx' V(x'), \tag{7.55a}$$

$$W_3(x) = -\frac{i\hbar}{2m\Delta x^2}[V(x_0)+V(x)-\frac{2}{\Delta x}\int_{x_0}^{x} dx' V(x')], \tag{7.55b}$$

and

$$W_4 = \frac{-1}{2m\Delta x^4}\left[\Delta x \int_{x_0}^{x} V(x')^2 dx' - [\int_{x_0}^{x} V(x')dx']^2\right]$$

$$- \frac{3\hbar^2}{2m^2\Delta x^4}\left[V(x_0)+V(x) - \frac{2}{\Delta x}\int_{x_0}^{x} V(x')dx' - \frac{\Delta x}{6}[V'(x)-V'(x_0)]\right], \tag{7.55c}$$

where $\Delta x = x - x_0$. We note that Eq. (7.55a) for $W_2(x)$ is the same exponent obtained in Section 2 using semiclassical arguments and also that expansion of the exponential factor involving $W_3(x)$ of Eq. (7.55b) through lowest order in t gives the corresponding Van Vleck determinant. Furthermore, the *first term* of Eq. (7.55c) is the same

third order term obtained before semiclassically. In the present fully quantum treatment, though, we obtain a "quantum correction" to this term,[7.15] the second term of Eq. (7.55c) (which is proportional to $\hbar^2$).

Finally, it is illuminating to see the limiting form taken by the various terms in Eq. (7.55) as $x \to x_0$. It is not hard to show that

$$\lim_{x \to x_0} W_2(x) = -V(x_0) \tag{7.56a}$$

$$\lim_{x \to x_0} W_3(x) = -\frac{i\hbar}{12m} V''(x_0) \tag{7.56b}$$

$$\lim_{x \to x_0} W_4(x) = -\frac{V'(x_0)^2}{24m} + \frac{\hbar^2}{240m^2} V''''(x_0). \tag{7.56c}$$

Thus for the case $t = -i\hbar\beta$, the equilibrium density is given by this single step propagator as

$$\langle x | e^{-\beta H} | x \rangle = \left[\frac{m}{2\pi\hbar^2\beta}\right]^{1/2} \exp[-\beta V(x) - \frac{\hbar^2\beta^2}{12m} V''(x)]$$

$$+ \frac{\hbar^2\beta^3}{24m}(V'(x)^2 - \frac{\hbar^2}{10m} V''''(x)) + O(\beta^4)]. \tag{7.57}$$

If one expands the exponential and keeps only the terms through order $\hbar^2$, then one obtains the well-known Wigner-Kirkwood [7.16] correction factor to the classical density,

$$\langle x | e^{-\beta H} | x \rangle = \left[\frac{m}{2\pi\hbar^2\beta}\right]^{1/2} e^{-\beta V(x)} [1 - \frac{\hbar^2\beta^2}{12m} V''(x) + \frac{\hbar^2\beta^3}{24m} V'(x)^2]. \tag{7.58}$$

4. Applications

To illustrate the ideas discussed in Sections 2 and 3 we present here some analytic and numerical examples.

a) Harmonic potential

With $V(x)=\frac{1}{2}m\omega^2x^2$, Equations (7.6), (7.28) and (7.29) give the following result for the first order propagator:

$$<x|e^{-iH\Delta t/\hbar}|x_0> = \sqrt{\frac{m}{2\pi i\hbar\Delta t}}\left[1+\frac{\omega^2\Delta t^2}{6}\right]^{1/2} e^{\frac{im}{2\hbar\Delta t}\Delta x^2-\frac{i\Delta t}{6}m\omega^2(x^2+xx_0+x_0^2)} . \quad (7.59)$$

In contrast, the "trapezoid rule" form of the Trotter product formula (Eq. 7.3) gives

$$<x|e^{-iH\Delta t/\hbar}|x_0> = \sqrt{\frac{m}{2\pi i\hbar\Delta t}}\, e^{\frac{im}{2\hbar\Delta t}\Delta x^2-\frac{i\Delta t}{4}m\omega^2(x^2+x_0^2)} . \quad (7.60)$$

One can readily check that Eq. (7.59) is the correct expansion through order Δt of the exact propagator for the harmonic oscillator,[7.1]

$$<x|e^{-iH\Delta t/\hbar}|x_0> = \sqrt{\frac{m\omega}{2\pi i\hbar\sin\omega\Delta t}}e^{\frac{im\omega}{2\hbar\sin\omega\Delta t}[(x^2+x_0^2)\cos\omega\Delta t-2xx_0]} , \quad (7.61)$$

while Eq. (7.60) is not.[7.17]

We now use the various short time approximations for the propagator in the discretized path integral, Eq. (7.1), to obtain the coordinate matrix element of the propagator for time $t=N\Delta t$. By straightforward algebra, it is possible to show that use of the Trotter product formula, Eq. (7.60), gives for $x_0=x_N=0$:

$$<0|e^{-iHt/\hbar}|0> = \sqrt{\frac{m}{2\pi i\hbar t}}\prod_{k=1}^{N-1}\left[1-\frac{\omega^2t^2}{4N^2\sin^2\frac{k\pi}{2N}}\right]^{-1/2} . \quad (7.62)$$

On the other hand, the first order propagator of Eq. (7.59) gives [7.13]

$$<0|e^{-iHt/\hbar}|0> = \sqrt{\frac{m}{2\pi i\hbar t}}\left[1+\frac{\omega^2t^2}{6N^2}\right]^{N/2}$$

$$\times\prod_{k=1}^{N-1}\left[\cot^2\frac{k\pi}{2N}-\frac{\omega^2t^2}{6N^2}-\frac{\omega^2t^2}{12N^2}\csc^2\frac{k\pi}{2N}\right]^{-1/2} , \quad (7.63)$$

and inclusion of the third term in the action, i.e., the semiclassical *third order*

propagator, gives [7.13]

$$<0|e^{-iHt/\hbar}|0> = \sqrt{\frac{m}{2\pi i\hbar t}}\left[1+\frac{\omega^2t^2}{6N^2}+\frac{7\omega^4t^4}{360N^4}\right]^{N/2}$$

$$\times\prod_{k=1}^{N-1}\left[\cot^2\frac{k\pi}{2N}-\frac{\omega^2t^2}{6N^2}-\frac{7\omega^4t^4}{360N^4}-\left(\frac{\omega^2t^2}{12N^2}+\frac{\omega^4t^4}{360N^4}\right)\csc^2\frac{k\pi}{2N}\right]^{-1/2}. \qquad (7.64)$$

Table 7-1

$<0|e^{-\beta H}|0>$ for harmonic potential (m=1000, ω=0.001)

$\hbar\omega\beta$	Exact [a]	1st order [b]	3rd order [c]	Trotter [d]
1.0	0.36801	0.36791	0.36804	0.36932
1.5	0.27340	0.27305	0.27353	0.27577
2.0	0.20948	0.20870	0.20978	0.21299
2.5	0.16219	0.16083	0.16272	0.16680
3.0	0.12604	0.12402	0.12684	0.13162
3.5	0.09809	0.09539	0.09917	0.10445
4.0	0.07637	0.07304	0.07775	0.08331
4.5	0.05947	0.05560	0.06114	0.06677
5.0	0.04631	0.04201	0.04825	0.05379
5.5	0.03607	0.03146	0.03827	0.04356
6.0	0.02809	0.02330	0.03053	0.03545

[a] Eq. (7.61) [b] Eq. (7.63), N=5 [c] Eq. (7.64), N=5 [d] Eq. (7.62), N=5

Table 7-1 compares the results of Equations (7.62), (7.63) and (7.64) to the exact result, Eq. (7.61), as a function of the imaginary time $t=-i\hbar\beta$ for N=5. A similar comparison is given in Table 7-2, where the different approximations are presented as a function of the imaginary time $\hbar\omega\beta$ with fixed time step $\hbar\omega\beta/N$=1. Finally, Fig. 7-3 compares the relative error given by Equations (7.62), (7.63), and (7.64) for the case of imaginary time $t=-i\hbar\beta$, as a function of N, the number of time "slices". The dimensionless imaginary time is $\hbar\omega\beta=\pi$. One sees that the results

given by the first order propagator converge to the correct value considerably faster than those of the conventional Trotter product, requiring only about half as large a value of N to reduce the error to a few percent. The third order propagator gives still faster convergence, requiring only about half the value of N as the first order result.

Table 7-2
$\langle 0|e^{-\beta H}|0\rangle$ for harmonic potential (m=1000, ω=0.001)

$\hbar\omega\beta$	N	Exact [a]	1st order [b]	3rd order [c]	Trotter [d]
1.0	1	0.36801	0.36418	0.36841	0.39894
2.0	2	0.20948	0.20358	0.21144	0.23033
3.0	3	0.12604	0.11981	0.12853	0.14105
4.0	4	0.07637	0.07092	0.07871	0.08706
5.0	5	0.04631	0.04201	0.04825	0.05379
6.0	6	0.02809	0.02489	0.02959	0.03325

[a] Eq. (7.61) [b] Eq. (7.63) [c] Eq. (7.64) [d] Eq. (7.62)

Finally, it is easy to show that the quantum correction to the third order term of the semiclassical expression [the $\hbar^2$ term of Eq. (7.55c)] vanishes. This is in agreement with the well known fact that the WKB approximation is exact in the case of the harmonic oscillator.

b) Double well potential

We illustrate the use of the power series expansion of Section 3, Eq. (7.35) with W_n determined from (7.49), by calculating the off-diagonal coordinate matrix element of the Boltzmann operator,

$$\langle x_-|e^{-\beta H}|x_+\rangle, \tag{7.65}$$

for the case of an electron in a one-dimensional symmetric double well potential,

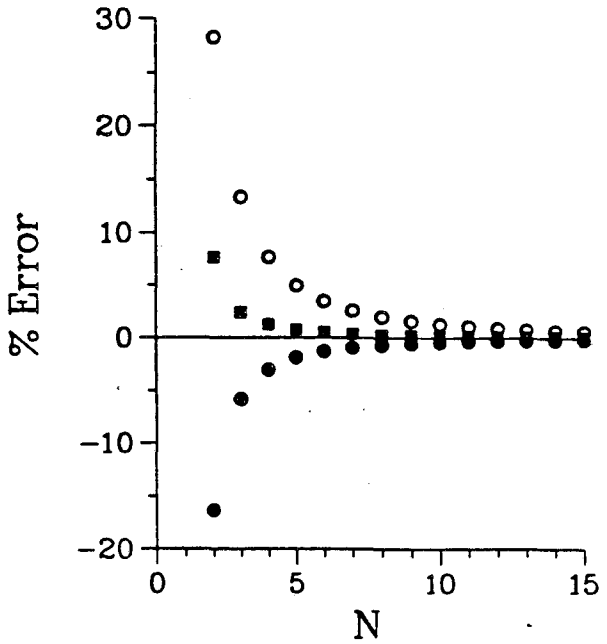

Fig. 7-3

The relative error, (approximate-exact)/exact, made by the three propagators discussed in Section 2 for the 0-0 coordinate matrix element of the Boltzmann operator with a harmonic potential for the value of $\hbar\omega\beta=\pi$, as a function of N [cf. Eqs. (7.62), (7.63), and (7.64)]. Open circles: Trotter product formula, Eq. (7.62). Solid circles: first order propagator, Eq. (7.63). Squares: third order propagator, Eq. (7.64).

$$V(x) = -\frac{1}{2}a_0x^2 + \frac{1}{4}c_0x^4. \tag{7.66}$$

This quantity is closely related to the tunneling splitting between the two lowest eigenstates of the double well.[7.18] The coefficients are chosen so that the barrier height is 4.2 eV and the two minima are located at $x_\pm = \pm 2.66\text{Å}$. [7.15]

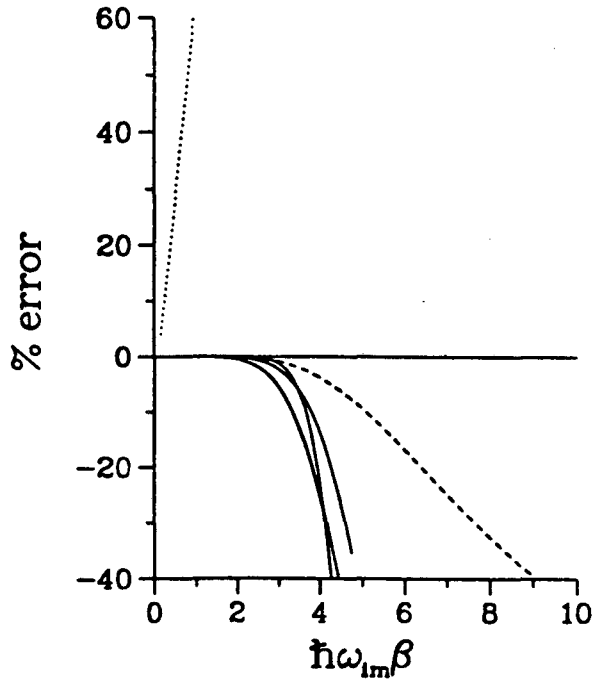

Fig. 7-4

Percentage error, 100×(approximate-exact)/exact, in the tunneling matrix element [Eq. (7.65)] for an electron in a double well potential [Eq. (7.66)], for the single step propagator in pure imaginary time ($t=-i\hbar\beta$). The barrier height is 4.2 eV and the two minima are located at ±2.66 Å. The dotted line is the result of the standard short time propagator [Eq. (7.3)], and the solid lines the results of the exponential power series [Eq. (7.35)] for n_{max} = 6, 8, and 10. The dashed line is the result of the Padé approximant, Eq. (7.54), with L=5, M=3. In the abscissa, ω_{im} is the imaginary frequency at the top of the barrier.

Fig. 7-4 shows the relative error made by truncating Eq. (7.35) at n_{max}=6, 8 and 10 , for *a single* (imaginary) *time step*, as a function of the dimensionless quantity $\hbar\omega_{im}\beta$, where ω_{im} is the imaginary frequency at the top of the barrier. Each successive higher order is seen to reduce the error over a larger range of β. Eventually [i.e., beyond some $\beta_{max}=\beta_{max}(n)$], of course, the error begins to grow very rapidly;

one would then need to include many more terms in the power series to obtain convergent results, or the series may not converge at all, if β exceeds its radius of convergence. A successful way of overcoming this problem is to use rational expansions such as Padé approximants.[7.19] As seen in Fig. 7-4, the [5/3] Padé approximant (computed from the n=0,...,8 terms of the Taylor series) converges significantly better over a much broader range of β than the corresponding Taylor expansion. It is thus seen that the recursive evaluation of the propagator according to Eq. (7.49) shows promise for calculating short or intermediate (complex) time dynamics *analytically*. It should then be useful in studying the dynamical (or equilibrium statistical mechanical) properties of *multidimensional* systems in a simple and economical way. Finally, Fig. 7-4 also shows the error made by using the standard Trotter formula, Eq. (7.3). As anticipated, the error increases *linearly* with β in this case, and very soon grows out of the scale of the figure.

In order to illustrate graphically the scaling with time of the various approximations discussed above, we plot in Fig. 7.5 the absolute error in the same quantity made by these approximations as a function of $\hbar\omega_{im}\beta$ (for small β) on a logarithmic scale. The slope of the line that corresponds to the Trotter propagator is equal to 1, while that corresponding to the first order propagator is equal to 3, clearly in agreement with the statements made in Sections 2 and 3.

Next, we apply the various approximations discussed above for the short time propagator to the path integral evaluation of the same quantity according to Eq. (7.1). With the standard Trotter product formula, the path integral representation for the imaginary time propagator becomes

$$\langle x_N | e^{-\beta H} | x_0 \rangle = \left[\frac{mN}{2\pi\hbar^2\beta}\right]^{N/2} \int_{-\infty}^{\infty} dx_1 \cdots \int_{-\infty}^{\infty} dx_{N-1} \times e^{-\frac{mN}{2\hbar^2\beta}\sum_{k=1}^{N}(x_k - x_{k-1})^2 - \frac{\beta}{2N}\sum_{k=1}^{N}[V(x_k)+V(x_{k-1})]} . \quad (7.67)$$

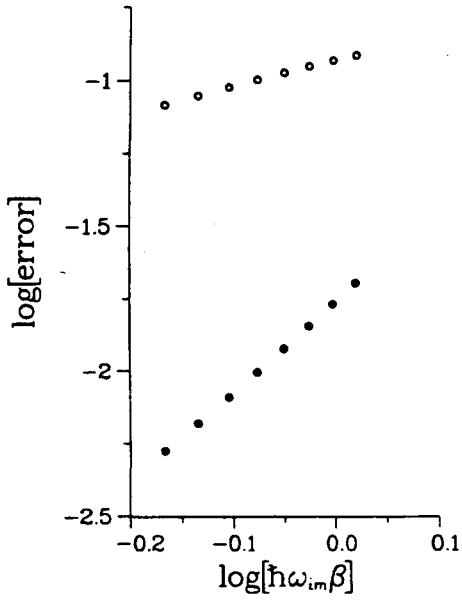

Fig. 7-5

The absolute error in the tunneling matrix element [Eq. (7.65)] for an electron in a double well potential [Eq. (7.66)], for the single step propagator in pure imaginary time ($t=-i\hbar\beta$). The parameters are the same as in Fig. 7-4. Open circles: Trotter formula, Eq. (7.3). Solid circles: semiclassical first order propagator, Eq. (7.6), with S given by Eq. (7.28). The error is seen to grow linearly with β in the first case, whereas it grows as t^3 in the second case.

As explained in Chapter V, exactly equivalent to this is Coalson's [7.14] quasi-Fourier representation,

$$<x_N|e^{-\beta H}|x_0> = \sqrt{\frac{m}{2\pi\hbar^2\beta}}\, e^{-\frac{m}{2\hbar^2\beta}(x_N-x_0)^2}$$

$$\times \int_{-\infty}^{\infty} da_1 \cdots \int_{-\infty}^{\infty} da_{N-1} e^{-\pi\sum_{k=1}^{N-1} a_k^2 - \frac{\beta}{2N}\sum_{k=1}^{N}[V(x_k)+V(x_{k-1})]} \tag{7.68}$$

where

$$x_k = x_0 + (x_N-x_0)\frac{k}{N} + \sqrt{\frac{\pi\hbar t}{m}}\frac{1}{N}\sum_{k'=1}^{N-1} a_{k'}\frac{\sin(\pi kk'/N)}{\sin(\pi k'/2N)}; \tag{7.69}$$

i.e., Eq. (7.68) is obtained from (7.67) simply by changing integration variables from $\{x_k\}$ to $\{a_k\}$ according to Eq. (7.69). It is useful to carry out the Monte Carlo integration in the $\{a_k\}$ variables because the kinetic energy part of the action is diagonal in them.

The path integral expression corresponding to Eq. (7.68) that results from using the first (or third) order semiclassical or quantum short time propagator of Sections 2 and 3 is obtained simply by replacing the average potential $\frac{1}{2}[V(x_k)+V(x_{k-1})]$ in Eq. (7.68) by the corresponding corrected expressions derived in these Sections and also modifying the integrand by the appropriate pre-exponential factor. For the first order semiclassical short time propagator, for example, the replacement in Eq. (7.68) is

$$\frac{1}{2}[V(x_k)+V(x_{k-1})] \rightarrow \frac{1}{x_k-x_{k-1}}\int_{x_{k-1}}^{x_k} V(x)dx\,, \tag{7.70a}$$

and the extra factor arising from the Van Vleck determinants is

$$\prod_{k=1}^{N-1}\left[1-\left[\frac{\hbar\beta}{N}\right]^2\frac{1}{2m(x_k-x_{k-1})^2}\left[\frac{V(x_k)+V(x_{k-1})}{2}-\frac{1}{x_k-x_{k-1}}\int_{x_{k-1}}^{x_k}V(x)dx\right]\right]^{1/2}. \tag{7.70b}$$

Since the Monte Carlo integration over the variables $\{a_k\}$ in Eq. (7.68) – either as it stands or with the modifications given by Eq. (7.70) – is an un-normalized Monte Carlo average,[7.20] one must use the charging algorithm [7.21] as in Chapter V to calculate the integral.

The calculation is performed with fixed $\hbar\omega_{im}\beta/N=\pi/4$. Shown in Fig. 7-6 are results obtained using the expansion of Eq. (7.35) truncated after the n=3 and n=5 term. Also shown are results obtained from the corresponding (i.e., of the same order) *semiclassical* expressions. Although no net quantum term appears in the n=2 or 3 terms in the present treatment, the effect of retaining the *exponential* form (rather than expanding it to lowest order to produce the Van Vleck determinant of the semiclassical expression) is the reduction of the error by roughly a factor of 2. The

semiclassical third order propagator is seen to further reduce the error, and the corresponding quantum version yields results which are essentially indistinguishable from the exact ones within the resolution of the figure. The error made by the Trotter formula, Eq. (7.3), is again large compared to that of the power series.

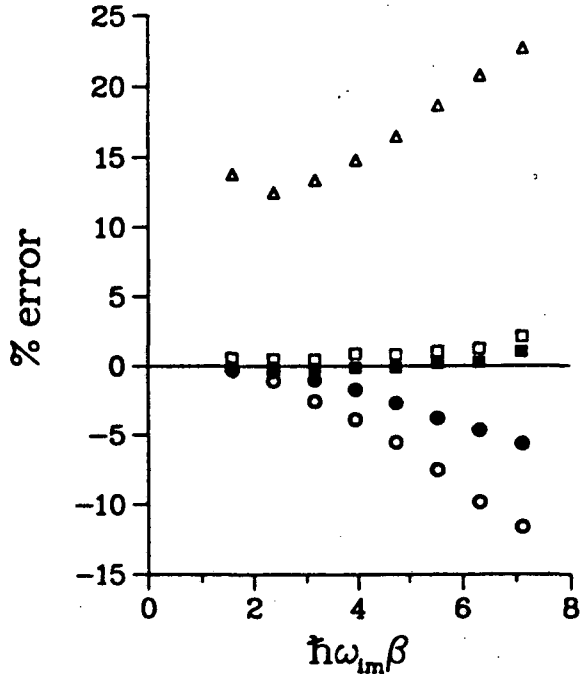

Fig. 7-6

Percentage error in the path integral evaluation of the off-diagonal coordinate matrix element of the Boltzmann operator, Eq. (7.65), for an electron in a double well potential, with the short time propagator given by the various approximations discussed in Sections 2 and 3. The parameters are the same as in Fig. 7-4. Triangles: Trotter formula. Open circles: semiclassical first order propagator. Open squares: semiclassical third order propagator. Solid circles: quantum version of the first order propagator (terms up to W_3 included in the power series). Solid squares: quantum version of the third order propagator (power series with terms up to W_5).

c) Reactive flux correlation functions

One potentially powerful use of path integral methodology is to evaluate reactive flux correlation functions, the integral of which gives the thermal [$\beta=(kT)^{-1}$] rate constant for a chemical reaction,

$$k(\beta) = Q_R^{-1} \int_0^\infty dt\ C_f(t), \tag{7.71}$$

where Q_R is the partition function for reactants. The version of the correlation function given by Miller, Schwartz, and Tromp [7.22] involves the propagator for complex time $t_c=t-i\hbar\beta/2$,

$$C_f(t) = \mathrm{tr}\,[Fe^{iHt_c^*/\hbar}Fe^{-iHt_c/\hbar}] \tag{7.72}$$

where F is the flux operator,

$$F = \frac{1}{2m}[\delta(\hat{s}-s_0)\hat{p}_s + \hat{p}_s\delta(\hat{s}-s_0)]; \tag{7.73}$$

s is the (Cartesian) reaction coordinate, $\hat{p}_s$ its conjugate momentum operator, and $s=s_0$ is the dividing surface that defines reactants and products. Evaluating the trace in a coordinate representation gives the following expression for the correlation function:

$$C_f(t) = \frac{\hbar^2}{2m^2}\int d\mathbf{Q}\int d\mathbf{Q}'\ \mathrm{Re}[\langle s'\mathbf{Q}'|e^{-iHt_c/\hbar}|s\mathbf{Q}\rangle^* \frac{\partial^2}{\partial s\,\partial s'}\langle s'\mathbf{Q}'|e^{-iHt_c/\hbar}|s\mathbf{Q}\rangle$$

$$- \frac{\partial}{\partial s'}\langle s'\mathbf{Q}'|e^{-iHt_c/\hbar}|s\mathbf{Q}\rangle^* \frac{\partial}{\partial s}\langle s'\mathbf{Q}'|e^{-iHt_c/\hbar}|s\mathbf{Q}\rangle], \tag{7.74}$$

where Re denotes "real part of", where $s=s'=s_0$ after differentiation, and where $\mathbf{Q}$ are the (Cartesian) coordinates for the degrees of freedom in addition to the reaction coordinate.

Since it is often the case in applications that one needs only the short time behavior of the flux correlation function, we consider in this Section the possibility of using the single step propagator developed in Section 3 to evaluate it. Specializing

to the case of one dimension [and thus no coordinate **Q** in Eq. (7.74)] and writing the coordinate matrix element of the propagator in the form of Section 3, i.e.,

$$<s'|e^{-iHt_c/\hbar}|s> \equiv \frac{1}{t_c^{1/2}} e^{iW(s,s';t_c)/\hbar}, \tag{7.75}$$

it is not hard to show that Eq. (7.74) becomes

$$C_f(t) = \frac{1}{2m^2|t_c|}\, e^{-\frac{2}{\hbar}\,\mathrm{Im}W(0,0;t_c)}\left[-\hbar\,\mathrm{Im}\frac{\partial^2 W(s,s';t_c)}{\partial s\,\partial s'} - 2\left[\mathrm{Re}\frac{\partial W(s,0;t_c)}{\partial s}\right]^2\right], \tag{7.76}$$

with $s=s'=0$ after differentiation (where the dividing surface s_0 has been chosen as $s_0=0$). Now expanding the exponent $W(s,s';t_c)$ in a power series as in Eq. (7.35b) gives the final expression

$$C_f(t) = C_f^{(0)}(t)\exp[-\frac{2}{\hbar}\mathrm{Im}\sum_{n=2} t_c^{n-1} W_n(0,0)]$$

$$\times\left[1 - \frac{2|t_c|^2}{m\hbar\beta}\mathrm{Im}\sum_{n=2} t_c^{n-1}\frac{\partial^2 W_n(s,s')}{\partial s\,\partial s'} - \frac{4|t_c|^2}{m\hbar^2\beta}[\mathrm{Re}\sum_{n=2} t_c^{n-1}\frac{\partial W_n(s,0)}{\partial s}]^2\right], \tag{7.77a}$$

with $s=s'=0$, and where $C_f^{(0)}(t)$ is the free particle correlation function [7.22]

$$C_f^{(0)}(t) = \frac{kT}{2\pi\hbar}\frac{(\frac{\hbar\beta}{2})^2}{[t^2+(\frac{\hbar\beta}{2})^2]^{3/2}}. \tag{7.77b}$$

If the standard short time approximation, Eq. (7.3), is used for the propagator, then it is easy to show that Eq. (7.77) gives the free particle correlation function multiplied simply by a classical Boltzmann factor,

$$C_f(t) = C_f^{(0)}(t)\, e^{-\beta V(0)}. \tag{7.78}$$

Having the propagator expressed as a power series in time, as it is in the present methodology, is especially convenient for Boltzmann correlation functions because complex time is as easily dealt with as real (or pure imaginary) time.

We demonstrate the *analytic* calculation of the reactive flux correlation function using the single step, complex time propagator of Eq. (7.35) for an Eckart barrier,[7.15]

$$V(x) = \frac{V_0}{\cosh^2(ax)}. \tag{7.79}$$

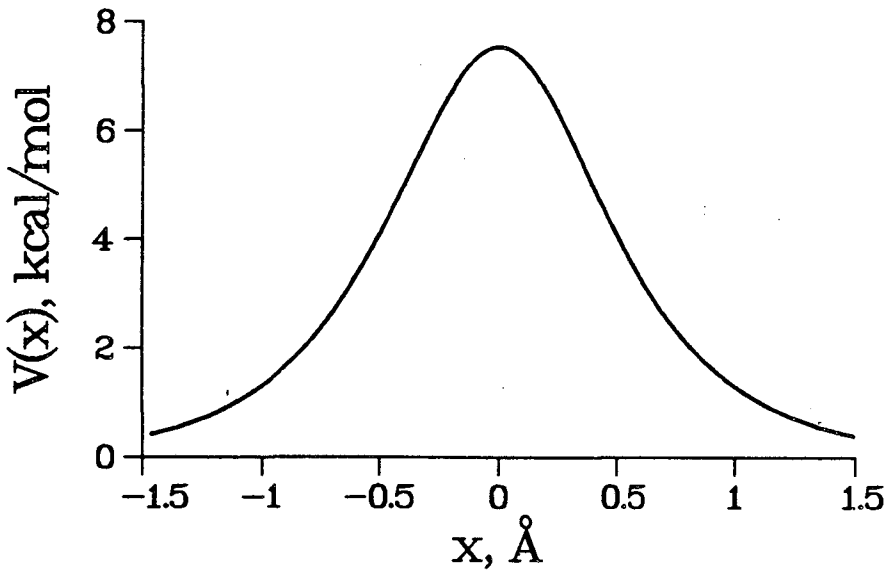

Fig. 7-7
The Eckart potential, Eq. (7.79).

The mass is taken to be that of a hydrogen atom, the temperature is $T \approx 630$ K (β=500 hartree^{-1}), and V_0=7.5 kcal/mol, a=3.15 Å^{-1} are typical of a hydrogen atom transfer reaction. A plot of the potential is shown in Fig. 7-7. The Eckart potential is simple enough that the necessary integrations involved in Eq. (7.49) can be performed analytically. However, it is useful to point out that one actually need *not* carry out all the algebra with the full potential for the flux correlation function. Since the right hand side of Eq. (7.77a) is evaluated at $s=s'=0$, one can readily see that only a *finite* number of terms in the Taylor expansion of the potential contribute

to a certain order in t_c. The calculation is thus greatly simplified by expanding the potential as a polynomial, without loss of accuracy for a given order in the complex time. Symbolic algebra programs are particularly efficient in dealing with polynomials, and complex time is no more difficult to manipulate than purely imaginary (or real) time, so that the analytic calculation of the flux correlation function as described above is straightforward and free of numerical errors. The results of this procedure are shown and compared to those obtained by an accurate basis set calculation in Fig. 7-8. For comparison, the result obtained using the standard short time propagator, i.e., Eq. (7.78), is also shown.

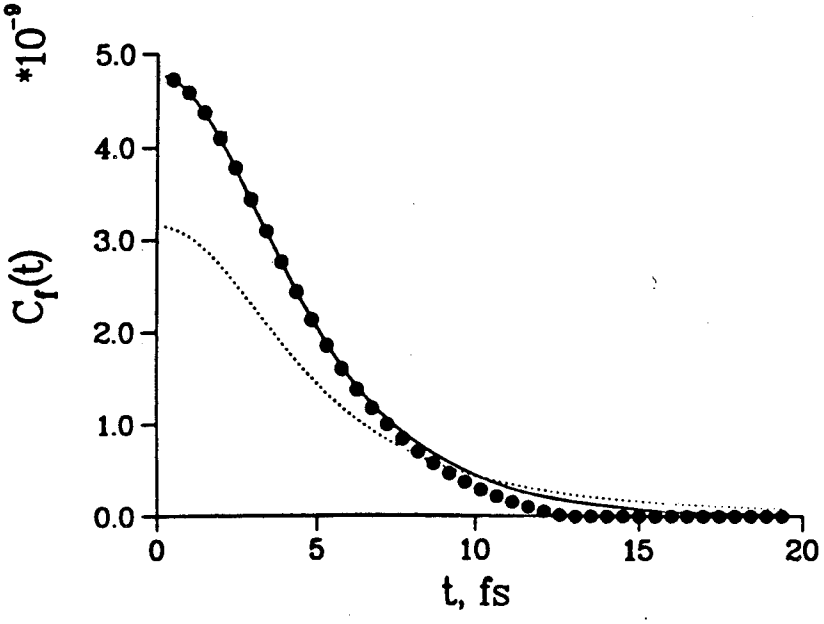

Fig. 7-8

The flux correlation function, Eq. (7.72), for an Eckart barrier [cf. Eq. (7.79)]. The mass is that of a hydrogen atom, and the temperature is 630° K. The barrier height is 7.5 kcal/mol and the imaginary frequency of the barrier is 1022 cm^{-1}. Solid line: exact results. Circles: analytic, single step calculation by power series expansion [cf. Eq. (7.77)], with n_{max}=4. Dotted line: single step evaluation of the flux correlation function using the Trotter formula [cf. Eq. (7.78)].

5. Hamiltonian with vector potential

For completeness we show here how the results of Sections 2 and 3 are modified if the Hamiltonian includes a vector potential that arises from an electromagnetic field,[7.1a,7.2]

$$\hat{H} = \frac{1}{2m}[\hat{\mathbf{p}} - \frac{e}{c}\mathbf{A}(\hat{\mathbf{x}})]^2 + V(\hat{\mathbf{x}}). \tag{7.80}$$

The same *ansatz* as Eq. (7.35) is chosen, and the analogous procedure leads here to the following equations for the functions $\{W_n(\mathbf{x})\}$:

$$0 = i\hbar\frac{F}{2}\delta_{n,1} + (n-1)W_n(\mathbf{x}) - \frac{i\hbar}{2m}\nabla^2 W_{n-1} + \frac{1}{2m}\sum_{n'=0}^{n}\nabla W_{n'}\cdot\nabla W_{n-n'}$$

$$+ \delta_{n,2}[V(\mathbf{x}) + \frac{e^2}{2mc^2}|\mathbf{A}(\mathbf{x})|^2 + \frac{i\hbar e}{2mc}\nabla\cdot\mathbf{A}] - \frac{e}{mc}\mathbf{A}\cdot\nabla W_{n-1}, \tag{7.81}$$

n=0,1,2,... ($W_{-1}\equiv 0$). If the vector potential is set to zero, then Eq. (7.81) reverts to Eq. (7.39).

For n=0 and 1, Eq. (7.81) gives

$$W_0(\mathbf{x}) = \frac{1}{2m}|\nabla W_0|^2, \tag{7.82a}$$

$$0 = i\hbar\frac{F}{2} + \frac{1}{m}\nabla W_0\cdot\nabla W_1 - \frac{i\hbar}{2m}\nabla^2 W_0 - \frac{e}{mc}\mathbf{A}\cdot\nabla W_0. \tag{7.82b}$$

The solution of (7.82a) for $W_0(\mathbf{x})$ is the same as before, Eq. (7.36a), and Eq. (7.82b) then becomes

$$(\mathbf{x}-\mathbf{x}_0)\cdot\nabla W_1 = \frac{e}{c}(\mathbf{x}-\mathbf{x}_0)\cdot\mathbf{A}(\mathbf{x}). \tag{7.83}$$

Utilizing Equations (7.42) and (7.43), the solution to Eq. (7.83) is found to be [7.15]

$$W_1(\mathbf{x}) = W_1^{(0)} + \frac{e}{c}\int_0^1 d\xi\ (\mathbf{x}-\mathbf{x}_0)\cdot\mathbf{A}(\mathbf{x}_0+(\mathbf{x}-\mathbf{x}_0)\xi)$$

$$= W_1^{(0)} + \frac{e}{c}\int_{\mathbf{x}_0}^{\mathbf{x}} d\mathbf{x}'\cdot\mathbf{A}(\mathbf{x}') \tag{7.84}$$

where the constant $W_1^{(0)}$ is the field free result of Eq. (7.36b).

Utilizing the above results for W_0 and W_1, it is not hard to show that for n=2,3,4,..., Eq. (7.81) gives equations *identical* to the field free case, Eq. (7.41); i.e., all terms involving the vector potential cancel out. The solution of Eq. (7.41a) for $W_2(\mathbf{x})$ is thus the same as the field free case, i.e., Eq. (7.48), but the solution for $W_3(\mathbf{x})$ given by Eq. (7.49) for n=3,

$$W_3(\mathbf{x}) = \int_0^1 d\xi\, \xi \left[\frac{i\hbar}{2m}\nabla^2 W_2(\mathbf{x}') - \frac{1}{m}\nabla W_2(\mathbf{x}')\cdot\nabla W_1(\mathbf{x}') \right] |_{\mathbf{x}'=\mathbf{x}_0+(\mathbf{x}-\mathbf{x}_0)\xi}, \tag{7.85}$$

is different from the field free case because here $\nabla W_1(\mathbf{x})\neq 0$. From Eq. (7.84), in fact, one has

$$\nabla W_1(\mathbf{x}) = \frac{e}{c}\mathbf{A}(\mathbf{x}), \tag{7.86}$$

so that Eq. (7.85) becomes

$$W_3(\mathbf{x}) = W_3^{(0)}(\mathbf{x}) - \frac{e}{mc}\int_0^1 d\xi\, \xi \nabla W_2(\mathbf{x}')\cdot\mathbf{A}(\mathbf{x}')|_{\mathbf{x}'=\mathbf{x}_0+(\mathbf{x}-\mathbf{x}_0)\xi} \tag{7.87}$$

where $W_3^{(0)}(\mathbf{x})$ is the field-free result given by Eq. (7.51). Using the solution for $W_2(\mathbf{x})$, one obtains the following explicit result for W_3:

$$W_3(\mathbf{x}) = W_3^{(0)}(\mathbf{x}) + \frac{e}{mc}\int_0^1 d\xi \int_0^\xi d\xi' \frac{\xi'}{\xi}\mathbf{A}(\mathbf{x}')\cdot\nabla V(\mathbf{x}''), \tag{7.88}$$

with $\mathbf{x}'=\mathbf{x}_0+(\mathbf{x}-\mathbf{x}_0)\xi$ and $\mathbf{x}'' = \mathbf{x}_0 + (\mathbf{x}-\mathbf{x}_0)\xi'$.

In summary, therefore, the terms $W_0(\mathbf{x})$ and $W_2(\mathbf{x})$ are the same as the field free results of Section 3, but $W_1(\mathbf{x})$ and $W_3(\mathbf{x})$, given by Equations (7.84) and (7.88), have a contribution involving the vector potential. Eq. (7.84) is particularly interesting in clarifying the ambiguity associated with the discretized path integral representation of the propagator in the presence of a vector potential.[7.1a,7.2] Namely, it is well known that evaluating the vector potential at the midpoint,

$$(\mathbf{x}-\mathbf{x}_0)\cdot\mathbf{A}(\tfrac{1}{2}(\mathbf{x}_0+\mathbf{x})), \tag{7.89a}$$

or taking the average of the vector potential,

$$(\mathbf{x}-\mathbf{x}_0)\cdot[\mathbf{A}(\mathbf{x}_0)+\mathbf{A}(\mathbf{x})]/2 \qquad (7.89b)$$

in the short time propagator gives the correct time evolution of a wavefunction through first order in the time, while evaluating A at either one of the two endpoints,

$$(\mathbf{x}-\mathbf{x}_0)\cdot\mathbf{A}(\mathbf{x}) \quad \text{or} \quad (\mathbf{x}-\mathbf{x}_0)\cdot\mathbf{A}(\mathbf{x}_0), \qquad (7.90)$$

does not satisfy the Schrödinger equation. It is now clear from Eq. (7.84) why this is the case. The midpoint rule or the average potential rule correspond to a correct evaluation of the line integral of Eq. (7.84) through first order in Δx, while the endpoint formula does not.

6. Concluding remarks

The short time propagators developed in Sections 2 and 3 are thus seen to constitute a significant improvement over the conventional one. The first order propagator requires calculation of the average of the potential over the time increment, while the third order propagator requires in addition the variance of the potential. If the potential is not too complicated, these quantities can be analytically calculated; use of these better propagators should not increase the complexity of a path integral calculation in that case, while it will result in much faster convergence, thus permitting one to use much larger time increments Δt in the path integral. If on the other hand the potential is not available in analytic form, the necessary integrals can still computed by quadrature, or the potential can be expanded in a Taylor series (see the discussion following the Eckart barrier calculation). Which of these schemes is advantageous to adopt will in general depend on the characteristics of the particular problem.

The primary purpose we envision for this single step propagator is thus as an improved short time propagator for use in a path integral, Eq. (7.1). If time evolution is needed for only relatively short times, however - as is often the case for the

reactive flux correlation function of Section 4c - then it may be possible to use it for the entire time increment. The example treated in Section 4c is very encouraging in this regard. Having the propagator as a power series in time is especially convenient for Boltzmann correlation functions because one is able to deal with complex time $(t - i\hbar\beta/2)$ in a very simple way.

By reducing the number of "time slices" that are required to evaluate a path integral, Eq. (7.1), we believe that the single step propagator described in this Chapter will significantly increase the feasibility of path integral calculations.

References

7.1 (a) R. P. Feynman, *Rev. Mod. Phys.* **20**, 367 (1948).

(b) R. P. Feynman and A. R. Hibbs, *Quantum Mechanics and Path Integrals*, McGraw-Hill, N.Y., 1965.

7.2 L. S. Schulman, *Techniques and Applications of Path Integration*, Wiley, N.Y., 1981.

7.3 M. F. Trotter, *Proc. Am. Math. Soc.* 10, 545 (1959).

7.4 E. Nelson, *J. Math. Phys.* **5**, 332 (1964).

7.5 (a) J. D. Doll, R. D. Coalson, and D. L. Freeman, *Phys. Rev. Lett.* 55, 1 (1985);

(b) R. D. Coalson, D. L. Freeman, and J. D. Doll, *J. Chem. Phys.* 85, 4567 (1986).

7.6 D. Thirumalai and B. Berne, *J. Chem. Phys.* 79, 5029 (1983).

7.7 M. Takahashi and M. Imada, *J. Phys. Soc. Jpn.* 53, 3765 (1984).

7.8 K. S. Schweizer, R. M. Stratt, D. Chandler, and P. G. Wolynes, *J. Chem. Phys.* **75**, 1347 (1981).

7.9 H. Kono, A. Takasaka, and S. H. Lin, *J. Chem. Phys.* **88**, 6390 (1988).

7.10 H. Goldstein, *Classical Mechanics*, 2nd Edition, Addison-Wesley.

7.11 (a) J. H. Van Vleck, *Proc. Nat. Acad. U.S. Sci.* **14**, 178 (1928);

(b) C. Morette, *Phys. Rev.* **81**, 848 (1952);

(c) B. DeWitt, *Rev. Mod. Phys.* **29**, 377 (1957).

7.12 V. P. Maslov and M. V. Fedoriuk, *Semiclassical Approximation in Quantum Mechanics*, Reidel, Boston, 1981.

7.13 The semiclassical derivation of the short time propagator of Section 2 appeared previously in the following article:

N. Makri and W. H. Miller, *Chem. Phys. Lett.* **151**, 1 (1988).

7.14 R. D. Coalson, *J. Chem. Phys.* **85**, 926 (1986).

7.15 The exponential power series expansion of the propagator appeared previously in the following article:

N. Makri and W. H. Miller, *J. Chem. Phys.* 90, 904 (1989).

7.16 E. P. Wigner, *Phys. Rev.* **40**, 749 (1932).

7.17 It was this observation, that the standard short time approximation, Eq. (7.3), is not correct to order Δt even for the harmonic oscillator, that led us to search for the correct result.

7.18 (a) D. Chandler and P. G. Wolynes, *J. Chem. Phys.* 74, 4078 (1981);
(b) D. M. Ceperley and G. Jacucci, *Phys. Rev. Lett.* 58, 1648 (1987).

7.19 G. A. Baker, Jr., *Essentials of Padé Approximants*, Academic Press, New York, 1975.

7.20 N. Metropolis, A. W. Rosenbluth, M. N. Rosenbluth, H. Teller, and E. Teller, *J. Chem. Phys.* 21, 1087 (1953);
J. P. Valleau and S. G. Whittington, in *Modern Theoretical Chemistry*, B.J. Berne, Ed., Phenum, New York, 1977, vol. 5, pp. 137-168.

7.21 C. H. Bennett, *J. Comp. Phys.* 22, 245 (1976).

7.22 W. H. Miller, S. D. Schwartz, and J. W. Tromp, *J. Chem. Phys.* 79, 4889 (1983).

7.23 W. H. Miller, *Adv. Chem. Phys.* 25, 69 (1974).

7.24 Y. Fujiwara, T. A. Osborn, and S. F. J. Wilk, *Phys. Rev.* A 25, 14 (1982).

LAWRENCE BERKELEY LABORATORY
TECHNICAL INFORMATION DEPARTMENT
1 CYCLOTRON ROAD
BERKELEY, CALIFORNIA 94720